Mediators of Inflammation

Metabolic Syndrome, Inflammation, and Cancer

Lead Guest Editor: Yong Wu
Guest Editors: Yunzhou Dong, Shengzhong Duan, Yingqiu Xie, Donghui Zhu, and Lin Deng

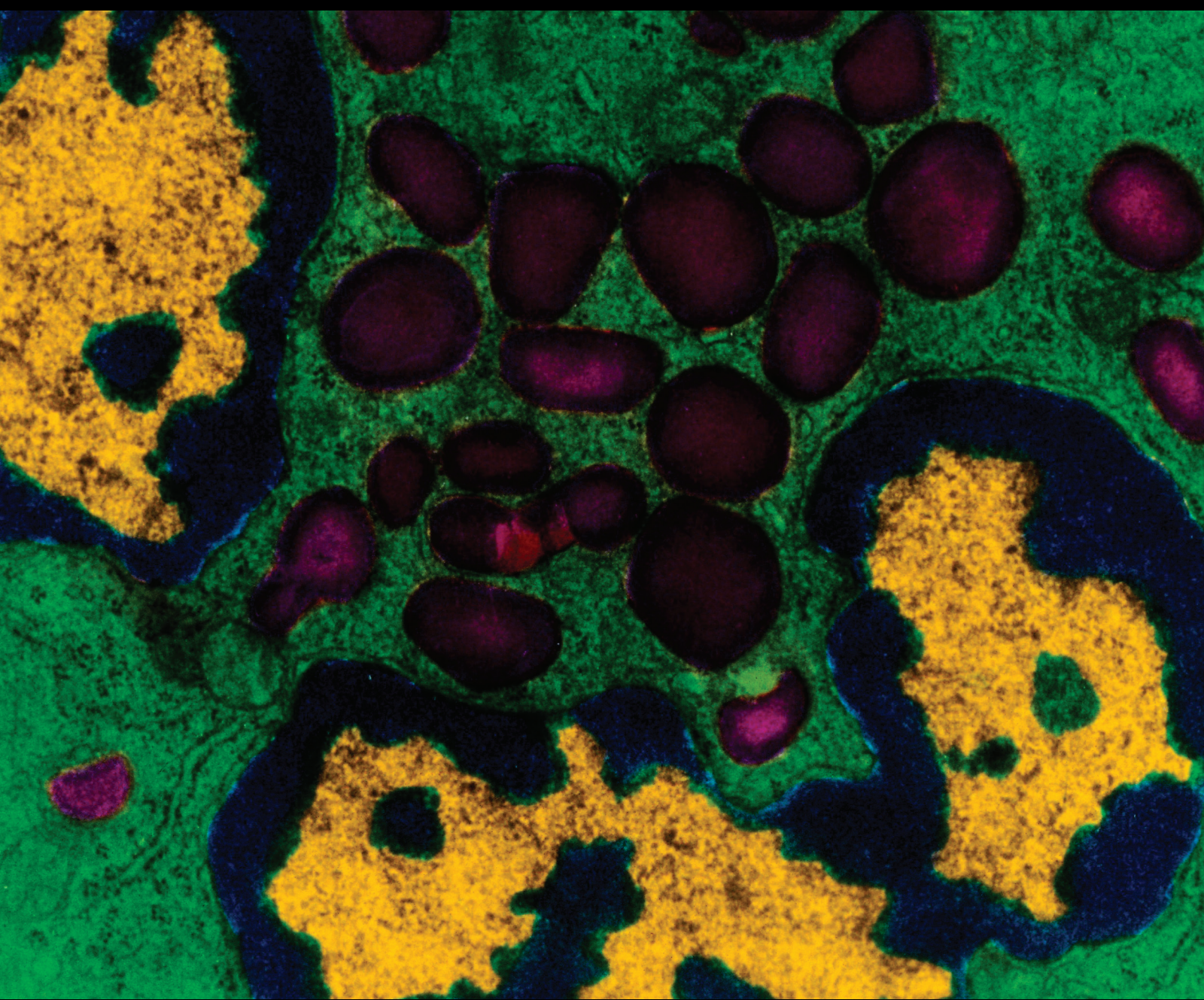

Metabolic Syndrome, Inflammation, and Cancer

Mediators of Inflammation

Metabolic Syndrome, Inflammation, and Cancer

Lead Guest Editor: Yong Wu
Guest Editors: Yunzhou Dong, Shengzhong Duan, Yingqiu Xie, Donghui Zhu, and Lin Deng

Editorial Board

Contents

Hindawi
Mediators of Inflammation
Volume 2017, Article ID 8259356, 2 pages
https://doi.org/10.1155/2017/8259356

Editorial

Metabolic Syndrome, Inflammation, and Cancer

Yong Wu,[1,2] Yunzhou Dong,[3] Shengzhong Duan,[4] Donghui Zhu,[5] and Lin Deng[6]

[1]*Division of Cancer Research and Training, Department of Internal Medicine, Charles R. Drew University of Medicine and Science, Los Angeles, CA, USA*
[2]*David Geffen UCLA School of Medicine and UCLA Jonsson Comprehensive Cancer Center, University of California, Los Angeles, CA, USA*
[3]*Department of Surgery, Boston Children's Hospital and Harvard Medical School, Boston, MA 02115, USA*
[4]*Laboratory of Oral Microbiology, Shanghai Research Institute of Stomatology, Shanghai Key Laboratory of Stomatology, Ninth People's Hospital, Shanghai Jiao Tong University School of Medicine, Shanghai 200011, China*
[5]*University of North Texas, Denton, TX, USA*
[6]*Dana-Farber Cancer Institute, Harvard Medical School, Boston, MA 02115, USA*

Correspondence should be addressed to Yong Wu; yongwu@cdrewu.edu

Received 14 June 2017; Accepted 14 June 2017; Published 6 July 2017

The inflammatory condition associated with overweight/obesity represents a triggering factor in the pathogenesis of the metabolic syndrome and primarily contributes to the related pathological outcomes. Stimuli including overnutrition, physical inactivity, and ageing might lead to oversecretion of proinflammatory cytokine, ultimately resulting in insulin resistance, diabetes, and its cardiovascular complications. Furthermore, inflammation has also been associated with several types of cancers by influencing growth, apoptosis, and proliferation of cancer and stromal cells.

Previous studies propose that the metabolic syndrome may play an imperative role in the initiation, progression, and poor prognosis of some tumors. Currently, the causal association between the metabolic syndrome and cancer is more commonly recognized; nevertheless, the precise mechanisms mediating this relationship remain poorly understood. It has become evident that the inflammatory condition associated with metabolic syndrome contributes to the development and progression of cancer. Ascertaining the link between the metabolic syndrome and cancer, the role of inflammation in these diseases and identification of new therapeutic targets are of great significance. This special issue contributes original research papers and review articles that motivate the continuous efforts to comprehend the mechanisms, production, and management related to cancers associated with the metabolic syndrome.

In this special issue, the link between the metabolic syndrome and cancer was extensively discussed. Both cancer and diabetes are associated with abnormal lactate metabolism, and high lactate level is the crucial biological feature of these diseases. On the other hand, high lactate results in a higher insulin-resistant status and a more malignant phenotype of cancer cells, favoring diabetes and cancer development. Considering an interactive relationship between diabetes and cancers, the role of high lactate production in diabetes and cancer interaction should not be neglected. Understanding the molecular mechanisms underlying metabolic remodeling of diabetes- and cancer-related signaling would provide novel preventive and therapeutic approaches for diabetes and cancer treatment. In addition, S. Harlid et al. interrogated the association between the metabolic syndrome and colorectal cancer risk in human subjects. Out of 178 inflammatory and cancer biomarkers, 12 proteins were associated with the metabolic syndrome and/or its components. FGF21, one of the 12 proteins, was also associated with an increased risk for colorectal cancer, exemplifying the intimate relationship between the metabolic syndrome and cancer.

In the present special issue, the anti-inflammatory role and tissue-/organ-protective effects of different reagents and drugs were also studied. Y. Gao et al. revealed that H2 saline has a protective effect against doxorubicin-

induced cardiotoxicity and hepatotoxicityin rats by inhibiting inflammation and apoptosis. K. Su et al. demonstrated that FTY720, a new chemical substance derived from the ascomycete *Isaria sinclairii*, is able to attenuate sphingosine-1-phosphate- (S1P-) induced podocyte damage via reducing inflammatory cytokines. Using system pharmacological analysis, X. Shen et al. suggested that combined application of Bupleuri Radix and Scutellaria Radix not only directly inhibit the synthesis and release of inflammatory cytokines but also have potential therapeutic effects against inflammation-induced pain. Additionally, a combination therapy of these two drugs exhibited systemic treatment efficacy and provided a theoretical basis for the development of drugs against inflammatory diseases. Y. Dong et al. elicited the role of lysophosphatidic acid (LPA), a naturally occurring bioactive phospholipid, in the regulation of cell survival and apoptosis in HeLa cells. Under pathological conditions, high concentration of LPA triggers apoptosis by the upregulation of TNFR21 (DR6) expression, one of the death receptors in inflammation, which solved a controversial question in different literatures. In clinical studies, X. Liu et al. revealed that the antidiabetic drugs metformin, sitagliptin, and pioglitazone have an anti-inflammatory role in atherosclerosis, suggesting a therapeutic role of these drugs in preventing diabetic atherosclerosis, and furthermore, combinational therapy was beneficial to reduce atherosclerosis. Another clinical study by X. Ding et al. suggest that the components of the metabolic syndrome may associate with the higher risks of thyroid nodule (TN) in women than in men. Furthermore, S. S. Chung et al. proposed that proinflammatory cytokines induced cancer cell invasiveness and this was mediated by a signal transducer and activator of transcription 3- (STAT3-) regulated mechanism in colorectal cancer cells. Their data suggest that withaferin A could be a promising anticancer agent that effectively inhibits the progression of colorectal cancer.

We anticipate that the present special issue will not only be valuable to the extensive readership by providing insights into novel and chief aspects associated with inflammation and its mediators in the context of the metabolic syndrome and cancer but also inspire innovative research ideas and revolutionized therapeutic strategies in this field.

Acknowledgments

We would like to thank all the authors for their outstanding work and all the reviewers for their time, efforts, and critical comments in refining these manuscripts.

Yong Wu
Yunzhou Dong
Shengzhong Duan
Donghui Zhu
Lin Deng

Hindawi
Mediators of Inflammation
Volume 2017, Article ID 5432818, 8 pages
https://doi.org/10.1155/2017/5432818

Research Article

Role of ARPC2 in Human Gastric Cancer

Jun Zhang,[1] Yi Liu,[2] Chang-Jun Yu,[2] Fu Dai,[1] Jie Xiong,[1] Hong-Jun Li,[1] Zheng-Sheng Wu,[2] Rui Ding,[1] and Hong Wang[1]

[1]*Department of General Surgery, Third Affiliated Hospital (Hefei First People's Hospital) of Anhui Medical University, Hefei, China*
[2]*Department of Gastrointestinal Surgery, First Affiliated Hospital of Anhui Medical University, Hefei, China*

Correspondence should be addressed to Yi Liu; yliu20harvard@126.com

Received 4 December 2016; Accepted 6 March 2017; Published 13 June 2017

Academic Editor: Yingqiu Xie

Gastric cancer continues to be the second most frequent cause of cancer deaths worldwide. However, the exact molecular mechanisms are still unclear. Further research to find potential targets for therapy is critical and urgent. In this study, we found that ARPC2 promoted cell proliferation and invasion in the human cancer cell line MKN-28 using a cell total number assay, MTT (3-(4,5-dimethyl-2-thiazolyl)-2,5-diphenyl-2-H-tetrazolium bromide) assay, cell colony formation assay, migration assay, invasion assay, and wound healing assay. For downstream pathways, CTNND1, EZH2, BCL2L2, CDH2, VIM, and EGFR were upregulated by ARPC2, whereas PTEN, BAK, and CDH1 were downregulated by ARPC2. In a clinical study, we examined the expression of ARPC2 in 110 cases of normal human gastric tissues and 110 cases of human gastric cancer tissues. ARPC2 showed higher expression in gastric cancer tissues than in normal gastric tissues. In the association analysis of 110 gastric cancer tissues, ARPC2 showed significant associations with large tumor size, lymph node invasion, and high tumor stage. In addition, ARPC2-positive patients exhibited lower RFS and OS rates compared with ARPC2-negative patients. We thus identify that ARPC2 plays an aneretic role in human gastric cancer and provided a new target for gastric cancer therapy.

1. Introduction

Despite the rapid progression in the therapies used to treat gastric cancer patients, it continues to be the second most common cause of cancer deaths worldwide [1–4]. Patients with gastric cancer usually lack symptoms in the early stages, and efficient early detection methods are limited. Hence, gastric cancers are usually diagnosed only at advanced stages. Combinations of surgery, chemotherapy, and radiotherapy are common treatment options for advanced gastric cancer, but the prognosis is always poor [4, 5]. Many scientists have focused on the molecular mechanisms underlying the development and progression of gastric cancer, but the exact mechanisms remain unclear. Further studies are therefore warranted to find potential therapeutic targets for gastric cancers.

Actin-related protein 2/3 complex subunit 2 (ARPC2) is one of the evolutionarily conserved subunits of actin-related protein 2/3 complex (Arp2/3). The other subunits are ARPC1, ARPC3, ARPC4, and ARPC5 and two actin-related proteins Arp2 and Arp3 [6–9]. In the Arp2/3 complex, ARPC2 subunit holds a central structural position and helps relay both signals and conformational changes [7, 10, 11]. Ghouleh et al. demonstrated that ARPC2 participated in promoting smooth muscle cell migration [6]. Melboucy-Belkhir et al. determined that ARPC2 was regulated by Forkhead box F1 (FOXF1) and might be involved in cell growth of lung fibroblasts [12]. To date, there is no publication that documents the relation between ARPC2 and tumor proliferation or invasion.

In this article, we determined that ARPC2 promotes both proliferation and invasion in the human gastric cancer cell line MKN-28 by using a cell total number assay, MTT assay, cell colony formation assay, migration assay, invasion assay, and wound healing assay. For downstream genes, we found that cancer-promoting genes were upregulated while tumor suppress genes were downregulated by ARPC2. Moreover, in clinical tissues, ARPC2 was associated with tumor size, lymph node invasion, and tumor stage but not with patients' age, gender, or tumor grade. ARPC2 expressed higher levels

in gastric cancer tissues than in normal gastric tissues. Furthermore, ARPC2-positive patients exhibited both a lower RFS rate ($P = 0.009$) and a lower OS rate ($P = 0.030$) than did ARPC2-negative patients. As a result, ARPC2 played a destructive role in human gastric cancer cells and can be used as a potential target for the diagnosis and therapy of gastric cancer.

2. Materials and Methods

2.1. Cell Lines and Cell Culture. Human gastric cancer cell MKN-28 was obtained from ATCC (the American Type Culture Collection) (Rockville, MD, USA). As recommended, MKN-28 was cultured in a humidified incubator at 37°C and 5% CO_2.

2.2. RNA Oligonucleotides and Transfection. Small-interfering RNAs used in this article contained two types of ARPC2-siRNA (designated as siARPC2-1 and siARPC2-2 or siAR-1 and siAR-2) and negative control (designated as siNC). They were obtained from GenePharma (Shanghai, China). Lipofectamin 2000 (Invitrogen, Carlsbad, CA, USA) was used to perform siRNA transfection.

2.3. RT-Quantitative PCR (qPCR). We used RT-qPCR to evaluate the mRNA levels of CTNND1, EZH2, BCL2L2, CDH2, VIM, EGFR, PTEN, BAK, and CDH1, which was performed as described in the previous studies [13]. GAPDH was used as the endogenous control.

2.4. Cell Proliferation and Invasion Assays. In this study, the cell total number assay, MTT assay, cell colony formation assay, migration assay, invasion assay, and wound healing assay were carried out to test cell proliferation and invasion. They were all carried out as previously described [13–15].

2.5. Western Blot Analysis. Western blot analysis was carried out to test the protein level of ARPC2, which was performed as described previously [13]. β-Actin was used as the endogenous control.

2.6. Patients and Tissue Samples. In total, 110 paraffin-embedded surgical gastric cancer tissue specimens and 110 paraffin-embedded surgical normal gastric tissue specimens were collected at the First Affiliated Hospital of Anhui Medical University (Hefei, Anhui, China) between 2009 and 2015. All experimental protocols were approved by the Ethical Committee of Anhui Medical University and conform to the principles outlined in the Declaration of Helsinki. The pathohistological diagnosis and grade of the patients was based on the World Health Organization grading systems. This study protocol was approved by the institutional review board. Informed consent forms were obtained from all patients. We followed up the patients with gastric cancer, and the average duration was approximately 5 years.

2.7. Immunohistochemistry (IHC). Immunohistochemistry analysis was carried out as described earlier [16]. In this study, we tested the protein level of ARPC2. The stained sections were reviewed and scored using an Olympus microscope (Olympus America Inc., Melville, NY). ARPC2-positive was designated as more than 20% percent of the tumor cells stained, and ARPC2-negative was designated as 20% percent or less of the tumor cells stained.

2.8. Statistical Analyses. For the in vitro experiments, the differences were analyzed using unpaired two-tailed t-test. For the experiments involving clinical tissues, the differences were analyzed using Pearson's chi-square test. Patient relapse-free survival (RFS) and overall survival (OS) were analyzed using Kaplan-Meier curves, and the differences were analyzed using the log-rank test. $P < 0.05$ was considered statistically significant.

3. Results

3.1. ARPC2 Promoted Proliferation of MKN-28 Cells. Human gastric cancer MKN-28 cells were tranfected with ARPC2-siRNA-1, ARPC2-siRNA-2, or negative control (designated as siARPC2-1 and siARPC2-2 or siAR-1, siAR-2, and siNC, resp.). Figure 1(a) showed that protein level of ARPC2 was dramatically decreased after being tranfected with ARPC2-siRNA-1 and ARPC2-siRNA-2, as determined using western blot. Over a period of 5 days, the cell total number assay showed that the number of MKN-28 cells decreased significantly after being transfected with ARPC2-siRNA-1 and ARPC2-siRNA-2 compared with the negative control (Figure 1(b)). Concordantly, the MTT assay showed that the cell viability of the MKN-28 cells decreased significantly after being transfected with ARPC2-siRNA (Figure 1(c)). Moreover, Figure 1(d) showed that the cell colony formation of MKN-28 cells decreased apparently after being transfected with ARPC2-siRNA-1 and ARPC2-siRNA-2 compared with the negative control. Therefore, ARPC2 promoted the proliferation of human gastric cancer cells.

3.2. ARPC2 Promoted Invasion of MKN-28 Cells. To further evaluate whether ARPC2 could promote the invasion of MKN-28 cells, migration assay, invasion assay, and wound healing assay were carried out. After transfection with ARPC2-siRNA-1 and ARPC2-siRNA-2, both the migration (Figure 2(a)) and invasion (Figure 2(b)) of MKN-28 cells decreased remarkably compared with the negative control. Additionally, the wound closing of MKN-28 cells was significantly decreased in MKN-28 cells with a decreased expression of ARPC2 (Figure 2(c)). As a result, ARPC2 also promoted the invasion of human gastric cancer cells.

3.3. ARPC2 Regulated the Expression of Several Genes. In addition, we carried out large-scale RT-qPCR to screen for genes that were regulated by ARPC2. It has been reported previously that CTNND1, EZH2, BCL2L2, CDH2, VIM, and EGFR have positive correlation to proliferation, invasion, and poor prognosis of gastric cancer. As shown in Figure 3(a), the mRNA levels of those genes were clearly decreased after being transfected with ARPC2-siRNA-1 and ARPC2-siRNA-2, which indicated that ARPC2 upregulated them. In contrast, the mRNA levels of tumor suppress genes (PTEN, BAK, and CDH1) were increased significantly after the blocking of ARPC2, which indicated that ARPC2 downregulated them (Figure 3(b)). Therefore, we may conclude

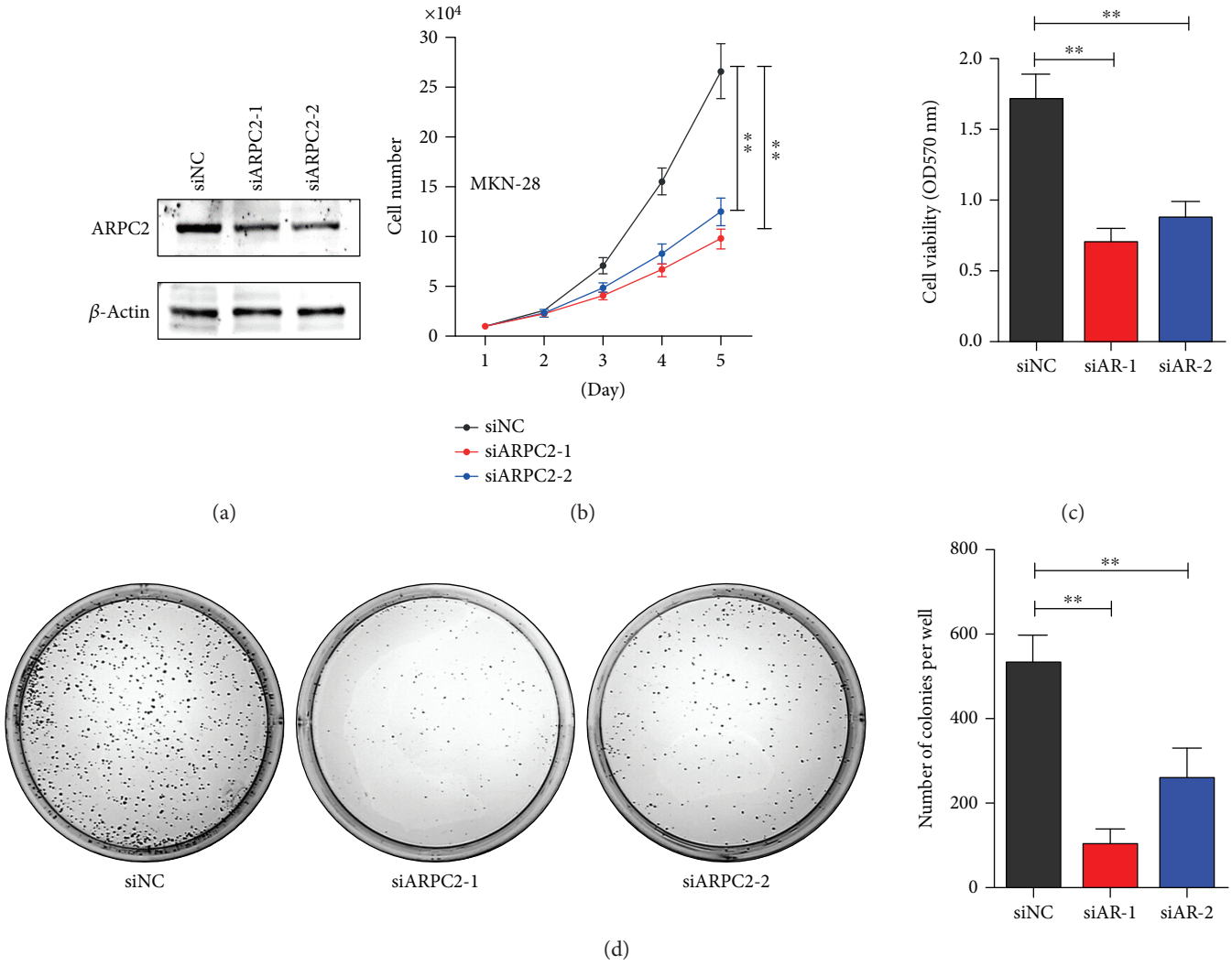

Figure 1: ARPC2 promoted proliferation of MKN-28 cells. MKN-28 cells were transfected with ARPC2-siRNA-1, ARPC2-siRNA-2, or negative control (siNC). (a) Protein level of ARPC2 was evaluated by western blot. (b) Cell total number assay; (c) MTT assay; and (d) cell colony formation assay were performed in MKN-28 cells after transfection. $^{*}P < 0.05$. $^{**}P < 0.01$.

that these genes might participate in the role that ARPC2 plays in promoting the cell proliferation and invasion of human gastric cancer cells.

3.4. Association of ARPC2 Expression with Clinic-Pathological Features from Patients with Gastric Cancer. We collected 110 normal gastric tissues and 110 gastric cancer tissues of archived formalin-fixed paraffin-embedded specimens and detected the protein level of ARPC2 using immunohistochemistry. The positive signal of ARPC2 protein was mainly located in the cytoplasm. As shown in Table 1, in gastric cancer tissues, 40 of the 110 cases negatively expressed ARPC2 and 70 of the 110 cases positively expressed ARPC2; in normal gastric tissues, 70 of the 110 cases negatively expressed ARPC2 and 40 of the 110 cases positively expressed ARPC2. As a result, the percentage of ARPC2-positive tissues in gastric cancer specimens was much higher than that in the normal gastric specimens. Figure 4(a) shows the typical pictures.

For further study, we associated ARPC2 expression with clinic-pathological features from patients with gastric cancer. The patients' age, gender, tumor size, lymph node invasion, tumor grade, and tumor stage were included. The expression of ARPC2 was markedly higher in patients with a tumor size > 5 cm than in those with a tumor size ≤ 5 cm ($P = 0.001$); higher in tumors with lymph node invasion than in tumors without lymph node invasion ($P = 0.004$); and higher in higher-stage (stages III-IV) tumors than in lower-stage (stages I-II) tumors ($P = 0.001$). However, there was no significant difference between ARPC2 expression and other clinic-pathological features, including patients' age, gender, and tumor grade (Table 2).

3.5. Correlation between ARPC2 Expression and Survival of Patients with Gastric Cancer. To evaluate the RFS and OS rates of gastric cancer patients with different levels of ARPC2 expression, Kaplan-Meier analyses were performed in the 110 gastric cancer tissues. Every patient was followed

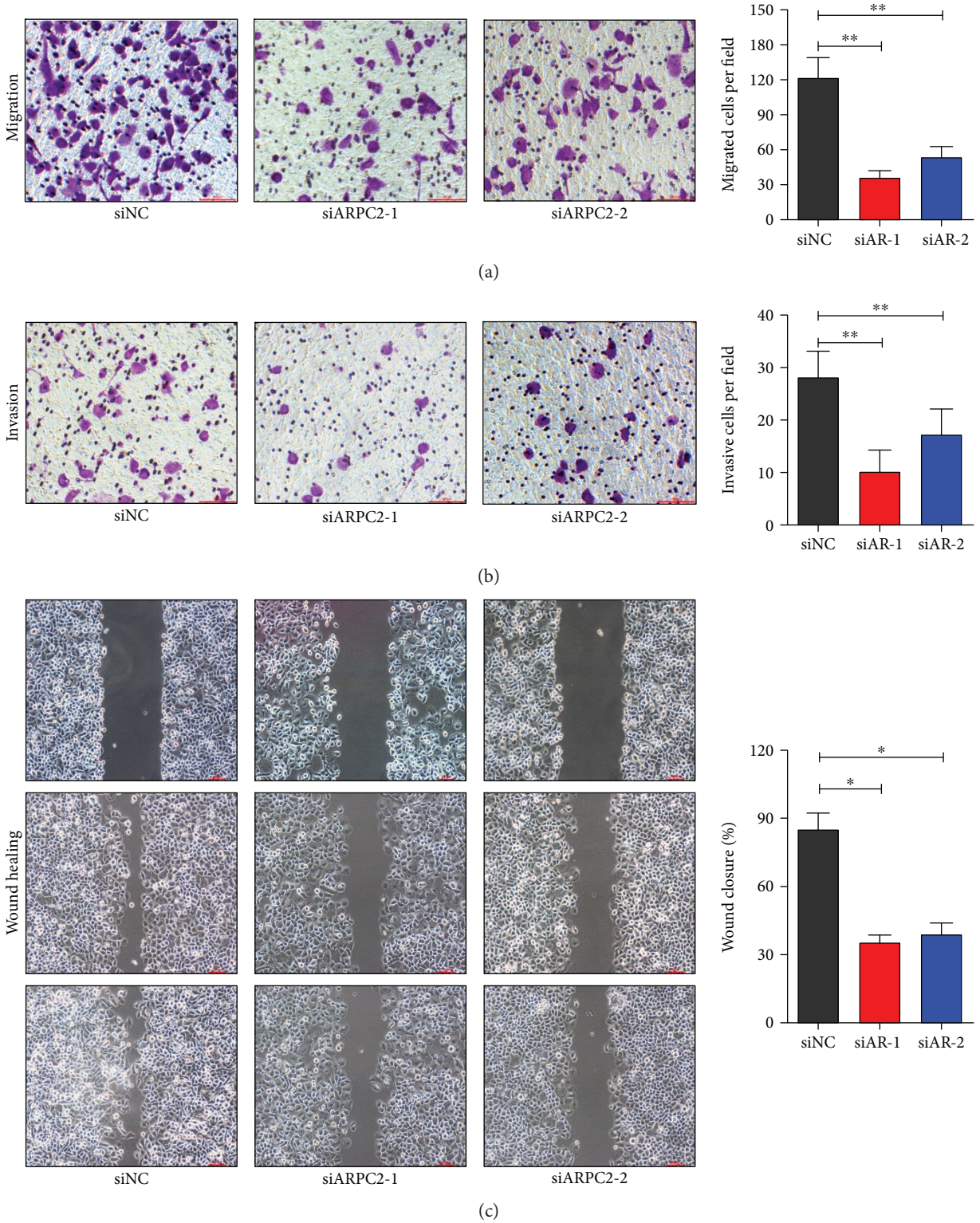

Figure 2: ARPC2 promoted invasion of AGS cells. MKN-28 cells were transfected with ARPC2-siRNA-1, ARPC2-siRNA-2, or negative control. (a) Migration assay; (b) invasion assay; and (c) wound healing assay were performed in MKN-28 cells after transfection. $^{*}P < 0.05$. $^{**}P < 0.01$.

up for more than 5 years. As shown in Figure 4(b), the ARPC2-positive patients exhibited both a lower RFS rate ($P = 0.009$) and a lower OS rate ($P = 0.030$) than did the ARPC2-negative patients.

4. Discussion

Herein, we confirmed for the first time that ARPC2 had adverse effects in human gastric cancer, and this was the first

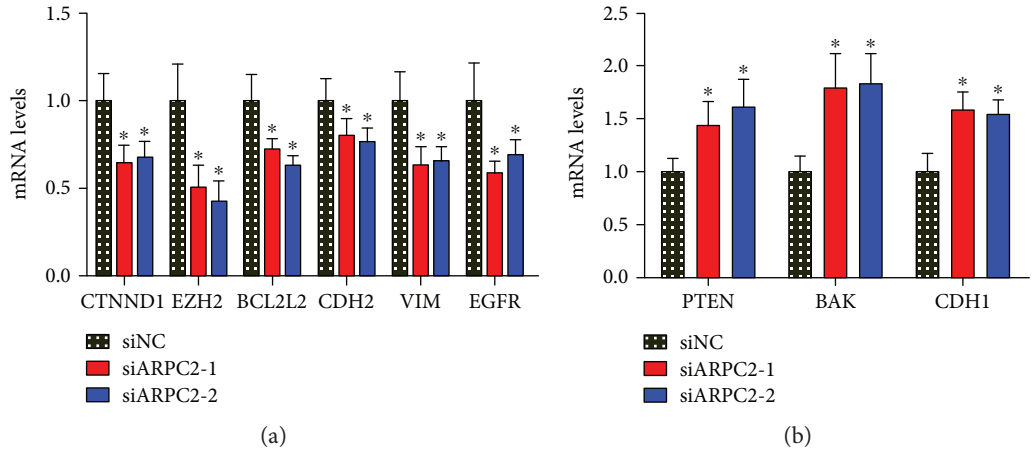

Figure 3: ARPC2 regulated proliferation and invasion-related genes. (a) mRNA levels of CTNND1, EZH2, BCL2L2, CDH2, VIM, and EGFR were decreased after transfected with ARPC2-siRNA-1 and ARPC2-siRNA-2 compared with the negative control using RT-qPCR. (b) mRNA levels of PTEN, BAK, and CDH1 were increased after transfected with ARPC2-siRNA-1 and ARPC2-siRNA-2 compared with the negative control. GAPDH was used as the endogenous control. $^{*}P < 0.05$. $^{**}P < 0.01$.

Table 1: Expression of ARPC2 in gastric cancer and normal tissues.

Group	n	ARPC2 expression	
		Negative, n (%)	Positive, n (%)
Cancer	110	40 (36.4)	70 (63.6)*
Normal	110	70 (63.6)	40 (36.4)

Note: $^{*}P < 0.001$.

report on the role of ARPC2 in human cancers. Combining multiple methods that were used in our study, we drew conclusions that ARPC2 promoted both the cell proliferation and invasion of human gastric cancer cells. In clinical samples, the expression level of APRC2 was much higher in gastric cancer tissues than in normal gastric tissues. Furthermore, the expression of ARPC2 was associated with aggressive behaviors of gastric cancer, including large tumor size, lymph node invasion, high tumor stage, and poor prognosis.

As for recurrent, metastatic, or advanced gastric cancer, the traditional therapeutic methods, including surgery, chemotherapy, and radiotherapy, showed poor curative effects and patient prognoses [4, 12, 17]. Trastuzumab, a monoclonal antibody that targets HER2, is one of a mere few targeted therapies that have been used in human gastric cancer [17, 18]. Trastuzumab could partly prolong survival and improve the quality of life of gastric cancer patients. However, only 15–20% of patients with gastric cancer overexpressed HER2 and could benefit from trastuzumab [17, 19]. Currently, searching for new genes as potential targets for therapy is urgent. In this study, we found that blocking ARPC2 by using the siRNA method can dramatically decrease the cell proliferation and invasion of the human gastric cancer cell line MKN-28. Clinically, an elevated ARPC2 level was associated with a lower survival rate in gastric cancer patients. These results imply that ARPC2 participates in the development of gastric cancer and that function-inhibiting drugs targeted at ARPC2 may be a new approach for its therapy.

As reported previously, Arp2/3 complex is essential for cell motility [11, 20]. As one of the subunits of Arp2/3, ARPC2 also promoted tumor development and progression. For downstream genes, we found that CTNND1, EZH2, BCL2L2, CDH2, VIM, and EGFR were upregulated by ARPC2 and that PTEN, BAK, and CDH1 were downregulated by ARPC2. In previous studies, CTNND1 was documented to promote many types of human cancers, including hepatocellular carcinoma and lung cancer [21, 22]. EZH2 was demonstrated to be oncogenic in esophageal cancer, lung cancer, and breast cancer, among others [23–25]. Moreover, Liu et al. and Chen et al. proved that EZH2 promoted the progression and invasion of human gastric cancer [26, 27]. BCL2L2 was determined to promote tumorigenicity and invasion in human glioblastoma, non-small-cell lung cancer, and colon cancer [28–30]. CDH2 was reported to be related to the epithelial-mesenchymal transition (EMT) in non-small-cell lung cancer [31]. Vimentin (VIM) is a famous EMT marker that promotes tumor invasion and drug resistance in ovarian cancer, colon cancer, and gastric cancer [32–34]. EGFR is also a famous oncogene in ovarian cancer, breast cancer, and gastric cancer [35–37]. Moreover, PTEN is a well-studied gene that inhibits tumor growth and invasion in nearly all types of human cancers, including gastric cancer, breast cancer, and lung cancer [38–41]. BAK was demonstrated to promote tumor apoptosis and chemosensitivity to chemotherapeutic drugs in non-small-cell lung cancer and gastric cancer [42, 43]. CHD1 was also reported to be a tumor suppressor gene in many human cancers [44, 45]. These publications all supported our result. Thus, CTNND1, EZH2, BCL2L2, CDH2, VIM, EGFR, PTEN, BAK, and CDH1 all contributed to the bad role of ARPC2 in human gastric cancer.

In this study, we reported for the first time the destructive role of ARPC2 in human gastric cancer cells. Both in vitro and clinical studies were performed. A high expression of

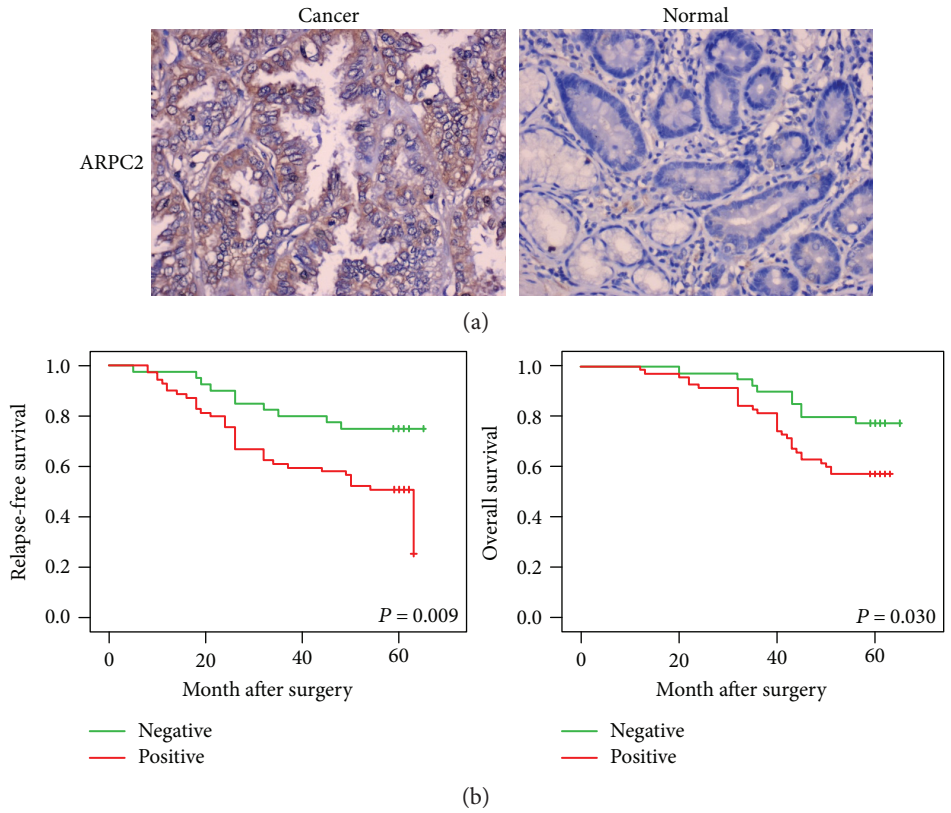

Figure 4: Relapse-free and overall survival curves stratified by ARPC2 expression. (a) Expression of ARPC2 protein in normal gastric tissues and gastric cancer tissues was detected using immunohistochemistry method, and representative pictures are shown. Magnification: 200. (b) Gastric cancer patients with positive expression of ARPC2 were associated with worse relapse-free survival and overall survival.

Table 2: Correlation of ARPC2 expression with clinicopathological parameters from gastric cancer patients.

Parameter	n	ARPC2 expression	
		Positive, n (%)	P value
Age (years)			
≤60	57	34 (59.6)	0.367
>60	53	36 (67.9)	
Gender			
Male	60	34 (56.7)	0.096
Female	50	36 (72.0)	
Tumor size (cm)			
≤5	73	38 (52.1)	0.001
>5	37	32 (86.5)	
Lymph node metastasis			
No	34	15 (44.1)	0.004
Yes	76	55 (72.4)	
Grade			
I	11	8 (72.7)	0.638
II	71	43 (60.6)	
III	28	19 (67.9)	
Stage			
I-II	57	25 (43.9)	0.001
III-IV	53	45 (84.9)	

ARPC2 was associated with both poor RFS and OS rates in gastric cancer patients. Therefore, we propose ARPC2 as a new potential biomarker and therapeutic target for patients with gastric cancer.

Conflicts of Interest

The authors declare no conflict of interests.

Acknowledgments

This work was supported by the National Natural Science Foundation (Grant no. 81472493).

References

[1] A. Jemal, F. Bray, M. M. Center, J. Ferlay, E. Ward, and D. Forman, "Global cancer statistics," *CA: A Cancer Journal for Clinicians*, vol. 61, pp. 69–90, 2011.

[2] D. H. Wang, Z. S. Fan, F. L. Liu, and J. Zuo, "Hsa-miR-21 and Hsa-miR-29 in tissue as potential diagnostic and prognostic biomarkers for gastric cancer," *Cellular Physiology and Biochemistry*, vol. 37, pp. 1454–1462, 2015.

[3] S. H. Wu, F. Liu, L. M. Xie et al., "miR-125b suppresses proliferation and invasion by targeting MCL1 in gastric cancer," *BioMed Research International*, vol. 2015, Article ID 365273, p. 10, 2015.

[4] C. Yan, J. C. Yu, Y. Q. Liu, W. M. Kang, Z. Q. Ma, and L. Zhou, "MiR-32 promotes gastric carcinoma tumorigenesis by

targeting Kruppel-like factor 4," *Biochemical and Biophysical Research Communications*, vol. 467, pp. 913–920, 2015.

[5] H. L. Tang, Y. N. Kong, J. L. Guo et al., "Diallyl disulfide suppresses proliferation and induces apoptosis in human gastric cancer through Wnt-1 signaling pathway by up-regulation of miR-200b and miR-22," *Cancer Letters*, vol. 340, pp. 72–81, 2013.

[6] I. Al Ghouleh, A. Rodriguez, P. J. Pagano, and G. Csanyi, "Diallyl disulfide suppresses proliferation and induces apoptosis in human gastric cancer through Wnt-1 signaling pathway by up-regulation of miR-200b and miR-22," *International Journal of Molecular Sciences*, vol. 14, pp. 20220–20235, 2013.

[7] K. M. Daugherty and B. L. Goode, "Functional surfaces on the p35/ARPC2 subunit of Arp2/3 complex required for cell growth, actin nucleation, and endocytosis," *Journal of Biological Chemistry*, vol. 283, pp. 16950–16959, 2008.

[8] L. M. Machesky, S. J. Atkinson, C. Ampe, J. Vandekerckhove, and T. D. Pollard, "Purification of a cortical complex containing two unconventional actins from Acanthamoeba by affinity chromatography on profilin-agarose," *The Journal of Cell Biology*, vol. 127, pp. 107–115, 1994.

[9] M. D. Welch, A. H. DePace, S. Verma, A. Iwamatsu, and T. J. Mitchison, "The human Arp2/3 complex is composed of evolutionarily conserved subunits and is localized to cellular regions of dynamic actin filament assembly," *The Journal of Cell Biology*, vol. 138, pp. 375–384, 1997.

[10] H. Gournier, E. D. Goley, H. Niederstrasser, T. Trinh, and M. D. Welch, "Reconstitution of human Arp2/3 complex reveals critical roles of individual subunits in complex structure and activity," *Molecular Cell*, vol. 8, pp. 1041–1052, 2001.

[11] L. Havelkova, G. Nanda, J. Martinek et al., "Arp2/3 complex subunit ARPC2 binds to microtubules," *Plant Science: An International Journal of Experimental Plant Biology*, vol. 241, pp. 96–108, 2015.

[12] S. Melboucy-Belkhir, P. Pradere, S. Tadbiri et al., "Forkhead box F1 represses cell growth and inhibits COL1 and ARPC2 expression in lung fibroblasts in vitro," *American Journal of Physiology. Lung Cellular and Molecular Physiology*, vol. 307, pp. L838–L847, 2014.

[13] J. Kang, J. K. Perry, V. Pandey et al., "Artemin is oncogenic for human mammary carcinoma cells," *Oncogene*, vol. 28, pp. 2034–2045, 2009.

[14] S. Tan, K. S. Ding, R. Li et al., "Identification of miR-26 as a key mediator of estrogen stimulated cell proliferation by targeting CHD1, GREB1 and KPNA2," *Breast Cancer Research*, vol. 16, 2014.

[15] Z. Y. Ding, G. N. Jin, W. Wang et al., "Reduced expression of transcriptional intermediary factor 1 gamma promotes metastasis and indicates poor prognosis of hepatocellular carcinoma," *Hepatology*, vol. 60, pp. 1620–1636, 2014.

[16] A. Giatromanolaki, E. Sivridis, A. Mitrakas et al., "Autophagy and lysosomal related protein expression patterns in human glioblastoma," *Cancer Biology & Therapy*, vol. 15, pp. 1468–1478, 2014.

[17] T. Namikawa, E. Munekage, M. Munekage et al., "Evaluation of a trastuzumab-containing treatment regimen for patients with unresectable advanced or recurrent gastric cancer," *Molecular and Clinical Oncology*, vol. 5, pp. 74–78, 2016.

[18] J. H. Kang, S. I. Lee, D. H. Lim et al., "Salvage chemotherapy for pretreated gastric cancer: a randomized phase III trial comparing chemotherapy plus best supportive care with best supportive care alone," *Journal of Clinical Oncology*, vol. 30, pp. 1513–1518, 2012.

[19] Y. Kurokawa, N. Matsuura, Y. Kimura et al., "Multicenter large-scale study of prognostic impact of HER2 expression in patients with resectable gastric cancer," *Gastric Cancer*, vol. 18, pp. 691–697, 2015.

[20] H. I. Balcer, K. Daugherty-Clarke, and B. L. Goode, "The p40/ARPC1 subunit of Arp2/3 complex performs multiple essential roles in WASp-regulated actin nucleation," *The Journal of Biological Chemistry*, vol. 285, pp. 8481–8491, 2010.

[21] B. Tang, F. Tang, Z. Wang et al., "Overexpression of CTNND1 in hepatocellular carcinoma promotes carcinous characters through activation of Wnt/β-catenin signaling," *Journal of Experimental & Clinical Cancer Research*, vol. 35, no. 1, p. 82, 2016.

[22] S. D. Castillo, B. Angulo, A. Suarez-Gauthier et al., "Gene amplification of the transcription factor DP1 and CTNND1 in human lung cancer," *The Journal of Pathology*, vol. 222, pp. 89–98, 2010.

[23] Y. Wang, F. Gao, M. Zhao et al., "Prognostic significance of EZH2 expression in patients with oesophageal cancer: a meta-analysis," *Journal of Cellular and Molecular Medicine*, vol. 20, pp. 836–841, 2016.

[24] H. Zhang, J. Qi, J. M. Reyes et al., "Oncogenic deregulation of EZH2 as an opportunity for targeted therapy in lung cancer," *Cancer Discovery*, vol. 6, no. 9, pp. 1006–1021, 2016.

[25] S. Guo, X. Li, J. Rohr et al., "EZH2 overexpression in different immunophenotypes of breast carcinoma and association with clinicopathologic features," *Diagnostic Pathology*, vol. 11, p. 41, 2016.

[26] S. Liu, D. Chen, W. Shen et al., "EZH2 mediates the regulation of S100A4 on E-cadherin expression and the proliferation, migration of gastric cancer cells," *Hepato-Gastroenterology*, vol. 62, pp. 737–741, 2015.

[27] D. L. Chen, D. S. Zhang, Y. X. Lu et al., "microRNA-217 inhibits tumor progression and metastasis by downregulating EZH2 and predicts favorable prognosis in gastric cancer," *Oncotarget*, vol. 6, pp. 10868–10879, 2015.

[28] H. J. Chung, Y. E. Choi, E. S. Kim, Y. H. Han, M. J. Park, and I. H. Bae, "miR-29b attenuates tumorigenicity and stemness maintenance in human glioblastoma multiforme by directly targeting BCL2L2," *Oncotarget*, vol. 6, pp. 18429–18444, 2015.

[29] T. Yang, A. Thakur, T. Chen et al., "MicroRNA-15a induces cell apoptosis and inhibits metastasis by targeting BCL2L2 in non-small cell lung cancer," *Tumour Biology: The Journal of the International Society for Oncodevelopmental Biology and Medicine*, vol. 36, pp. 4357–4365, 2015.

[30] J. Qu, L. Zhao, P. Zhang et al., "MicroRNA-195 chemosensitizes colon cancer cells to the chemotherapeutic drug doxorubicin by targeting the first binding site of BCL2L2 mRNA," *Journal of Cellular Physiology*, vol. 230, pp. 535–545, 2015.

[31] T. Ma, Y. Zhao, K. Wei et al., "MicroRNA-124 functions as a tumor suppressor by regulating CDH2 and epithelial-mesenchymal transition in non-small cell lung cancer," *Cellular Physiology and Biochemistry: International Journal of Experimental Cellular Physiology, Biochemistry, and Pharmacology*, vol. 38, pp. 1563–1574, 2016.

[32] Y. Yanaka, T. Muramatsu, H. Uetake, K. Kozaki, and J. Inazawa, "miR-544a induces epithelial-mesenchymal

transition through the activation of WNT signaling pathway in gastric cancer," *Carcinogenesis*, vol. 36, pp. 1363–1371, 2015.

[33] Y. Huo, Z. Zheng, Y. Chen, Q. Wang, Z. Zhang, and H. Deng, "Downregulation of vimentin expression increased drug resistance in ovarian cancer cells," *Oncotarget*, vol. 7, no. 29, pp. 45876–45888, 2016.

[34] D. L. Lazarova and M. Bordonaro, "Vimentin, colon cancer progression and resistance to butyrate and other HDACis," *Journal of Cellular and Molecular Medicine*, vol. 20, pp. 989–993, 2016.

[35] D. Li, Q. J. Wu, F. F. Bi et al., "Effect of the BRCA1-SIRT1-EGFR axis on cisplatin sensitivity in ovarian cancer," *American Journal of Translational Research*, vol. 8, pp. 1601–1608, 2016.

[36] X. Meng, B. Hu, M. M. Hossain, G. Chen, Y. Sun, and X. Zhang, "ADAM17-siRNA inhibits MCF-7 breast cancer through EGFR-PI3K-AKT activation," *International Journal of Oncology*, vol. 49, pp. 682–690, 2016.

[37] C. C. Su and T. L. Chiu, "Tanshinone IIA decreases the protein expression of EGFR, and IGFR blocking the PI3K/Akt/mTOR pathway in gastric carcinoma AGS cells both in vitro and in vivo," *Oncology Reports*, vol. 36, pp. 1173–1179, 2016.

[38] R. Xin, F. Bai, Y. Feng et al., "MicroRNA-214 promotes peritoneal metastasis through regulating PTEN negatively in gastric cancer," *Clinics and Research in Hepatology and Gastroenterology*, vol. 40, no. 6, pp. 748–754, 2016.

[39] Y. F. Pei, R. Tao, J. F. Li et al., "TET1 inhibits gastric cancer growth and metastasis by PTEN demethylation and re-expression," *Oncotarget*, vol. 7, no. 21, pp. 31322–31335, 2016.

[40] R. Golmohammadi, M. H. Rakhshani, A. R. Moslem, and A. Pejhan, "Prognostic role of PTEN gene expression and length of survival of breast cancer patients in the north east of Iran," *Asian Pacific Journal of Cancer Prevention: APJCP*, vol. 17, no. S3, pp. 305–309, 2016.

[41] J. Gu, W. Ou, L. Huang et al., "PTEN expression is associated with the outcome of lung cancer: evidence from a meta-analysis," *Minerva Medica*, vol. 107, no. 5, pp. 342–351, 2016.

[42] M. Matsumoto, W. Nakajima, M. Seike, A. Gemma, and N. Tanaka, "Cisplatin-induced apoptosis in non-small-cell lung cancer cells is dependent on Bax- and Bak-induction pathway and synergistically activated by BH3-mimetic ABT-263 in p53 wild-type and mutant cells," *Biochemical and Biophysical Research Communications*, vol. 473, pp. 490–496, 2016.

[43] T. Kubo, Y. Kawano, N. Himuro et al., "BAK is a predictive and prognostic biomarker for the therapeutic effect of docetaxel treatment in patients with advanced gastric cancer," *Gastric Cancer*, vol. 19, pp. 827–838, 2016.

[44] W. Zeng, J. Zhu, L. Shan et al., "The clinicopathological significance of CDH1 in gastric cancer: a meta-analysis and systematic review," *Drug Design, Development and Therapy*, vol. 9, pp. 2149–2157, 2015.

[45] Q. Yu, Q. Guo, L. Chen, and S. Liu, "Clinicopathological significance and potential drug targeting of CDH1 in lung cancer: a meta-analysis and literature review," *Drug Design, Development and Therapy*, vol. 9, pp. 2171–2178, 2015.

Hindawi
Mediators of Inflammation
Volume 2017, Article ID 5958429, 11 pages
https://doi.org/10.1155/2017/5958429

Research Article

Proinflammatory Cytokines IL-6 and TNF-α Increased Telomerase Activity through NF-κB/STAT1/STAT3 Activation, and Withaferin A Inhibited the Signaling in Colorectal Cancer Cells

Seyung S. Chung,[1,2,3] Yong Wu,[1,2,3] Quincy Okobi,[1,2] Debbie Adekoya,[1,2] Mohammad Atefi,[1,2] Orette Clarke,[1,2] Pranabananda Dutta,[1,2] and Jaydutt V. Vadgama[1,2,3,4]

[1]*Division of Cancer Research and Training, Department of Internal Medicine, Charles R. Drew University of Medicine and Science, 1731 East 120th street, Los Angeles, CA 90059, USA*
[2]*Charles R. Drew University of Medicine and Science, 1731 East 120th street, Los Angeles, CA 90059, USA*
[3]*David Geffen UCLA School of Medicine, Los Angeles, CA, USA*
[4]*Jonsson Comprehensive Cancer Center, Los Angeles, CA, USA*

Correspondence should be addressed to Seyung S. Chung; seyungchung@cdrewu.edu

Received 12 December 2016; Revised 10 March 2017; Accepted 4 April 2017; Published 6 June 2017

Academic Editor: Fumio Tsuji

There are increasing evidences of proinflammatory cytokine involvement in cancer development. Here, we found that two cytokines, IL-6 and TNF-α, activated colorectal cancer cells to be more invasive and stem-like. Combined treatment of IL-6 and TNF-α phosphorylated transcription factors STAT3 in a synergistic manner. STAT3, STAT1, and NF-κB physically interacted upon the cytokine stimulation. STAT3 was bound to the promoter region of human telomerase reverse transcriptase (hTERT). IL-6 and TNF-α stimulation further enhanced STAT3 binding affinity. Stem cell marker Oct-4 was upregulated in colorectal cancer cells upon IL-6 and TNF-α stimulation. Withaferin A, an anti-inflammatory steroidal lactone, inhibited the IL-6- and TNF-α-induced cancer cell invasion and decreased colonosphere formation. Notably, withaferin A inhibited STAT3 phosphorylation and abolished the STAT3, STAT1, and NF-κB interactions. Oct-4 expression was also downregulated by withaferin A inhibition. The binding of STAT3 to the hTERT promoter region and telomerase activity showed reduction with withaferin A treatments. Proinflammatory cytokine-induced cancer cell invasiveness is mediated by a STAT3-regulated mechanism in colorectal cancer cells. Our data suggest that withaferin A could be a promising anticancer agent that effectively inhibits the progression of colorectal cancer.

1. Introduction

Inflammation is one of the complex biological responses to the damages caused either by injury or microbial infection, where the immune system attempts to neutralize an injury. The role of inflammation in tumorigenesis is now widely accepted. In many cases, chronic inflammation in the microenvironment is essential for the initiation and progression of cancers. Although the molecular mechanisms by which the inflammation promotes cancer are explained, the molecular roles of inflammation in tumorigenesis, progression, and metastasis need to be better understood. Epidemiological evidence first points to a link between inflammation and a development of cancer [1]. It was reported that 15~20% of various cancer types have direct initiation cues from chronic inflammation in the same tissue or organ preceding the cancer development [2]. The risk of developing cancer from inflammation is often time-dependent on the type of cancer. Hepatitis or chronic inflammation caused by hepatitis B or C virus initiated hepatocellular carcinoma [3]. Chronic

inflammatory diseases of small and large intestines, ulcerative colitis, and Crohn's disease provoked the development of colitis-related cancer [4].

Chronic inflammation is a risk factor for colorectal cancer development. Colorectal cancer is the second cancer-related mortality in the western world [5]. Over 50% of colorectal cancer patients eventually developed metastasis and recurrent colorectal cancer disease. There is an important association between colorectal cancer prognosis and cytokine levels in the serum of patients. When IL-6 (interleukin 6) and TNF-α (tumor necrosis factor α) coexpression is elevated, the prognosis of the patient is significantly poorer. It has been reported that IL-6 and TNF-α serum levels were elevated in colorectal cancer patients [6] and can be used as a prognosis factor [7]. Similarly, in breast cancer, the coexpression levels of IL-6 and TNF-α have been tightly associated with a negative prognosis [8]. Another study has shown that elevated serum levels of IL-6 were closely associated with the progress and prognosis of metastatic breast cancer [9]. Finally, patients with metastatic prostate cancer had significantly higher levels of serum IL-6 and TNF-α than primary cancer patients [10]. Taken together, these clinical reports implicate that IL-6 and TNF-α may function as a driver for cancer advancement, metastasis, and poor disease prognosis.

There is a notion that protumorigenic inflammation signaling pathways are subject to a feed-forward loop. We hypothesized that IL-6 and TNF-α contribute to the cancer initiation and progression by promoting cancer stemness and telomerase activity. To test this, we investigate the key transcription factors STAT3 (signal transducer and activator of transcription 3) and NF-κB. STAT3 is a latent transcription factor that conveys the signals of growth factors and cytokines from the cellular membrane to nucleus onto its target genes [11]. STAT3 functions in a variety of physiological processes including embryonic development, immunity, and inflammation [12]. In addition, STAT3 transcriptionally activates the oncogenes, proliferative and angiogenesis-related genes in responding to the stimuli from outside, hence contributes to cancer progression [13]. NF-κB (nuclear factor κB) is a prominent transcription factor involved in immune response and inflammation. NF-κB target genes are associated with the regulation of cell survival as well as apoptosis. Herein, we tried to identify the mechanisms of STAT3-NF-κB-induced cancer cell activation. STAT3 activation resulted in the upregulation of stemness gene Oct-4. The activated transcription factors and increased telomerase were accordingly attributed to the cell invasiveness in the transwell migration assay.

Natural compounds are major sources of current chemotherapeutic agents. Mounting evidence demonstrates the chemotherapeutic effects of natural compounds in preclinical and clinical studies. In an effort to find the novel natural compound to inhibit the cytokine signaling, we tried the withaferin A compound, which is abundant in Indian winter cherry. It is a steroidal lactone abundant in the plant *Withania somnifera* that has been used historically in oriental medicine, to treat inflammation and some neurological disorders [14, 15]. It has potent anti-inflammatory properties through the inhibition of Akt and NF-κB signaling pathways [16, 17]. The antitumor, antimetastasis, and antiangiogenic activities of withaferin A have been reported from various cancer types [18]. The antiangiogenic property is linked to the degradation-enhancing modification of vimentin by withaferin A [19]. Recently, withaferin A showed the efficacious effects as an adjunct agent for chemotherapeutic agents, implicating to be well suited for an amplifier or supplementary agent alongside the conventional drug [20]. Withaferin A is an attractive anticancer agent based on the broad range of responses for the multiple cancers with a low toxicity. In this study, we investigated the molecular effects of withaferin A on cytokine-stimulated colorectal cancer cells. We have demonstrated that IL-6 and TNF-α cotreatments induce cancer cells to be more invasive and aggressive. We also report that withaferin A can inhibit the STAT3 activation, reduce the stem cell-like traits, and decrease the telomerase activity. These findings suggest the possible value of withaferin A in a novel therapy for the metastatic colorectal cancer.

2. Materials and Methods

2.1. Cell Culture and Reagents. DLD1 and HT-29 colorectal cancer cell lines were purchased from the American Type Culture Collection (ATCC, Manassas, VA, U.S.A.). Cancer cells were maintained in a monolayer culture in DMEM/F12 (Dulbecco's modified Eagle medium) with 10% fetal bovine serum, 1% L-glutamine, and 0.5% penicillin/streptomycin. Interleukin 6 was purchased from EMD Millipore (Temecula, CA, U.S.A. Catalog number: IL006). IL-6 was used at the concentration of 10 ng/ml to stimulate the cancer cells. We used the IL-6 concentration of 10 ng/ml according to the manufacturer's instruction. TNF-α was purchased from the R&D Systems (Minneapolis, MN; Catalog number: 210-TA-020). TNF-α was prepared as 100 μg/ml stock solution. TNF-α concentration was decided based on the manufacturer's instructions. TNF-α was used at 25 ng/ml to activate cancer cells. Withaferin A was purchased from Sigma Aldrich company (Sigma Aldrich, St. Louis, MO; Catalog number: W4394). Withaferin A was prepared in 10 mM stock solution in methanol. The working concentration was 10 μM for withaferin A in this study. Withaferin A concentration was decided based on the IC50 value from our dose-dependent cell growth study.

2.2. Western Blot Analyses. Monolayer cultures of respective cell lines at 80–90% confluence were lysed using 100 μl of RIPA buffer (Thomas Scientific Inc. Swedesboro, NJ). Tris-glycine (Bio-Rad, Irvine, CA) gels were loaded with 100 μg of total proteins. After electrophoresis, the gel was transferred to a nitrocellulose membrane for 1 hour.

The membrane was blocked for 30 min in 5% skim milk at room temperature. The membrane was briefly rinsed with 1xTTBS and incubated overnight with the respective primary antibodies at 4°C. Primary antibodies of STAT3, pSTAT3, NF-κB, pNF-κB, CD44, and Oct-4 were purchased from Cell Signaling Technology (Danvers, MA). Primary antibody for β-actin was purchased from the Santa Cruz Biotech (Santa Cruz, CA). After incubation with the secondary antibodies

conjugated with horseradish peroxidase (HRP), the protein bands were developed with the chemiluminescent reagents.

2.3. Coimmunoprecipitation. Coimmunoprecipitation assay was performed as previously described [21]. Briefly, cells were washed once with PBS buffer and lysed in immunoprecipitation lysis buffer (Thomas Scientific Company). Antibodies to STAT3 (Cell signaling technology) were added to the cell lysates and incubated for one hour at 4°C. Protein A agaroses (Santa Cruz Biotechnology) were added to the cell lysates 20 μl each, incubated for overnight at 4°C. After the immunoprecipitation, cell lysates were briefly spun and washed three times with 1X PBS buffer. Immunopellets were resuspended in 40 μl of loading dye (Bio Rad) and run on a polyacrylamide gel electrophoresis. Immunoblots were probed for either NF-κB or STAT1 proteins for interactions with STAT3 via western blot analyses.

2.4. CHIP (Chromatin Immunoprecipitation) Assay. Chromatin immunoprecipitation (ChIP) Assay Kit (Millipore, Catalog number: 17–295) was utilized to study STAT3 binding to hTERT promoter region. DLD1 or HT-29 cells were incubated with 1% formaldehyde for 20 minutes at 37°C. Cells were collected, lysed, sonicated, and incubated with 4 μg of antibodies to STAT3 overnight. PCR was used to amplify DNA bound to the immunoprecipitated histones after reversing the histone-DNA cross-links. Primer sets were designed flanking the possible STAT3 binding regions. Primer sequences: *hTERT* promoter primer sequence 1, forward primer 5′- CCAAACCTGTGGACAGAACC-3′ and reverse primer 5′-AGACTGACTGCCTCCATCGT-3′ and *hTERT* promoter primer sequence 2, forward primer 5′-GGGGTGTCTTCTGGGTATCA-3′ and reverse primer 5′-AAGGGCTGTGTTTGTGAATTG-3′.

2.5. Telomerase Activity Assay. Telomerase activity assay was performed as previously described [22]. Briefly, cells were processed according to the manufacturer's protocol for the TeloTAGGG Telomerase PCR ELISA kit (Roche, Orange, CA. Catalog number: 11854666910). Briefly, cell pellets were thawed in lysis reagent, incubated on ice for 30 minutes, and centrifuged at 16,000*g* for 20 minutes at 4°C. Telomerase activity was immediately measured in the resultant supernatant using the telomeric repeat amplification protocol in which telomerase, if present in the cell lysate, adds telomeric repeats to the 3′ end of a biotin-labeled synthetic P1-TS primer. Samples were amplified by polymerase chain reaction (PCR), with P1-TS and P2 primers creating an elongated telomere. The PCR product was denatured and hybridized to a digoxigenin-labeled probe that detects telomeric repeats in a subsequent enzyme-linked immunosorbent assay (ELISA). Samples were considered positive for telomerase activity if the ELISA resulted in a background-corrected absorbance of ≥0.2 units. Telomerase assays were performed three times independently, and p values less than 0.05 were considered statistically significant.

2.6. Colonosphere Formation Assay. Colonosphere formation was examined as previously described [21]. Matrigel (BD, Cambridge, MA), 200 μl was spread as a thick layer on wells of a 24-well plate and allowed to polymerize at 37°C for 15 minutes. 2×104 cancer cells grown in monolayer were trypsinized to single cells and plated on top of the precoated matrigel. Plates were incubated at 37°C to allow cells to fully settle down before media was replaced with appropriate culture media containing 5% matrigel. Cells were grown for 15 days; fresh growth media with matrigel was replenished every two days. Images of representative fields were taken.

2.7. Cell Invasion Assay. Cell invasion assay was performed as previously described [22]. Mouse fibroblasts (NIH-3T3) were used as a chemo-attractant and grown in a 24-well plate in 2 ml of DMEM/F12 media. Boyden chambers were prepared with 25 μl of 1 : 6 diluted matrigel and allowed to incubate for 2 hours to solidify. Each chamber received the different treatments: methanol (vehicle) and withaferin A. After cell synchronization, an invasion was allowed to occur for 40 hours. The cells were then fixed with 0.5% glutaraldehyde and stained with 5% toluidine blue for cell counting.

2.8. Receptor Tyrosine Kinase Signaling Antibody Array Study. The receptor tyrosine kinase signaling antibody array kit was purchased from Cell Signaling Technology (Cell Signaling Technology, Beverly, MA; Catalog number: 7982). Each colorectal cancer cell line had stimulation by the IL-6 and TNF-α alone or in combination. Whole protein lysates were prepared using the provided lysis buffer from the kit. 100 μl of each lysate was placed onto the membrane window of the antibody slide. The treated slide was incubated overnight at 4°C on an orbital shaker. The slide was then washed with 100 μl 1X Array Wash Buffer and incubated on an orbital shaker for 5 minutes at room temperature. This washing procedure was repeated three more times. 75 μl of 1X Detection Antibody Cocktail was added to each of the 8 wells, and the plate was covered with the provided sealing tape. It was incubated for 1 hour at room temperature on an orbital shaker. Next, three wash cycles were performed and the slide was incubated for 30 minutes with 75 μl 1X HRP-linked Streptavidin. The slide was washed and treated with Lumi Glo and peroxide. We took the picture of the slides with a camera of gel documentation system (Bio-Rad, Gel Doc XRS) using Quantity One software.

2.9. Statistical Analysis. Student t-tests were used to evaluate the significance of changes in all combination treatment assays compared to controls. Data collected from each experiment was used to calculate the mean values and standard deviations (SD). Experiments were repeated three times independently. Differences were considered statistically significant if $p < 0.05$.

3. Results

3.1. IL-6 and TNF-α Cotreatments Activated STAT3 Synergistically Whereas Withaferin A Abolished the Activation. STAT3 and NF-κB are key transcription factors activated in cells responding to inflammation. We first tested the effects of IL-6 and TNF-α cotreatments on the phosphorylation of STAT3 and NF-κB (p65) in colorectal cancer cells. To this end, we performed the western blots for STAT3 and NF-κB

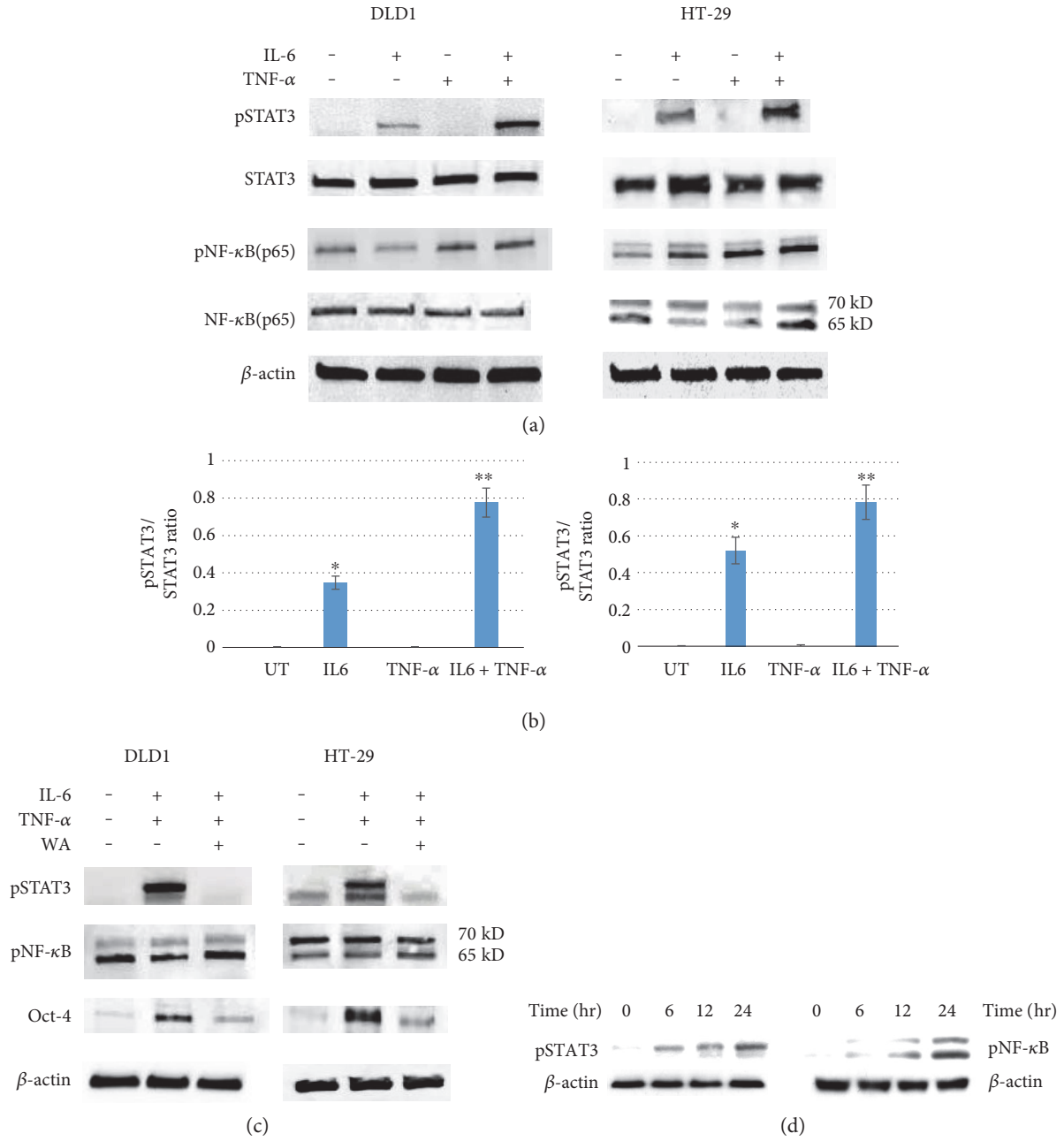

Figure 1: STAT3 was activated by IL-6 and TNF-α treatments whereas inhibited by withaferin A in human colorectal cancer cells. (a) Western blot analysis of DLD1 and HT-29 for pSTAT3, total STAT3, pNF-κB, and total NF-κB. Cells were treated with IL-6 (10 ng/ml) and TNF-α (25 ng/ml) alone and in combination for 24 hours, then subjected to protein analysis for pSTAT3, total STAT3, pNF-κB, and total NF-κB. (b) A quantitative graph of pSTAT3: STAT3 ratio was presented from DLD1 and HT-29 ($^{*}p < 0.05$, $^{**}p < 0.001$). (c) Western blot analysis of DLD1 and HT-29 for pSTAT3, pNF-κB, and Oct-4. Cells were treated with either IL-6 (10 ng/ml) and TNF-α (25 ng/ml) alone or in combination for 24 hours. Withaferin A was treated at 10 μM concentrations for 24 hours as indicated. (d) STAT3 and NF-κB phosphorylation was measured with IL-6 and TNF-α stimulation on a time course. DLD1 cells were treated with combined IL-6 and TNF-α and monitored the phosphorylation status on different time points of 0, 6, 12, and 24 hours.

with the cancer cells treated with IL-6 alone, TNF-α alone, or IL-6 and TNF-α combined. As shown in Figure 1(a), IL-6 phosphorylated STAT3 whereas TNF-α did not phosphorylate it. When we cotreated cells with IL-6 and TNF-α, however, STAT3 phosphorylation levels were further elevated (Figure 1(a)). TNF-α may activate STAT3 indirectly as it enhances the IL-6 induction. We quantified the pSTAT3/STAT3 ratio using Image J software. IL-6 alone activated pSTAT3 to the 0.38 folds of total STAT3, but IL-6 and TNF-α cotreatments elevated the pSTAT3 level to 0.97 folds of STAT3 in DLD1 cell line (Figure 1(b)). Similarly, IL-6 alone increased pSTAT3 to 0.52 folds and combined IL-6 and TNF-α elevated pSTAT3 to 0.83 folds of STAT3 in HT-29. Our data suggest that IL-6 and TNF-α cotreatments

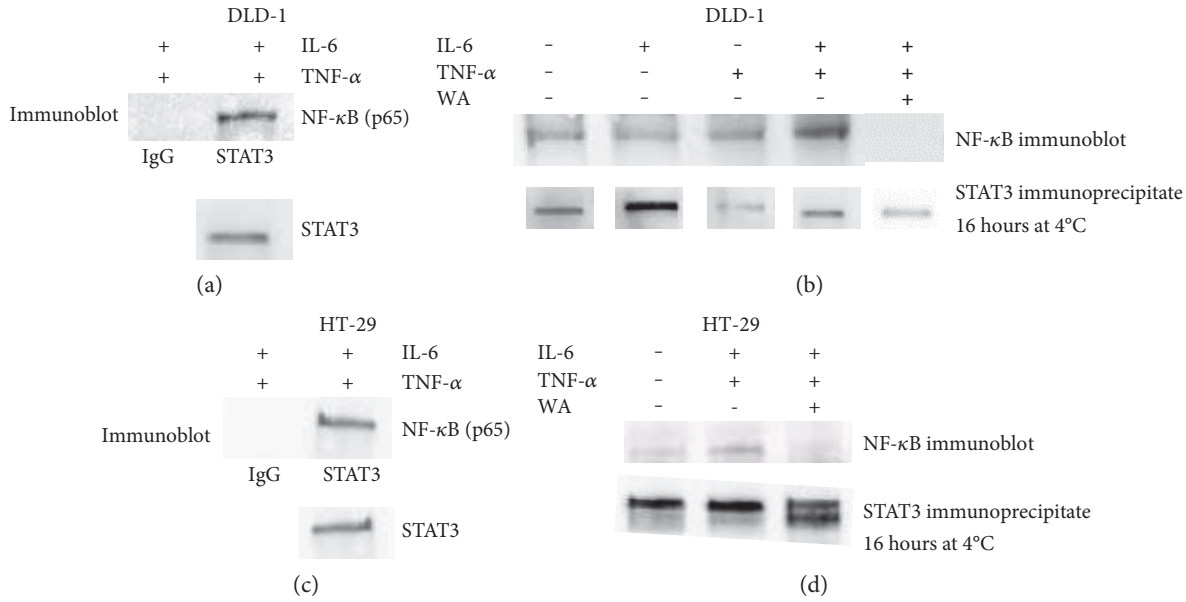

Figure 2: STAT3 and NF-κB bind upon IL-6 and TNF-α treatments in colorectal cancer cell lines DLD and HT-29. (a) Immunoprecipitation with STAT3 antibody revealed that NF-κB was bound to STAT3 in DLD1 cell line. STAT3 pull-down was performed in the presence of IL-6 (10 ng/ml) and TNF-α (25 ng/ml). (b) In the presence of withaferin A (10 μM), pull-down assay with STAT3 antibody showed that STAT3 interaction with NF-κB was abolished in DLD1 cell line. (c) Immunoprecipitation with STAT3 antibody showed the interactions with NF-κB in HT-29 cell line. (d) With the withaferin A challenge (10 μM), STAT3 and NF-κB interactions were abolished in HT-29.

activate STAT3. NF-κB was phosphorylated by TNF-α alone or IL-6/TNF-α cotreatments. The NF-κB activation was modest. Total STAT3 and NF-κB levels were not changed upon IL-6 and TNF-α treatments.

Next, we tested if anti-inflammatory steroidal lactone withaferin A can deactivate pSTAT3 induced by IL-6 and TNF-α cotreatments. We hypothesized that withaferin A may exert anti-inflammatory effects through the downregulation of STAT3 phosphorylation. Indeed, withaferin A treatments inhibited the STAT3 phosphorylation in both DLD1 and HT-29 cancer cells (Figure 1(c)). NF-κB phosphorylation levels were not changed upon withaferin A. Our results indicate that withaferin A may inhibit STAT3 activation selectively. With IL-6 and TNF-α stimulation, we wished to investigate Oct-4 expression levels. Tumor dedifferentiation is a well-known phenomenon, and it may involve in tumor progression [23]. Aberrant expression of Oct-4 is associated with abnormal tissue growth or tumorigenesis. Oct-4 is the most critical transcription factor since it can reprogram adult stem cells to iPS (induced pluripotent stem) cells as a single factor [24]. Oct-4 expression was also upregulated upon IL-6 and TNF-α cotreatments; however, in the presence of withaferin A, Oct-4 expression was downregulated (Figure 1(c)). IL-6 and TNF-α cotreatments activated STAT3 synergistically and upregulated Oct-4. Withaferin A abolished the STAT3 activation and prevented upregulation of Oct-4 expressions.

To examine time-dependent STAT3 and NF-κB activation, we treated DLD1 cells with IL-6 and TNF-α on time points of 0, 6, 12, and 24 hours and examined the phosphorylation status. As shown in the Figure 1(d), both pSTAT3 and pNF-κB were expressed from 6 hours and increased their expression levels to the 24 hour time points (Figure 1(d)).

3.2. STAT3 Physically Binds NF-κB upon IL-6 and TNF-α Stimulation; However, Withaferin A Inhibits the STAT3-NF-κB Interactions. Both STAT3 and NF-κB are involved in gene regulation of inflammation and activated by IL-6 and TNF-α. We have previously shown that STAT3 and NF-κB formed a complex and transcriptionally activated human telomerase reverse transcriptase in breast cancer lines of MDA-MB-231 and MCF7-HER2 [25]. We next wished to find out whether treatment with the combination of IL-6 and TNF-α can induce the interactions between STAT3 and NF-κB in colorectal cancer cells. To uncover this, a coimmunoprecipitation assay was performed with cell extracts treated with IL-6 alone, TNF-α alone, or IL-6 and TNF-α combined. As shown in Figure 2, STAT3 was bound to NF-κB with the IL-6 and TNF-α stimulations in both DLD1 and HT-29, respectively (Figures 2(a) and 2(c)). In DLD1 cells, IL-6 or TNF-α alone treatments were not sufficient to induce the STAT3-NF-κB interactions (Figure 2(b)). Untreated cells also showed very weak binding to NF-κB in HT-29 (Figure 2(d)). Our data suggest that activated STAT3 and NF-κB physically interact upon IL-6 and TNF-α treatments.

Since withaferin A inhibited STAT3 activation, we tested whether the STAT3 interactions were abolished by withaferin A challenge. We performed the coimmunoprecipitation on the cell extracts treated with IL-6 and TNF-α with 10 μM withaferin A this time. As withaferin A inhibited STAT3 phosphorylation, it also abolished the STAT3 interactions with NF-κB in DLD1 and HT-29 (Figures 2(b) and

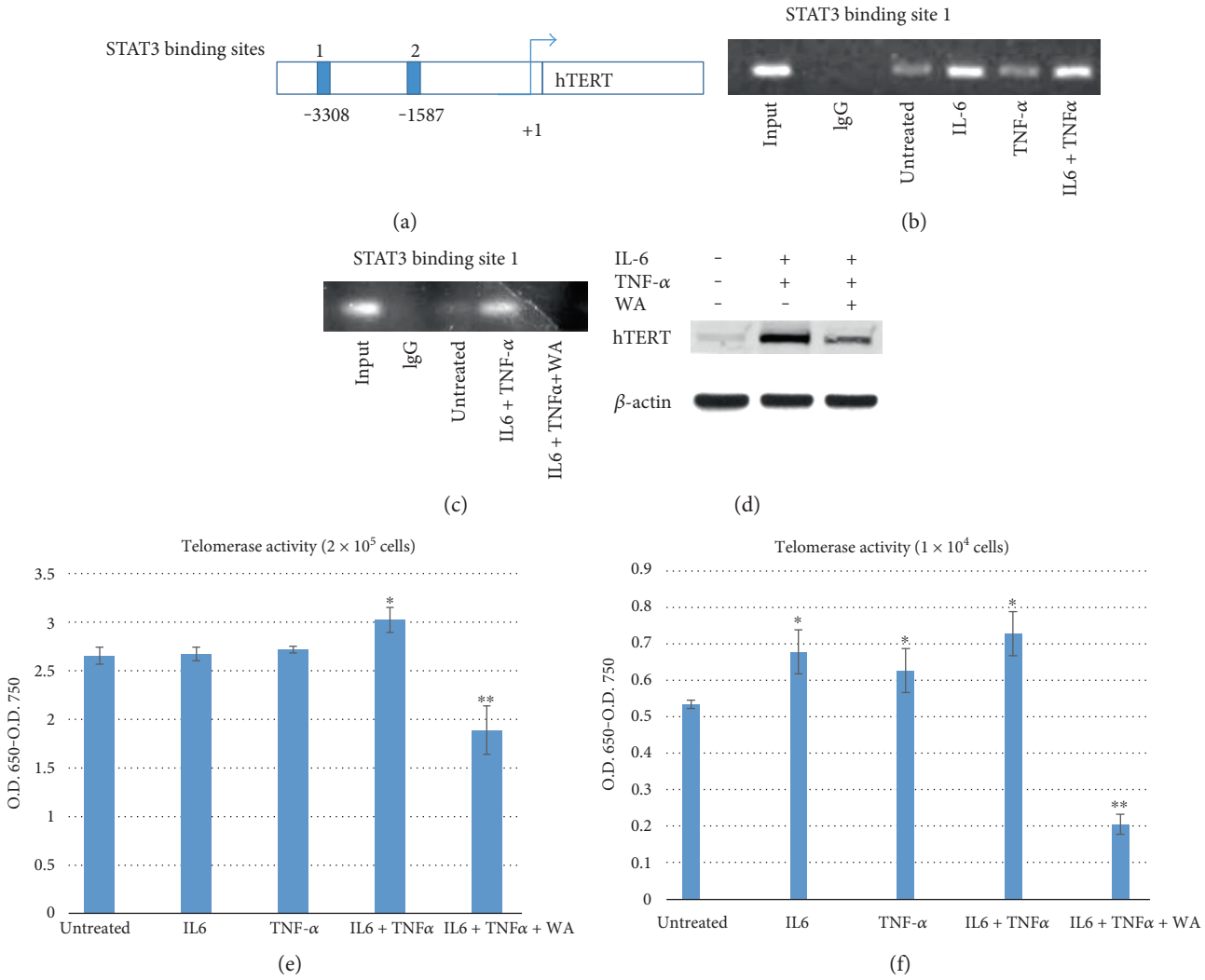

Figure 3: STAT3 binds hTERT promoter region. There are two STAT3 binding sites located in the promoter region of hTERT. Primer sets were designed flanking the putative STAT3-binding sites 1 and 2. Chip assay was performed with the primers. (a) Diagram of hTERT promoter with location of consensus STAT3-binding sites 1 and 2 indicated. (b) Chip assay was performed with the DLD1 lysates using anti-STAT3 antibody. Cells were pretreated with IL-6 and TNF-α alone or in combination. (c) Chip assay was performed with DLD1 cells stimulated with IL-6 and TNF-α, and DLD1 cells cotreated with IL-6, TNF-α, and withaferin A. (d) Western blot of hTERT proteins. DLD1 cells were treated with IL-6 and TNF-α and cotreated with IL-6, TNF-α, and withaferin A and monitored for the hTERT expression levels. (e) TRAP-PCR-ELISA assay for telomerase activity. DLD1 cells of 2×105 were treated with IL-6 (10 ng/ml) for 24 h, TNF-α (25 ng/ml) for 24 h alone, and in combination. Withaferin A (10 μM) was treated with the cytokines and applied to TRAP-PCR-ELISA assay to monitor telomerase assay. Telomerase activities were measured three times independently. All of the data are presented as mean $\pm$ SD ($n = 3$ in each group). $^{*}p < 0.05$, $^{**}p < 0.01$ versus untreated control. (f) Less amount of cells, 1×104, was treated with IL-6 and TNF-α alone and in combination. We decreased the cell amounts to discern cytokine and withaferin A effects on telomerase more clearly. $^{*}p < 0.05$, $^{**}p < 0.01$ versus untreated control.

2(d)). Our results revealed the IL-6 and TNF-α cotreatments stimulated STAT3-NF-κB complex, and withaferin A inhibited the STAT3-NF-κB interactions.

3.3. STAT3 Binds to hTERT Promoter and Increases Telomerase Activity upon IL-6 and TNF-α Stimulation Whereas Withaferin A Inhibits STAT3 Binding and Decreases Telomerase. We next determined the STAT3 binding to hTERT (human telomerase reverse transcriptase) promoter region. It has been reported that STAT3 regulated the expression of hTERT in glioblastoma and primary cells [26]. We wished to determine whether transcription factor STAT3 was bound to hTERT promoter and further when stimulated by IL-6 and TNF-α if the binding was enhanced by these cytokines. To test this, we performed the Chip (chromatin immunoprecipitation) assay as described in Section 2. Consensus STAT3 binding sites (TTCNNNGAA) reside within the hTERT promoter. Chip assay was performed on the two putative STAT3-binding sites (Figure 3(a)). Cells were treated with IL-6, TNF-α alone, and combined. In DLD1 cells, we found that STAT3 was bound to the first STAT3 binding site located at −3308 base pair upstream hTERT open reading frame (Figure 3(b)). STAT3 binding affinity was approximately

the same within the untreated control and TNF-α alone-treated samples. However, IL-6 and TNF-α cotreatments clearly enhanced STAT3 binding to the hTERT promoter region. These results suggest that transcription factor STAT3 is directly binding hTERT promoter and IL-6, and TNF-α cotreatments stimulate this binding. We investigated the telomerase activity upon activation and inhibition of STAT3 binding to hTERT promoter later.

STAT3 is phosphorylated in the cytoplasm, homodimerized with pSTAT3, and translocated into the nucleus to activate target genes. Since withaferin A inhibited STAT3 phosphorylation and its interactions with NF-κB, we hypothesized that withaferin A may block the STAT3 binding to hTERT promoter. As shown in the Figure 3(c), 10 μM withaferin A challenge blocked the STAT3 binding to the first STAT3 site within the hTERT promoter in our Chip assay (Figure 3(c)). This can be the effect of the reduced level of pSTAT3 in the presence of withaferin A since mainly pSTAT3 can translocate into nucleus and bind to the target gene promoters.

To measure the actual hTERT expression levels, we performed the western blots for hTERT with the IL-6-and TNF-α-treated cells and cytokine- and withaferin A-cotreated cells (Figure 3(d)). As shown in the figure, hTERT expression was upregulated with IL-6 and TNF-α stimulation whereas withaferin A cotreatment decreased hTERT expression. Our data show that STAT3 binding was enhanced by cytokine stimulation and translated into increased hTERT protein expression.

Finally, we examined the telomerase activity of colorectal cancer cells treated with IL-6, TNF-α, and withaferin A using TeloTAGGG Telomerase PCR ELISA kit as described in the methods section. Untreated DLD1 cells showed telomerase activity 2.67 (O.D. 450-O.D. 750). IL-6-treated cells and TNF-α-treated cells showed the telomerase activities of 2.68 and 2.72, respectively. Those activities are not statistically significant. However, when cells were cotreated with IL-6 and TNF-α, telomerase activity has been increasing to 3.04 (Figure 3(e)). This is 14% activity increase and out of standard deviation range. Withaferin A challenge clearly reduced the telomerase activity to 1.89. This is 29% decreased telomerase compared to the untreated control. To discern the telomerase difference more clearly, we reduced the cancer cell numbers from 2×105 to 1×104 and repeated the telomerase assay. Telomerase activity was increased from 0.58 to 0.77 with the IL-6 and TNF-α treatments whereas withaferin A (10 μM) challenge decreased the activity to 0.255 (Figure 3(f)). Taken together, these results suggest that STAT3 directly bind to hTERT promoter, thereby regulating telomerase expressions; IL-6 and TNF-α cotreatments enhanced the STAT3 binding and increased effector protein telomerase activity. Anti-inflammatory withaferin A inhibited the STAT3 phosphorylation, blocked the binding to the hTERT promoter, and decreased telomerase activity.

3.4. Cotreatments with IL-6 and TNF-α Increased Cell Invasiveness Whereas Withaferin A Decreased both Colonosphere Formation and Trans-Well Invasion. As we found out the molecular mechanisms of STAT3 activation by cytokines of IL-6 and TNF-α, we next examined the cell-level invasiveness of colorectal cancer cells. To measure the cell invasiveness, we used two methods, colonosphere formation and trans-well invasion assays. For colonosphere formation, we created three-dimensional culture conditions by adding 5% matrigel to the 24-well plates. Cancer cells were seeded onto the wells with culture medium with or without IL-6 and TNF-α. Withaferin A treatment was done as a pretreatment in a 10 μM withaferin A for 24 hours, and cells were seeded onto the wells. Formed colonospheres were counted after 14 days incubation. As shown in the Figure 4(a), untreated DLD1 cells formed ~29 spheres per wells whereas cytokine-treated cells showed increased spheres of ~71 (Figures 4(a) and 4(b)). However, withaferin A pretreatments almost abolished the sphere formation from the assay. Similarly, trans-well invasion assay showed ~30% of cell invasion with untreated ontrol while cytokine-treated cells showed 66% invasion. When cells were pretreated with withaferin A, the cell invasion has been decreased to 16% (Figures 4(c) and 4(d)). These data are consistent with the Chip assay and telomerase assay data in that cytokine-increased STAT3 binding and telomerase activity. On the contrary, withaferin A inhibited STAT3 activation decreased telomerase and cell invasiveness.

3.5. IL-6 Activated STAT3 and TNF-α Activated STAT1, STAT3, and STAT1 Heterodimerize upon IL-6 and TNF-α Cotreatments. Both IL-6 and TNF-α are pleiotropic cytokines stimulating more than one signaling pathways. We next investigated that which receptor tyrosine kinases were activated by IL-6 and TNF-α alone and in combination. To this end, we used the PathScan RTK Signaling Antibody Array Kit (Cell Signaling Technology) to screen the receptor tyrosine kinases. We were able to detect 28 receptor tyrosine kinases simultaneously using this array kit. We treated two cancer cell lines DLD1 and HT-29, then observed the receptor tyrosine kinase activation. When we treated with IL-6, STAT3 (Tyr 705) was phosphorylated whereas TNF-α treatment induced STAT1 (Tyr 701) phosphorylation in both DLD1 and HT-29 (Figures 5(a) and 5(b)). STAT1 is involved in upregulating genes due to a signal by either types I, II, or III interferons [27]. In response to stimulation, STAT1 forms homodimers or heterodimers with STAT3 that bind to the GAS (interferon-gamma-activated sequence) promoter element.

We next tested if STAT1 heterodimerize with STAT3, and furthermore, the interactions were enhanced by cytokine stimulation. To this end, we pulled down with STAT3 antibody and probed for STAT1 protein in the coimmunoprecipitation assay. As shown in the Figure 6(a), STAT1 heterodimerized with STAT3. When treated with IL-6 and TNF-α, the interaction was enhanced as the bound STAT1 protein amount was increased. We treated cells with chemotherapy agent 5-FU and withaferin A, then monitored the STAT3-STAT1 interactions. As shown in Figure 6(b), withaferin A abolished the STAT3-STAT1 interactions whereas 5-FU modestly reduced the interactions.

We have shown that STAT3 and NF-κB physically bind from the previous coimmunoprecipitation study (Figure 2).

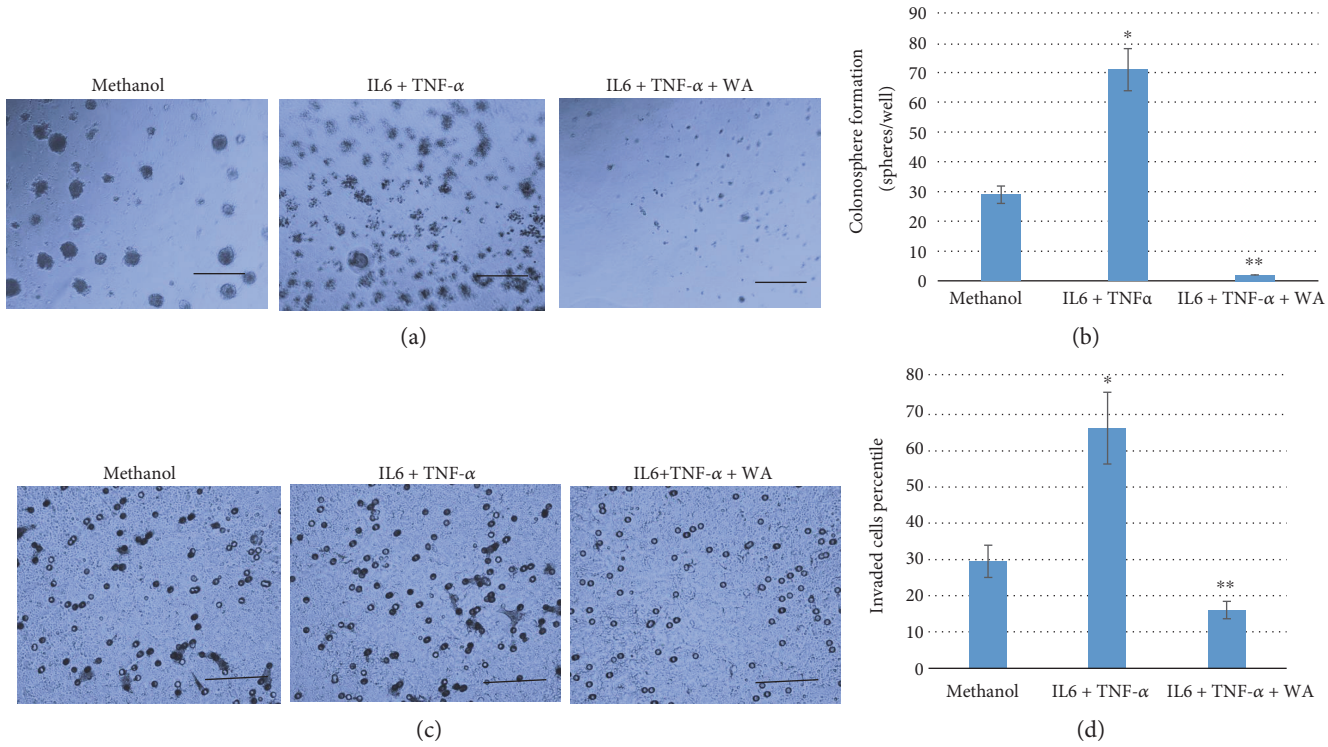

Figure 4: IL-6 and TNF-α cotreatments increased colonosphere formation and cell invasion whereas withaferin A decreased the sphere formation and cell invasiveness. (a) Colonosphere formation assay. DLD1 cells were cotreated with IL-6 and TNF-α for 24 hours, then subjected to the three-dimensional culture condition. Withaferin A (10 μM) was pretreated with IL-6 and TNF-α, then applied to three-dimensional culture. Representative images were taken after 7 days. Scale bar represents 50 μm in length. (b) Quantitative representation of colonospheres formed in IL-6 and TNF-α cotreatments in the absence and presence of withaferin A. $^{*}p < 0.05$, $^{**}p < 0.01$ versus untreated control. (c) Boyden chamber assay. Cell invasiveness was examined by employing Boyden chamber assay. Human colorectal cancer DLD1 cells were subjected to Boyden chamber cell invasion assay. Cells were treated with IL-6 and TNF-α in the absence or presence of withaferin A. Assays were done for 48 hours. Representative images were taken. Scale bar represents 50 μm in length. (d) The cell invasion assay was quantitatively measured in graphic representation. $^{*}p < 0.05$, $^{**}p < 0.01$ versus untreated control.

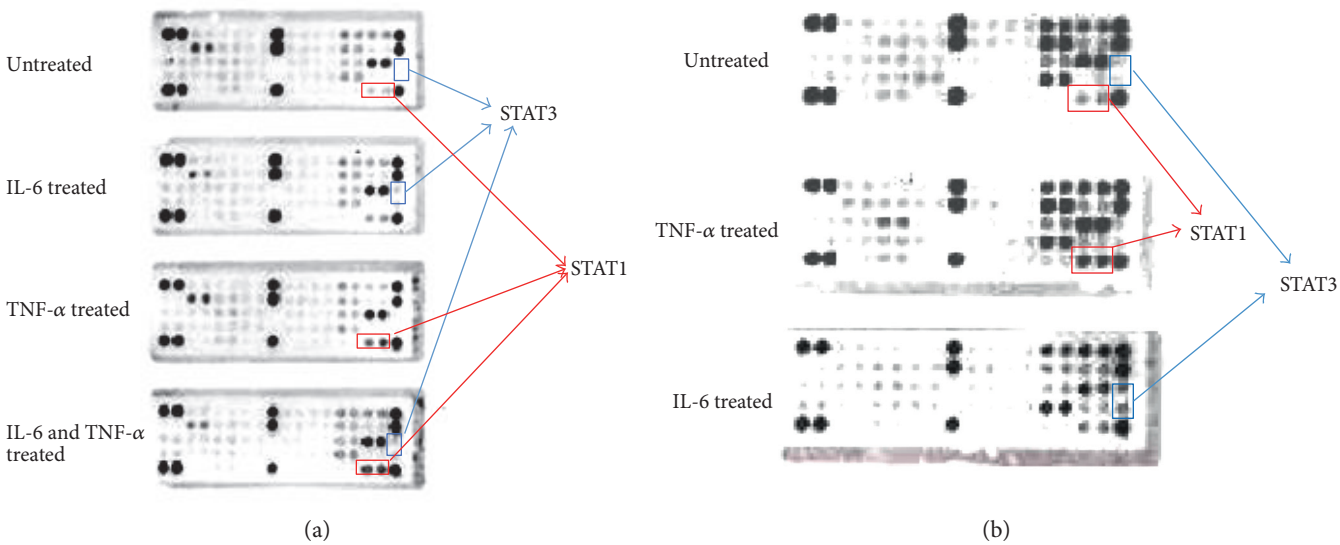

Figure 5: IL-6 activated STAT3 (Tyr 705) and TNF-α activated STAT1 (Tyr 701) in human colorectal cancer cells. We investigated the receptor tyrosine kinase phosphorylation with IL-6 and TNF-α treatments in DLD1 and HT-29. (a) When DLD1 cell was treated with IL-6 (10 ng/ml), STAT3 was activated. TNF-α treatment activated STAT1 (Tyr 701). IL-6 and TNF-α cotreatments activated both STAT1 and STAT3. (b) HT-29 was treated with TNF-α and IL-6. TNF-α treatments activated STAT1 (Tyr 701). IL-6 treatment activated STAT3 (Tyr 705).

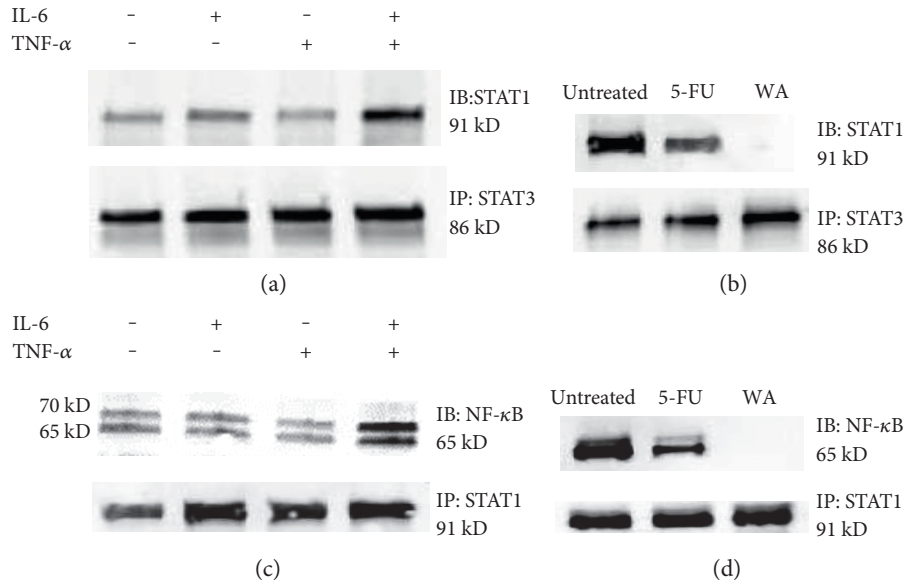

Figure 6: STAT3 dimerize with STAT1 and STAT1 dimerize with NF-κB. Withaferin A abolished the protein-protein interactions. (a) STAT1 was heterodimerized with STAT3 from the pull-down assay with an STAT3 antibody. The binding affinity was increased upon IL-6 and TNF-α cotreatments. (b) Withaferin A (10 μM) treatment has abolished the STAT3-STAT1 interactions. (c) Coimmunoprecipitation with STAT1 antibody revealed that STAT1 was bound to NF-κB. STAT1-NF-κB interaction was enhanced by the IL-6 and TNF-α stimulation. (d) These interactions were also abolished by withaferin A (10 μM) treatment.

We next tested if STAT1 also binds NF-κB as STAT1 and STAT3 bind as well as STAT3 and NF-κB bind. STAT1 pull-down assay showed that NF-κB was bound to STAT1 (Figure 6(c)). When IL-6 and TNF-α were treated, the STAT1-NF-κB interaction was also enhanced. We also treated 5-FU and withaferin A, then tested the STAT1-NF-κB interactions. Withaferin A abolished the STAT1-NF-κB interactions while 5-FU modestly decreased the binding. Our results suggest that IL-6 and TNF-α activate STAT3 and STAT1 on the receptor tyrosine kinase levels, then form the triplet complex with NF-κB, subsequently induce cell invasiveness through the converged STAT3, STAT1, and NF-κB regulations on the target genes in colorectal cancer cells.

4. Discussion

In this study, we found that STAT3 was synergistically activated by IL-6 and TNF-α. STAT3, STAT1, and NF-κB formed triplet complexes with IL-6 and TNF-α stimulation, thereby increasing telomerase activity by binding hTERT promoter more tightly. Cell-level invasion assay revealed that cytokine treatments contributed to the cell invasiveness. An anti-inflammatory steroidal lactone withaferin A abolished the cancer stem cell traits and decreased telomerase activity significantly. Our data suggest the novel molecular mechanisms by which proinflammatory cytokines drive the colorectal tumorigenesis and a link between inflammation and cancer.

STAT3 and NF-κB are transcription factors activated in the majority of cancers. They activate genes that control cell survival, proliferation, angiogenesis, invasiveness, and cytokine production [28, 29]. STAT3 and NF-κB enhance resistance to apoptosis-based tumor surveillance of preneoplastic and malignant cells [30]. We found that combined treatments of IL-6 and TNF-α activate STAT3 in a synergistic manner, and promoted STAT3 and NF-κB physically bind each other. With cytokine stimulation, STAT3 and NF-κB formed a complex and activated their target genes, like hTERT. The IL-6-TNFα synergistic activation of STAT3 may result in the enhanced STAT3 activation on its target genes. Human TERT promoter region is likely one of the converging points of these activations elicited by the cytokines of IL-6 and TNF-α. In accordance, the telomerase activity was increased with the activation of STAT3 and NF-κB. The next step of cytokine signaling characterization will be to monitor the changes in IL-6 and TNF-α production levels from the activated, telomerase-increased, and invasive cancer cells employing Elisa assays. If STAT3-NF-κB signaling feed-forward loop working, the cytokine production possibly significantly increased in the invasive cells. More in vivo studies are warranted for the cytokine-stimulated tumorigenesis and withaferin A antitumor effects. The enhanced tumor formation with cytokines and tumor regression by withaferin A in an animal model is underway.

The cytokines, IL-6 and TNF-α, and transcription factors, STAT3 and NF-κB, are critical for both inflammation and cancer, thus they can constitute a central signaling pathway that promotes inflammation and tumor growth concurrently. It has been shown that pharmacological interference on the cytokine signaling has decreased the tumorigenesis and cancer progression [31, 32]. Withaferin A has abolished the STAT3 activation in colorectal cancer cells. More importantly, withaferin A inhibited Oct-4, stem cell marker, expression in the cancer cells. Oct-4 is the most critical

transcription factor for stemness, and aberrant Oct-4 expression is closely associated with abnormal tissue growth or tumorigenesis [33, 34]. There were multiple putative STAT3 binding sites in the Oct-4 promoter (Qiagen, Epi Tect ChIP qPCR data base). We also searched the current literature for the Oct-4 promoter binding proteins. The upstream signals that regulate Oct-4 expression and its gene circuitry are not well documented. More detailed Oct-4 gene regulation studies remain to be seen.

In addition, withaferin A decreased STAT3-NF-κB interaction and significantly decreased telomerase activity. Presently, there is only one clinical trial going on with withaferin A at the University of Pittsburgh on Schizophrenia (Clinical Trial ID, NCT01793935). Based on our study and data from others, withaferin A is likely to be subject to new clinical trial for metastatic cancer. Considering withaferin A characteristics as a natural compound, it would be reasonable to use it as an amplifier or supplement for the standard chemotherapy agent for recurrent or metastatic cancers.

Our receptor tyrosine kinase array screen revealed that IL-6 induced STAT3 (Tyr 705) and TNF-α induced STAT1 (Tyr 701) activations. There has been a report that a low STAT1 and high STAT3 ratio showed faster tumor growth in a xenograft [35]. Accordingly, these results reflected the similar clinical outcomes from the colorectal cancer patients. When STAT1 is low and STAT3 is high, the prognosis was poor. It was proposed that the ratio of STAT1 to STAT3 expression was a key determinant of colorectal cancer progression and that STAT1 counteracts protumorigenic STAT3 signaling. Our data indicate that TNF-α elicits STAT1 pathway and IL-6 activates STAT3 pathway in terms of receptor tyrosine kinase levels. STAT3 and STAT1 activation and dimerization can be a regulation mechanism for IL-6 and TNF-α signaling. One step further, NF-κB also complexed with STAT3 and STAT1 and contributed to the target gene activation. One similar study to our work has been reported from the breast cancer area. Snyder and associates have shown that STAT3-NF-κB complex was necessary for the expression of fascin in metastatic breast cancer cells in response to IL-6 and TNF-α [36]. In there, they showed that treatment of IL-6 and TNF-α led to the formation of STAT3 and NF-κB, binding to the fascin promoter region. STAT3-NF-κB complex was necessary for the fascin expression and migration of breast cells. More characterization of the STAT3-STAT1 dual regulation on the cancer stemness and telomerase studies remains to be seen.

Conflicts of Interest

All of the authors declare that there is no conflict of interest with the publication of this study.

Authors' Contributions

Seyung S. Chung and Yong Wu contributed equally to this work.

Acknowledgments

This work was supported by the National Institutes of Health (NIH, NCI, NIMHD, NCATS) Grants to Jaydutt V. Vadgama: U54 CA143931, U54 MD007598, and UL1TR000124. Seyung S. Chung is a scholar supported by the Clinical Research Education and Career Development by the NIMHD R25 MD 007610, pilot project award from U54 MD 007598 and Emerging Scientist Award from the Urban Health Institute-CDU S21 MD 000103. Research reported in this publication was also supported by Accelerating Excellence in Translational Science Pilot Grants G0812D05, pilot project award from the National Institutes of Health (NCI, NIMHD) Grants U54 CA143931 and U54MD0075984, and NIH/NCI SC1CA200517 to Yong Wu. The content is solely the responsibility of the authors and does not necessarily represent the official views of the National Institutes of Health. We deeply thank the division of cancer research and training members for their helpful comments and suggestions.

References

[1] L. M. Coussens and Z. Werb, "Inflammation and cancer," *Nature*, vol. 420, no. 6917, pp. 860–867, 2002.

[2] S. I. Grivennikov, F. R. Greten, and M. Karin, "Immunity, inflammation, and cancer," *Cell*, vol. 140, no. 6, pp. 883–899, 2010.

[3] M. V. Lin, L. Y. King, and R. T. Chung, "Hepatitis C virus-associated cancer," *Annual Review Pathology*, vol. 10, pp. 345–370, 2015.

[4] T. A. Ullman and S. H. Itzkowitz, "Intestinal inflammation and cancer," *Gastroenterology*, vol. 140, no. 6, pp. 1807–1816, 2011.

[5] R. Siegel, J. Ma, Z. Zou, and A. Jemal, "Cancer statistics 2014," *CA: A Cancer Journal for Clinicians*, vol. 64, no. 1, pp. 9–29, 2014.

[6] T. Ueda, E. Shimada, and T. J. Urakawa, "Serum levels of cytokines in patients with colorectal cancer: possible involvement of interleukin-6 and interleukin-8 in hematogenous metastasis," *Journal of Gastroenterology*, vol. 29, no. 4, pp. 23–29, 1994.

[7] P. H. Chang, Y. P. Pan, C. W. Fan et al., "Pretreatment serum interleukin-1β, interleukin-6 and tumor necrosis factor α levels predict the progression of colorectal cancer," *Cancer Medicine*, vol. 5, no. 3, pp. 426–433, 2016.

[8] G. Tripsianis, E. Papadopoulou, K. Romanidis et al., "Co-expression of IL-6 and TNF-α: prognostic significance on breast cancer outcome," *Neoplasma*, vol. 61, no. 2, pp. 205–212, 2014.

[9] G. J. Zhang and I. Adachi, "Serum interleukin-6 levels correlate to tumor progression and prognosis in metastatic breast carcinoma," *Anticancer Research*, vol. 19, no. 2, pp. 1427–1432, 1999.

[10] V. Michalaki, K. Syrigos, P. Charles, and J. Axman, "Serum levels of IL-6 and TNF-α correlate with clinicopathological features and patient survival in patients with prostate cancer," *British Journal of Cancer*, vol. 90, no. 12, pp. 2312–2316, 2004.

[11] T. Hirano, K. Ishihara, and M. Hibi, "Roles of STAT3 in mediating the cell growth, differentiation and survival signals relayed through the IL-6 family of cytokine receptors," *Oncogene*, vol. 19, no. 21, pp. 2548–2556, 2000.

[12] H. Yu, D. Pardoll, and R. Jove, "STATs in cancer inflammation and immunity: a leading role for STAT3," *Nature Reviews. Cancer*, vol. 9, no. 11, pp. 798–809, 2009.

[13] L. Lin, A. Liu, Z. Peng et al., "STAT3 is necessary for proliferation and survival in colon cancer-initiating cells," *Cancer Research*, vol. 71, no. 23, p. 7226, 2011.

[14] M. H. Mirjalili, E. Moyano, M. Bonfill, R. M. Cusido, and J. Palazón, "Steroidal lactones from *Withania somnifera*, an ancient plant for novel medicine," *Molecules*, vol. 14, no. 7, pp. 2373–2393, 2009.

[15] M. Winters, "Ancient medicine, modern use: *Withania somnifera* and its potential role in integrative oncology," *Alternative Medicine Review*, vol. 11, no. 4, pp. 269–277, 2006.

[16] S. Suman, T. P. Das, S. Sirimulla, H. Alatassi, M. K. Ankem, and C. Damodaran, "Withaferin-A suppress AKT induced tumor growth in colorectal cancer cells," *Oncotarget*, vol. 7, no. 12, pp. 13854–13864, 2016.

[17] K. Heyninck, M. Lahtela-Kakkonen, P. Van der Veken, G. Haegeman, and B. W. Vanden, "Withaferin A inhibits NF-kappaB activation by targeting cysteine 179 in IKKβ," *Biochemical Pharmacology*, vol. 91, no. 4, pp. 501–509, 2014.

[18] P. Bargagna-Mohan, A. Hamza, Y. E. Kim, A. Khuan, and Y. Ho Y, et al., "The tumor inhibitor and antiangiogenic agent withaferin A targets the intermediate filament protein vimentin," *Chemistry & Biology*, vol. 14, no. 6, pp. 623–634, 2007.

[19] J. T. Thaiparambil, L. Bender, T. Ganesh et al., "Withaferin A inhibits breast cancer invasion and metastasis at sub-cytotoxic doses by inducing vimentin disassembly and serine 56 phosphorylation," *International Journal of Cancer*, vol. 129, no. 11, pp. 2744–2755, 2011.

[20] S. S. Kakar, V. R. Jala, and M. Y. Fong, "Synergistic cytotoxic action of cisplatin and withaferin A on ovarian cancer cell lines," *Biochemical and Biophysical Research Communications*, vol. 423, no. 4, pp. 819–825, 2012.

[21] S. S. Chung, D. Adekoya, I. Enenmoh et al., "Salinomycin abolished STAT3 and STAT1 interactions and reduced telomerase activity in colorectal cancer cells," *Anticancer Research*, vol. 37, no. 2, pp. 445–453, 2017.

[22] S. S. Chung, B. Oliva, S. Dwabe, and J. V. Vadgama, "Combination treatment with flavonoid morin and telomerase inhibitor MST-312 reduces cancer stem cell traits by targeting STAT3 and telomerase," *International Journal of Oncology*, vol. 49, no. 2, pp. 487–498, 2016.

[23] H. Gabbert, R. Wagner, R. Moll, and C. D. Gerharz, "Tumor dedifferentiation: an important step in tumor invasion," *Clinical & Experimental Metastasis*, vol. 3, no. 4, pp. 257–279, 1985.

[24] J. B. Kim, V. Sebastiano, G. Wu et al., "Oct4-induced pluripotency in adult neural stem cells," *Cell*, vol. 136, no. 3, pp. 411–419, 2009.

[25] S. S. Chung, C. Aroh, and J. V. Vadgama, "Constitutive activation of STAT3 signaling regulates hTERT and promotes stem cell-like traits in human breast cancer cells," *PloS One*, vol. 8, no. 12, article e83971, 2013.

[26] L. Konnikova, M. C. Simeone, M. M. Kruger, M. Kotecki, and B. H. Cochran, "Signal transducer and activator of transcription 3 (STAT3) regulates human telomerase reverse transcriptase (hTERT) expression in human cancer and primary cells," *Cancer Research*, vol. 65, no. 15, pp. 6516–6520, 2005.

[27] C. P. Leonidas, "Mechanisms of type-I- and type-II-interferon-mediated signaling," *Nature Reviews Immunology*, vol. 5, no. 5, pp. 375–386, 2005.

[28] S. Grivennikov and M. Karin, "Dangerous liasons: STAT3 and NF-κB collaboration and crosstalk in cancer," *Cytokine & Growth Factor Reviews*, vol. 21, no. 1, pp. 11–19, 2010.

[29] H. Yu, M. Kortylewski, and D. Pardoll, "Crosstalk between cancer and immune cells: role of STAT3 in the tumour microenvironment," *Nature Reviews. Immunology*, vol. 7, no. 1, pp. 41–51, 2007.

[30] F. Yihui, M. Renfang, and Y. Jianhua, "NF-κB and STAT3 signaling pathways collaboratively link inflammation to cancer," *Protein & Cell*, vol. 4, no. 3, pp. 176–185, 2013.

[31] C. Becker, M. C. Fantini, C. Schramm et al., "TGF-β suppresses tumor progression in colon cancer by inhibition of IL-6 *trans*-signaling," *Immunity*, vol. 21, no. 4, pp. 491–501, 2004.

[32] M. Hedvat, D. Huszar, A. Herrmann et al., "The JAK2 inhibitor AZD1480 potently blocks Stat3 signaling and oncogenesis in solid tumors," *Cancer Cell*, vol. 16, no. 6, pp. 487–497, 2009.

[33] C. Hadjimichael, K. Chanoumidou, N. Papadopoulou, P. Arampatzi, J. Papamatheakis, and A. Kretsovali, "Common stemness regulators of embryonic and cancer stem cells," *World Journal of Stem Cells*, vol. 7, no. 9, pp. 1150–1184, 2015.

[34] F. Hassiotou, A. R. Hepworth, A. S. Beltran et al., "Expression of the Pluripotency transcription factor OCT4 in the normal and aberrant mammary gland," *Frontiers in Oncology*, vol. 3, p. 79, 2013.

[35] H. Nivarthi, C. Gordziel, M. Themanns et al., "The ratio of STAT1 to STAT3 expression is a determinant of colorectal cancer growth," *Oncotarget*, vol. 7, no. 32, pp. 51096–51106, 2016.

[36] M. Snyder, J. Huang, and J. Zhang, "A signal transducer and activator of transcription 3·nuclear factor κB (Stat3·NFκB) complex is necessary for the expression of Fascin in metastatic breast cancer cells in response to interleukin (IL)-6 and tumor necrosis factor (TNF)-α," *The Journal of Biological Chemistry*, vol. 289, no. 43, pp. 30082–30089, 2014.

Hindawi
Mediators of Inflammation
Volume 2017, Article ID 8481049, 11 pages
https://doi.org/10.1155/2017/8481049

Research Article

Gender Disparity in the Relationship between Prevalence of Thyroid Nodules and Metabolic Syndrome Components: The SHDC-CDPC Community-Based Study

Xiaoying Ding,[1,2] Ying Xu,[3] Yufan Wang,[1] Xiaohua Li,[1] Chunhua Lu,[4] Jing Su,[1] Yuting Chen,[1] Yuhang Ma,[1] Yanhua Yin,[1] Yong Wu,[3] Yaqiong Jin,[3] Lihua Yu,[4] Junyi Jiang,[5] Naisi Zhao,[6] Qingwu Yan,[2] Andrew S. Greenberg,[2] Haiyan Sun,[1] Mingyu Gu,[1] Li Zhao,[1] Yunhong Huang,[1] Yijie Wu,[1] Chunxian Qian,[3] and Yongde Peng[1]

[1]*Department of Endocrinology and Metabolism, Shanghai General Hospital, Shanghai Jiao Tong University School of Medicine, Shanghai 200080, China*
[2]*Jean Mayer USDA Human Nutrition Research Center on Aging, Tufts University, Boston, MA 02111, USA*
[3]*Department of Internal Medicine, Sijing Hospital, Shanghai 201601, China*
[4]*Department of Chronic Disease Prevention and Control, Sijing Community Health Service Centre of Songjiang District, Shanghai 201601, China*
[5]*Shanghai Pudong New Area Center for Disease Control and Prevention, Shanghai 200136, China*
[6]*Department of Public Health and Community Medicine, Tufts University School of Medicine, Boston, MA 02111, USA*

Correspondence should be addressed to Chunxian Qian; dxy_gh@sina.com and Yongde Peng; pengyongde0908@126.com

Received 22 October 2016; Accepted 20 February 2017; Published 21 May 2017

Academic Editor: Yong Wu

The study is aimed to investigate the pathogenesis underlying the increased prevalence of thyroid nodule (TN) in different levels of metabolic syndrome (MetS) components and analyze the relationships between TN and MetS components. A total of 6,798 subjects, including 2201 patients with TN, were enrolled in this study. Anthropometric, biochemical, thyroid ultrasonographic, and other metabolic parameters were all measured. There was obviously sexual difference in the prevalence of TN (males 26.0%, females 38.5%, resp.). The prevalence of TN in hyperuricemia (45.7% versus 37.4%, $P = 0.001$), NAFLD (41.2% versus 36.4%, $P < 0.05$), and MetS (41.4% versus 35.4%, $P < 0.001$) groups was significantly increased only in females. Insulin resistance [OR = 1.31 (1.15, 1.49)], MetS [OR = 1.18 (1.03, 1.35)], and diabetes [OR = 1.25 (1.06, 1.48)] were all independent risk factors for TN in total subjects, whereas, after stratified analysis of gender, MetS [OR = 1.29, (1.09, 1.53)] and diabetes [OR = 1.47, (1.17, 1.84)] are still strongly and independently associated with the higher risks of TN in female subjects, but not in males. Our results suggest that the components of MetS might associate with the higher risks of TN in women than in men, but further cohort study of this gender disparity in the association between TN and MetS is required.

1. Introduction

Thyroid nodule (TN), one of the most common clinical thyroid diseases, has been becoming increasingly prevalent all over the world in the last decades and its associated risk factors have received much attention [1]. It is estimated that TN affects 4% to 7% of adults by palpation and 19% to 67% with ultrasonography [2], with 5 to 10% being malignant worldwide [3, 4]. Thus, more thyroid nodule diagnoses mean more possibilities of the thyroid cancer occurrence in the future. Further study of the relevant risk factors of the TN is required.

Previous studies have showed that impaired glucose metabolism is an independent risk factor for increased thyroid volume and nodule prevalence [5–7]. Obesity was

associated with higher risks of TN and thyroid cancer [8–10]. Insulin resistance (IR) was also shown to promote the formation and growth of TN [11]. Recently, it has been suggested that metabolic syndrome (MetS) was associated with the functional and morphological alterations of the thyroid gland and may be involved in the pathogenesis of TN [12, 13]. Although the metabolic risk factors such as obesity, insulin resistance, and abnormal glucose metabolism are involved in the pathogenesis of TN in patients and these have been targeted for therapeutic intervention [14, 15], however, up to now, the metabolic mechanisms facilitating TN in individuals still have not been fully investigated, but also there has been scarce literature investigating the different levels of MetS risk factors in subjects with or without TN. Little is known about the relationships between TN and the components of MetS components [16], which limits the understanding of the mechanisms of the relative crosstalk between TN and MetS. TN are most frequently observed in females and in the elderly [17, 18]; nevertheless, there is very little epidemiological data related to the gender disparity in the relationship between TN and the components of MetS in aged populations.

Based on this issue, the main purpose of this study was to investigate the prevalence of TN among a population aged over 45 years with different glucose metabolic status and to comprehensively investigate the association between TN diagnosed on ultrasonography and the MetS components in the SHDC-CDPC Community-based Study (Shenkang Hospital Development Center for Chronic Disease Prevention and Control project, Shanghai, China). A total of 7,920 individuals with age above 45 years were enrolled in the epidemiological investigation in a rural Chinese population. The different levels of metabolic indices between the TN group and control group were measured and compared. Our study would strengthen the associations between TN and the components of MetS and increase knowledge in gender disparity on the prevalence of TN.

2. Subjects and Methods

2.1. Participants and Data Collection. From October 2014 to July 2015, a total of 7,920 local inhabitants aged 45 years or older who had been living in Sijing, Shanghai, for 1 year or longer before the enrollment and represented ten rural communities, were enrolled in this cross-section survey. A comprehensive survey was administered by the trained research staff to obtain a detailed questionnaire, anthropometry index, medical history, family histories of chronic diseases, and current medication use. Meanwhile, smoking and drinking status were also recorded. Through multiple screenings, 476 individuals were excluded from the study with missing data on questionnaire, anthropometry index, demographic variables, physical examination data, or the glucose metabolic indexes. Furthermore, subjects who met the exclusion criteria, including illnesses, such as hypothyroidism, hyperthyroidism, chronic renal failure, excessive drinking (an alcohol intake > 140 g/week for men or >70 g/week for women), or current medication use affecting body composition, thyroid function, lipid profile, serum UA level, and glucose metabolic status, were excluded in the data analysis. In the end, a total of 6798 subjects and 2201 of them with TN were included in the final data analysis. The study protocol has been approved by the Committee on Human Research at Shanghai General Hospital, Shanghai Jiao Tong University School of Medicine. Written informed consent was obtained from each participant.

2.2. Anthropometric Measurement and Ultrasonography. All subjects had a physical examination in a fasting state. Blood pressure was measured in the all participants seated quietly for at least five minutes thrice consecutively and the average of three measurements was recorded. Waist circumference (WC) was measured in standing subjects, midway between the lower edge of the costal arch and the top of the iliac crest. Hip circumference (HC) was measured in standing subjects, around the widest portion of the buttocks. Body mass index (BMI) was calculated as body weight/height^2 in kg/m^2. Waist-to-hip ratio (WHR) was calculated as WC divided by HC. In a supine position and the hyperextended neck of all participants, ultrasound examination of the thyroid nodules, including the TN number and location, was performed and evaluated independently by the two senior experts using a B-mode high-resolution tomographic ultrasound system (Toshiba, Tokyo, Japan).

2.3. Biochemical Measurements and Calculation. Venous blood samples were collected from all participants in the morning after an overnight fasting for at least 10 hours. The subjects without diagnosis of diabetes underwent the oral standard 75 g glucose tolerance test (OGTT) and the previously diagnosed diabetes underwent the steamed bread meal test. Biochemical measurements, including plasma glucose concentrations, uric acid (UA), serum lipid profile containing levels of total cholesterol (TCH), low-density lipoprotein cholesterol (LDL-C), high-density lipoprotein cholesterol (HDL-C), and triglycerides (TG), were measured enzymatically using an automatic biochemistry analyzer (HITACHI 7600). Fasting plasma insulin (FINS) concentration, serum level of thyroid-stimulating hormone (TSH), free triiodothyronine (FT3) concentration, free tetraiodothyronine (FT4) concentration, and thyroid peroxidase antibody (TPOAB) concentration were measured by electrochemiluminescence analyzer (Roche Diagnostics, Basel, Switzerland). The homoeostasis model assessment for insulin resistance index (HOMA-IR) was calculated by multiplying fasting plasma insulin (mIU/l) and fasting plasma glucose (FPG) (mM) and dividing the result by 22.5. Beta cell function (HOMA-beta) was calculated as 20x fasting plasma insulin (mIU/l)/(FPG (mM) −3.5) ×100%. Glycosylated hemoglobin (HbA1c) was measured by high-performance liquid chromatography (D10; Bio-Rad Laboratories, Inc., CA).

2.4. Definition and Diagnostic Criteria. The MetS was defined according to the IDF criteria [19] with modification on WC cutoff point for an Asian population: the central obesity (defined as WC ≥ 90 cm for men or ≥ 80 cm for women; [20]),

plus any two or more: (1) raised TG (≥1.7 mmol/l or specific treatment for this lipid abnormality); (2) reduced HDL-C (<1.03 mmol/l in men and <1.29 mmol/l in women or specific treatment for this lipid abnormality); (3) raised blood pressure (≥130/85 mmHg or treatment of previously diagnosed hypertension); (4) raised fasting plasma glucose (≥5.6 mmol/l or previously diagnosed type 2 diabetes). The diabetes and prediabetes were defined using criteria recommended by the ADA 2010 [21]. BMI ≥25 kg/m^2 was defined as overweight or ≥30 kg/m^2 was defined as obesity using criteria recommended by the World Health Organization [22]. Insulin resistance was evaluated using HOMA-IR of 2.8 or higher [23]. Hyperuricemia was defined as serum uric acid level of 420 umol/L or higher in men and 360 umol/L or higher in women, respectively [24]. Current smoking status (Yes or No) was defined according to smoking more than one cigarette daily for at least 6 months. Current alcohol consumption status (Yes or No) was defined according to drink more than one time of any type monthly. A thyroid nodule is a discrete lesion within the thyroid gland that is radiologically distinct from the surrounding thyroid parenchyma [25]. NAFLD was defined according to the "Diagnostic Criteria of Nonalcoholic Fatty Liver Disease by the Chinese Society of Hepatology" after exclusion of viral or autoimmune liver disease and excessive alcohol consumption [26]. NAFLD was ascertained using hepatic ultrasonography that revealed ultrasound beam attenuation, a diffusely increased echogenicity in the liver parenchyma or poor visualization of intrahepatic structures by two trained ultrasonographists [27].

2.5. Statistical Analysis. All statistical analyses were performed using the SAS version 9.2 (SAS Institute Inc., Cary, NC, USA). Demographic, metabolic features and other clinical parameters were described by sex using frequency (percentage) for categorical variables and median (interquartile range) for continuous variables, respectively. Additionally, we divided the participants into different subgroups with and without thyroid nodules according to the different levels of MetS components and clinical characteristics. Differences on metabolic characteristics in subjects with or without TN were evaluated using χ^2 test for the categorical variables or using nonparameter Wilcoxon test for analysis for the continuous variables. To further explore whether metabolic syndrome is associated with the risk of TN, unconditional sex-stratified logistic regression models were used to estimate the adjusted odds ratios (ORs) and 95% confident intervals (CIs) of MetS components with TN prevalence. Significance tests were two-tailed, with P value less than 0.05 considered of statistical significance.

3. Results

3.1. General Characteristics of Subjects with or without Thyroid Nodules. Clinical characteristics of the total of 6,798 participants including 3289 males and 3509 females, with a median age of 58.8 years (52.5–66.0), stratified by gender with and without thyroid nodules, were presented in Table 1. Of the 6798 subjects, the prevalence of TN was 32.4%. The prevalence of TN in women was significantly higher (38.5%) than in men (26.0%) ($P < 0.001$). Regardless of gender, analysis of the clinical risk factors revealed that subjects with TN were significantly older and had higher levels of SBP, FPG, PPG, HbA1c, FINS, HOMA-IR, HOMA-beta, FT4, and TPOAB than subjects without TN. Furthermore, all subjects with TN had significantly lower levels of DBP, FT3, and TSH than those without TN. However, after further gender stratification, there were still significant differences of SBP, UA, FPG, PPG, FINS, HOMA-IR, and TSH between the two groups in females.

3.2. Stratified Analysis of Prevalence of Thyroid Nodules according to the Different Metabolic Status. To explore the association of TN and related metabolic risk factors, the subjects were classified into different subgroups according to the different levels of MetS components and clinical characteristics (Table 2). The prevalence of TN was significantly increasing in the elder subjects (P for trend <0.001) and insulin resistance group (31.0% in the total control group, 37.0% in the total IR group, $P < 0.001$; 24.9% in the male control group, 30.1% in the male IR group, $P < 0.001$; 37.2% in the female control group, 42.0% in the female IR group, $P < 0.01$), respectively. However, there were no significant differences in the prevalence of TN between the male and female subgroups with the different levels of body fat accumulation (divided by BMI; by WHR quartile; by waist circumference) except for higher prevalence of TN in total subjects with central obesity. The prevalence of TN with normal glucose metabolism, prediabetes, and diabetes was 29.9%, 31.4%, and 37.2%, respectively, whereas the significant differences were only in female subjects (33.3%, 37.9%, and 46.0%, resp., $P < 0.001$). To explore whether MetS and the associated other metabolic parameters contributed to the pathogenesis of TN, all subjects were further divided into different subgroups according to being with or without MetS, with or without NAFLD, and with or without hyperuricemia, respectively. The results showed that the prevalence of TN with hyperuricemia (45.7% versus 37.4%, $P = 0.001$), NAFLD (41.2% versus 36.4%, $P < 0.05$), and MetS (41.4% versus 35.4%, $P < 0.001$) groups was statistically significantly higher in females, but not in males.

3.3. Logistic Regression Analyses of the Associated Metabolic Risk Factors of TN in Male and Female Subjects. Finally, to explore whether the MetS and the associated other metabolic parameters were independently associated with TN. A multiple logistic regression analysis for the risk factors of TN involving all the significant different anthropometric and metabolic parameters, such as central obesity, HOMA-IR, HOMA-beta, FPG, PPG, FINS, hyperuricemia, NAFLD, and MetS, were applied in subjects with or without TN (Figure 1). We next performed the stratified analysis in the subgroups divided according to the serum UA levels, glucose metabolic status, HOMA-IR, FINS, thyroid function, waist circumference, NAFLD, and MetS. Analysis of logistic regression indicated that diabetes [OR = 1.254, (1.061, 1.481)], insulin resistance [OR = 1.309, (1.149, 1.490)], and MetS [OR = 1.178,

Table 1: Clinical characteristics of the participants according to the presence or absence of thyroid nodules stratified by gender.

Parameters	Total subjects (n = 6798)		Statistic	P	Male (n = 3289)		Statistic	P	Female (n = 3509)		Statistic	P
	Thyroid nodules	Nonthyroid nodules			Thyroid nodules	Nonthyroid nodules			Thyroid nodules	Nonthyroid nodules		
Participants	2201 (32.4)	4597 (67.6)			854 (26.0)	2435 (74.0)			1352 (38.5)	2157 (61.5)		
General indices												
Age (years)	60.8 (55.1,67.9)	57.9 (51.4,64.9)	11.911	<0.001	61.1 (55.6,67.7)	58.1 (52,65)	8.12	<0.001	60.6 (54.8,68)	57.6 (50.7,64.8)	9.09	<0.001
Smoking, *n*, (%)	470 (22.1)	1342 (30.2)	48.20	<0.001	465 (55.4)	1332 (56.2)	0.170	0.680	5 (0.4)	10 (0.5)	0.17	0.684
Drinking, *n* (%)	226 (10.7)	802 (18.2)	60.32	<0.001	216 (26.3)	785 (33.6)	14.97	<0.001	10 (0.8)	17 (0.8)	0.02	0.883
SBP (mmHg)	136.0 (124.7,149.0)	134.0 (122.7,146.3)	4.43	<0.001	135.3 (123.7,148.3)	134.0 (123.3,146.3)	1.71	0.088	136.7 (125.3,149)	133.7 (122.3,146.3)	4.29	<0.001
DBP (mmHg)	77.0 (70.7,83.3)	77.7 (71.0,84.3)	−2.82	0.005	78.0 (71.3,84.3)	79 (72,86)	−2.81	0.005	76.7 (70.3,82.7)	76.3 (70,82.7)	0.257	0.797
Metabolic indices												
BMI (kg/m^2)	24.2 (22.1,26.5)	24.3 (22.1,26.5)	−0.66	0.512	24.4 (22.4,26.5)	24.6 (22.3,26.6)	−0.42	0.672	24.1 (21.9,26.5)	24 (21.9,26.3)	0.23	0.822
WC (cm)	86 (80,92)	86 (80,93)	−0.58	0.564	88 (82,93)	87 (81,94)	0.93	0.354	84 (78,91)	84 (78,91)	0.66	0.506
WHR	0.9 (0.9,1)	0.9 (0.9,0.9)	−0.51	0.611	0.9 (0.9,1.0)	0.9 (0.9,1.0)	1.29	0.199	0.9 (0.9,0.9)	0.9 (0.8,0.9)	0.78	0.437
TCH (mmol/l)	5.1 (4.5,5.8)	5.1 (4.5,5.7)	1.90	0.057	4.8 (4.3,5.4)	4.9 (4.4,5.5)	−2.15	0.032	5.3 (4.7,5.9)	5.2 (4.7,5.9)	1.57	0.117
TG (mmol/l)	1.4 (1.0,1.9)	1.3 (0.9,2.0)	0.67	0.500	1.4 (1.0,2.0)	1.4 (0.9,2.1)	−0.12	0.902	1.4 (1,1.9)	1.3 (0.9,1.9)	1.64	0.102
HDL-C (mmol/l)	1.5 (1.3,1.8)	1.5 (1.3,1.8)	0.75	0.451	1.4 (1.2,1.6)	1.4 (1.2,1.7)	−2.95	0.003	1.6 (1.4,1.9)	1.6 (1.4,1.9)	0.03	0.973
LDL-C (mmol/l)	2.9 (2.4,3.4)	2.8 (2.4,3.3)	1.65	0.099	2.7 (2.2,3.2)	2.7 (2.3,3.2)	−1.510	0.131	3 (2.5,3.5)	2.9 (2.5,3.5)	1.24	0.215
UA (μmol/l)	306 (256,363)	313 (261,369)	−2.73	0.006	353 (304,404)	350 (302,404)	0.09	0.930	280 (237,329)	273 (235,318)	3.20	0.001
FPG (mmol/l)	5.7 (5.3,6.3)	5.7 (5.3,6.2)	2.48	0.013	5.7 (5.3,6.3)	5.7 (5.3,6.3)	−0.08	0.938	5.7 (5.4,6.3)	5.7 (5.3,6.1)	4.01	<0.001
PPG (mmol/l)	7.6 (6.2,10.0)	7.3 (6.0,9.4)	5.07	<0.001	7.3 (5.9,10.1)	7.2 (5.8,9.6)	1.49	0.135	7.8 (6.5,9.9)	7.3 (6.1,9.2)	4.96	<0.001
HbA1c (%)	5.6 (5.3,6.0)	5.6 (5.3,5.9)	4.76	<0.001	5.6 (5.3,6)	5.6 (5.3,5.9)	2.26	0.024	5.6 (5.4,5.9)	5.6 (5.3,5.8)	4.71	<0.001
FINS (mIU/l)	7.2 (4.9,10.7)	6.8 (4.6,9.9)	4.10	<0.001	6.4 (4.2,9.6)	6.2 (4.1,9.2)	1.21	0.225	7.7 (5.3,11)	7.5 (5.2,10.6)	2.15	0.032
HOMA-IR	1.9 (1.2,2.9)	1.8 (1.1,2.6)	4.73	<0.001	1.7 (1,2.7)	1.7 (1,2.5)	1.65	0.098	2 (1.3,3)	1.9 (1.3,2.8)	3.03	0.002
HOMA-beta	61.6 (42.2,89.1)	59.9 (40.6,85.2)	2.18	0.029	54.3 (34.6,82.6)	53.7 (35.4,79.2)	0.61	0.545	65.5 (47.1,93)	66.7 (47,90.9)	−0.27	0.789
Thyroid indices												
FT3 (pmol/l)	4.9 (4.5,5.4)	5.1 (4.7,5.5)	−8.79	<0.001	5.2 (4.7,5.7)	5.3 (4.9,5.7)	−3.70	<0.001	4.8 (4.4,5.2)	4.9 (4.5,5.3)	−4.01	<0.001
FT4 (pmol/l)	15.9 (14.7,17.4)	15.8 (14.5,17.3)	2.29	0.022	16.2 (14.8,18)	16 (14.7,17.5)	2.50	0.013	15.8 (14.5,17.1)	15.6 (14.3,17)	2.58	0.010
TSH (mIU/l)	2.0 (1.5,2.7)	2.1 (1.5,2.8)	−2.24	0.025	1.8 (1.4,2.5)	1.9 (1.4,2.6)	−1.31	0.191	2.1 (1.6,2.8)	2.3 (1.7,3)	−4.38	<0.001
TPOAB (IU/ml)	13.8 (8.7,22.8)	12.5 (8.4,20.1)	4.23	<0.001	14.4 (9,23.5)	12.4 (8.2,19.1)	5.14	<0.001	13.3 (8.4,22.4)	12.7 (8.6,21.5)	0.851	0.395

SBP, systolic blood pressure; DBP, diastolic blood pressure; BMI, body mass index; WC, waist circumference; WHR, waist-to-hip ratio; TCH, total cholesterol; TG, triglyceride; HDL-C, high-density lipoprotein cholesterol; LDL-C, Low-density lipoprotein cholesterol; UA, uric acid; FPG, fasting plasma glucose; PPG, postprandial plasma glucose; HbA1c, Hemoglobin A1c; FINS, fasting plasma insulin; FT3, free triiodothyronine; FT4, free thyroxine; TSH, thyroid-stimulating hormone; TPOAB, thyroid peroxidase antibody.

Table 2: Stratified analysis of prevalence of thyroid nodules according to the different levels of metabolic syndrome components.

Parameters	Total subjects (n = 6798)		Males (n = 3289)		Females (n = 3509)	
	Thyroid nodules	Nonthyroid nodules	Thyroid nodules	Nonthyroid nodules	Thyroid nodules	Nonthyroid nodules
Age (years)						
<55	540 (24.1)	1700 (75.9)	194 (18.5)	854 (81.5)	346 (29.0)	846 (71.0)
55–65	912 (34.2)	1756 (65.8)	362 (27.2)	967 (72.8)	550 (41.1)	789 (58.9)
65–75	497 (39.4)	765 (60.6)	203 (32.3)	426 (67.7)	294 (46.5)	339 (53.6)
≥75	252 (41.0)	362 (59.0)	93 (34.1)	180 (65.9)	159 (46.6)	182 (53.4)
Chi-square	123.139		53.725		75.329	
P value	<0.001		<0.001		<0.001	
P for trend	<0.001		<0.001		<0.001	
BMI (kg/m^2)						
<25.0	1270 (32.8)	2602 (67.2)	465 (26.1)	1319 (73.9)	805 (38.6)	1283 (61.5)
25.0–30.0	755 (32.1)	1601 (68.0)	314 (25.3)	929 (74.7)	441 (39.6)	672 (60.4)
≥30.0	122 (32.5)	254 (67.6)	48 (28.9)	118 (71.1)	74 (35.2)	136 (64.8)
Chi-square	0.380		1.076		1.479	
P value	0.827		0.584		0.477	
P for trend	0.618		0.888		0.806	
WHR						
Q1	504 (31.1)	1115 (68.9)	187 (24.0)	593 (76.0)	317 (37.8)	522 (62.2)
Q2	515 (31.8)	1105 (68.2)	196 (24.7)	597 (75.3)	319 (38.6)	508 (61.4)
Q3	520 (32.1)	1099 (67.9)	203 (26.3)	568 (73.7)	317 (37.4)	531 (62.6)
Q4	544 (33.9)	1062 (66.1)	208 (26.8)	567 (73.2)	336 (40.4)	495 (59.6)
Chi-square	3.034		2.222		1.941	
P value	0.386		0.528		0.585	
P for trend	0.101		0.144		0.372	
Waist circumference (cm)						
<90 in men <80 in women	812 (29.3)	1964 (70.8)	454 (25.1)	1356 (74.9)	358 (37.1)	608 (62.9)
≥90 in men ≥80 in women	1281 (34.6)	2425 (65.4)	345 (26.2)	973 (73.8)	936 (39.2)	1452 (60.8)
Chi-square	20.506		0.479		1.324	
P value	<0.001		0.489		0.250	
HOMA-IR						
<2.8	1603 (31.0)	3566 (69.0)	649 (24.9)	1954 (75.1)	954 (37.2)	1612 (62.8)
≥2.8	597 (37.0)	1016 (63.0)	203 (30.1)	472 (69.9)	394 (42.0)	544 (58.0)
Chi-square	20.194		7.366		6.758	
P value	<0.001		0.001		0.009	

Table 2: Continued.

Parameters	Total subjects (n = 6798)		Males (n = 3289)		Females (n = 3509)	
	Thyroid nodules	Nonthyroid nodules	Thyroid nodules	Nonthyroid nodules	Thyroid nodules	Nonthyroid nodules
Glucose metabolic status						
NGR, n (%)	472 (29.9)	1106 (70.1)	195 (26.1)	652 (73.9)	277 (33.3)	554 (66.7)
Prediabetes, n (%)	1094 (31.4)	2390 (68.6)	397 (24.1)	1248 (75.9)	697 (37.9)	1142 (62.1)
Diabetes, n (%)	526 (37.2)	889 (62.8)	208 (28.8)	515 (71.2)	318 (46.0)	374 (54.1)
Chi-square	20.773		5.746		25.896	
P value	<0.001		0.057		<0.001	
P for trend	<0.001		0.253		<0.001	
UA (μmol/l)						
≤420 in men ≤360 in women	1856 (32.5)	3862 (67.5)	702 (26.6)	1933 (73.4)	1154 (37.4)	1929 (62.6)
>420 in men >360 in women	341 (32.2)	719 (67.8)	150 (23.4)	492 (76.6)	191 (45.7)	227 (54.3)
Chi-square	0.034		2.881		10.622	
P value	0.854		0.090		0.001	
NAFLD						
Without NAFLD	760 (32.2)	1599 (67.8)	254 (26.3)	713 (73.7)	506 (36.4)	886 (63.7)
NAFLD	535 (33.4)	1069 (66.7)	214 (26.0)	610 (74.0)	321 (41.2)	459 (58.9)
Chi-square	0.561		0.020		4.892	
P value	0.454		0.887		0.027	
Metabolic syndrome						
Without MetS	1168 (30.1)	2716 (69.9)	539 (25.6)	1566 (64.3)	629 (35.4)	1150 (64.6)
MetS	876 (35.3)	1605 (64.7)	249 (25.8)	716 (74.2)	627 (41.4)	889 (58.6)
Chi-square	19.041		0.014		12.500	
P value	<0.001		0.908		<0.001	

BMI, body mass index; WHR, waist-to-hip ratio; NGR, normal glucose regulation; UA, uric acid; NAFLD, nonalcoholic fatty liver disease; MetS, metabolic syndrome.

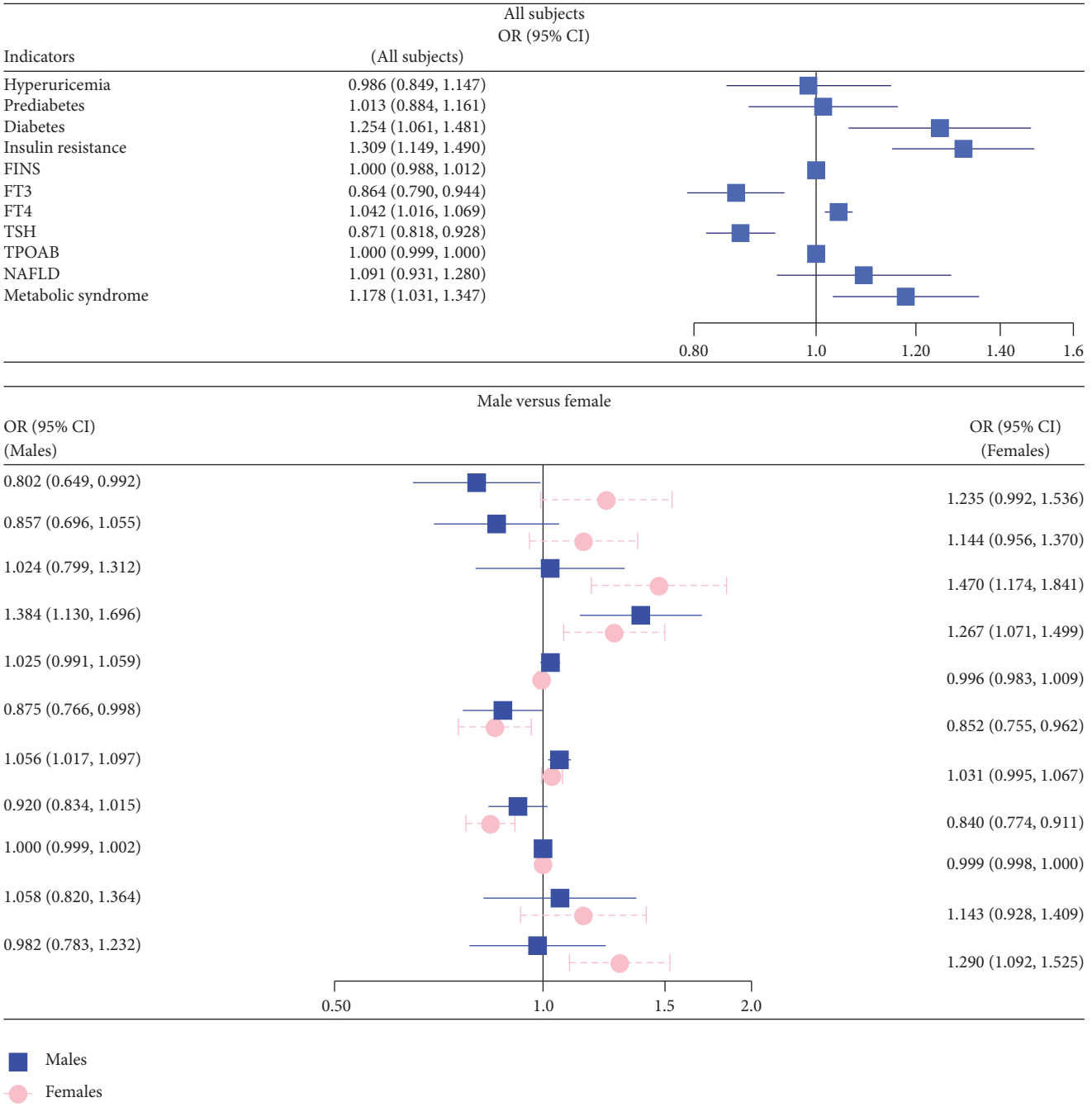

Figure 1: Metabolic risk factors of thyroid nodules were analyzed using logistic regression in total, male and female subjects. Adjustment of age, drinking, smoking, and family history of thyroid disease; FINS, fasting plasma insulin; FT3, free triiodothyronine; FT4, free thyroxine; TSH, thyroid-stimulating hormone; TPOAB, thyroid peroxidase antibody; NAFLD, nonalcoholic fatty liver disease.

(1.031, 1.347)], but neither hyperuricemia nor FINS, were all independently significant risk factors for the increased prevalence of TN in all subjects after additional adjusting for age, smoking, drinking status, and family history of thyroid disease. Additionally, the most pronounced sex disparity was found in the relationship between the prevalence of thyroid nodules and metabolic syndrome. After stratified analysis of gender, MetS [OR = 1.29, (1.092, 1.525)] and diabetes [OR = 1.47, (1.174, 1.841)] are still strongly and independently associated with the higher risks of TN in female subjects, but not in males (Figure 1).

4. Discussion

The prevalence of TN and the accompanying thyroid tumors are the increasing public health problems [1, 28, 29].

Guo et al. [30] reported the population aged over 40 years had a higher prevalence (46.6%) of TN previously. Our cross-sectional study was performed in a large community-based population in rural China. Among men and women aged over 45 years, the prevalence of TN was one-third higher in women than in men (38.5% versus 26%, resp.). This frequency was higher with advancing age, among females and in subjects with insulin resistance. But, up to now, the mechanisms of the higher prevalence of TN in females as compared to the males are not completely understood. So we investigated the prevalence of TN in different levels of MetS components and examined whether MetS components and the associated metabolic risk factors contributed to the pathogenesis of TN in male and female subjects, respectively. Our results were partially comparable to previous studies, suggesting that females and the elderly were all risk factors for TN [18, 31, 32]. Moreover, we found that diabetes and MetS were independent risk factors for TN after adjusting for age, smoking, and alcohol consumption only in female subjects, but not in males.

Metabolic syndrome is a complex clinical disorder characterized by dyslipidemia, obesity, NAFLD, insulin resistance, hyperuricemia, and a disturbance of glucose metabolism. In our study, to further explore whether MetS components and the other metabolic risk parameters related to the pathogenesis of TN in subjects, all subjects were divided into different subgroups according to different metabolic status. Nearly 35.3% of subjects with MetS had TN. The results showed that the subjects with TN had significantly higher levels of FPG, PPG, HbA1c, FINS, HOMA-IR, HOMA-beta, and TPOAB than those without TN after adjusting for age. However, in addition to the above findings, after further stratified analysis of gender, there were still significant differences of FPG, PPG, FINS, HOMA-IR, and TSH between the groups with or without TN in females, but not in males. The females with hyperuricemia, NAFLD, or MetS had much higher prevalence of TN as compared with controls, whereas there were no such associations in males. Perhaps the most intriguing finding of our study was that the MetS were significantly associated with TN only in women. The one plausible explanation for this gender disparity in TN formation was the hormone testosterone, which might contribute to the protective roles against the harmful effects of MetS cluster in men compared to women. We concluded from our data that the prevalence of TN was more closely associated with the components of MetS in women than in men. Female subjects with MetS were at increased risk for TN. Few studies assessed gender disparity in the pathogenesis of TN formation [33]. The gender dichotomy of MetS-induced TN formation may underlie the increased propensity to TN in women. The gender differences observed in this study contributed to an increased theoretical understanding of TN in MetS and might suggest future studies into the sex-specific pathophysiology of TN in MetS, which remains to be further determined. Clinically, awareness of gender differences in the relationship between thyroid nodules and the components of MetS might help to detect TN in women with MetS. Therefore, better intervention strategies against the components of MetS might be performed to reduce the risks of TN occurrence.

Researchers have recently focused their interest on the pathogenesis of TN in subjects with abnormal glucose metabolism [6, 34]; however, the mechanisms facilitating TN in individuals with impaired glucose metabolism have not been investigated thoroughly [5]. In previous studies, strong correlations between thyroid volume, BMI, and WC were demonstrated [8, 16, 35–37]. Because the fat deposition in abdomen was linked to IR and MetS, the prevalence of TN in patients with central obesity or IR, which were the high risk states for development of diabetes, were significantly higher than that of controls in total subjects in our study. Ayturk et al. [38] discovered that IR was an independent risk factor for TN formation in iodine-sufficient areas, but the pathophysiologic mechanisms for the increased risk were still not fully understood. It has been reported that metformin which could improve IR might result in a significant decrease in the nodular size in patients with IR [39]. Nonetheless, there was limited data about the interaction between insulin resistance and the pathogenesis of TN [11, 40]. In this study, the prevalence of TN in diabetes group was 37.2%, which was significantly higher than 31.4% in the prediabetes and 29.9% in normal glucose tolerance (NGR). IR as an important metabolic factor in the development of the diabetes may have had an impact on the incidence of TN. We also found the risks of prevalence of TN were increased by 1.384 times in male and 1.267 times in female, with IR, respectively. It has been indicated that insulin receptors were overexpressed in most thyroid tumors. All these findings suggested the level of IR was the key factor most independently and strongly correlated with TN in all subjects. After stratified analysis of gender, MetS and diabetes were still strongly and independently associated with the higher risks of TN in female subjects, but not in males. These results indicated that there is a need for better understanding of gender disparity in the relationship between prevalence of TN and MetS components. Additional studies are required to discern how these findings may impact future research, diagnosis, and treatment of TN.

Recently, extensive studies have found the roles of NAFLD and hyperuricemia in IR. Up to now, we were unable to find any published studies to explore the role of NAFLD in pathogenesis of TN in a large population [41, 42]. The literature about the relationships between NAFLD, hyperuricemia, and TN remains scant. Concerns have been given to the relationship between hyperuricemia, inflammation, and IR recently. Since others have shown positive correlations between the levels of UA and IR [40], we inferred that the hyperuricemia may lead to the formation of thyroid nodules. The results of our study also showed that the prevalence of TN with hyperuricemia and NAFLD groups was statistically significantly higher in females. It has previously been reported that NAFLD and hyperuricemia, which by themselves are risk factors for the activation of inflammation pathways, share many predisposing metabolic risk factors with IR [43, 44]. We tentatively put forward that IR, hyperuricemia, NAFLD, and MetS might play the important roles in TN formation. Therefore, in female subjects with IR, NAFLD, hyperuricemia, or MetS, more attention should be paid to the early and the timely medical management.

Ayturk et al. reported that higher serum TSH level was an independent risk factor for increased thyroid volume in MetS patients but failed to find the relationship between TSH and TN formation [38]. In our study, regarding free thyroid hormones, results appeared contradictory at TN prevalence. Higher FT3 and serum thyroid-stimulating hormone levels were related to a decreased risk of TN in female subjects, while higher FT4 level was related to an increased risk of TN in male subjects. A recent study reported that FT3 and FT3/FT4 were positively related to BMI, waist, TG, and FPG, while FT4 was negatively related to the above metabolic parameters [45]. Few studies have explored this apparent paradox between the free THs (thyroid hormones) and TN. Taken together, although the difference of the study populations might be responsible for the above inconsistency, it was still difficult to explain the independent association between TN formation and the free THs levels. A possible explanation could be that free T3 and free T4 might be affecting the prevalence of MetS in opposite ways [45–47]. In addition, our study should be acknowledged with several potential limitations. This study was cross-sectional in design and therefore no causal inferences can be drawn. Although we found different levels of SBP, UA, HOMA-IR, FT3, and FT4 as well as plasm glucose between subjects with or without TN, it was still hard to get any causal relationships. Furthermore, the findings of single-centre study could not have been used to all TN population regarding urbanization, economic development, and geographic distribution. Given these findings, prospective studies on a larger scale are required to clarify the causal associations of MetS, IR, and hyperuricemia with TN in subjects. Therefore, the early integrated intervention involving uric acid-lowering, lipid-regulating therapy, and insulin-sensitizing medication might more effectively delay the formation of TN than either intervention alone in women with MetS.

5. Conclusion

Although the components of metabolic syndrome lie among the risk factors for TN both in men and women, our results suggested that MetS components had the much stronger effects on the risk of TN in women than in men. In conclusion, age, gender, IR, MetS, and abnormal glucose metabolic status as well as hyperuricemia independently played the important roles in the pathological mechanisms of thyroid nodules. The prevalence of TN in female patients with MetS was significantly increased, which was significantly associated with the different levels of MetS components. The prevalence of TN in DM group was significantly higher than those in NGR and prediabetes groups only in females. The right managements of MetS aimed to adjust hyperuricemia, central obesity, abnormal glucose metabolism, and IR might be beneficial in the blocking of TN formation, especially in females. Our data supported the possible metabolic clues to the gender disparity of nodule formation. Hence, in the future, more cross-sectional and long-term cohort multicenter study on a large scale will be necessary to further verify and clarify the findings in this study.

Abbreviations

WHR: Waist-to-hip ratio
SBP: Systolic blood pressure
DBP: Diastolic blood pressure
BMI: Body mass index
WC: Waist circumference
HC: Hip circumference
NAFLD: Nonalcoholic fatty liver disease
TCH: Total cholesterol
TG: Triglyceride
HDL-C: High-density lipoprotein cholesterol
LDL-C: Low-density lipoprotein cholesterol
UA: Uric acid
FPG: Fasting plasma glucose
PPG: Postprandial plasma glucose
HbA1c: Hemoglobin A1c
FINS: Fasting plasma insulin
NGR: Normal glucose regulation
NAFLD: Nonalcoholic fatty liver disease
MetS: Metabolic syndrome
FT3: Free triiodothyronine
FT4: Free thyroxine
TSH: Thyroid-stimulating hormone
TPOAB: Thyroid peroxidase antibody.

Conflicts of Interest

The authors declare that there are no conflicts of interest.

Authors' Contributions

Xiaoying Ding, Ying Xu, and Yufan Wang contributed equally to this work.

Acknowledgments

The study was supported by grants from the Shanghai Shenkang Hospital Development Center for chronic disease prevention and control project (SHDC12015304), the Shanghai municipal health bureau key project fund (201440033), 2015 Wang Kuancheng medicine fund, 2015 Shanghai General Hospital Excellent physician project, the Songjiang district health bureau medical climbing project (0702N14003), and The science and technology committee project of Songjiang district (15SJGG54). The authors thank all the study participants and all the research staff for their participation and contribution.

References

[1] G. Pellegriti, F. Frasca, C. Regalbuto, S. Squatrito, and R. Vigneri, "Worldwide increasing incidence of thyroid cancer: update on epidemiology and risk factors," *Journal of Cancer Epidemiology*, vol. 2013, Article ID 965212, 10 pages, 2013.

[2] L.-Z. He, T.-S. Zeng, L. Pu, S.-X. Pan, W.-F. Xia, and L.-L. Chen, "Thyroid hormones, autoantibodies, ultrasonography, and clinical parameters for predicting thyroid cancer," *International*

Journal of Endocrinology, vol. 2016, Article ID 8215834, 11 pages, 2016.

[3] I. S. Nam-Goong, H. Y. Kim, G. Gong et al., "Ultrasonography-guided fine-needle aspiration of thyroid incidentaloma: correlation with pathological findings," *Clinical Endocrinology*, vol. 60, no. 1, pp. 21–28, 2004.

[4] E. Papini, R. Guglielmi, A. Bianchini et al., "Risk of malignancy in nonpalpable thyroid nodules: predictive value of ultrasound and color-doppler features," *Journal of Clinical Endocrinology and Metabolism*, vol. 87, no. 5, pp. 1941–1946, 2002.

[5] C. Anil, A. Akkurt, S. Ayturk, A. Kut, and A. Gursoy, "Impaired glucose metabolism is a risk factor for increased thyroid volume and nodule prevalence in a mild-to-moderate iodine deficient area," *Metabolism: Clinical and Experimental*, vol. 62, no. 7, pp. 970–975, 2013.

[6] Y. Yeo, S. H. Ma, Y. Hwang et al., "Diabetes mellitus and risk of thyroid cancer: a meta-analysis," *PLoS ONE*, vol. 9, no. 6, Article ID e98135, 2014.

[7] A. O. Duran, C. Anil, A. Gursoy et al., "Thyroid volume in patients with glucose metabolism disorders," *Arquivos Brasileiros de Endocrinologia e Metabologia*, vol. 58, no. 8, pp. 824–827, 2014.

[8] A. Arduc, B. A. Dogan, M. M. Tuna et al., "Higher body mass index and larger waist circumference may be predictors of thyroid carcinoma in patients with Hürthle-cell lesion/neoplasm fine-needle aspiration diagnosis," *Clinical Endocrinology*, vol. 83, no. 3, pp. 405–411, 2015.

[9] W. Xu, Z. Chen, and N. Li, "Relationship of anthropometric measurements to thyroid nodules in a Chinese population," *BMJ Open*, vol. 5, no. 12, Article ID e008452, 2015.

[10] P. A. Sousa, M. Vaisman, J. R. Carneiro et al., "Prevalence of goiter and thyroid nodular disease in patients with class III obesity," *Arq Bras Endocrinol Metabol*, vol. 57, no. 2, pp. 120–125, 2013.

[11] Z. Heidari, M. A. Mashhadi, and S. Nosratzehi, "Insulin resistance in patients with benign thyroid nodules," *Archives of Iranian Medicine*, vol. 18, no. 9, pp. 572–576, 2015.

[12] J. Shin, M.-H. Kim, K.-H. Yoon, M.-I. Kang, B.-Y. Cha, and D.-J. Lim, "Relationship between metabolic syndrome and thyroid nodules in healthy Koreans," *Korean Journal of Internal Medicine*, vol. 31, no. 1, pp. 98–105, 2016.

[13] E. Blanc, C. Ponce, D. Brodschi et al., "Association between worse metabolic control and increased thyroid volume and nodular disease in elderly adults with metabolic syndrome," *Metabolic Syndrome and Related Disorders*, vol. 13, no. 5, pp. 221–226, 2015.

[14] C. Anil, A. Kut, B. Atesagaoglu, A. Nar, N. B. Tutuncu, and A. Gursoy, "Metformin decreases thyroid volume and nodule size in subjects with insulin resistance: A Preliminary Study," *Medical Principles and Practice*, vol. 25, no. 3, pp. 233–236, 2016.

[15] M. Karimifar, A. Aminorroaya, M. Amini et al., "Effect of metformin on thyroid stimulating hormone and thyroid volume in patients with prediabetes: a randomized placebo-controlled clinical trial," *Journal of Research in Medical Sciences*, vol. 19, no. 11, pp. 1019–1026, 2014.

[16] J. Yin, C. Wang, Q. Shao et al., "Relationship between the prevalence of thyroid nodules and metabolic syndrome in the iodine-adequate area of Hangzhou, China: a cross-sectional and cohort study," *International Journal of Endocrinology*, vol. 2014, Article ID 675796, 7 pages, 2014.

[17] H. Jiang, Y. Tian, W. Yan et al., "The prevalence of thyroid nodules and an analysis of related lifestyle factors in Beijing communities," *International Journal of Environmental Research and Public Health*, vol. 13, no. 4, article no. 442, 2016.

[18] N. Kwong, M. Medici, T. E. Angell et al., "The influence of patient age on thyroid nodule formation, multinodularity, and thyroid cancer risk," *Journal of Clinical Endocrinology and Metabolism*, vol. 100, no. 12, pp. 4434–4440, 2015.

[19] K. G. M. M. Alberti, P. Zimmet, and J. Shaw, "The metabolic syndrome—a new worldwide definition," *The Lancet*, vol. 366, no. 9491, pp. 1059–1062, 2005.

[20] Y. Xu, L. Wang, and J. He, "Prevalence and control of diabetes in Chinese adults," *JAMA*, vol. 310, no. 9, pp. 948–959, 2013.

[21] American Diabetes Association, "Diagnosis and classification of diabetes mellitus," *Diabetes Care*, vol. 34, supplement 1, pp. S62–S69, 2011.

[22] WHO, "Obesity: preventing and managing the global epidemic. Report of a WHO consultation," World Health Organization Technical Report Series 894, 2000.

[23] W. Jia, "Status of insulin resistance in Chinese population," *International Journal of Endocrinology and Metabolism*, vol. 22, no. 4, p. 264, 2002.

[24] D. I. Feig, D.-H. Kang, and R. J. Johnson, "Medical progress: uric acid and cardiovascular risk," *New England Journal of Medicine*, vol. 359, no. 17, pp. 1811–1821, 2008.

[25] D. S. Cooper, G. M. Doherty, B. R. Haugen et al., "Revised American thyroid association management guidelines for patients with thyroid nodules and differentiated thyroid cancer," *Thyroid*, vol. 19, no. 11, pp. 1167–1214, 2009.

[26] F. Jian-gao, "Guidelines for management of nonalcoholic fatty liver disease: an updated and revised edition," *Chinese Journal of Hepatology*, vol. 18, no. 3, pp. 163–166, 2010.

[27] M. D. Zeng, J. G. Fan, L. G. Lu et al., "Guidelines for the diagnosis and treatment of nonalcoholic fatty liver diseases," *Journal of Digestive Diseases*, vol. 9, no. 2, pp. 108–112, 2008.

[28] S. R. Bomeli, S. O. LeBeau, and R. L. Ferris, "Evaluation of a thyroid nodule," *Otolaryngologic Clinics of North America*, vol. 43, no. 2, pp. 229–238, 2010.

[29] L. G. T. Morris, A. G. Sikora, T. D. Tosteson, and L. Davies, "The increasing incidence of thyroid cancer: the influence of access to care," *Thyroid*, vol. 23, no. 7, pp. 885–891, 2013.

[30] H. Guo, M. Sun, W. He et al., "The prevalence of thyroid nodules and its relationship with metabolic parameters in a Chinese community-based population aged over 40 years," *Endocrine*, vol. 45, no. 2, pp. 230–235, 2014.

[31] K. Kiseljak-Vassiliades and M. Xing, "Association of cigarette smoking with aberrant methylation of the tumor suppressor gene RARβ2 in papillary thyroid cancer," *Frontiers in Endocrinology*, vol. 2, article 99, 2011.

[32] Y. S. Balhara and K. Deb, "Impact of alcohol use on thyroid function," *Indian Journal of Endocrinology and Metabolism*, vol. 17, no. 4, pp. 580–587, 2013.

[33] L. J. Bessey, N. B. K. Lai, N. E. Coorough, H. Chen, and R. S. Sippel, "The incidence of thyroid cancer by fine needle aspiration varies by age and gender," *Journal of Surgical Research*, vol. 184, no. 2, pp. 761–765, 2013.

[34] B. Aschebrook-Kilfoy, M. M. Sabra, A. Brenner et al., "Diabetes and thyroid cancer risk in the national institutes of Health-AARP diet and health study," *Thyroid*, vol. 21, no. 9, pp. 957–963, 2011.

[35] S. Semiz, U. Şenol, O. Bircan, S. Gümüşlü, S. Bilmen, and I. Bircan, "Correlation between age, body size and thyroid volume in an endemic area," *Journal of Endocrinological Investigation*, vol. 24, no. 8, pp. 559–563, 2001.

[36] L. Hegedus, H. Perrild, L. R. Poulsen et al., "The determination of thyroid volume by ultrasound and its relationship to body weight, age, and sex in normal subjects," *Journal of Clinical Endocrinology and Metabolism*, vol. 56, no. 2, pp. 260–263, 1983.

[37] R. Sari, M. K. Balci, H. Altunbas, and U. Karayalcin, "The effect of body weight and weight loss on thyroid volume and function in obese women," *Clinical Endocrinology*, vol. 59, no. 2, pp. 258–262, 2003.

[38] S. Ayturk, A. Gursoy, A. Kut, C. Anil, A. Nar, and N. B. Tutuncu, "Metabolic syndrome and its components are associated with increased thyroid volume and nodule prevalence in a mild-to-moderate iodine-deficient area," *European Journal of Endocrinology*, vol. 161, no. 4, pp. 599–605, 2009.

[39] J. Rezzónico, M. Rezzónico, E. Pusiol, F. Pitoia, and H. Niepomniszcze, "Metformin treatment for small benign thyroid nodules in patients with insulin resistance," *Metabolic Syndrome and Related Disorders*, vol. 9, no. 1, pp. 69–75, 2011.

[40] J. N. Rezzónico, M. Rezzónico, E. Pusiol, F. Pitoia, and H. Niepomniszcze, "Increased prevalence of insulin resistance in patients with differentiated thyroid carcinoma," *Metabolic Syndrome and Related Disorders*, vol. 7, no. 4, pp. 375–380, 2009.

[41] T. Geach, "Thyroid function: poor thyroid function linked to NAFLD," *Nature Reviews Endocrinology*, vol. 12, no. 8, p. 434, 2016.

[42] Y. Nakade and M. Yoneda, "Relationship between non-alcoholic fatty liver disease and thyroid dysfunction," *Internal Medicine*, vol. 55, no. 15, pp. 1941–1942, 2016.

[43] F. Martinon, "Update on biology: uric acid and the activation of immune and inflammatory cells," *Current Rheumatology Reports*, vol. 12, no. 2, pp. 135–141, 2010.

[44] S. Becker, L. Dossus, and R. Kaaks, "Obesity related hyperinsulinaemia and hyperglycaemia and cancer development," *Archives of Physiology and Biochemistry*, vol. 115, no. 2, pp. 86–96, 2009.

[45] S. Jing, D. Xiaoying, X. Ying et al., "Different levels of thyroid hormones between impaired fasting glucose and impaired glucose tolerance: free T3 affects the prevalence of impaired fasting glucose and impaired glucose tolerance in opposite ways," *Clinical Endocrinology*, vol. 80, no. 6, pp. 890–898, 2014.

[46] Y. Ye, X. Gai, H. Xie, L. Jiao, and S. Zhang, "Association between serum free thyroxine (FT4) and uric acid levels in populations without overt thyroid dysfunction," *Annals of Clinical and Laboratory Science*, vol. 45, no. 1, pp. 49–53, 2015.

[47] G. L. Roef, E. R. Rietzschel, C. M. Van Daele et al., "Triiodothyronine and free thyroxine levels are differentially associated with metabolic profile and adiposity-related cardiovascular risk markers in euthyroid middle-aged subjects," *Thyroid*, vol. 24, no. 2, pp. 223–231, 2014.

Hindawi
Mediators of Inflammation
Volume 2017, Article ID 5032708, 6 pages
https://doi.org/10.1155/2017/5032708

Clinical Study

Comparison of Antidiabetic Medications during the Treatment of Atherosclerosis in T2DM Patients

Xiaojie Liu,[1,2] Tao Mei,[3] Wei Chen,[4] and Shandong Ye[1,5]

[1]*School of Medicine, Shandong University, Jinan, Shandong, China*
[2]*Department of Geriatrics, Anhui Provincial Hospital Affiliated to Anhui Medical University, Hefei, China*
[3]*Department of MEC, Anhui Provincial Hospital Affiliated to Anhui Medical University, Hefei, China*
[4]*Department of Nephrology, Anhui Provincial Hospital Affiliated to Anhui Medical University, Hefei, China*
[5]*Department of Endocrinology, Anhui Provincial Hospital Affiliated to Anhui Medical University, Hefei, China*

Correspondence should be addressed to Shandong Ye; ysdcwsd@163.com

Received 16 December 2016; Accepted 6 February 2017; Published 30 April 2017

Academic Editor: Yunzhou Dong

Type 2 diabetes is often associated with arterial atherosclerosis in large blood vessels. We set out to elucidate whether commonly used antidiabetic drugs metformin, sitagliptin, and pioglitazone will reduce atherosclerosis in T2DM patients. We enrolled 176 individuals with type 2 diabetes, which were divided into four treatment groups according to different oral drugs: metformin alone, sitagliptin alone, pioglitazone alone, or combination of metformin and sitagliptin. We assessed changes in glycometabolism, lipid metabolism, cytokine released, and carotid artery intima-media thickness as the readout for improvement in atherosclerosis. HbA1c levels were significantly decreased in all treatment groups ($p < 0.05$), and FBG levels were also decreased in metformin and combined groups ($p < 0.05$). In addition, we found IL-6 levels significantly decreased in all treatment groups ($p < 0.05$). Treatment with pioglitazone showed a significant increase in BMI, HDL, and ADPN levels ($p < 0.05$). We also observed a significant decrease in NHDL levels in the combined treatment group ($p < 0.05$). Our data revealed that in addition to hypoglycemic properties of metformin, sitagliptin, and pioglitazone, these drugs also have the potential to promote an anti-inflammatory response. Therefore, combination therapy may be more beneficial for reducing atherosclerosis in patients with type 2 diabetes. The clinical trial is registered with ChiCTR-ORC-17010835.

1. Introduction

Atherosclerosis is one of the most severe complications associated with Type 2 diabetes mellitus (T2DM), often progressing to myocardial infarction and cerebral stroke. Accordingly, atherosclerosis is an important cause of disability and mortality in T2DM patients [1]. Risk factors that contribute to the development of atherosclerosis include hyperglycemia, increased low density lipoprotein-cholesterol (LDL-C), and elevated triglyceride levels [2]. Previously, Ross et al. reported that an inflammatory response occurs during the development of atherosclerosis [3].

Inflammation associated with T2DM is performed mainly by the release of proinflammatory cytokines, such as Interleukin-6 (IL-6) and tumor necrosis factor-alpha (TNF-α), by multiple tissues. Meanwhile, the secretion of antiinsulin resistance cytokines, such as adiponectin (ADPN) and IL-10, is reduced [4]. Proinflammatory cytokines act upon vascular endothelial cells (VECs) leading to the reduction of nitric oxide (NO) production, followed by VEC damage [5]. In addition, these cytokines attract and promote the attachment of mononuclear cells, granular cells, and T cells to VECs, which lead to artery wall inflammation, followed by atherosclerosis [4, 5]. IL-6, which is produced by activated leucocytes, adipocytes, and VECs, is a crucial proinflammatory cytokine and can affect insulin sensitivity through multiple mechanisms. IL-6 level positively correlates with the degree of insulin resistance [6]. On the contrary, ADPN is secreted by adipose tissue and works as an insulin sensitive hormone. ADPN promotes fatty acid oxidation in hepatocytes and myocytes, suppresses

the production of inflammatory cytokines, protects VEC function, and reduces atherosclerosis [7].

The carotid artery is the most frequently affected blood vessel by atherosclerosis and also can serve as a window for the measurement. Early symptoms of atherosclerosis include increased thickness of intimal layer of the carotid artery. Measurement of carotid artery intima-media thickness (CCA-IMT) with ultrasonography is a safe approach for identifying and quantifying atherosclerosis in early clinical diagnosis.

The pathogenesis of T2DM is caused by damage to pancreatic islet β-cells and insulin resistance [8]. Metformin reduces hepatic glucose and increases insulin sensitivity of peripheral tissue thereby reducing insulin resistance. It can act on the AMP-activated protein kinase (AMPK) to modulate multiple energy pathways and promote lipid metabolism, which in turn alleviates atherosclerosis [9]. The DPP-4 inhibitor sitaglipin increases the secretion of insulin by enhancing the activities of glucagon-like peptide-1(GLP-1) and glucose-dependent insulinotropic polypeptide (GIP), delaying gastric emptying, and protecting islet β-cell function [10]. Previous studies have shown that sitagliptin decreases the production of proinflammatory cytokines, increases the biological availability of NO, and protects VECs, thus reducing the formation of atherosclerotic plaques [10, 11]. Pioglitazone is a highly selective PPARγ agonist. It can reduce the levels of fasting insulin, hemoglobin A1c (HbA1c), and the homeostasis model of assessment for insulin resistance index (HOMA-IR). In addition, key transcription factors involved in the inflammatory response, such as nuclear factor-kappa B (NF-κB) and activator protein-1 (AP-1), are suppressed by pioglitazone [12]. The purpose of this study is to investigate whether these antidiabetic drugs reduce atherosclerosis by measuring the activities of glycometabolism and lipid metabolism, release of inflammatory cytokines, and CCA-IMT.

2. Materials and Methods

2.1. Patients. We enrolled 176 T2DM patients (160 male and 16 female) at Anhui Provincial Hospital Medical Center (Hefei, China) during the period of January 2015 and November. All of the enrolled T2DM patients met the WHO-1999 T2DM diagnostic criteria. The duration of diabetes was 1–5 years. The following criteria were used for excluding patients: severe hepatic and kidney dysfunction; cardiac function grades 3-4; any systemic immune disorders; chronic inflammatory disease or tumor; severe diabetic complications; or an acute stress state within 2 months (surgical operation, active infection). Statin, ARB (angiotensin receptor blocker), and ACEI (angiotensin converting enzyme inhibitor) had not been taken. The protocol of this study was ethically approved by the Institutional Review Board of both Shandong University and Anhui Provincial Hospital in accordance with the Declaration of Helsinki.

2.2. Antidiabetic Medication Treatment Regimens. The 176 enrolled T2DM patients were divided into four treatment groups based on the type of antidiabetic treatment used: metformin group ($n = 77$), sitagliptin group ($n = 31$), pioglitazone group ($n = 40$), and combined treatment group ($n = 28$). For the metformin group, patients received oral administration of 1000–1500 mg of metformin daily. For the sitagliptin group, patients received oral administration of 100 mg of sitagliptin daily. For the pioglitazone group, patients received oral administration of 30 mg of pioglitazone daily. For the combined treatment group, patients received oral administration of 1000–1500 mg of metformin and 100 mg of sitagliptin daily. Dietary control and exercise options were provided.

2.3. Serum Cytokine ELISA. Serum was obtained from patient venous blood through centrifugation for 10 min at 1500 rpm and stored at −80°C prior to analysis. Serum IL-6 and ADPN levels were measured by enzyme-linked immunosorbent assay (ELISA) (R&D systems Minneapolis, MN, USA) according to the manufacturer's protocols.

2.4. Measurement of Carotid Artery Intima-Media Thickness (CCA-IMT). The CCA-IMT value is measured at the bifurcations of the bilateral common carotid within 10 mm, in three cardiac cycles for a total for six measurements. The average of the six measurements was used to calculate the CCA-IMT. Any CCA-IMT that is below 0.9 mm was not recorded.

2.5. Monitoring Parameters. Patients were assessed for fasting blood glucose (FBG), hemoglobin A1c (HbA1c), triglycerides (TG), total cholesterol (TC), low density lipoproteins (LDL), high density lipoproteins (HDL), uric acid (UA), creatinine (Cr), recorded systolic pressure (SBD), measured CCA-IMT, calculated body mass index (BMI), and non-high density lipoproteins (NHDL, where NHDL = TC-HDL) at enrollment to determine baseline and subsequently reassessed following 12 months treatment. When TC level is in 2.3–5.6 mmol/L or LDL level is not high, international lipid guidelines recommend NHDL for lipid monitoring [13], especially in patients with T2DM.

2.6. Statistics. All statistical analysis was carried out using Graphpad and Excel using Student's t-test (two-tailed). Differences between multigroups were compared using one-way ANOVA.

3. Results

We did not observe hypoglycemia at the endpoint of the study, although 13 patients opted out due to poor blood glucose control. We compared and analyzed the parameters of four groups (Tables 1–4). We found that HbA1c levels were significantly decreased in all four treatment groups (Figure 1, $p < 0.05$), which indicates that all three antidiabetic agents show good efficacy. FBG levels were significantly decreased in both the metformin group and the combined treatment group (Figure 2, $p < 0.05$), which suggests metformin is beneficial for T2DM that inhibited elevated FBG levels. We found IL-6 levels were significantly decreased in all four treatment groups (Figure 3, $p < 0.05$), which indicates that each of the antidiabetic drugs has anti-inflammatory

Table 1: Metabolic group parameters of patients at the beginning and at the end of the study.

Parameters	Beginning ($n = 77$)	End ($n = 71$)	P
FBG (mmol/L)	7.54 ± 1.77	7.00 ± 1.25	0.04
SBP (mmHg)	131.36 ± 15.25	131.46 ± 14.27	0.97
HbA1c (%)	6.80 ± 0.99	6.46 ± 0.77	0.03
BMI (kg/m^2)	28.35 ± 2.19	27.91 ± 1.99	0.20
TC (mmol/L)	4.69 ± 0.91	4.51 ± 0.75	0.19
TG (mmol/L)	2.19 ± 1.82	2.03 ± 1.33	0.55
NHDL (mmol/L)	3.75 ± 0.91	3.47 ± 0.77	0.06
HDL (mmol/L)	0.99 ± 0.21	1.03 ± 0.18	0.29
LDL (mmol/L)	2.75 ± 0.78	2.57 ± 0.82	0.21
UA (μmol/L)	336.29 ± 90.55	324.77 ± 92.08	0.44
IMT (mm)	1.22 ± 0.14	1.16 ± 0.14	0.07
Cr (μmol/L)	84.90 ± 14.18	85.96 ± 14.43	0.65
IL-6 (pg/mL)	14.59 ± 5.95	12.63 ± 5.45	0.04
ADPN (ng/mL)	12.18 ± 3.79	13.06 ± 3.80	0.16

Table 2: Combined treatment group parameters of patients at the beginning and at the end of the study.

Parameters	Beginning ($n = 28$)	End ($n = 26$)	P
FBG (mmol/L)	7.14 ± 1.39	6.38 ± 1.31	0.04
SBP (mmHg)	132.36 ± 15.52	133.35 ± 18.70	0.83
HbA1c (%)	7.32 ± 0.91	6.64 ± 1.08	0.02
BMI (kg/m^2)	29.53 ± 2.02	28.63 ± 1.51	0.07
TC (mmol/L)	4.50 ± 0.64	4.35 ± 0.57	0.37
TG (mmol/L)	2.23 ± 1.81	2.06 ± 1.66	0.72
NHDL (mmol/L)	3.89 ± 0.85	3.25 ± 1.10	0.03
HDL (mmol/L)	1.01 ± 0.24	1.08 ± 0.28	0.46
LDL (mmol/L)	2.64 ± 0.76	2.36 ± 0.67	0.18
UA (μmol/L)	351.18 ± 87.69	345.35 ± 79.11	0.80
IMT (mm)	1.27 ± 0.12	1.15 ± 0.15	0.05
Cr (μmol/L)	87.29 ± 12.72	90.31 ± 11.65	0.37
IL-6 (pg/mL)	18.70 ± 5.28	15.18 ± 5.18	0.02
ADPN (ng/mL)	11.02 ± 3.40	11.93 ± 3.40	0.33

Table 3: Sitagliptin group parameters of patients at the beginning and at the end of the study.

Parameters	Beginning ($n = 31$)	End ($n = 29$)	P
FBG (mmol/L)	7.59 ± 1.98	7.03 ± 1.93	0.27
SBP (mmHg)	132.87 ± 16.65	137.66 ± 13.10	0.22
HbA1c (%)	7.14 ± 1.16	6.50 ± 0.70	0.03
BMI (kg/m^2)	22.02 ± 1.14	21.93 ± 1.24	0.77
TC (mmol/L)	4.81 ± 0.94	4.56 ± 1.02	0.33
TG (mmol/L)	1.43 ± 1.14	1.36 ± 0.92	0.79
NHDL (mmol/L)	3.68 ± 0.90	3.20 ± 1.48	0.29
HDL (mmol/L)	1.00 ± 0.23	1.09 ± 0.25	0.30
LDL (mmol/L)	2.65 ± 0.87	2.53 ± 0.76	0.64
UA (μmol/L)	377.65 ± 81.56	379.00 ± 72.47	0.95
IMT (mm)	1.18 ± 0.16	1.15 ± 0.10	0.59
Cr (μmol/L)	87.35 ± 13.62	86.72 ± 16.82	0.87
IL-6 (pg/mL)	15.82 ± 6.20	12.78 ± 4.30	0.03
ADPN (ng/mL)	11.73 ± 3.67	12.15 ± 3.97	0.67

Table 4: Pioglitazone group parameters of patients at the beginning and at the end of the study.

Parameters	Beginning ($n = 40$)	End ($n = 37$)	P
FBG (mmol/L)	7.64 ± 1.99	7.14 ± 1.62	0.23
SBP (mmHg)	137.88 ± 16.89	137.44 ± 19.38	0.92
HbA1c (%)	6.94 ± 0.91	6.45 ± 0.70	0.04
BMI (kg/m^2)	25.94 ± 1.45	26.99 ± 1.87	0.01
TC (mmol/L)	4.61 ± 0.91	4.55 ± 0.79	0.75
TG (mmol/L)	1.88 ± 1.44	1.90 ± 1.44	0.95
NHDL (mmol/L)	3.68 ± 0.92	3.40 ± 1.32	0.37
HDL (mmol/L)	1.01 ± 0.24	1.16 ± 0.23	0.02
LDL (mmol/L)	2.69 ± 0.96	2.52 ± 0.76	0.42
UA (μmol/L)	371.28 ± 73.87	370.76 ± 75.33	0.98
IMT (mm)	1.20 ± 0.14	1.16 ± 0.12	0.26
Cr (μmol/L)	84.48 ± 15.06	82.43 ± 13.49	0.53
IL-6 (pg/mL)	14.32 ± 3.97	12.27 ± 3.91	0.03
ADPN (ng/mL)	11.77 ± 3.36	14.06 ± 4.44	0.01

property. In addition, we observed a significant decrease in NHDL levels in the combined treatment group (Figure 4, $p < 0.05$) but not in any of the single agent groups, which suggests combination treatment of metformin with sitagliptin offers additional benefits in modulating lipid metabolism. Finally, we found that BMI, HDL, and ADPN levels were significantly increased in the pioglitazone group (Figures 5–7, $p < 0.05$), which demonstrates that improved lipid metabolism and weight gain are effects of pioglitazone treatment. When IL-6 declining levels were compared in different treatment groups, no significant difference was found between each treatment group. In addition, we did not observe significant improvement of blood pressure and uric acid levels in patients.

4. Discussion

Our results suggest that all three antidiabetic treatments, metformin, sitagliptin, and pioglitazone, showed efficacy in reducing blood glucose levels. Metformin effectively reduced the level of HbA1C. Metformin has been considered as the first line of treatment for T2DM in many countries [14]. Although many studies have found that metformin could decrease the BMI in T2DM patients, we were unable to observe the same phenomenon in this study. This may be due to the notion that metformin-mediated weight loss is more prominent during the early stages of treatment, whereas the T2DM patients in our study had already been prescribed metformin for more than one year.

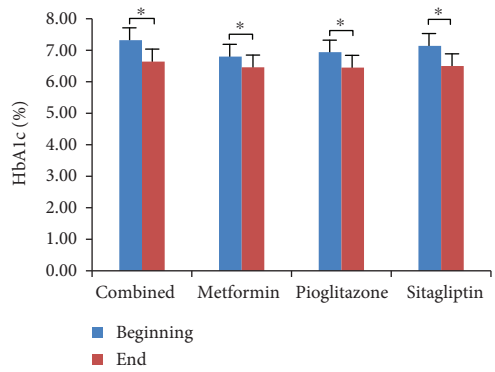

Figure 1: Comparison of HbA1c levels in four treatment groups. Serum HbA1c was measured by high efficiency liquid chromatography (HPLC). Data were shown as mean ± SD. HbA1c levels are significantly decreased in each treatment group ($^*p < 0.05$).

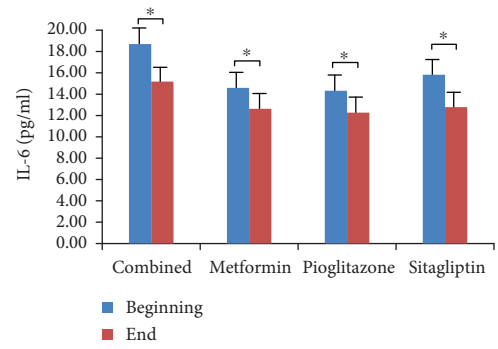

Figure 3: Comparison of IL-6 levels in each treatment group. Determination of serum IL-6 was by ELISA. Data were shown as mean ± SD. IL-6 levels are significantly reduced in all four groups ($^*p < 0.05$).

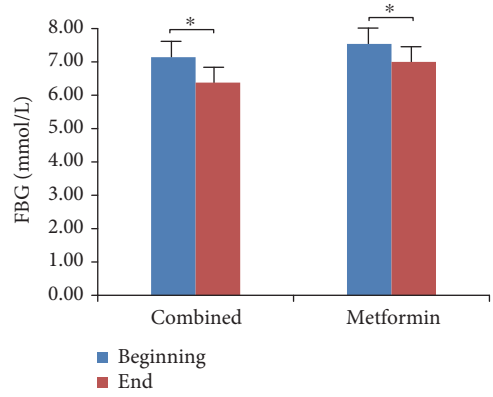

Figure 2: Comparison of FBG levels in metformin and combined treatment groups. Detection of FBG wanted patients with fasting 8 hours or more. Data were shown as mean ± SD. FBG levels are significantly decreased in both the metformin group and the combined treatment group ($^*p < 0.05$).

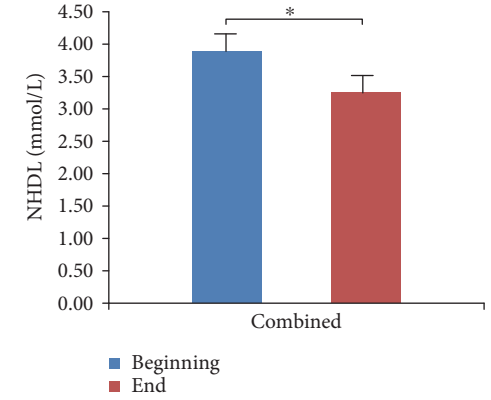

Figure 4: Comparison of NHDL levels in the combined treatment group. NHDL was obtained from TC-HDL. Data were shown as mean ± SD. NHDL levels are decreased in the combined treatment group ($^*p < 0.05$).

The DPP-4 inhibitor, sitagliptin, is a novel antidiabetic treatment with the ability to reduce postprandial blood glucose levels and maintain glucagon levels, improving the sensitivity of pancreatic α-cells to changes in blood glucose levels [15]. Two meta-analyses studies assessing how DPP-4 inhibitors influence blood lipid levels showed that they could decrease TG and TC levels but failed to improve HDL level [16, 17]. In addition, these studies imply that DPP-4 inhibitors do not directly act upon blood lipid metabolism, rather DPP-4 inhibitors activate the sympathetic nervous system and thus increase fat mobilization and oxidation [16, 17]. In our study, we did not observe a change in blood lipid level in the sitagliptin treatment group. This could be due to small sample size and short treatment duration. While metformin treatment or sitagliptin treatment alone did not decrease NHDL, combined metformin and sitagliptin treatment significantly decreased NHDL. Further investigation is warranted to elucidate the molecular mechanism of this combination efficacy on decreasing NHDL. Interestingly, a previous report identified that metformin could increase GLP-1 levels, which augmented the effects of DPP-4 inhibitors [18]. Here, we show that combined metformin and sitaglipin treatment is beneficial for T2DM patient in terms of HbA1c, NHDL, and IL-6 levels.

It has been previously demonstrated that pioglitazone treatment leads to an increase of lipoprotein lipase (LPL) expression and the acceleration of triglyceride degradation by activating PPAR-γ. Pioglitazone can also partially activate PPAR-α, which leads to effect similar to fibrates and an increase of HDL-C [19]. We did not observe an improvement of CCA-IMT in any of the treatment groups, which could be due to the short treatment duration and less severity of the atherosclerosis in the enrolled patient population.

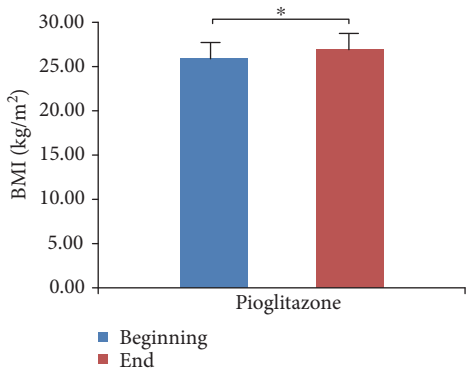

Figure 5: Comparison of BMI in pioglitazone treatment group. BMI = weight (kg)/height (m^2). Data were shown as mean ± SD. BMI is significantly increased in the pioglitazone group ($^*p < 0.05$).

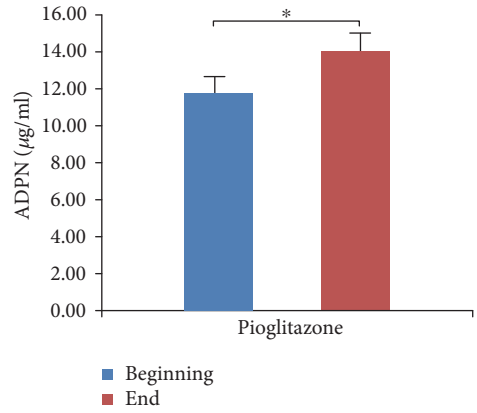

Figure 7: ADPN levels in the pioglitazone treatment group. Determination of serum ADPN was by ELISA. Data were shown as mean ± SD. ADPN levels are significantly increased in the pioglitazone group ($^*p < 0.05$).

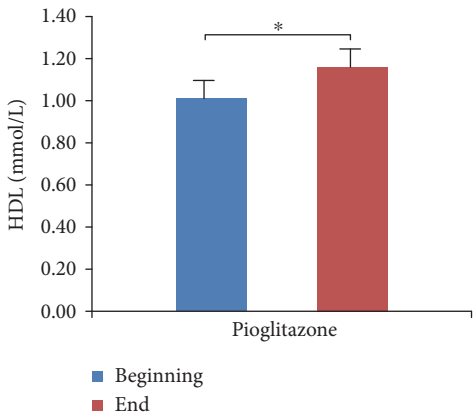

Figure 6: Comparison of HDL levels in the pioglitazone treatment group. Data were shown as mean ± SD. HDL levels are significantly increased in the pioglitazone group ($^*p < 0.05$).

5. Conclusion

Taken together, our study demonstrates that metformin, sitagliptin, and pioglitazone all showed safety and efficacy in reducing blood glucose levels, as well as in promoting an anti-inflammatory effect. Our results suggest that combined metformin and sitagliptin treatment may be more beneficial for the improvement of atherosclerosis in patients with T2DM; however, further studies would need to be performed that are extended in duration or recruit a patient population showing signs of increased CCA-IMT prior to treatment to potentially observe an effect directly on development of atherosclerosis.

Conflicts of Interest

The authors declare no conflict of interest regarding the publication of this paper.

References

[1] S. Y. Rhee and Y. S. Kim, "Peripheral arterial disease in patients with type 2 diabetes mellitus," *Diabetes and Metabolism Journal*, vol. 39, no. 4, pp. 283–290, 2015.

[2] N. A. Kotb, R. Gaber, M. Salama, H. M. Nagy, and A. Elhendy, "Clinical and biochemical predictors of increased carotid intima-media thickness in overweight and obese adolescents with type 2 diabetes," *Diabetes & Vascular Disease Research*, vol. 9, no. 1, pp. 35–41, 2012.

[3] R. Ross, "Atherosclerosis—an inflammatory disease," *The New England Journal of Medicine*, vol. 340, no. 2, pp. 115–126, 1999.

[4] T. Mazurek and G. Opolski, "Pericoronary adipose tissue: a novel therapeutic target in obesity-related coronary atherosclerosis," *Journal of the American College of Nutrition*, vol. 34, no. 3, pp. 244–254, 2015.

[5] K. Smitka and D. Maresova, "Adipose tissue as an endocrine organ: an update on pro-inflammatory and anti-inflammatory microenvironment," *Prague Medical Report*, vol. 116, no. 2, pp. 87–111, 2015.

[6] H. Mukumoto, Y. Takahashi, M. Ando, M. Nishikawa, and Y. Takakura, "Expression profile-dependent improvement of insulin sensitivity by gene delivery of interleukin-6 in a mouse model of type II diabetes," *Molecular Pharmaceutics*, vol. 10, no. 10, pp. 3812–3821, 2013.

[7] R. S. Lindsay, T. Funahashi, R. L. Hanson et al., "Adiponectin and development of type 2 diabetes in the pima Indian population," *Lancet*, vol. 360, no. 9326, pp. 57–58, 2002.

[8] V. T. Samuel and G. I. Shulman, "The pathogenesis of insulin resistance: integrating signaling pathways and substrate flux," *The Journal of Clinical Investigation*, vol. 126, no. 1, pp. 12–22, 2016.

[9] W. Y. Shi, D. Xiao, L. Wang et al., "Therapeutic metformin/AMPK activation blocked lymphoma cell growth via inhibition of mTOR pathway and induction of autophagy," *Cell Death and Disease*, vol. 3, article e275 2041 4889, 2012.

[10] J. Koska, M. Sands, C. Burciu, and P. Reaven, "Cardiovascular effects of dipeptidyl peptidase-4 inhibitors in patients with type 2 diabetes," *Diabetes & Vascular Disease Research*, vol. 12, no. 3, pp. 154–163, 2015.

[11] A. Makdissi, H. Ghanim, M. Vora et al., "Sitagliptin exerts an antinflammatory action," *The Journal of Clinical Endocrinology and Metabolism*, vol. 97, no. 9, pp. 3333–3341, 2012.

[12] M. Ricote, A. C. Li, T. M. Willson, C. J. Kelly, and C. K. Glass, "The peroxisome proliferator-activated receptor-gamma is a negative regulator of macrophage activation," *Nature*, vol. 391, no. 6662, pp. 79–82, 1998.

[13] T. A. Jacobson, M. K. Ito, K. C. Maki et al., "National lipid association recommendations for patient-centered management of dyslipidemia: part 1—full report," *Journal of Clinical Lipidology*, vol. 9, no. 2, pp. 129–169, 2015.

[14] S. E. Inzucchi, R. M. Bergenstal, J. B. Buse et al., "Management of hyperglycemia in type 2 diabetes: a patient-centered approach: position statement of the American Diabetes Association (ADA) and the European Association for the Study of Diabetes (EASD)," *Diabetes Care*, vol. 35, no. 6, pp. 1364–1379, 2012.

[15] M. Barbieri, M. R. Rizzo, R. Marfella et al., "Decreased carotid atherosclerotic process by control of daily acute glucose fluctuations in diabetic patients treated by DPP-IV inhibitors," *Atherosclerosis*, vol. 227, no. 2, pp. 349–354, 2013.

[16] M. Monami, C. Lamanna, C. M. Desideri, and E. Mannucci, "DPP-4 inhibitors and lipids: systematic review and meta-analysis," *Advances in Therapy*, vol. 29, no. 1, pp. 14–25, 2012.

[17] M. Terasaki, M. Nagashima, T. Watanabe et al., "Effects of PKF275-055, a dipeptidyl peptidase-4 inhibitor, on the development of atherosclerotic lesions in apolipoprotein E-null mice," *Metabolism*, vol. 61, no. 7, pp. 974–977, 2012.

[18] Y. Liu and T. Hong, "Combination therapy of dipeptidyl peptidase-4 inhibitors and metformin in type 2 diabetes: rationale and evidence," *Diabetes, Obesity & Metabolism*, vol. 16, no. 2, pp. 111–117, 2014.

[19] U. Khanderia, R. Pop-Busui, and K. A. Eagle, "Thiazolidinediones in type 2 diabetes: a cardiology perspective," *The Annals of Pharmacotherapy*, vol. 42, no. 10, pp. 1466–1474, 2008.

Hindawi
Mediators of Inflammation
Volume 2017, Article ID 4803156, 9 pages
https://doi.org/10.1155/2017/4803156

Research Article

The Metabolic Syndrome, Inflammation, and Colorectal Cancer Risk: An Evaluation of Large Panels of Plasma Protein Markers Using Repeated, Prediagnostic Samples

Sophia Harlid, Robin Myte, and Bethany Van Guelpen

Department of Radiation Sciences, Oncology, Umeå University, Umeå, Sweden

Correspondence should be addressed to Bethany Van Guelpen; bethany.vanguelpen@umu.se

Received 15 December 2016; Accepted 27 February 2017; Published 22 March 2017

Academic Editor: Shengzhong Duan

Metabolic syndrome (MetS), a set of metabolic risk factors including obesity, dysglycemia, and dyslipidemia, is associated with increased colorectal cancer (CRC) risk. A putative biological mechanism is chronic, low-grade inflammation, both a feature of MetS and a CRC risk factor. However, excess body fat also induces a proinflammatory state and increases CRC risk. In order to explore the relationship between MetS, body size, inflammation, and CRC, we studied large panels of inflammatory and cancer biomarkers. We included 138 participants from the Västerbotten Intervention Programme with repeated sampling occasions, 10 years apart. Plasma samples were analyzed for 178 protein markers by proximity extension assay. To identify associations between plasma protein levels and MetS components, linear mixed models were fitted for each protein. Twelve proteins were associated with at least one MetS component, six of which were associated with MetS score. MetS alone was not related to any protein. Instead, BMI displayed by far the strongest associations with the biomarkers. One of the 12 MetS score-related proteins (FGF-21), also associated with BMI, was associated with an increased CRC risk (OR 1.71, 95% CI 1.19–2.47). We conclude that overweight and obesity, acting through both inflammation and other mechanisms, likely explain the MetS-CRC connection.

1. Introduction

Metabolic syndrome (MetS) is associated with numerous adverse health outcomes, such as cardiovascular disease (CVD), type 2 diabetes mellitus (T2DM), and several types of cancer [1–4]. It comprises metabolic abnormalities including central obesity, hypertension, dysglycemia, and dyslipidemia [5, 6]. The western lifestyle, with a diet high in fat and simple carbohydrates combined with low physical activity, likely contributes to the current rise in incidence [7].

One hallmark of MetS is a state of chronic inflammation. Several previous studies have reported protein biomarkers associated with MetS [8], with a large proportion directly related to inflammation, for example, tumor necrosis factor alpha (TNF-α) and interleukin 6 (IL-6). Visceral adiposity appears to play a central role in driving the inflammatory state, as this type of adipose tissue secretes monocyte chemoattractant protein-1 (MCP-1) and proinflammatory cytokines, which in turn induce macrophage infiltration of the tissue [9]. The chronic, low-grade inflammation resulting from visceral adiposity may therefore be a major mechanism behind the established association between MetS and colorectal cancer (CRC) [10, 11]. However, whether this connection is dependent on actual MetS development, or is solely an artefact of obesity, remains to be elucidated.

We hypothesized that the connection between MetS and CRC is driven by inflammation, with body composition as an important component, and that inflammatory proteins associated with MetS would therefore also associate with CRC risk. Using a unique collection of repeated samples from the Västerbotten Intervention Programme (VIP) in northern Sweden, we analyzed large panels of inflammatory and cancer biomarkers in relation to MetS and its components. The MetS-related biomarkers identified were examined in relation to the risk of developing CRC.

2. Materials and Methods

2.1. Study Population. All study participants were selected from the Västerbotten Intervention Programme (VIP), initiated in 1985 and still ongoing [12]. All residents of the county are invited to a general health exam at 10-year intervals (starting at 40 years). They also donate a blood sample and fill out an extensive questionnaire on health and lifestyle.

Samples for this study were originally selected as part of a prospective study of CRC biomarkers. All CRC cases had to have a verified CRC diagnosis within five years after the latest sampling (excluding samples collected within three months of diagnosis) and have at least two available blood samples in the biobank. All but one case set had samples collected ten years apart. We selected an equal number of control subjects, matched on age (±12 months), sex, and sampling dates (±12 months). Controls had to be cancer-free at the latest follow-up (Dec. 31, 2014). For both cases and controls, only samples collected after at least eight hours of fasting were included, and none of the samples had previously been thawed. After all inclusions and exclusions, the study included repeated samples from 69 prospective CRC cases and 69 matched controls, resulting in 276 samples analyzed.

The project was approved by the Regional Ethical Review Board of Umeå University, Sweden. All VIP participants provide a written informed consent before donating their samples for research purposes, and they retain the right to withdraw that consent at any time in the future.

2.2. MetS Variables. MetS components were measured as body mass index (BMI), triglyceride levels, total cholesterol levels, mid-blood pressure (mean of systolic and diastolic blood pressure), and fasting glucose levels. The variables were scaled to mean 0 and standard deviation (SD) 1 (z-transformed) separately for sex and sampling occasion. Due to a skewed distribution, triglycerides were log transformed first. We calculated a composite MetS score by summing all scaled variables except total cholesterol, which could distort the score depending on the proportions of HDL and LDL/VLDL within the total cholesterol measurement. The MetS score was also scaled separately by sex and sampling occasion. As a sensitivity analysis, we defined a dichotomous MetS variable according to the International Diabetes Federation criteria of obesity (BMI $\geq 30\,kg/m^2$) and at least two of elevated triglyceride levels (≥1.7 mmol/l or lipid-lowering medication), hypertension (SBT ≥ 130 mm Hg or DBT ≥ 85 mm Hg or antihypertension medication), and elevated fasting glucose levels (≥5.6 mmol/l or self-reported diabetes).

2.3. Protein Biomarkers. All 276 samples were analyzed simultaneously for 178 unique protein biomarkers on two predesigned Proseek Multiplex® immunoassay panels (Olink Proteomics, Uppsala, Sweden) related to inflammation and cancer (all proteins are listed in Supplementary Table S1 available online at https://doi.org/10.1155/2017/4803156). Processing, output data quality check, and normalization were performed by Olink Proteomics. All data were delivered as Normalized Protein eXpression (NPX) values on a log2 scale. The log2 NPX values were scaled to mean 1 and SD 1 before data analysis, to facilitate comparisons between protein associations. Data values below the level of detection (LOD) were removed from the dataset. Proteins with <50% missing values (IL-20RA, IL-2RB, IL-1-alpha, IL-2, TSLP, IL-10RA, IL-22.RA1, IL-24, IL-13, ARTN, TNF, IL-20, IL-33, IFN-gamma, IL-4, LIF, NRTN, and IL-5) were excluded, leaving 160 proteins for further analysis.

2.4. Statistics. All computations were conducted in R v.3.3.1 (R Foundation for Statistical Computing, Vienna, Austria).

Associations between protein markers and MetS were determined by fitting linear mixed models for each protein using the lme function in the lmer R-package. The mixed models included participant as a random factor (random intercept) and MetS and covariates as fixed factors. Two models were fitted for each protein, one including MetS score and one including each individual MetS component. Other covariates adjusted for the models were CRC status (case, control), age (continuous), sex (male, female), physical activity (5-level scale from never to >3 times/week), smoking (non-, current, and ex-smoker), and level of education (elementary school, upper secondary school, and university). The contribution of MetS and its components to protein variance was tested by an analysis of variance approach using the anova.lme function. For evaluation of variation in protein levels within and between individuals, we calculated intraclass correlations (ICC), defined as the proportion of total variance due to variation between individuals, using the variance estimates from the mixed models. We also calculated variance explained by fixed factors (R^2_m) and variance explained by fixed and random factors (R^2_c) using the RsqGLMM function in the MuMIn package. Model assumptions were evaluated by visually inspecting the Pearson standardized residuals. Outliers, defined as standardized residuals >3, were excluded separately for each protein. Coefficients from the mixed models are interpreted as SD change in protein levels per 1SD change in MetS variable.

We assessed MetS and lifestyle-adjusted associations between the MetS-associated proteins by calculating partial Spearman's correlations on the estimated residuals from the mixed models using the core function on pairwise complete observations.

All P values were adjusted for multiple testing using the Bonferroni method. P values below 0.05 were considered significant.

We also examined MetS and the MetS-associated proteins in relation to CRC risk using conditional logistic regression models stratified on the matched case sets. Odds ratios (ORs) were estimated per 1SD change in the MetS variables. To evaluate whether associations differed depending on the follow-up time from sampling to CRC diagnosis, we tested for an interaction between sampling time point, MetS, and the protein variables.

3. Results

3.1. Participant Characteristics. Characteristics of the participants at the first and second sampling occasion are

Table 1: (a) Characteristics of study participants, stratified by sampling occasion. (b) Characteristics of study participants, stratified by colorectal cancer (CRC) status at the second sampling occasion.

(a)

Characteristics	Sample 1 ($n = 138$[a]) Median (range)	Sample 2 ($n = 138$[a]) Median (range)	P[b]
Age	49.9 (30.0–52.4)	59.9 (40.0–60.5)	—
Height	173 (157–195)	172 (155–196)	<0.001
Weight	76.5 (51–128)	80.0 (51–139)	<0.001
Triglycerides, mmol/l	1.0 (0.4-5.2)	1.1 (0.5–3.8)	0.98
Total cholesterol, mmol/l	5.5 (3.5–9.5)	5.5 (3.4–10.1)	0.18
Diastolic bp	79.0 (60.0–120.0)	80.0 (60.0–110.0)	0.12
Systolic bp	120.0 (94.0–180.0)	126.0 (90.0–179.0)	0.04
Fasting plasma glucose, mmol/l	5.4 (4.0–6.9)	5.5 (1.0–13.1)	0.003
BMI	25.3 (18.8–41.3)	26.0 (18.4–44.9)	<0.001
Categorized BMI (N, (%))	—	—	0.08
<18.5 (underweight)	0	1 (1)	—
18.5–24.9 (normal)	62 (45)	52 (38)	—
25–29.9 (overweight)	60 (43)	56 (41)	—
30+ (obese)	16 (16)	29 (21)	—
MetS (yes, %)	12 (9)	24 (17)	0.05

[a]Number of samples.
[b]Paired t-tests for differences in continuous variables between measurements 1 and 2. Chi-square test or Fisher's exact test (if expected cell count is below 5) for differences in categorical variables.

(b)

Characteristics	Case ($n = 69$) Median (range)	Control ($n = 69$) Median (range)	P[b]
Age (at sampling occasion)	59.9 (40.3–60.4)	59.9 (40.0–60.5)	—
Height	172.5 (156–196)	172 (155–191)	0.99
Weight	81.0 (56–114)	78.0 (51–139)	0.95
Triglycerides, mmol/l	1.1 (0.6–3.5)	1.1 (0.5–3.8)	0.99
Total cholesterol, mmol/l	5.4 (3.8–7.6)	5.6 (3.4–10.1)	0.03
Diastolic bp	82.0 (62.0–105.0)	80.0 (60.0–110.0)	0.14
Systolic bp	126.0 (90.0–163.0)	126.0 (90.0–179.0)	0.80
Fasting plasma glucose, mmol/l	5.7 (1.0–11.1)	5.5 (4.1–13.1)	0.73
BMI	26.1 (21.0–36.0)	26.0 (18.4–44.9)	0.82
Categorized BMI (N, (%))	—	—	0.12
<18.5 (underweight)	0	1 (1)	—
18.5–24.9 (normal)	22 (32)	30 (43)	—
25–29.9 (overweight)	34 (50)	22 (32)	—
30+ (obese)	12 (18)	16 (23)	—
MetS score	−0.02 (−0.60–0.54)	−0.06 (−0.80–0.51)	0.26
MetS (yes, %)	9 (13)	15 (22)	—

All data refer to characteristics at the second sampling as depicted in Table 1(a).
[b]Paired t-tests for differences in continuous variables between matched cases and controls. Chi-square test or Fisher's exact test (if expected cell count is below 5) for differences in categorical variables.

presented in Table 1(a), and characteristics stratified by case status in Table 1(b). Median age at first sampling was 49.9 years. Systolic blood pressure and fasting plasma glucose increased slightly over time. BMI also increased modestly with time, with more individuals categorized as obese at the second sampling occasion. The prevalence of MetS increased from 9% at the first sampling occasion to 17% at the second (Table 1(a)). BMI had a larger proportion of total variance between, and less within, participants compared to the other MetS components (ICC = 0.86, Supplementary Figure S1). Total cholesterol was higher in cases compared to controls ($P = 0.03$, Table 1(b)). There were no other large differences

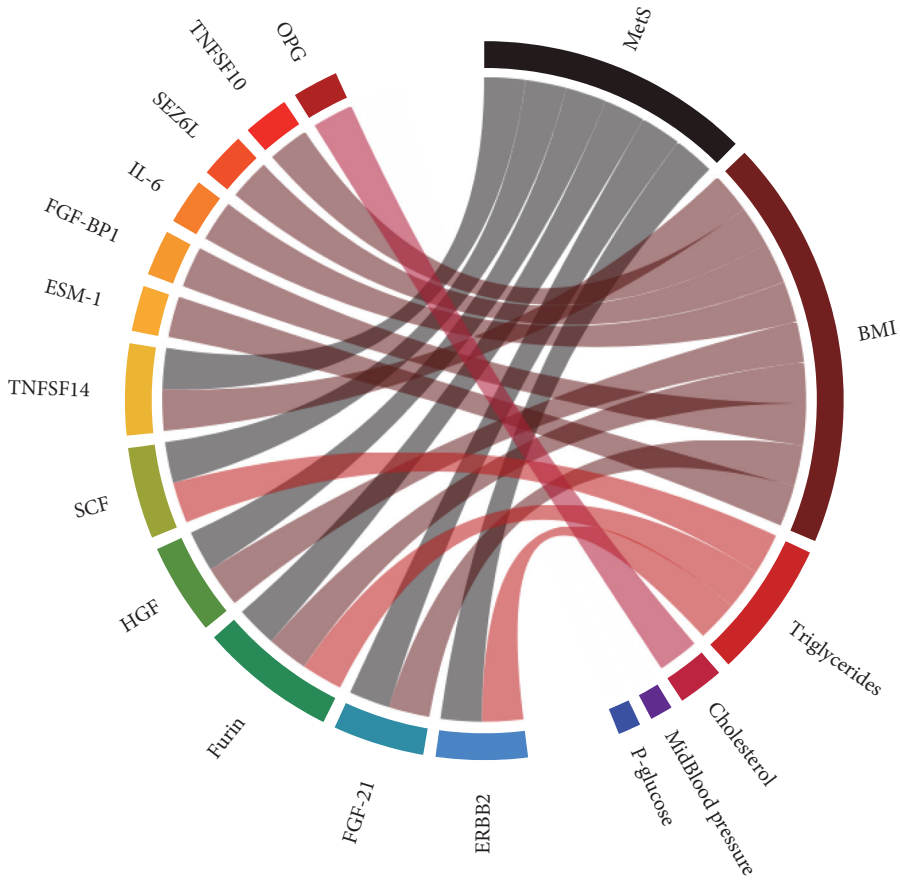

Figure 1: Significant associations between metabolic syndrome (MetS) and its components and each protein. Connections illustrate significant contributions to protein variance (Bonferroni corrected P value < 0.05).

Table 2: List of proteins significantly associated with MetS score or one of its components.

Protein name	UniProt number	Associated with	Direction of association	Original Olink panel
IL-6	P05231	BMI	Positive	Inflammation panel and oncology panel
TNFSF10	P50591	BMI	Positive	Inflammation panel and oncology panel
SEZ6L	Q9BYH1	BMI	Negative	Oncology panel
FGF-BP1	Q14512	BMI	Negative	Oncology panel
ESM-1	Q9NQ30	BMI	Negative	Oncology panel
FGF-21	Q9NSA1	MetS and BMI	Positive	Inflammation panel
TNFSF14	O43557	MetS and BMI	Positive	Inflammation panel
HGF	P14210	MetS and BMI	Positive	Inflammation panel and oncology panel
Furin	P09958	MetS, BMI, and triglycerides	Positive	Oncology panel
ERBB2	P04626	MetS and triglycerides	Positive	Oncology panel
SCF	P21583	MetS and triglycerides	Negative	Inflammation panel and oncology panel
OPG	O00300	Total cholesterol	Positive	Inflammation panel

in MetS components, MetS score, or MetS prevalence between CRC cases and controls. The same pattern was seen at the first sampling occasion.

3.2. Protein Levels. Out of 160 proteins that passed quality control, six were associated with the MetS score: three (TNFSF14, HGF, and FGF-21) with MetS score and BMI, two (SCF and ERBB2) with MetS score and triglyceride levels, and one (Furin) with MetS score, BMI, and triglyceride levels. An additional five proteins were associated with BMI alone (TNFSF10, SEZ6L, IL-6, FGF-BP1, and ESM-1), and one (OPG) was associated with total cholesterol (Figure 1, Table 2). The direction of the significant associations was inverse for SCF, ESM-1, SEZ6L, and FGF-BP1 and positive

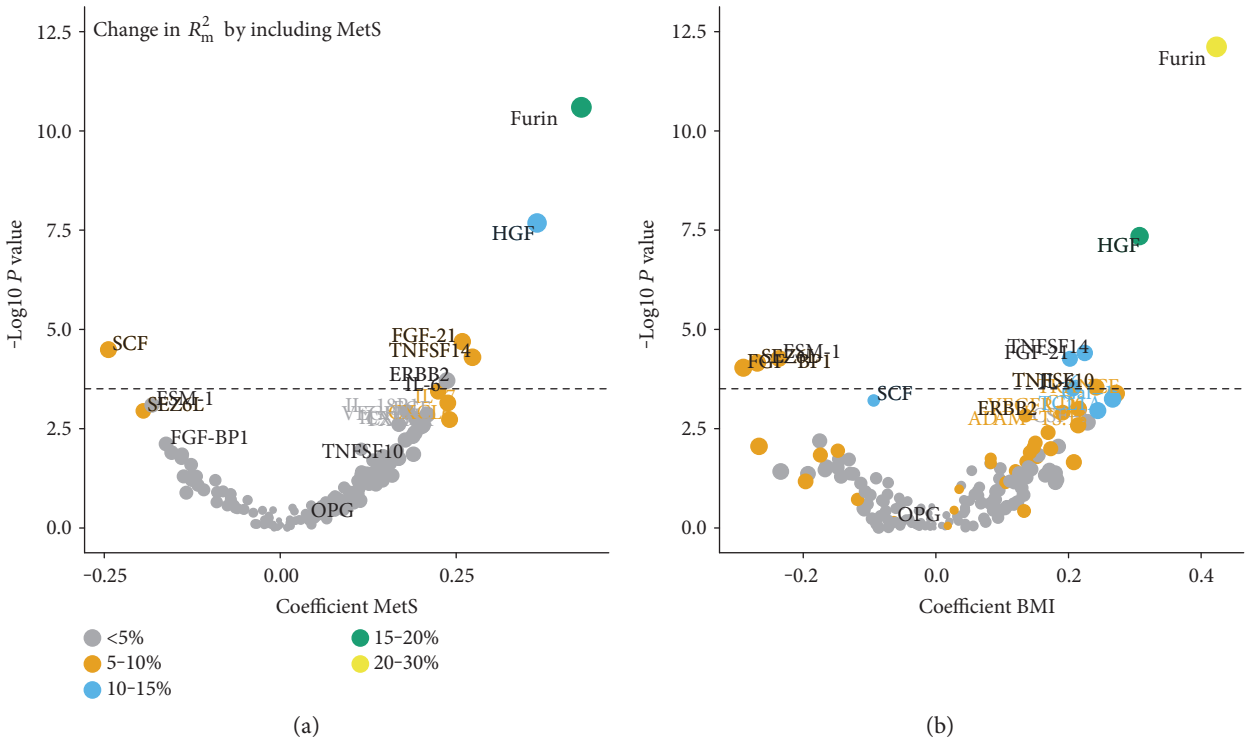

Figure 2: Volcano plots for metabolic syndrome (MetS) (a) and BMI (b). The dashed line indicates the Bonferroni-adjusted significance threshold. Coefficients are interpreted as SD change in protein levels by 1SD change in MetS score and BMI, respectively. R^2_m is the proportion of variance explained by the included fixed factors.

for OPG, TNFSF10, IL-6, ERBB2, TNFSF14, FGF-21, HGF, and Furin (Figure 2, Supplementary Figure S2).

The proportion of variance in protein levels explained by the fixed factors in our models, R^2_m, varied between 0 and 35% (Figure 3). The proportion of variance attributable to MetS was 5–30% for the proteins identified. IL-6, FGF-21, and TNFSF14 varied more within participants between the measurements compared with the other significant proteins (ICC < 0.50, Supplementary Figure S3), whereas the intraindividual variation between sampling occasions was lower for SEZ6L, TNFSF10, and FGF-BP1 (ICC: 0.69–0.71).

Furin and HGF showed the strongest associations with MetS. The relations were driven largely by BMI, with 20–30 percentage points of the variation explained by the fixed factors attributed to BMI (Figure 3). OPG was significantly associated with total cholesterol, yet only a small proportion (5 percentage points) of the variance explained by the included fixed factors was attributable to MetS components. Instead, a large part (25%) of the variance in OPG was explained by age. Inthe sensitivity analyses, using predefined cut-offs to define MetS and MetS components gave similar results but with fewer significant protein associations (data not shown).

Partial correlations between the MetS-associated proteins are presented in Supplementary Figure S4. Almost all correlations were positive. Two clusters of more correlated proteins were present: cluster 1: SCF, OPG, ERBB2, SEZ6L, ESM-1, and FGF-BP1; cluster 2: HGF, TNFSF14, Furin, IL-6, FGF-21, and TNFSF10.

3.3. MetS, Protein Levels, and CRC Risk. None of the MetS components was significantly associated with CRC risk in conditional logistic regression models adjusting for age, sex, and sampling date by case-set stratification, and additionally by smoking status and educational level by regression (Figure 4). MetS score was associated with an insignificant increased risk of CRC (OR per 1SD increase in MetS score: 1.28, 95% CI: 0.97–1.70). For the 12 proteins significantly associated with MetS and/or its components, five were associated with CRC risk. Higher levels of FGF-21, which in our dataset were directly associated with MetS score and BMI, were associated with an increased CRC risk (OR per 1SD increase in protein levels: 1.71, 95% CI: 1.19–2.47). Higher levels of SEZ6L, TNFSF10, HGF, and ESM-1 were associated with a lower CRC risk (ORs per 1SD increase in protein levels: 0.59 to 0.39). Most protein risk estimates were enlarged by including MetS score in the models. The OR for MetS score was markedly enlarged when including SCF, TNFSF10, and HGF and attenuated when including FGF-21 and SEZ6L (Figure 4). Similar changes in ORs were seen for BMI. There were no significant interactions between MetS and the proteins, or between MetS or MetS-related proteins, and sampling time point.

4. Discussion

Metabolic syndrome is becoming increasingly common, and many studies indicate a direct association between MetS and the risk of developing CRC and other forms of cancer, likely

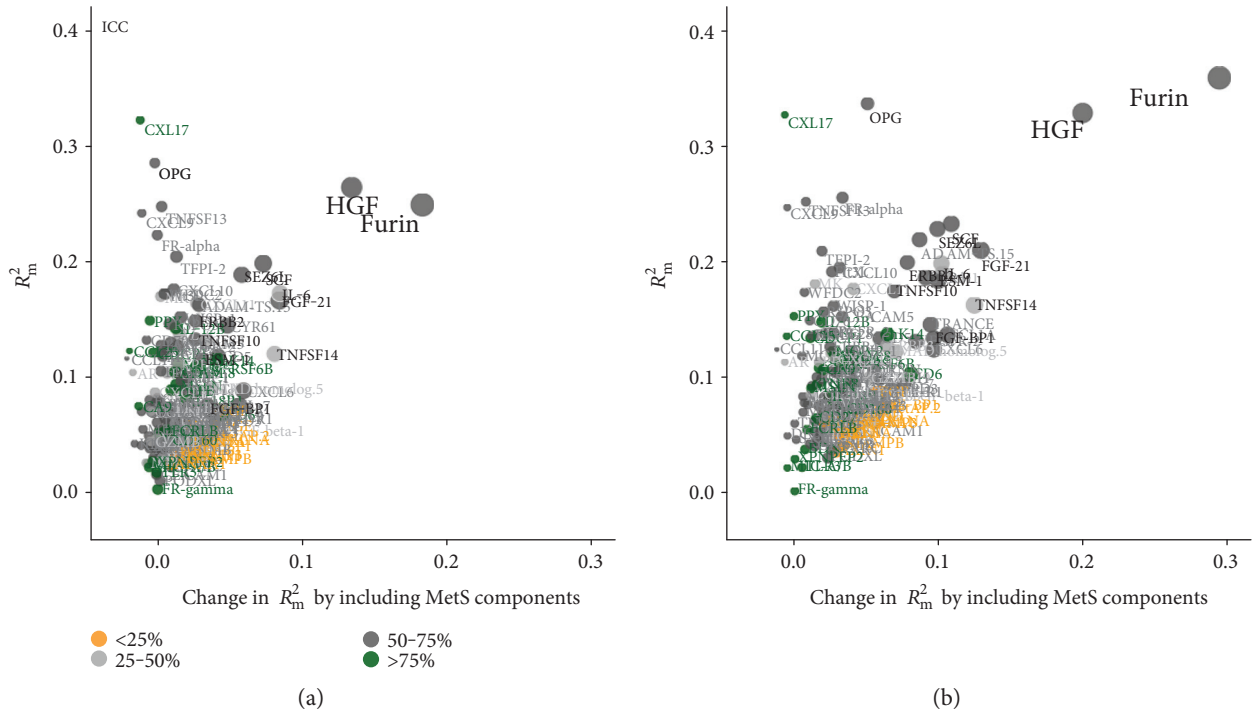

Figure 3: Contribution to variance explained by metabolic syndrome (MetS) and other included covariates. (a) Variance explained by including MetS (*x*-axis). (b) Variance explained by including MetS components. The proteins are color coded according to ICC, that is, proportion of interindividual variance to total variance. Proteins with high ICC vary less within and more between participants, whereas proteins with low ICC vary less between and more within participants. Proteins in black were significantly associated with MetS or any MetS component.

driven, at least in part, by body composition and inflammation [13, 14]. In order to investigate the hypothesis that inflammation is the driving factor between MetS and CRC, we evaluated 160 unique protein biomarkers, known to be related to cancer or inflammation, in repeated samples from 138 individuals (of which half developed CRC within 5 years after the second sampling occasion). Twelve proteins were associated with at least one MetS component, six of which were also associated with MetS score. One of the six, FGF-21, was positively associated with CRC risk.

Interestingly, five of the 12 proteins identified were associated with BMI only, all of which were included in the predefined oncology protein marker panel due to a potential relation to cancer (with or without an inflammatory connection). However, of the six proteins associated with MetS score, there was an equal distribution between inflammatory and cancer proteins. Thus, body composition likely contributes to cancer development not only through chronic inflammation but also through other pathways.

Of the MetS-associated proteins, only one, which was also associated with BMI, was positively associated with CRC risk, FGF-21 (fibroblast growth factor 21). Inclusion of MetS strengthened the association between FGF-21 and CRC risk and attenuated the association between MetS and CRC risk, suggesting a mediating effect. Increases in BMI and MetS score contributed to a significant amount of the FGF-21 protein level variation, and it was the protein with the largest change in level per MetS score increase. Consistent with our observations, the associations between FGF-21, BMI, and MetS have been previously described [15, 16] and appear to be robust in plasma or serum samples. FGF-21 is part of the family of fibroblast growth factors, which includes 18 mammalian proteins (FGF1-FGF10 and FGF16-FGF23) [17]. However, FGF-21 is not a clear-cut growth factor but serves as a metabolic hormone as it lacks the FGF-heparin-binding domain and therefore can diffuse away from its tissue of origin [18, 19]. FGF-21 is expressed in a wide variety of tissues [17] and mediates signaling by binding to the tyrosine kinase FGF-receptors. One of the main functions of FGF-21 appears to be the regulation of metabolic function and stimulation of glucose uptake [20]. It has been shown to increase in patients with T2DM [21]. More recently, the possibility of using FGF-21 as a prognostic or diagnostic cancer marker has been raised and evaluated for renal cancer, with promising results [22]. To the best of our knowledge, FGF-21 has not previously been evaluated as a biomarker for CRC risk. Our results indicate that it might be suitable for this purpose. However, FGF-21 levels were subject to a fairly high intraindividual variation (0.46), meaning variation over time is common. Intraindividual variation would need to be taken into consideration for all future applications including FGF-21 as a potential biomarker [23].

Two proteins were strongly associated with both MetS and BMI, namely, HGF (hepatocyte growth factor) and Furin. Both of these proteins have been previously implicated in MetS [24, 25]. HGF is a cytokine secreted from adipocyte tissue, known to increase with hypertension and obesity and most likely regulated by genetic factors [26]. In the

Metabolic syndrome		OR	95% CI	*P*		
P-glucose		1.28	0.91–1.81	0.16		
BMI		1.13	0.81–1.58	0.48		
Mid-BP		1.07	0.80–1.42	0.67		
Triglycerides		1.04	0.74–1.47	0.80		
Total cholesterol		0.76	0.55–1.06	0.10		
MetS score		1.28	0.97–1.70	0.09		
Proteins	OR crude	OR adjusted	95% CI	*P*	MetS score OR	MetS score P
FGF-21	1.47	1.71	1.19–2.47	0.0037	1.06	0.70
SGF	1.07	1.32	0.92–1.88	0.13	1.42	0.03
FGF-BP1	1.05	1.08	0.78–1.49	0.64	1.29	0.08
Furin	1.23	1.06	0.74–1.52	0.75	1.25	0.18
ERBB2	0.96	0.88	0.62–1.26	0.50	1.31	0.07
IL-6	0.95	0.88	0.65–1.19	0.41	1.32	0.06
TNFSF14	0.94	0.84	0.61–1.18	0.32	1.34	0.05
OPG	0.83	0.74	0.51–1.09	0.13	1.31	0.06
SEZ6L	0.68	0.59	0.40–0.84	0.0082	1.19	0.24
TNFSF10	0.65	0.53	0.36–0.78	0.0015	1.61	0.0050
HGF	0.68	0.51	0.33–0.77	0.0016	1.70	0.0032
ESM-1	0.54	0.47	0.31–0.70	0.0003	1.34	0.07

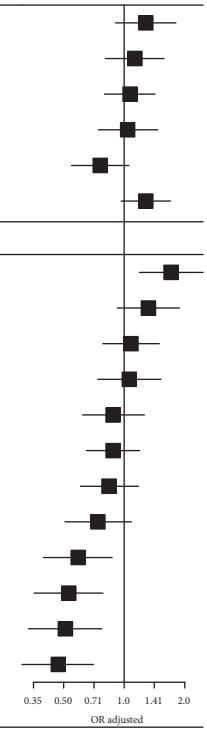

Figure 4: Associations between metabolic syndrome (MetS) score, MetS components, protein levels, and CRC risk. All odds ratios (ORs) were calculated using conditional logistic regression, stratified for the case-sets. For MetS, odds ratios (ORs) were adjusted for smoking status and education level. For protein models, ORs are adjusted for smoking status and education level. ORs adjusted are additionally adjusted for the MetS score. MetS score OR and MetS score P are ORs and corresponding *P* values for the MetS score in the protein models.

present study, HGF was positively related to both MetS score and BMI but inversely associated with CRC risk, an effect that was strengthened by adjusting for MetS score. This contradicts a previous study in which elevated serum HGF levels were proposed as a biomarker for tumor progression and suggested to enhance angiogenesis and tumor cell invasion [27]. Furin belongs to the proprotein convertase family and processes inactive proteins into their active forms [28]. It is the most studied protein in this family, and its function and expression have been investigated in relation to several types of cancer. Furin's role in protein activation makes it important for tumor progression and metastasis. Inhibitors of Furin activity are therefore potential targets for cancer therapy [29]. At the same time, overexpression of Furin has been linked to tumor suppression and better prognosis in hepatocellular carcinoma [30]. We found no significant association between Furin and CRC in our dataset, possibly due to the prospective study design, with plasma samples collected prior to CRC diagnosis. However, the null relationship was apparent even at the second sampling occasion, at which cases were more likely to have a premalignant or malignant process in the colorectum.

The protein most strongly associated with CRC risk was ESM-1 (endothelial cell-specific molecule-1), which was inversely associated with both BMI and CRC in our dataset but not associated with MetS. ESM-1 has previously been shown to be overexpressed in CRC patients and associated with poor prognosis [31]. The fact that increased levels in our dataset were indicative of reduced CRC risk shows the difficulty in translating markers identified at diagnosis to prospective samples. ESM-1 does appear to have an active role in CRC by regulating growth and metastasis and may be useful as a therapeutic target [32], but further investigation of the mechanisms behind the inverse association we observed using prediagnostic samples is warranted.

One other protein, SEZ6L (seizure 6-like protein), was also inversely associated with both BMI and CRC. It controls synaptic connectivity and motor coordination and is also a substrate for the β-secretase BACE1, which is highly expressed in the nervous system and an important drug target in Alzheimer's disease [33]. Although it has not previously been implicated in CRC, one study found an association between a genetic polymorphism in the SEZ6L gene and increased risk of lung cancer [34].

Weaknesses of our study include lack of a central obesity measurement (substituted with BMI) and HDL cholesterol measurements. Total cholesterol was evaluated in relation to protein measurements but not included in the MetS score definition because of the conflicting roles of HDL and LDL, both of which contribute to total cholesterol. In addition, CRP (c-reactive protein), an established and important marker of inflammation previously connected to MetS [35], was not included in the Olink inflammation panel, and TNF-alpha (a well-known marker of inflammation and

characteristic of MetS [8]) was omitted due to missing values. Hence, neither of these were addressed in our study.

Major strengths of the study included the use of high-quality blood samples collected prospectively with respect to CRC diagnosis, with all participants fasting for at least eight hours prior to sampling, and with no previous thaw-freeze cycles. The VIP cohort also provided a unique opportunity to use repeated samples from both cases and time-matched controls, allowing us to account for intra-individual variation. Finally, an important strength of the study was the large number of protein biomarkers evaluated simultaneously using a highly sensitive platform.

5. Conclusions

In our study MetS does not, in itself, appear to contribute to the inflammation cancer-connection. MetS score was associated with six different proteins in our investigation. However, all were also associated with BMI and/or triglyceride levels. Of the individual MetS components assessed, BMI displayed by far the strongest associations with inflammatory and cancer biomarkers. Although external replication is needed, our data indicate that the relationship between MetS and CRC risk is likely driven primarily by excess body fat, acting through both pro-inflammation and other pro-carcinogenic mechanisms.

Conflicts of Interest

The authors declare that they have no conflicts of interest.

Authors' Contributions

Sophia Harlid and Robin Myte contributed equally to this work.

Acknowledgments

This study was funded by the Lion's Cancer Research Foundation, Umeå University; the Cancer Research Fund in Northern Sweden; the Swedish Society of Medicine; the Swedish Cancer Society; the Young Scientist and other research grants from the County Council of Västerbotten, Sweden, through the regional agreement between Umeå University and Västerbotten County Council in cooperation in the field of medicine, odontology, and health; and the Faculty of Medicine at Umeå University, Umeå, Sweden.

References

[1] K. Esposito, P. Chiodini, A. Colao, A. Lenzi, and D. Giugliano, "Metabolic syndrome and risk of cancer: a systematic review and meta-analysis," *Diabetes Care*, vol. 35, no. 11, pp. 2402–2411, 2012.

[2] E. S. Ford, "Risks for all-cause mortality, cardiovascular disease, and diabetes associated with the metabolic syndrome: a summary of the evidence," *Diabetes Care*, vol. 28, no. 7, pp. 1769–1778, 2005.

[3] A. Galassi, K. Reynolds, and J. He, "Metabolic syndrome and risk of cardiovascular disease: a meta-analysis," *The American Journal of Medicine*, vol. 119, no. 10, pp. 812–819, 2006.

[4] J. Harding, M. Sooriyakumaran, K. J. Anstey et al., "The metabolic syndrome and cancer: is the metabolic syndrome useful for predicting cancer risk above and beyond its individual components?" *Diabetes & Metabolism*, vol. 41, no. 6, pp. 463–469, 2015.

[5] S. M. Grundy, J. I. Cleeman, S. R. Daniels et al., "Diagnosis and management of the metabolic syndrome: an American Heart Association/National Heart, Lung, and Blood Institute Scientific Statement," *Circulation*, vol. 112, no. 17, pp. 2735–2752, 2005.

[6] J. Kaur, "A comprehensive review on metabolic syndrome," *Cardiology Research and Practice*, vol. 2014, Article ID 943162, p. 21, 2014.

[7] A. J. McCullough, "Epidemiology of the metabolic syndrome in the USA," *Journal of Digestive Diseases*, vol. 12, no. 5, pp. 333–340, 2011.

[8] K. Srikanthan, A. Feyh, H. Visweshwar, J. I. Shapiro, and K. Sodhi, "Systematic review of metabolic syndrome biomarkers: a panel for early detection, management, and risk stratification in the West Virginian population," *International Journal of Medical Sciences*, vol. 13, no. 1, pp. 25–38, 2016.

[9] F. K. Welty, A. Alfaddagh, and T. K. Elajami, "Targeting inflammation in metabolic syndrome," *Translational Research*, vol. 167, no. 1, pp. 257–280, 2016.

[10] K. Aleksandrova, H. Boeing, M. Jenab et al., "Metabolic syndrome and risks of colon and rectal cancer: the European prospective investigation into cancer and nutrition study," *Cancer Prevention Research (Philadelphia, Pa.)*, vol. 4, no. 11, pp. 1873–1883, 2011.

[11] K. Esposito, P. Chiodini, A. Capuano et al., "Colorectal cancer association with metabolic syndrome and its components: a systematic review with meta-analysis," *Endocrine*, vol. 44, no. 3, pp. 634–647, 2013.

[12] M. Norberg, S. Wall, K. Boman, and L. Weinehall, "The Vasterbotten Intervention Programme: background, design and implications," *Global Health Action*, vol. 3, 2010.

[13] S. Braun, K. Bitton-Worms, and D. LeRoith, "The link between the metabolic syndrome and cancer," *International Journal of Biological Sciences*, vol. 7, no. 7, pp. 1003–1015, 2011.

[14] F. M. Mendonça, F. R. de Sousa, A. L. Barbosa et al., "Metabolic syndrome and risk of cancer: which link?" *Metabolism, Clinical and Experimental*, vol. 64, no. 2, pp. 182–189, 2015.

[15] S. Kralisch, A. Tönjes, K. Krause et al., "Fibroblast growth factor-21 serum concentrations are associated with metabolic and hepatic markers in humans," *Journal of Endocrinology*, vol. 216, no. 2, pp. 135–143, 2013.

[16] X. Zhang, D. C. Yeung, M. Karpisek et al., "Serum FGF21 levels are increased in obesity and are independently associated with the metabolic syndrome in humans," *Diabetes*, vol. 57, no. 5, pp. 1246–1253, 2008.

[17] A. Beenken and M. Mohammadi, "The FGF family: biology, pathophysiology and therapy," *Nature Reviews. Drug Discovery*, vol. 8, no. 3, pp. 235–253, 2009.

[18] S. A. Kliewer and D. J. Mangelsdorf, "Fibroblast growth factor 21: from pharmacology to physiology," *The American Journal of Clinical Nutrition*, vol. 91, no. 1, 2010.

[19] S. Kralisch and M. Fasshauer, "Fibroblast growth factor 21: effects on carbohydrate and lipid metabolism in health and

disease," *Current Opinion in Clinical Nutrition and Metabolic Care*, vol. 14, no. 4, pp. 354–359, 2011.

[20] K. R. Markan, M. C. Naber, M. K. Ameka et al., "Circulating FGF21 is liver derived and enhances glucose uptake during refeeding and overfeeding," *Diabetes*, vol. 63, no. 12, pp. 4057–4063, 2014.

[21] X. Cheng, B. Zhu, F. Jiang, and H. Fan, "Serum FGF-21 levels in type 2 diabetic patients," *Endocrine Research*, vol. 36, no. 4, pp. 142–148, 2011.

[22] M. E. Knott, J. N. Minatta, L. Roulet et al., "Circulating fibroblast growth factor 21 (Fgf21) as diagnostic and prognostic biomarker in renal cancer," *Journal of Molecular Biomarkers & Diagnosis*, vol. 1, 2016Supplement 2, 2016.

[23] J. M. G. Taylor, D. P. Ankerst, and R. R. Andridge, "Validation of biomarker-based risk prediction models," *Clinical Cancer Research*, vol. 14, no. 19, pp. 5977–5983, 2008.

[24] A. Hiratsuka, H. Adachi, Y. Fujiura et al., "Strong association between serum hepatocyte growth factor and metabolic syndrome," *The Journal of Clinical Endocrinology and Metabolism*, vol. 90, no. 5, pp. 2927–2931, 2005.

[25] C. Ueyama, H. Horibe, Y. Yamase et al., "Association of FURIN and ZPR1 polymorphisms with metabolic syndrome," *Biomedical Reports*, vol. 3, no. 5, pp. 641–647, 2015.

[26] Y. Vistoropsky, S. Trofimov, I. Malkin, E. Kobyliansky, and G. Livshits, "Genetic and environmental determinants of hepatocyte growth factor levels and their association with obesity and blood pressure," *Annals of Human Biology*, vol. 35, no. 1, pp. 93–103, 2008.

[27] Y. Ren, B. Cao, S. Law et al., "Hepatocyte growth factor promotes cancer cell migration and angiogenic factors expression: a prognostic marker of human esophageal squamous cell carcinomas," *Clinical Cancer Research: An Official Journal of the American Association for Cancer Research*, vol. 11, no. 17, pp. 6190–6197, 2005.

[28] G. Thomas, "Furin at the cutting edge: from protein traffic to embryogenesis and disease," *Nature Reviews. Molecular Cell Biology*, vol. 3, no. 10, pp. 753–766, 2002.

[29] J. M. Coppola, M. S. Bhojani, B. D. Ross, and A. Rehemtulla, "A small-molecule furin inhibitor inhibits cancer cell motility and invasiveness," *Neoplasia (New York, N.Y.)*, vol. 10, no. 4, pp. 363–370, 2008.

[30] Y.-H. H. Huang, K.-H. H. Lin, C.-H. H. Liao, M. W. Lai, Y. H. Tseng, and C. T. Yeh, "Furin overexpression suppresses tumor growth and predicts a better postoperative disease-free survival in hepatocellular carcinoma," *PloS One*, vol. 7, no. 7, 2012.

[31] N. Y. Ji, Y.-H. H. Kim, Y. J. Jang et al., "Identification of endothelial cell-specific molecule-1 as a potential serum marker for colorectal cancer," *Cancer Science*, vol. 101, no. 10, pp. 2248–2253, 2010.

[32] Y. H. Kang, N. Y. Ji, S. R. Han et al., "ESM-1 regulates cell growth and metastatic process through activation of NF-κB in colorectal cancer," *Cellular Signalling*, vol. 24, no. 10, pp. 1940–1949, 2012.

[33] M. Pigoni, J. Wanngren, P.-H. H. Kuhn et al., "Seizure protein 6 and its homolog seizure 6-like protein are physiological substrates of BACE1 in neurons," *Molecular Neurodegeneration*, vol. 11, no. 1, p. 67, 2016.

[34] I. P. Gorlov, P. Meyer, T. Liloglou et al., "Seizure 6-like (SEZ6L) gene and risk for lung cancer," *Cancer Research*, vol. 67, no. 17, pp. 8406–8411, 2007.

[35] S. Devaraj, U. Singh, and I. Jialal, "Human C-reactive protein and the metabolic syndrome," *Current Opinion in Lipidology*, vol. 20, no. 3, pp. 182–189, 2009.

Hindawi
Mediators of Inflammation
Volume 2017, Article ID 2754756, 12 pages
https://doi.org/10.1155/2017/2754756

Research Article

Lysophosphatidic Acid Triggers Apoptosis in HeLa Cells through the Upregulation of Tumor Necrosis Factor Receptor Superfamily Member 21

Yunzhou Dong,[1,2] Yong Wu,[3,4] Mei-Zhen Cui,[1] and Xuemin Xu[1]

[1] *Department of Biomedical & Diagnostic Sciences, College of Veterinary Medicine, University of Tennessee, Knoxville, TN 37996, USA*
[2] *Vascular Biology Program, Boston Children's Hospital, Harvard Medical School, Boston, MA 02115, USA*
[3] *Division of Cancer Research and Training, Department of Internal Medicine, Charles R. Drew University of Medicine and Science, Los Angeles, CA 90059, USA*
[4] *David Geffen UCLA School of Medicine and UCLA Jonson Comprehensive Cancer Center, University of California, Los Angeles, CA 90095, USA*

Correspondence should be addressed to Mei-Zhen Cui; cuim@utk.edu and Xuemin Xu; xmx@utk.edu

Received 19 November 2016; Accepted 18 January 2017; Published 19 February 2017

Academic Editor: Anshu Agrawal

Lysophosphatidic acid (LPA), a naturally occurring bioactive phospholipid, activates G protein-coupled receptors (GPCRs), leading to regulation of diverse cellular events including cell survival and apoptosis. Despite extensive studies of the signaling pathways that mediate LPA-regulated cell growth and survival, the mechanisms underlying the apoptotic effect of LPA remain largely unclear. In this study, we investigated this issue in HeLa cells. Our data demonstrate that LPA induces apoptosis in HeLa cells at pathologic concentrations with a concomitant upregulation of the expression of TNFRSF21 (tumor necrosis factor receptor superfamily member 21), also known as death receptor number 6 (DR6) involved in inflammation. Moreover, treatment of cells with LPA receptor (LPAR) antagonist abolished the DR6 upregulation by LPA. LPA-induced DR6 expression was also abrogated by pertussis toxin (PTX), an inhibitor of GPCRs, and by inhibitors of PI3K, PKC, MEK, and ERK. Intriguingly, LPA-induced DR6 expression was specifically blocked by dominant-negative form of PKCδ (PKCδ-DN). LPA-induced DR6 expression was also dramatically inhibited by knockdown of ERK or CREB. These results suggest that activation of the MEK/ERK pathway and the transcription factor CREB mediate LPA-induced DR6 expression. More interestingly, knockdown of DR6 using siRNA approach remarkably attenuated LPA-induced apoptosis. In conclusion, our results suggest that LPA-induced apoptosis in HeLa cells is mediated by the upregulation of DR6 expression.

1. Introduction

Lysophosphatidic acid (1- or 2-acyl-lysophosphatidic acid, LPA) is a naturally occurring bioactive phospholipid. Under normal physiological conditions, LPA is present at a low level in plasma (~100 nM) [1] and its concentration elevates at sites of tissue injury and inflammation [1, 2]. LPA is produced during phospholipid biosynthesis of cell membranes. LPA is also produced extracellularly by several cell types including activated platelets, leukocytes, epithelial cells, neuronal cells, and tumor cells [3]. Increasing evidence suggests that LPA plays a role in various inflammatory disease [4–6]. LPA regulates various developmental, physiological, and pathophysiological processes including cell motility, invasion, proliferation, survival, and production of growth factors [7, 8] through G protein-coupled receptor (GPCR). Platelet-derived LPA plays an important role in tissue regeneration and wound healing [9, 10]. LPA also functions as a chemoattractant promoting motility of various types of human cancer cells [11]. Recent studies suggest that tumor cells stimulate the production of LPA from activated platelets, which enhances both tumor growth and cytokine-mediated bone destruction [12, 13], and that specific inhibition of LPA receptors abolishes the migration of cancer cell response

to malignant ascites containing LPA [14]. The increased expression of LPA receptors is associated with an increased level of invasiveness in ovarian cancer cells [15, 16]. Thus, LPA has diverse biological activities implicated in tumor initiation and progression, including increasing cell survival, angiogenesis, invasion, and metastasis. Paradoxically, LPA also induces apoptosis in certain cells, such as neuronal cells [17] and epithelial cells from different tissues [18–20], myeloid progenitor cells, hippocampal neurons, and PC12 cells [3]. However, the mechanism by which LPA induces apoptosis remains unclear.

Death receptor 6 (DR6), also known as TNFRSF21, is a relatively new member of the tumor necrosis factor (TNF) receptor family possessing a cytoplasmic death domain. Previous studies indicate that ectopic expression of DR6 in mammalian cells induces apoptosis [21]. Our recent study suggests that DR6 induces apoptosis through a mitochondria-dependent pathway [22]. In the current study, to determine the mechanism by which LPA induces apoptosis, we surprisingly found that LPA induced apoptosis via upregulating expression of the death receptor DR6 in HeLa cells. In addition, our results strongly suggest that PI3K/PKC/MEK/ERK pathway and activation of the transcription factor CREB are responsible for LPA-induced upregulation of DR6 expression and apoptosis.

2. Materials and Methods

2.1. Reagents, Chemicals, and Antibodies. Anti-DR6 antibody was purchased from Santa Cruz Biotechnology (Santa Cruz, CA). Phosphor antibodies for PKCα/β, PKCε, PKCζ/λ, PKC-delta, MEK, ERK1/2, p90RSK, CREB, cleaved caspases 9, 7, 3, and PARP were purchased from Cell Signaling Technology (Danvers, MA). Antibody against LPAR1 was purchased from Cayman Chemical (Ann Arbor, MI); antibodies for LPAR2 and LPAR3 were from LifeSpan BioScience (Seattle, WA). LPA (category number 857130, water-soluble) and LPS were from Avanti Polar Lipids (Alabaster, AL). TNF-α, angiotensin II, PMA, insulin, thrombin, NGF-β, Ro 31-8220 (PKC inhibitor), and SB203580 (p38 inhibitor) were bought from Sigma-Aldrich (St. Louis, MO). Pertussis toxin (PTX), UO126, and GF10293X were from Biomol International (Plymouth Meeting, PA). Wortmannin (PI3K inhibitor) and Ki16425 (LPA Receptor Antagonist) were from Cayman Chemical (Boston, MA). ERK and CREB siRNA were from Cell Signaling Technology. DR6 siRNA was bought from Santa Cruz Biotechnology (CA). JNK inhibitor was purchased from Calbiochem (Billerica, MA). MTT assay kit for cell viability was bought from R&D System (Minneapolis, MN). TUNEL assay kit was purchased from Roche Applied Science USA. Adenoviral vector construction kit was from Qbiogene. Cloning tools including restriction enzymes, T4 DNA ligase, and modifying enzymes were bought from New England Biolabs or Promega. All other chemicals were purchased from Sigma-Aldrich or other brand companies.

2.2. Cell Culture and Treatment. HeLa cells were cultured in DMEM with 10% DMEM and antibiotics (Penn/Strep). Cells were starved for 16 hours before LPA treatment or as indicated in each experiment. Inhibitors were usually pretreated for 30 min followed by LPA treatment except the PTX pretreatment for 15 hours.

2.3. Northern Blot. Northern blot was performed as described previously [23]. Total RNA was extracted using TRIzol reagent (Invitrogen) and subjected to formaldehyde-agarose gel electrophoresis. RNA was transferred to nylon membranes (Amersham Biosciences), UV-crosslinked and hybridized with dCTP-labeled 444-bp fragment (see Supplemental Figure 2, in Supplementary Material available online at https://doi.org/10.1155/2017/2754756) of human DR6 cDNA. 18S and 28S rRNA were used as internal controls. Intensities of hybridized bands were quantified using Image J software.

2.4. Western Blot. Western blot was conducted as previously described [24]. In brief, cells were washed with cold PBS one time and immediately lysed in lysis buffer containing 50 mM Tris-HCl, pH 6.8, 8 M urea, 5% β-mercaptoethanol, 2% SDS, 0.2 mM NaF, 0.1 mM Na_2VO_3, and protease inhibitors (Roche). Protein concentration was determined by BCA kit (Fisher Scientific) for equal amount of total protein loading. Proteins were separated in Tris-glycine SDS-PAGE gel and transferred to PVDF membrane (Fisher Scientific), followed by probing with different antibodies and visualized by ECL reagent.

2.5. PCR, Reverse Transcriptional PCR, and qPCR. PCR primers were designed for human LPAR1, LPAR2, and LPAR3 for regular PCR. DR6 primers were designed for the amplification of human DR6 message RNA for Reverse Transcriptional (RT-) PCR. Primers have also been designed for the DR6 for Quantitative PCR (qPCR) analysis. All primers for targeting gene amplification and the relative controls are supplemented in Supplemental Table 1. Regular and reverse transcriptional PCR were performed with a Bio-Rad thermocycler using the following program: 95°C 2 min, followed by 32 cycles of 95°C 15 s, 55°C 30 s, and 72°C 45 s followed by extension at 72°C for 7 min. For reverse transcriptional PCR, the cycle number was controlled between 15 and 20 cycles and the PCR products were subjected to 1% agarose gel electrophoresis. Quantitative PCR was performed as previously reported [25]. In brief, the qPCR mixture was heated to 95°C for 3 min and then subjected to 40 cycles at 95°C for 30 s, 57°C for 30 s, and 72°C for 1 min by using the MyiQ™ System (Bio-Rad). The cycle threshold (Ct) value was determined for each sample. All Ct values were normalized to the internal control gene β-actin. The relative expression of DR6 mRNA, as determined by Ct value, was calculated using the equation $2^{-\Delta ct}$.

2.6. Adenoviral Infection. Adenovirus harboring different dominant-negative (DN) PKC isoforms and DR6 was titrated and added to cell culture at the 50x MOI (multiplicity of infection) for 24 hrs.

2.7. Downregulation of the Expression of DR6, ERK, and CREB by siRNA. Downregulating the expression of ERK and CREB

by siRNA technology was performed following the protocol from the supplier. Two rounds of siRNA treatment were conducted for a better knockdown efficiency.

2.8. MTT and TUNEL Assay. Cells were treated with LPA in different concentration and time points as indicated and MTT assay was performed according to the recommendation by supplier. For terminal deoxynucleotidyl transferase-(TdT-) mediated dUTP nick end labeling (TUNEL) assay, cells were treated with 25 μM LPA for 24 hrs, fixed, and stained. Images were captured using Olympus fluorescent microscopy equipped with a digital camera.

2.9. Statistical Analysis. All experiments were repeated for at least three times. Image bands from Western blot, Northern blot, and PCR/qPCRs were quantified using Image J software (NIH website). Data was presented as mean ± SD. Statistical analysis was performed using Prism software for comparison by either Student's t-test (two groups) or one-way ANOVA (≥three groups). A P value of less than 0.05 was considered a significant difference.

3. Results

3.1. LPA Induces Apoptosis and DR6 Expression in Cultured HeLa Cells. To test whether LPA can induce apoptosis, HeLa cells were treated with various concentrations of LPA for up to 48 hrs. LPA-induced apoptosis in HeLa cells was determined by MTT and TUNEl assay. As shown in Figures 1(a) and 1(b), the reduction of cell viability determined by MTT assay and the increase in the number of TUNEL-positive cells indicate that the apoptotic effect was apparently dose-dependent with the lowest levels at 10 μM of LPA treatment. The proapoptotic effect of LPA in HeLa cells was confirmed with apoptotic signaling protein activation. As shown in Figure 1(c), LPA treatment (25 and 50 μM) significantly increased caspase-9, caspase-7, and caspase-3 activation and PARP cleavage. Interestingly, as shown in Figure 1(d), the dose-dependent proapoptotic effect of LPA was accompanied by gradual augmentation of expression of DR6, a recently identified death receptor member of TNF superfamily. Treatment with LPA did not change the levels of DR5 and TNFR1, the other two members of the same TNF superfamily.

3.2. LPA Increases DR6 mRNA and Protein Expression in Both Dose- and Time-Dependent Manner. Next, we compared the effects of different proapoptotic factors and growth factors on DR6 expression. HeLa cells were treated with various stimuli including 0.1 μM angiotensin II (AgII), 20 ng/mL insulin, 25 μM LPA, 1 μg/mL LPS, 50 ng/mL NGF-β, 0.1 unit/mL thrombin, 50 ng/mL TNF-α, and 100 ng/mL phorbol 12-myristate 13-acetate (PMA). The expression of DR6 mRNA was measured by Northern blot at different time points as indicated. As shown in Figure 2(a), it was noted that only TNF-α, PMA, and LPA significantly upregulated DR6 expression at 7 hrs. TNF-α has been known to induce DR6 in several cancer cell lines [26]. PMA has also been reported to upregulate DR6 expression during T-cell activation [27]. As shown in Figure 2(b), DR6 mRNA expression in HeLa cells treated with 25 μM LPA increased transiently, with a peak level at 5–7 hr. As shown in Figure 2(c), LPA upregulated DR6 mRNA expression in a dose-dependent manner and reached a plateau at 25–50 μM. This result is further confirmed by RT-PCR (Supplemental Figure 1). Next, we sought to determine whether LPA regulates DR6 protein expression following a similar time course. As shown in Figure 2(d), 25 μM LPA treatment transiently increased DR6 protein expression in HeLa cells as early as 9 hr, with a peak level at 15–17 hr.

3.3. LPA Receptors 1 and 3 Mediate LPA-Induced DR6 Upregulation. Our data revealed that LPA receptors 1–3 (LPAR1–3) were expressed in HeLa cells (Figures 3(a) and 3(b)). To determine the role of LPAR in LPA-stimulated DR6 upregulation, we treated the cells with Ki16425 (3 μM), an LPA1/3 antagonist prior addition of LPA. As shown in Figures 3(c) and 3(d), pretreatment of cells with Ki16425 strongly inhibited LPA-induced DR6 expression, suggesting that LPA-induced DR6 upregulation was mediated by LPA receptors 1 and 3.

3.4. PI3K, PKC, and MEK Pathways Are Responsible for LPA-Stimulated DR6 Expression. As shown in Figure 4(a), treatment with LPA significantly induced MEK, ERK, and p90RSK phosphorylation. To determine the mechanism underlying LPA-induced DR6 expression, we first examined the effect of pertussis toxin (PTX), which inactivates the LPA receptor-coupled Gi/o type G protein [28], as shown in Figure 4(a); treatment with PTX inhibited LPA-induced phosphorylation of MEK, ERK, and p90RSK. LPA-induced phosphorylation of MEK, ERK, and p90RSK was also inhibited by wortmannin, a PI3K inhibitor, Ro 31-8220, a PKC inhibitor, and U-0126, a MEK inhibitor (Figure 4(a)). Next, we examined the roles of these kinases in LPA-induced DR6 expression. As shown in Figure 4(b), LPA-induced increase in the level of DR6 mRNA was strongly inhibited by Ro 31-8220, a cell-permeable inhibitor of PKC isoforms PKCα, PKCβ, PKCγ, and PKCε. Another PKC inhibitor GF 109203X also significantly inhibited LPA-induced DR6 mRNA expression, but not as strongly as Ro 31-8220. In addition to PKC inhibitors, the MEK inhibitor U-0126 and PI3K inhibitor wortmannin also significantly inhibited LPA-induced DR6 mRNA expression. The G protein inhibitor, PTX, inhibited LPA-induced DR6 mRNA expression too, but to a lesser extent. On the other hand, inhibition of p38 and JNK activity with SB203580 and JNK inhibitor had no effect on LPA-induced increase in DR6 mRNA expression. Together, our results suggested that PI3K/PKC/MEK pathway mediates LPA-induced DR6 expression.

3.5. PKC-Delta Specifically Mediates LPA-Induced DR6 Expression. Data presented in Figure 4 strongly suggest that activation of PKC is functionally involved in LPA-induced DR6 expression. To determine the specific isoform of PKC that contributes to LPA-induced DR6 expression, we first determined the LPA-induced activation of major PKC isoforms, PKCα/β, PKCε, PKCζ/λ, and PKCδ. HeLa cells were treated with 25 μM LPA for different time as indicated and the activation of the PKC isoforms was detected by

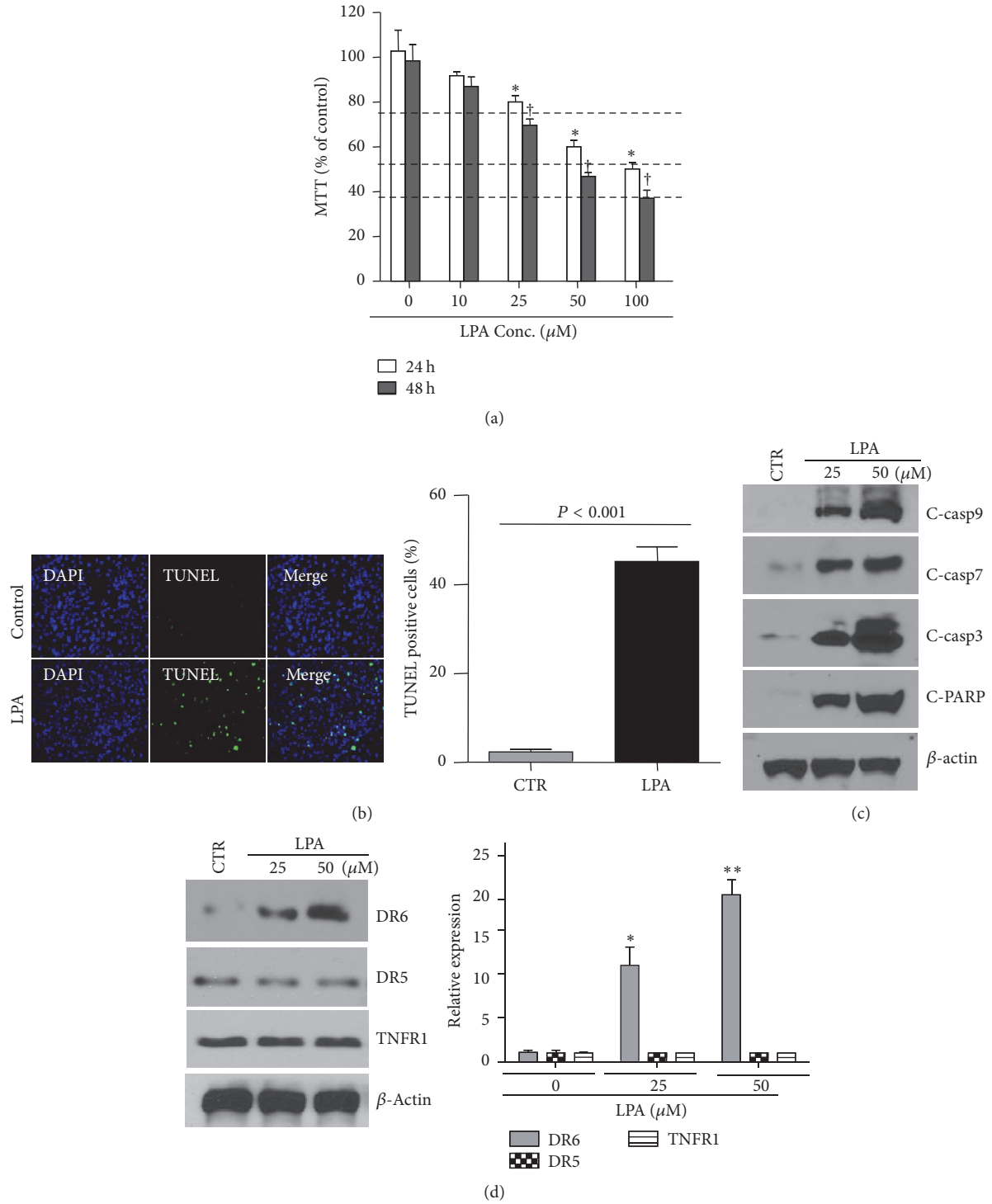

Figure 1: LPA induces apoptosis accompanied by upregulation of DR6 expression. (a) LPA treatment reduced cell viability in a concentration-dependent manner as determined by MTT assay. 10–25 μM LPA-induced significant cell viability reduction compared to control. $n = 4$, $^{*}P < 0.05$ versus control; †high concentration of LPA at 50–100 μM caused more cell viability reduction. $n = 4$. (b) LPA-triggered apoptosis was determined by TUNEL staining. HeLa cells were treated by 25 μM LPA for 24 hrs. $n = 3$. The bar graphs on the right panel represent quantification of TUNEL assay, $n = 3$, $P < 0.001$ versus control. (c and d) HeLa cells were exposed to different concentration of LPA for 18 hours. Activation of caspase-9, caspase-7, and caspase-3 and the cleavage of PARP (c), and expression levels of DR6, DR5, and TNFR (d) were determined by Western blot. The blot is a representative of 4 blots from 4 independent experiments ($n = 4$). The bar graphs on the right panel are densitometry analyses of DR6, DR5, and TNFR1 protein expression. $^{*}P < 0.05$, $^{**}P < 0.001$ versus control.

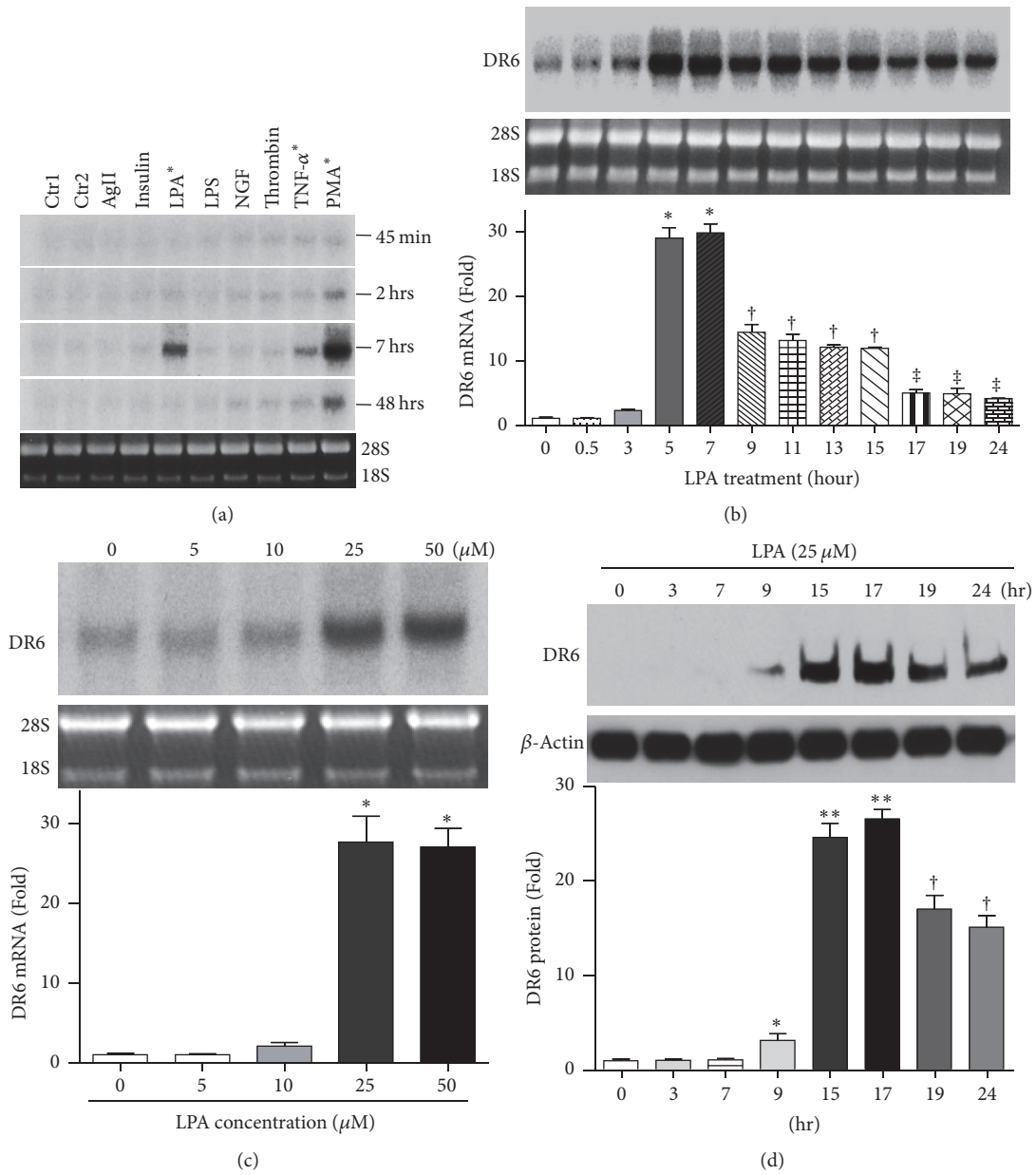

FIGURE 2: LPA upregulates DR6 expression in does- and time-dependent manner. (a) HeLa cells were exposed to various stimuli and the expression of DR6 was measured by Northern blot at different time points as indicated. Control 1: untreatment; Control 2: vehicle (DMSO) treatment. $^{*}P < 0.001$ versus control. (b) HeLa cells were treated with LPA (25 μM) for different times as indicated. Expression of DR6 was measured by Northern blot. $n = 3$. $^{*}P < 0.001$ versus control; $^{\dagger}P < 0.05$ versus 5–7 hr time point, $^{\ddagger}P < 0.05$ versus 9–15 hr time points. (c) HeLa cells were treated with various concentrations of LPA for 16 hrs. DR6 mRNA expression was measured by Northern blot. $n = 3$, $^{*}P < 0.001$ versus control. (d) HeLa cells were treated with LPA 25 μM for the times indicated. The cells were then lysed, and 50 μg of the cell lysates was analyzed by SDS-PAGE followed by Western blotting with anti-DR6 antibody and then were visualized by the enzyme-linked chemiluminescence system. The bar graphs below are densitometry analyses of DR6 protein expression. Data presented are mean ± SD from 3 independent experiments, with untreated controls set as 1. $^{*}P < 0.05$, $^{**}P < 0.001$ versus control; $^{\dagger}P < 0.05$ versus 15–17 time points.

Western blot analysis. As shown in Figure 5(a), upon treatment with LPA, all PKCs examined were activated to various extents. Among them, the high level of basal phosphorylation of PKCα/β was not significantly affected by LPA treatment. Similarly, the phosphorylation levels of PKCε and PKCζ/λ were also slightly increased by LPA treatment during the time course. On the other hand, PKCδ was remarkably activated upon treatment with LPA as determined by the rapid and robust increase in the phosphorylation level of it. Next, we determined the effect of expression of dominant-negative forms of these PKC isoforms on the LPA-induced DR6 expression. As shown in Figure 5(b), expression of dominant-negative forms of PKCα, PKCε, and PKCζ had no effect on LPA-induced DR6 expression. However,

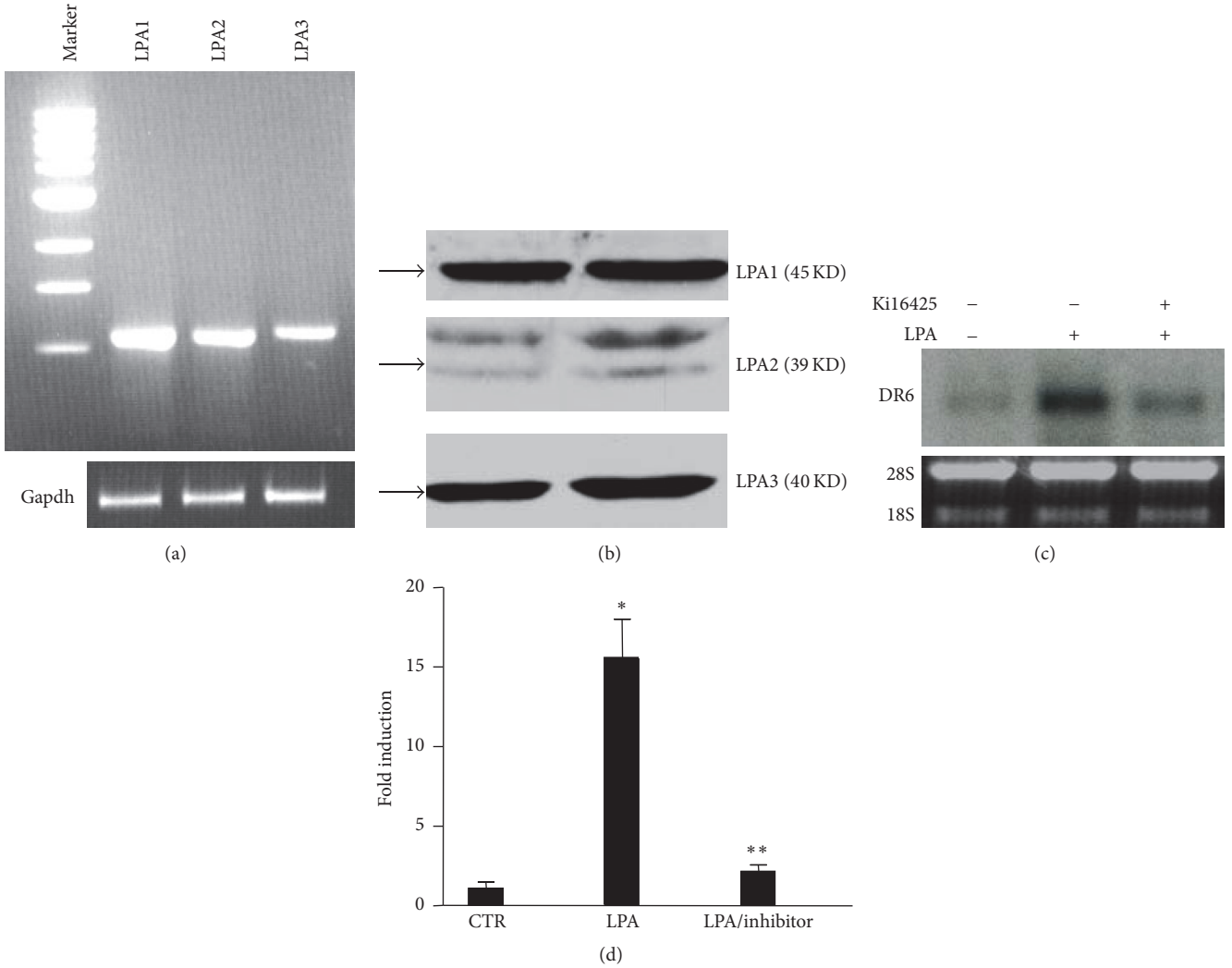

Figure 3: LPA-induced DR6 upregulation is mediated by LPA receptors 1/3 (LPAR1/3). (a and b), LPA1, LPA2, and LPA3 mRNA and protein are all expressed in HeLa cells, as indicated by PCR and Western blot, respectively. $n = 3$. (c) LPA1/3 antagonist Ki16425 (3 μM) attenuated the DR6 upregulation induced by LPA. $n = 4$. (d) The bar graphs are statistical analysis of DR6 expression. Data presented are mean ± SD from 4 independent experiments, with untreated controls set as 1. $^{*}P < 0.001$ versus control; $^{**}P < 0.001$ versus LPA.

expression of dominant-negative form of PKCδ almost completely blocked LPA-induced DR6 mRNA expression. Together, our data strongly suggest that PKCδ is the major PKC isoform that is functionally involved in signaling pathway that mediates LPA-induced DR6 expression. These data demonstrated for the first time PKC isoform-specific transcriptional regulation of LPA-induced DR6 expression.

3.6. Phosphorylated ERK and CREB Participate in LPA-Stimulated DR6 Expression. Data presented in Figure 4 showed that LPA induced the activation of both ERK and p90RSK. Previous study has reported that LPA can induce p90RSK activation through ERK [29]. The serine/threonine kinase p90Rsk is known to directly phosphorylate the transcriptional factor CREB (cAMP response element-binding protein) [30, 31]. Thus, we thought to determine whether LPA-induced activation of MEK-ERK-90RSK pathway leads to the activation of CREB and whether CREB is involved in LPA-induced expression of DR6. As shown in Figure 6(a), LPA induced activation of MEK and ERK1/2 at a very early time point. Moreover, LPA also strongly induced the activation of the transcription factor CREB in a time-dependent manner. To determine the role of these molecules in LPA-regulated DR6 expression, we employed a siRNA approach. As shown in Figure 6(b), knockdown of ERK and CREB strongly blocked LPA-induced DR6 mRNA expression. As shown in Figure 6(c), Western blot analysis confirmed the efficient knockdown of the expression of ERK and CREB. As expected, the protein level of DR6 was dramatically reduced in ERK- and CREB-knockdown cells. These observations suggest that LPA induces DR6 expression through activation of the PKCδ-ERK signaling pathway and the subsequent activation of CREB.

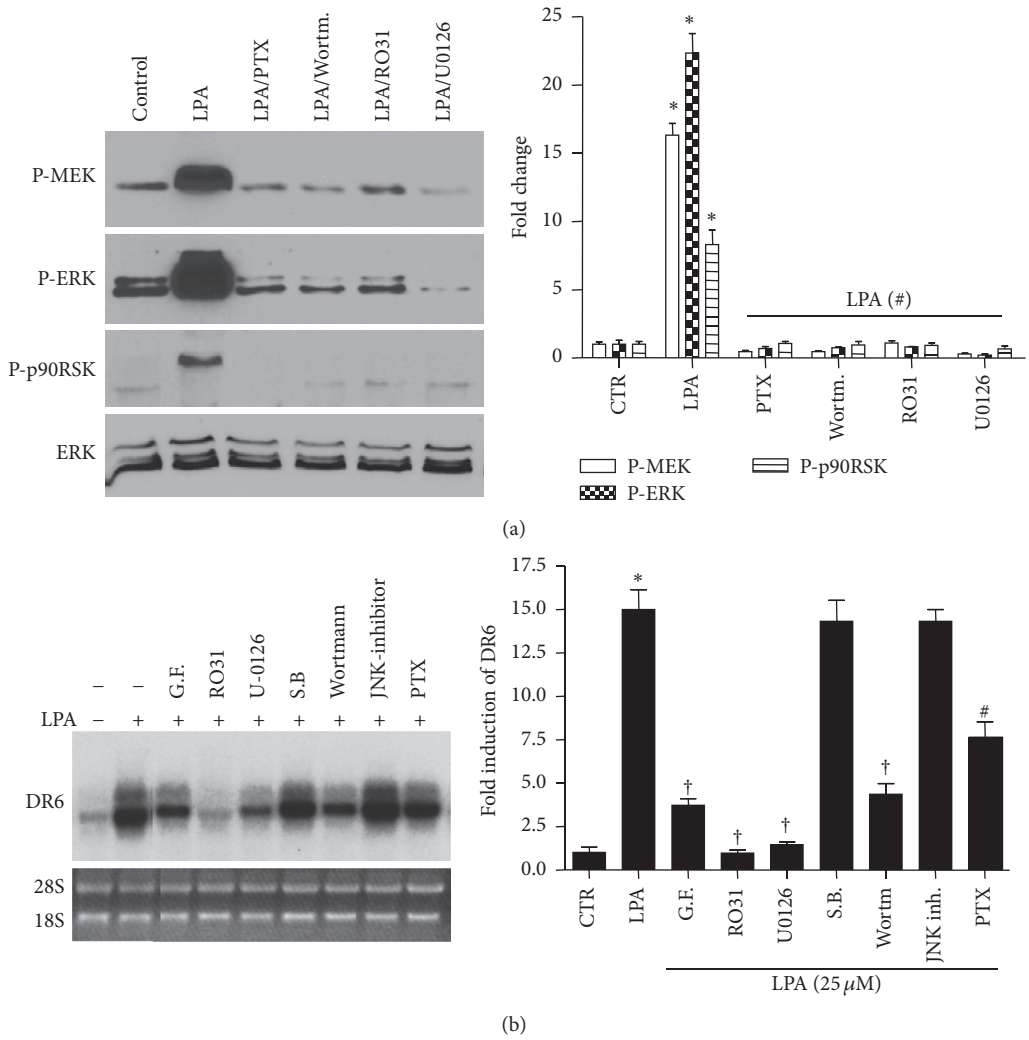

Figure 4: PI3K, PKC, and MEK pathways are involved in LPA-induced DR6 expression. (a) HeLa cells were treated with LPA (25 μM) in the presence or absence of the pathway inhibitors as indicated. The phosphorylation of MEK, ERK, and p90RSK was analyzed by Western blotting. The blot is a representative of 3 independent experiments. The bar graphs on the right panel are densitometry analyses of MEK, ERK, and p90RSK phosphorylation levels. $^{*}P < 0.001$ versus control; $^{\#}P < 0.001$ versus LPA-treated group. (b) HeLa cells were treated with LPA in the presence or absence of the pathway inhibitors as indicated and the expression of DR6 was measured by Northern blot. The bar graphs on the right panel are statistical analysis of DR6 expression. Data presented are mean ± SD from 3 independent experiments, with untreated controls set as 1. $^{*}P < 0.001$ versus control; $^{\dagger}P < 0.001$ versus LPA alone; $^{\#}P < 0.001$ versus LPA-treated group. PTX, pertussis toxin (100 ng/mL); GF10293X, PKC inhibitor (5 μM); wortmannin, PI3K inhibitor, (100 nM); Ro 31-8220, PKC inhibitor (5 μM); U-0126, MEK inhibitor (10 μM); SB203580, p38 inhibitor (2.5 μM) and JNK inhibitor (10 μM).

3.7. Downregulation of DR6 by siRNA Attenuates LPA-Induced Apoptosis. Next, we further substantiated the role of DR6 in LPA-induced apoptosis. First, to determine the apoptotic activity of DR6, HeLa cells were infected with adenoviruses expressing constitutively active DR6. As shown in Figure 7(a), infection of DR6-expressing adenovirus resulted in a dose-dependent apoptosis as determined by the cleavage of PARP, an indicator of apoptosis [32], and the activation of caspase-3. As a control, no apoptotic sign was detected in cells infected with virus expressing LacZ protein. Taken together, these results clearly indicate that overexpression of DR6 induces apoptosis in HeLa cells. Next, to determine whether LPA-upregulated DR6 expression accounts for the apoptosis induced by LPA, we determined the effect of knockdown of DR6 on LPA-induced apoptosis. As shown in Figure 7(b), as expected, treatment with DR6-specific siRNA strongly inhibited DR6 expression as determined by the reduction in the DR6 protein level. Interestingly, DR6-siRNA treatment also strongly inhibited LPA-induced apoptosis as determined by the reduction of caspase activation and PARP cleavage. These results strongly suggest that LPA-induced apoptosis is mediated by induction of DR6 expression.

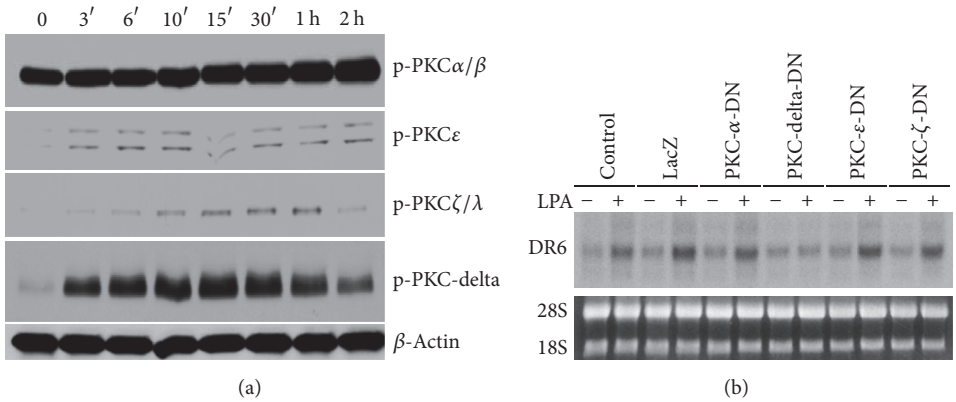

Figure 5: LPA-induced DR6 upregulation is specifically mediated by PKCδ isoform. (a) A time course of LPA-induced activation of PKC kinases. The blots were incubated in sequence with antibodies against several major PKC isoforms such as PKCα/β, PKCε, PKCζ/λ, and PKCδ. All isozymes stained as a dominant band of the expected molecular weight. $n = 3$. (b) HeLa cells were infected with adenoviral PKCα-DN, PKCδ-DN, PKCε-DN, and PKCζ-DN for up to 24 hrs. Cells were then starved in DMEM serum-free overnight and stimulated with 25 μM LPA (+) or vehicle (−) for 8 hrs, followed by Northern blotting for DR6 mRNA expression. $n = 3$.

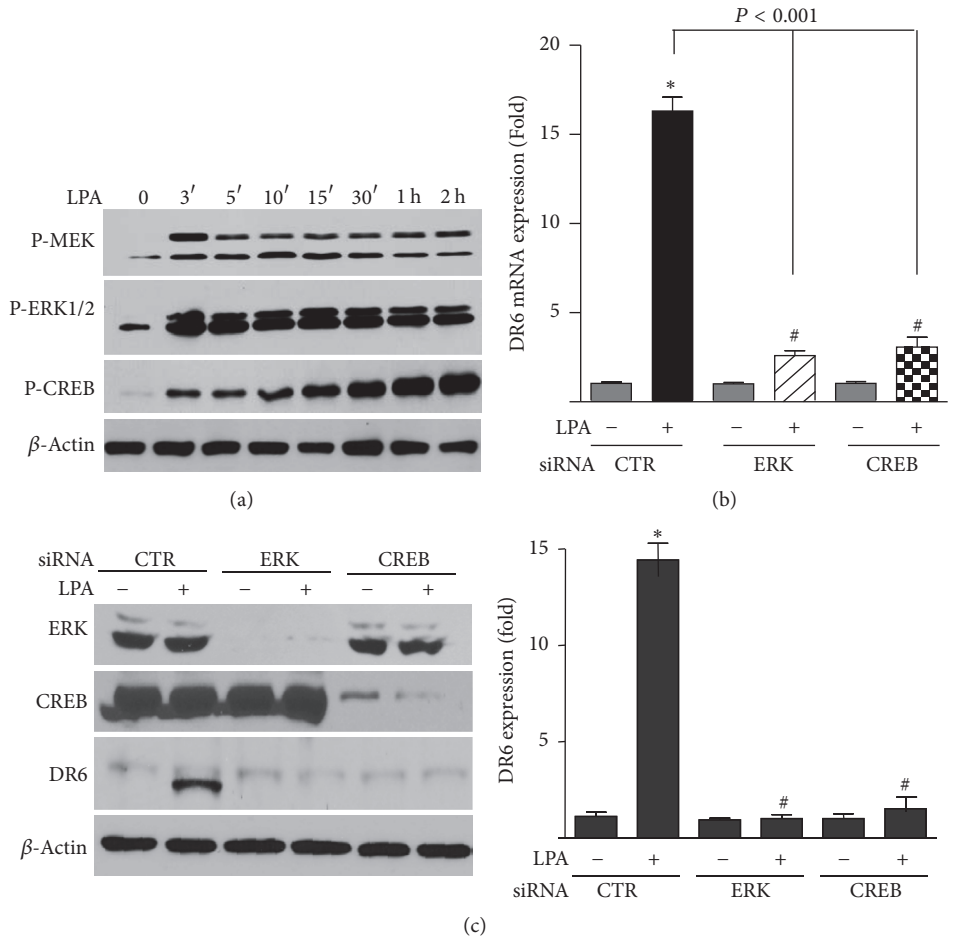

Figure 6: ERK and CREB pathway regulates LPA-induced DR6 expression. (a) HeLa cells were treated with LPA (25 μM) at various concentrations as indicated. The phosphorylation of MEK, ERK, and CREB was analyzed by Western blotting. The blot is a representative of 3 independent experiments ($n = 3$). (b and c) HeLa cells were treated with LPA in the presence of control siRNA and ERK- or CREB-specific siRNAs. The expressions of DR6 mRNA (b) and protein (c) were measured by q-PCR and Western analysis, respectively. The bar graphs on the right panel of (c) are statistical analysis of DR6 expression. Data presented are mean ± SD from 3 independent experiments, with nontreated controls set as 1. $^{*}P < 0.001$ versus control; $^{\#}P < 0.001$ versus LPA/control siRNA.

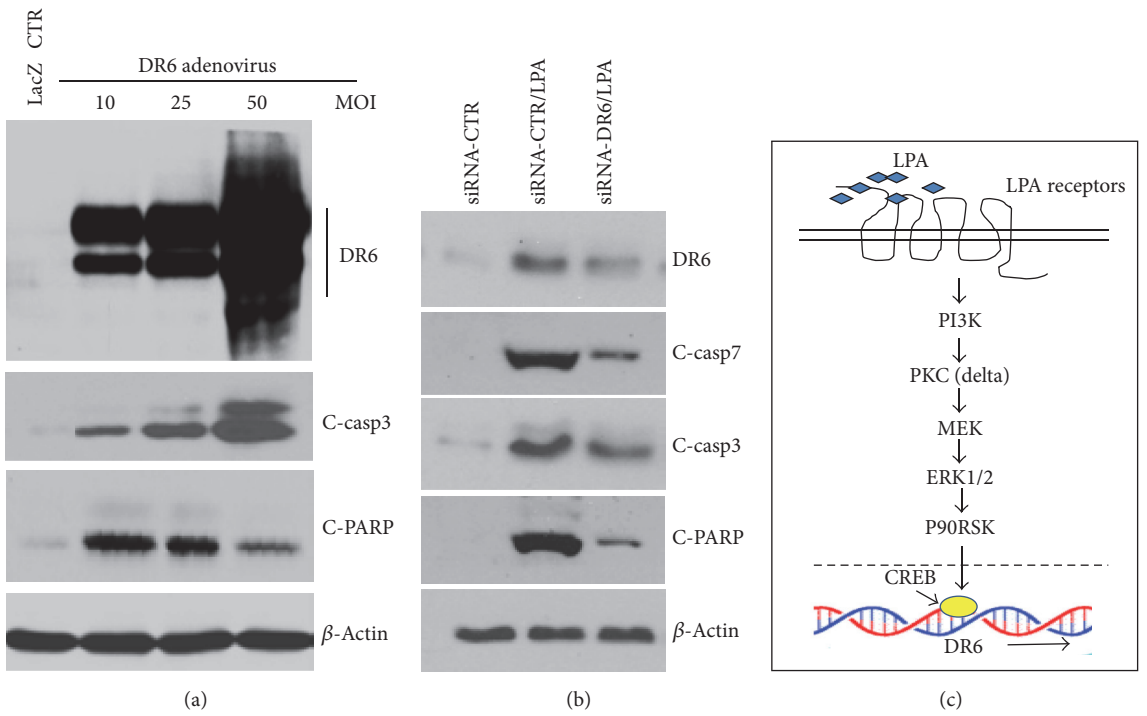

FIGURE 7: DR6 induction is responsible for LPA-induced apoptosis and sketch of mechanism. (a) Overexpression of DR6 induced apoptosis. HeLa cells were transiently infected with adenoviruses encoding constitutively active DR6 with different multiplicity of infection (MOI); or a control adenovirus carrying the LacZ gene (LacZ). After 24 hr infection, cells were harvested, and the lysates were separated by SDS-PAGE, followed by Western blot analysis for DR6 expression, caspase activation, and PARP cleavage. This membrane was also reprobed with anti-β-actin antibody to indicate relative loading of samples (bottom panel). The blot is a representative of 3 independent experiments ($n = 3$). (b) Downregulation of DR6 expression by siRNA attenuates LPA-triggered apoptosis. HeLa cells were treated with LPA in the presence of control siRNA or DR6 siRNA. The expressions of DR6 and activation of caspase-7, caspase-3, and PARP cleavage were measured by Western analysis. $n = 4$. (c) The proposed molecular mechanism of LPA-induced DR6 expression in HeLa cells. LPA ligand binds to its receptors LPAR1 or LPAR3 to initiate the cell signaling by activation PI3K, followed by the activation of PKC δ and MEK, which phosphorylate ERK1/2. ERK then activates CREB probably mediated by activation of P90-RSK.

4. Discussion

LPA, a simple bioactive phospholipid, is present in biological fluids such as plasma and cerebrospinal fluid (CSF). LPA concentrations in blood can range from 0.1 μM in plasma and up to 10 μM in serum [33]. In this study, most of the experiments were carried out using 25 μM LPA, which is in the range of pathological concentrations found in atherosclerotic lesions in vivo [34] and acute myocardial infarction [35]. This concentration range has been used to determine the apoptotic activity of LPA in other cell types, such as epithelial cells [18] and neuronal cells [17].

LPA, through its G protein-coupled receptors, regulates diverse cellular processes, including cell survival and apoptosis in many different cell types [28]. The function of LPA as a cell survival factor has been well studied; however, the mechanism by which LPA induces apoptosis remains elusive. In the current study, using pharmaceutical inhibitors, dominant-negative mutations, and siRNA approach, we explored the mechanism(s) underlying LPA-induced apoptosis. To this end, our results revealed several interesting findings. First, LPA induced apoptosis at pathologic concentrations in HeLa cells. Second, treatment with LPA resulted in remarkable upregulated expression of DR6. Third, knockdown of DR6 strongly blocked LPA-induced apoptosis. Fourth, LPA receptors 1 and 3 antagonist inhibited LPA-induced DR6 expression. Finally, inhibition of various kinases, PI3K/PKC/MEK/ERK, and their regulated transcription factor CREB strongly inhibited LPA-induced DR6 expression. Together, these results strongly suggest that LPA-induced apoptosis is mediated by upregulation of DR6 expression via activation of PI3K/PKC/MEK/ERK pathways leading to the activation of the transcription factor CREB, which controls the expression of DR6.

In this study, the first and novel finding is the identification of DR6 as an effector that mediates LPA-induced apoptosis. DR6 is a relatively less characterized member of the TNF death receptor family of protein. To date, DR6 still remains as an orphan receptor and no specific cognate ligand for it has yet been identified. Most of our current knowledge about the cellular and physiological role and biological function of DR6 comes from studying the effect of DR6 gene ablation in mice or ectopic expression of DR6 in cultured cells [36]. Recent studies reported that DR6

expression is upregulated in neurodegenerative disease such as Alzheimer's disease (AD) and amyotrophic lateral sclerosis (ALS) and the upregulated expression of DR6 may contribute to the pathogenesis of these neurodegenerative disorders [37, 38]. Interestingly, LPA has also been implicated in apoptotic neurodegeneration [17, 39–41]; however, the mechanism by which LPA induces apoptotic cell death remains elusive. In this study, our data demonstrated for the first time that LPA upregulated DR6 expression and that knockdown of DR6 strongly blocked LPA-induced apoptosis, strongly suggesting that LPA induces apoptosis via upregulating DR6 expression. Thus, our finding that LPA-induced apoptosis was mediated by upregulation of DR6 expression suggests a possibility that LPA may contribute to neurodegeneration through elevating DR6 protein level.

The second interesting discovery of this study is the finding that LPA-induced DR6 expression is mediated by activation of transcription factor CREB. Studies have reported that exogenous expression of DR6 could mimic ligand activation and triggered ligand-independent downstream apoptotic signaling cascades [21, 22]. However, although overexpression of DR6 causes apoptotic cell death, it has been found that the expression level of DR6 is elevated in several tumors in humans and the elevated expression of DR6 is regulated through activation of NF-kB [26]. Furthermore, these authors have also demonstrated that expression of DR6 expression could be induced by tumor necrosis factor-α (TNF-α) treatment and TNF-α-induced DR6 expression is also mediated by activation of NF-kB [26]. In contrast to this finding, it was recently reported that activation of NF-kB inhibited (E)-2,4-Bis(p-hydroxyphenyl)-2-butenal-induced DR6 expression in colon cancer cells [42]. These controversial observations might have resulted from the use of different experimental systems, such as different cell lines and different stimuli, in these studies. Interestingly, in the current study, our data demonstrated that LPA-induced DR6 expression is mediated by the activation of CREB. Our finding further supports the assumption that different stimuli activate different pathways and lead to activation of different transcriptional factors that govern the expression of DR6.

LPA is well known as a survival factor. However, it has also been reported that LPA can promote apoptosis in some cell types, including epithelial cells [18], the differentiated neuron model PC12 cells [39], and hippocampal neurons [40]. Regarding the seemingly contradictory effects of LPA on promoting cell survival and apoptosis, one possibility is that the concentration of LPA used in inducing apoptosis is higher than that used in cell survival. For example, the concentration of LPA in promoting cell survival is in the 10 μM range [43, 44]. On the other hand, the concentrations of LPA used to induce apoptosis are mostly higher than 20 μM [17, 18, 39, 40]. Other possibilities are that different cell types express different isoforms of LPA receptors and have unique gene expression and regulation patterns that are variably altered by LPA signals, as reviewed previously [3].

In summary, we have identified a signaling pathway implicated in LPA-induced apoptosis. This pathway is mediated by LPA receptor and its downstream PI3K/PKC/MEK/ERK signaling cascades. The most interesting and novel finding of current study is the identification of DR6 as a key factor that mediates LPA-induced apoptosis. The mechanism by which LPA functions as a survival factor has been extensively studied. However, the mechanism by which LPA regulates cell apoptosis remains largely unknown. Thus, our finding that LPA can stimulate DR6 expression leading to apoptotic cell death would contribute to better understanding of the mechanism by which LPA regulates apoptosis and identification of new therapeutic targets.

Competing Interests

The authors declare that they have no competing interests.

Authors' Contributions

Yunzhou Dong and Yong Wu contributed equally to this work.

Acknowledgments

This work was supported by National Institute of Health (NIH) R01AG026640, R21 AG039596, Alzheimer's Association grant, a grant from American Health Assistance Foundation (AHAF, to X. Xu), NIH Grant HL107466 (to M-Z Cui), a grant from Oklahoma Center for Advanced Science and Technology (OCAST) AR11-043, and a grant from AHA 12SDG8760002 (to Y. Dong) and partially supported by Accelerating Excellence in Translational Science Pilot Grants G0812D05, pilot project award from the National Institutes of Health (NCI, NIMHD) Grants U54 CA143931 and U54MD0075984, and NIH/NCI SC1CA200517 (to Y. Wu).

References

[1] S. Hosogaya, Y. Yatomi, K. Nakamura et al., "Measurement of plasma lysophosphatidic acid concentration in healthy subjects: strong correlation with lysophospholipase D activity," *Annals of Clinical Biochemistry*, vol. 45, no. 4, pp. 364–368, 2008.

[2] S. E. Gardell, A. E. Dubin, and J. Chun, "Emerging medicinal roles for lysophospholipid signaling," *Trends in Molecular Medicine*, vol. 12, no. 2, pp. 65–75, 2006.

[3] X. Ye, I. Ishii, M. A. Kingsbury, and J. Chun, "Lysophosphatidic acid as a novel cell survival/apoptotic factor," *Biochimica et Biophysica Acta—Molecular and Cell Biology of Lipids*, vol. 1585, no. 2-3, pp. 108–113, 2002.

[4] S. G. Bourgoin and C. Zhao, "Autotaxin and lysophospholipids in rheumatoid arthritis," *Current Opinion in Investigational Drugs*, vol. 11, no. 5, pp. 515–526, 2010.

[5] Y. Zhao and V. Natarajan, "Lysophosphatidic acid (LPA) and its receptors: role in airway inflammation and remodeling," *Biochimica et Biophysica Acta*, vol. 1831, no. 1, pp. 86–92, 2013.

[6] G. Tigyi, "Aiming drug discovery at lysophosphatidic acid targets," *British Journal of Pharmacology*, vol. 161, no. 2, pp. 241–270, 2010.

[7] E. J. van Corven, A. Groenink, K. Jalink, T. Eichholtz, and W. H. Moolenaar, "Lysophosphatidate-induced cell proliferation: identification and dissection of signaling pathways mediated by G proteins," *Cell*, vol. 59, no. 1, pp. 45–54, 1989.

[8] W. H. Moolenaar, L. A. Van Meeteren, and B. N. G. Giepmans, "The ins and outs of lysophosphatidic acid signaling," *BioEssays*, vol. 26, no. 8, pp. 870–881, 2004.

[9] W. H. Moolenaar, "Bioactive lysophospholipids and their G protein-coupled receptors," *Experimental Cell Research*, vol. 253, no. 1, pp. 230–238, 1999.

[10] O. Kranenburg and W. H. Moolenaar, "Ras-MAP kinase signaling by lysophosphatidic acid and other G protein-coupled receptor agonists," *Oncogene*, vol. 20, no. 13, pp. 1540–1546, 2001.

[11] J. Du, C. Sun, Z. Hu et al., "Lysophosphatidic acid induces MDA-MB-231 breast cancer cells migration through activation of PI3K/PAK1/ERK signaling," *PLoS ONE*, vol. 5, no. 12, Article ID e15940, 2010.

[12] A. Boucharaba, C.-M. Serre, S. Grès et al., "Platelet-derived lysophosphatidic acid supports the progression of osteolytic bone metastases in breast cancer," *The Journal of Clinical Investigation*, vol. 114, no. 12, pp. 1714–1725, 2004.

[13] A. Boucharaba, C.-M. Serre, J. Guglielmi, J.-C. Bordet, P. Clézardin, and O. Peyruchaud, "The type 1 lysophosphatidic acid receptor is a target for therapy in bone metastases," *Proceedings of the National Academy of Sciences of the United States of America*, vol. 103, no. 25, pp. 9643–9648, 2006.

[14] T. Yamada, K. Sato, M. Komachi et al., "Lysophosphatidic Acid (LPA) in Malignant Ascites Stimulates Motility of Human Pancreatic Cancer Cells through LPA1," *Journal of Biological Chemistry*, vol. 279, no. 8, pp. 6595–6605, 2004.

[15] X. Fang, D. Gaudette, T. Furui et al., "Lysophospholipid growth factors in the initiation, progression, metastases, and management of ovarian cancer," *Annals of the New York Academy of Sciences*, vol. 905, pp. 188–208, 2000.

[16] J. W. Choi, D. R. Herr, K. Noguchi et al., "LPA receptors: subtypes and biological actions," *Annual Review of Pharmacology and Toxicology*, vol. 50, pp. 157–186, 2010.

[17] M. R. Steiner, F. W. Holtsberg, J. N. Keller, M. P. Mattson, and S. M. Steiner, "Lysophosphatidic acid induction of neuronal apoptosis and necrosis," *Annals of the New York Academy of Sciences*, vol. 905, pp. 132–141, 2000.

[18] M. Funke, Z. Zhao, Y. Xu, J. Chun, and A. M. Tager, "The lysophosphatidic acid receptor LPA1 promotes epithelial cell apoptosis after lung injury," *American Journal of Respiratory Cell and Molecular Biology*, vol. 46, no. 3, pp. 355–364, 2012.

[19] Y. Meng, L. Graves, T.-V. Do, J. So, and D. A. Fishman, "Upregulation of FasL by LPA on ovarian cancer cell surface leads to apoptosis of activated lymphocytes," *Gynecologic Oncology*, vol. 95, no. 3, pp. 488–495, 2004.

[20] C.-C. Lin, C.-E. Lin, Y.-C. Lin et al., "Lysophosphatidic acid induces reactive oxygen species generation by activating protein kinase C in PC-3 human prostate cancer cells," *Biochemical and Biophysical Research Communications*, vol. 440, no. 4, pp. 564–569, 2013.

[21] G. Pan, K. O'Rourke, and V. M. Dixit, "Caspase-9, Bcl-X_L, and Apaf-1 form a ternary complex," *Journal of Biological Chemistry*, vol. 273, no. 10, pp. 5841–5845, 1998.

[22] L. Zeng, T. Li, D. C. Xu et al., "Death receptor 6 induces apoptosis not through type I or type II pathways, but via a unique mitochondria-dependent pathway by interacting with bax protein," *Journal of Biological Chemistry*, vol. 287, no. 34, pp. 29125–29133, 2012.

[23] M.-Z. Cui, E. Laag, L. Sun, M. Tan, G. Zhao, and X. Xu, "Lysophosphatidic acid induces early growth response gene 1 expression in vascular smooth muscle cells: CRE and SRE mediate the transcription," *Arteriosclerosis, Thrombosis, and Vascular Biology*, vol. 26, no. 5, pp. 1029–1035, 2006.

[24] X. Xu, Y.-C. Shi, W. Gao et al., "The novel presenilin-1-associated protein is a proapoptotic mitochondrial protein," *The Journal of Biological Chemistry*, vol. 277, no. 50, pp. 48913–48922, 2002.

[25] Y. Dong, Y. Wu, M. Wu et al., "Activation of protease calpain by oxidized and glycated LDL increases the degradation of endothelial nitric oxide synthase," *Journal of Cellular and Molecular Medicine*, vol. 13, no. 9, pp. 2899–2910, 2009.

[26] G. M. Kasof, J. J. Lu, D. Liu et al., "Tumor necrosis factor-α induces the expression of DR6, a member of the TNF receptor family, through activation of NF-κB," *Oncogene*, vol. 20, no. 55, pp. 7965–7975, 2001.

[27] M. Klíma, A. Broučková, M. Koc, and L. Anděra, "T-cell activation triggers death receptor-6 expression in a NF-κB and NF-AT dependent manner," *Molecular Immunology*, vol. 48, no. 12-13, pp. 1439–1447, 2011.

[28] X. Ye, I. Ishii, M. A. Kingsbury, and J. Chun, "Lysophosphatidic acid as a novel cell survival/apoptotic factor," *Biochimica et Biophysica Acta (BBA)—Molecular and Cell Biology of Lipids*, vol. 1585, no. 2-3, pp. 108–113, 2002.

[29] Y.-J. Xu, S. Ouk Kim, D.-F. Liao, S. Katz, and S. L. Pelech, "Stimulation of 90- and 70-kDa ribosomal protein S6 kinases by arginine vasopressin and lysophosphatidic acid in rat cardiomyocytes," *Biochemical Pharmacology*, vol. 59, no. 9, pp. 1163–1171, 2000.

[30] A. J. Shaywitz and M. E. Greenberg, "CREB: a stimulus-induced transcription factor activated by a diverse array of extracellular signals," *Annual Review of Biochemistry*, vol. 68, pp. 821–861, 1999.

[31] T. Mizutani, S. Fukushi, M. Saijo, I. Kurane, and S. Morikawa, "Regulation of p90RSK phosphorylation by SARS-CoV infection in Vero E6 cells," *FEBS Letters*, vol. 580, no. 5, pp. 1417–1424, 2006.

[32] L. Dubrez, I. Savoy, A. Hamman, and E. Solary, "Pivotal role of a DEVD-sensitive step in etoposide-induced and Fas-mediated apoptotic pathways," *The EMBO Journal*, vol. 15, no. 20, pp. 5504–5512, 1996.

[33] Y. C. Yung, N. C. Stoddard, and J. Chun, "LPA receptor signaling: pharmacology, physiology, and pathophysiology," *Journal of Lipid Research*, vol. 55, no. 7, pp. 1192–1214, 2014.

[34] W. Siess, K. J. Zangl, M. Essler et al., "Lysophosphatidic acid mediates the rapid activation of platelets and endothelial cells by mildly oxidized low density lipoprotein and accumulates in human atherosclerotic lesions," *Proceedings of the National Academy of Sciences of the United States of America*, vol. 96, no. 12, pp. 6931–6936, 1999.

[35] X. Chen, X. Y. Yang, N. D. Wang et al., "Serum lysophosphatidic acid concentrations measured by dot immunogold filtration assay in patients with acute myocardial infarction," *Scandinavian Journal of Clinical and Laboratory Investigation*, vol. 63, no. 7-8, pp. 497–503, 2003.

[36] R. Benschop, T. Wei, and S. Na, "Tumor necrosis factor receptor superfamily member 21: TNFR-related death receptor-6, DR6," in *Therapeutic Targets of the TNF Superfamily*, I. S. Grewal, Ed., pp. 186–194, Springer, New York, NY, USA, 2009.

[37] Y. Hu, X. Lee, Z. Shao et al., "A DR6/p75NTR complex is responsible for β-amyloid-induced cortical neuron death," *Cell Death & Disease*, vol. 4, no. 4, article e579, 2013.

[38] G. Huang, X. Lee, Y. Bian et al., "Death receptor 6 (DR6) antagonist antibody is neuroprotective in the mouse SOD1G93A

model of amyotrophic lateral sclerosis," *Cell Death and Disease*, vol. 4, no. 10, article e841, 2013.

[39] F. W. Holtsberg, M. R. Steiner, A. J. Bruce-Keller et al., "Lysophosphatidic acid and apoptosis of nerve growth factor-differentiated PC12 cells," *Journal of Neuroscience Research*, vol. 53, no. 6, pp. 685–696, 1998.

[40] F. W. Holtsberg, M. R. Steiner, J. N. Keller, R. J. Mark, M. P. Mattson, and S. M. Steiner, "Lysophosphatidic acid induces necrosis and apoptosis in hippocampal neurons," *Journal of Neurochemistry*, vol. 70, no. 1, pp. 66–76, 1998.

[41] Z.-Q. Zheng, X.-J. Fang, and J.-T. Qiao, "Dual action of lysophosphatidic acid in cultured cortical neurons: survival and apoptogenic," *Acta physiologica Sinica*, vol. 56, no. 2, pp. 163–171, 2004.

[42] J. O. Ban, Y.-S. Jung, D. H. Kim et al., "(E)-2,4-Bis(p-hydroxyphenyl)-2-butenal inhibits tumor growth via suppression of NF-κB and induction of death receptor 6," *Apoptosis*, vol. 19, no. 1, pp. 165–178, 2014.

[43] Y. Li, M. I. Gonzalez, J. L. Meinkoth, J. Field, M. G. Kazanietz, and G. I. Tennekoon, "Lysophosphatidic acid promotes survival and differentiation of rat Schwann cells," *The Journal of Biological Chemistry*, vol. 278, no. 11, pp. 9585–9591, 2003.

[44] F. Hao, F. Zhang, D. D. Wu et al., "Lysophosphatidic acid-induced vascular neointimal formation in mouse carotid arteries is mediated by the matricellular protein CCN1/Cyr61," *American Journal of Physiology—Cell Physiology*, vol. 311, no. 6, pp. C975–C984, 2016.

Hindawi
Mediators of Inflammation
Volume 2017, Article ID 3701385, 14 pages
https://doi.org/10.1155/2017/3701385

Research Article

FTY720 Attenuates Angiotensin II-Induced Podocyte Damage via Inhibiting Inflammatory Cytokines

Ke Su,[1] Ping Zeng,[1] Wei Liang,[1] Zhengyu Luo,[2] Yiman Wang,[1] Xifeng Lv,[1] Qi Han,[1] Miao Yan,[1] and Cheng Chen[1]

[1]*Department of Nephrology, Renmin Hospital of Wuhan University, 238 Jiefang Road, Wuhan 430060, China*
[2]*First School of Clinical Medicine, Renmin Hospital of Wuhan University, 238 Jiefang Road, Wuhan 430060, China*

Correspondence should be addressed to Cheng Chen; chencheng123@whu.edu.cn

Received 20 October 2016; Revised 8 December 2016; Accepted 26 December 2016; Published 7 February 2017

Academic Editor: Yong Wu

FTY720, a new chemical substance derived from the ascomycete *Isaria sinclairii*, is used for treating multiple sclerosis, renal cancer, and asthma. Sphingosine 1-phosphate (S1P) is a bioactive sphingolipid metabolite and exists in red blood cells. FTY720 is a synthetic S1P analog which can block S1P evoking physiological effects. Recently studies show that S1P was participating in activated inflammation cells induced renal injury. The objective of this study was to assess the protective effect of FTY720 on kidney damage and the potential mechanism of FTY720 which alleviate podocyte injury in chronic kidney disease. In this study, we selected 40 patients with IgA nephropathy and examined their clinical characteristics. Ang II-infusion rat renal injury model was established to evaluate the glomeruli and tubulointerstitial lesion. The result showed that the concentration of S1P in serum and urine was positively correlated with IgA nephropathy patients' renal injury. FTY720 could reduce renal histological lesions induced by Ang II-infusion in rats. Moreover, FTY720 decreased S1P synthesis in Ang II-infusion rats via downregulation of inflammatory cytokines including TNF-α and IL-6. In addition, FTY720 alleviated exogenous S1P-induced podocyte damage. In conclusion, FTY720 is able to attenuate S1P-induced podocyte damage via reducing inflammatory cytokines.

1. Introduction

Chronic kidney disease (CKD) includes a broad variety of pathologies, especially the chronic impairment of renal excretory function primarily arising from injury to renal structures. The majority forms of CKD are irretrievable and progressive. Renal damage comprises nephron loss, fibrosis, and renal vasculature changes [1]. CKD results from various causes including inflammatory and infiltrative diseases, nephritis, diabetes, hypertension, and renal and systemic infections. Renal inflammation, featured by the infiltration of inflammatory cells to kidney parenchyma, is a main pathologic process of various CKD [2–4]. Inflammatory infiltration results in the initiation and development of CKD. Inflammatory cell infiltration in the interstitium and persistent fibrogenesis involves several pathways, for example, stimulation of tubular chemokine expression, inflammatory cytokines, various growth factors, and monocyte chemotactic proteins [5]. Proteinuria represents a robust marker for progression of CKD [5]. The integrity of the glomerular filtration barrier relies on its three-layered structure such as endothelium, glomerular basement membrane (GBM), and podocytes. Augmented intraglomerular hydraulic pressure or glomerular filtration barrier impairment might cause glomerular/overload proteinuria [5]. Hematuria and proteinuria are the primary early-stage clinical features of CKD and can provoke proinflammatory and/or profibrotic effects, directly eliciting chronic tubulointerstitial damage.

Sphingosine 1-phosphate (S1P) is a bioactive sphingolipid metabolite that acts both as an extracellular mediator and as intracellular second messenger. S1P signaling mediates the pathogenesis of various diseases, such as inflammatory diseases, osteoporosis, and arthritis [6–8]. A number of cell types such as red blood cells (RBC), platelets, endothelial

cells, and neutrophils secrete S1P. RBC are the main source of S1P in plasma [9, 10]. Sphingosine kinases (SPHK) including two isoforms, SPHK1 and SPHK2 [11], are crucial regulators of S1P. SPHK1 is predominantly localized to the cytosol and translocates to the plasma membrane upon activation in eukaryotic cells. SPHK2 is found primarily in the nucleus [11]. S1P, via elevating its intracellular content through sphingolipid metabolism and binding to its receptors, controls a number of physiological/pathological processes, for example, cell proliferation, autophagy, migration, and angiogenesis. These processes are associated with tumor growth, metastasis, and invasion. S1P may interact with a family of G protein-coupled receptors (S1PRs), also known as endothelial differentiation gene (EDG) receptors [12], which affects the cellular responses to S1P. S1PRs, including S1P receptors 1 to 5 (S1PR1–S1PR5), are expressed in different tissue cells specifically [13, 14]. S1PR1 is extensively expressed in brain, heart, lung, liver, and spleen and, to a lesser extent, in thymus, kidney, renal medulla, glomeruli, and muscle [15–20]. Particularly, S1PR1 plays a critical role in the development of vascular lesions, progression of atherosclerosis, cancer, autoimmune disease, or multiple sclerosis [21–23]. Furthermore, deletion of S1PR1 intensifies kidney damage and inflammation [24] and S1PRs activation in kidneys and bone marrow-derived cells decreases inflammation [25, 26]. Overall, it is widely speculated that S1PR1 is implicated in regulating vascular tone and participating in renal damage under pathologic conditions. However, little is known about the role of S1PR1 in the development of renal damage.

FTY720, a synthetic S1P analog, is phosphorylated by SPHK1 and SPHK2 into its bioactive form, FTY720-phosphate [27–29]. FTY720-phosphate functions as a non-competitive inhibitor of various S1PRs [30, 31], such as S1PR1, S1PR3, S1PR4, and S1PR5, but not S1PR2, receptors [27, 32, 33]. FTY720-phosphate hinders S1P signaling through prompting the internalization and subsequent degradation of S1PRs [30]. Particularly, FTY720 has shown an extraordinary protective effect against autoimmune myocarditis [34], multiple sclerosis [27, 35], uveoretinitis [36], and atherosclerosis [37]. Clinical trials have been conducted to test its preventive effect on the rejection of renal transplant [38, 39]. Moreover, FTY720 administration relieved ovariectomy-induced osteoporosis [40] and mitigated lipopolysaccharide-induced arthritis in mice [41]. In this study, we used FTY720 to block S1P-elicited physiological effects. While previous studies suggested that FTY720 repressed immune response [38, 40], the mechanism(s) by which FTY720 modulates inflammatory diseases are poorly understood. In this study, we investigated the mechanisms behind FTY720 inhibition of the inflammatory response and alleviation of podocyte injury in chronic kidney disease.

2. Materials and Methods

2.1. Human Studies. Peripheral blood was collected from IgA nephropathy patient and healthy subjects. All patients were subjected to renal biopsy and the histological diagnoses of IgA nephropathy in Renmin Hospital of Wuhan University within 2014~2015. The histological grading of patients with IgA nephropathy was classified by Lee's grades I~IV. Patients who have systemic disease of SLE, Henoch-Schönlein Purpura Nephritis, and diabetic and chronic liver diseases were clinically excluded. Patients who received steroid therapy and immune depressant treatment were excluded. We collected patients' clinical information including age, sex, presence of hypertension (blood pressure > 140/95 mmHg or requirement for antihypertensive therapy), plasma creatinine, blood urea nitrogen, high-density lipoprotein, triglyceride, complement (C3 and C4), serum albumin, serum total protein, and 24 h urinary protein. The 24-hour urine protein excretion was tested by sulfosalicylic acid method. The renal biopsy tissues from patients with IgA nephropathy were stored immediately at −80°C for further tissue freezing section of pathological analysis. Renal tissue adjacent to carcinoma was collected as a normal control. These studies were approved by the hospital's Institutional Ethics Committee (Renmin Hospital of Wuhan University, China), and written informed consent was obtained from all patients.

2.2. ELISA. Plasma and urine S1P concentration in IgA nephropathy patient, healthy person, and rats were assessed by S1P ELISA (Echelon Biosciences, Salt Lake City, UT). Blood was allowed to clot and was then centrifuged and aliquots of serum were stored at −70°C before S1P analyses. The 24 h urine was collected for S1P level analyses. Plasma and urine were applied to the ELISA plate at 30 μg protein/well. ELISA was performed according to manufacturer's instructions. Results were confirmed by comparison to S1P concentration determined by microplate reader (BioTek, VT, USA) at OD 450 nm. Concentration of S1P was calculated in the samples by comparing the OD of the samples to the standard curve.

2.3. Animal. Animal experiments were performed according to the Guide for the Care and Use of Laboratory Animals of Wuhan University. Thirty-six male SPF Wistar rats weighing 160 ± 10 g were purchased from SJA experimental animals company (Hunan, China) and were maintained at a controlled temperature (23 ± 2°C) and humidity (55 ± 5%) with a light/dark cycle of 12/12 h and ad libitum fed with rodent chow and water. The rats were embedded with osmotic mini-pump (Alzet model 2002 or 2004, CA), mini-pump subcutaneous implant method as described in our previous studies [42, 43]. Rats were randomly subjected to normal saline infusion, or subcutaneous continuous Ang II-infusion at 400 ng/kg·min concentration, or Ang II at 400 ng/kg·min + FTY720 0.5 g/kg·d by means of intragastric administration for 14 or 28 days. 24-hour urine was collected in metabolic cages and urinary albumin excretion rate was measured at days 14 and 28. At the end of 14- or 28-day treatment, rats were sacrificed. Blood samples were immediately collected in EDTA-containing tubes and serum-separating tubes to separate the plasma and serum. Serum Ang II concentration, S1P concentration, kidney function blood urea nitrogen (BUN) and creatinine, and serum albumin level were measured. 24-hour urine protein excretion was tested by sulfosalicylic acid

method. The kidneys were dissected and rinsed with cold isotonic saline and weighed. The right kidney tissues were fixed in 10% neutralized formalin for histological analysis.

2.4. Angiotensin II Radioimmunoassay. Rat plasma and kidney angiotensin II radioimmunoassay was performed in 12 × 75 mm polypropylene culture tubes as described in the Amersham RIA procedure (Amersham Corporation, Arlington Heights, IL). Radioactivity was determined in a T Tri-Carb 4810TR Liquid Scintillation Analyzer (PerkinElmer, Boston, USA).

2.5. Hematoxylin-Eosin Staining. Sections of rat kidney were stained with hematoxylin for 10 minutes. Subsequently, they were washed under running tap water for 5 minutes, dried on a hot plate, and stained with 0.5% eosin in 96% ethanol for 5 minutes. The sections were rapidly rinsed in 95% ethanol and dehydrated in 2 changes of absolute ethanol for 5 minutes each. Slides were dehydrated, cleared in xylene, and mounted in resinous medium.

2.6. Immunohistochemical Staining. The sections were washed with PBS (pH 7.5) and incubated in protein blocking solution (0.5% normal goat serum in PBS, v/v) for 30 min. The sections were then incubated with antibody against rat TNF-α (1 : 100, GTX110520, Novus, Saint Charles, MI, USA) and rat IL-6 (1 : 100, Novus, Saint Charles, MI, USA) in a humidified chamber for 4°C overnight [44], rinsed with PBS 3 times, and incubated with peroxidase-conjugated secondary antibody (1 : 100, DAKO, Glostrup, Denmark) for 1 h at room temperature. To detect positive reactions, the slides were incubated with stable 3,39-diaminobenzidine (DAB) for 5–10 min (Zhongshan Jinqiao Biotechnology, Beijing, China). The sections were rinsed with distilled water, counterstained with Gill's hematoxylin for 1 min (Sigma, St. Louis, MO), and observed under a BX53 Olympus microscope.

To quantify glomerular and tubulointerstitial lesion, immunoperoxidase kidney sections were examined under ×20 magnification, using an Olympus BX40 microscope (Olympus Optical, London, UK) mounted with a Photonic Science Color Coolview digital camera (Photonic Science, East Sussex, UK). Digital images were captured and analyzed using Image-Pro Plus software (Media Cybernetics, Silver Spring, MD, USA), and color segmentation was performed for each slide individually, defining pixels that contained appropriate coloration. For each slide, 20 consecutive glomeruli or cortical areas were defined as an "area of interest," and the percentage of each cross-sectional area stained with the defined color was calculated. The final value for each slide was derived as the mean percentage area stained from 20 areas.

2.7. Cell Culture and Treatment. A conditionally immortalized murine podocytes were kindly provided by Dr. Peter Mundel (Mount Sinai School of Medicine, New York). Podocytes were maintained in RPMI 1640 medium (HyClone, USA) containing 10% heat-inactivated fetal calf serum (Gibco, USA), 100 U/mL penicillin G, and 100 μg/mL streptomycin in an incubator with 5% CO_2. During podocyte proliferation, the medium was mixed with 10 U/mL recombinant mouse interferon-γ (Sigma, USA), and the cells were maintained at 33°C. Then podocytes were cultured at 37°C to induce differentiation without interferon-γ for 10–14 days. 15–25 passages of podocytes were used in the following experiments.

Cells were cultured in serum-free RPMI 1640 for at least 8 h and pretreated with 5 μmol/L FTY720 (Cayman Chemicals, Ann Arbor, MI, USA) for 30 min followed by treatment with 2 μmol/L S1P (Sigma Chemical Co.) for 24 h.

2.8. Western Blot. Western blot was executed as previously described [45]. Briefly, 30 μg protein lysates were resuspended in a reduced sample buffer and electrophoresed on a Tris gel, blotted to NC membrane, and subsequently probed with primary antibodies including FAK (1 : 500; Abcam, Cambridge, MA, USA), rabbit polyclonal to SPHK1 (1 : 500; Abcam, Cambridge, MA, USA), Alexa Fluor 680 (Invitrogen), and IRDye 800 (LI-COR Biosciences). A horseradish peroxidase-conjugated goat anti-rabbit antibody was then added. The signal was detected through autoradiography using enhanced chemiluminescence (ECL Plus, General Electric Healthcare, Milwaukee, WI) with the Odyssey infrared imaging system (LI-COR Biosciences) and quantification was performed using Odyssey software. Western blot data were evaluated as follows: the gray value of the western blot bandings was examined by Image-Pro Plus (Media Cybernetics, Inc.) in the control and experimental groups; the gray value of interest protein of each group was divided by the gray value of internal reference protein itself.

2.9. Real-Time PCR. Total RNA was extracted with Trizol (Invitrogen). Total RNA (2 mg) was used for first-strand cDNA synthesis with RevertAid™ First-Strand cDNA Synthesis Kit (Fermentas, Vilnius, LTU). PCR was performed in the presence of SYBR green using a 7500 Fast Real-Time PCR System. All PCR reactions were run in triplicate and repeated at least three times. Differences were calculated according to the relative quantization method using the β-actin gene to calibrate. The primers for rat IL-6 forward: 5′-TGATGGATGCTTCCAAACTG-3′, reverse: 5′-GAGCATTGGAAGTTGGGGTA-3′; rat TNF-α forward: 5′-ACTGAACTTCGGGGTGATTG-3′, reverse: 5′-GCTTGGTGGTTTGCTACGAC-3′.

2.10. Immunofluorescence. Conditionally immortalized murine podocytes were cultured on coverslips in a 24-well plate. Cells were fixed with 4% paraformaldehyde for 30 min at room temperature, washed, and permeabilized with 0.5% Triton X-100 for 5 min. The cells were incubated with phalloidin-Alexa 488 (1 : 40, Invitrogen, Carlsbad, CA) 4°C for 20 min. ProLong Gold Antifade reagent along with DAPI (Invitrogen) was used to mount the coverslips to slides. The cells were visualized using a confocal for fluorescence to detect the subcellular distribution of the actin cytoskeleton.

The green fluorescence represents F-actin; and the blue fluorescence represents the cell nucleus.

2.11. Electron Microscopy. Renal cortex (1 mm^3) from each rat was cut into small pieces and fixed in 2.5% glutaraldehyde in 0.1 mol/L phosphate buffer (pH 7.4) at 4°C for several days. After washing in phosphate buffer and postfixing in 1% OsO_4 for 2 h, the fixed material was dehydrated and embedded in Epon 812 (Okenshoji, Tokyo, Japan). Ultrathin sections were prepared and stained with uranyl acetate and lead citrate and examined with a Hitachi H7100 electron microscope (Hitachi, Yokohama, Japan).

2.12. Wound-Healing Assay. Wound-healing assay was executed as previously described [46]. Cells were plated at a density of 1×10^6 cells/mL in a 6-well plate and grown to 100% confluence. The cells were serum starved for 12 h. A wound was scratched at the inner bottom of each well using a P-200 pipette tip. The cells were washed twice with phosphate buffer saline (PBS) to remove the cell debris; then serum-free RPMI 1640 medium containing 10 μg/mL mitomycin C and irritant was added to each well. Cells within the same field were photographed at 0 and 24 h after the cells were scratched. The percentage of wound closure was calculated using the following formula, in which S is the surface area of the wound field.

2.13. Cell Adhesion Assay. Cell adhesion assay was executed as previously described [46]. The 96-well plates were coated with 50 μL fibronectin (Fn) (20 μg/mL) or Matrigel (200 μg/mL) (Becton Dickinson, Heidelberg, Germany) at 37°C for 2 h, then washed twice with PBS, and blocked with serum-free DMEM + 2% BSA for 30 min at 37°C. The cells were treated with irritant for 24 h at 37°C in a humidified incubator supplemented with 5% carbon dioxide. The treated podocyte cells were harvested with 0.25% trypsin-EDTA and resuspended to a density of 1×10^5 cells/mL in serum-free RPMI 1640 medium and then seeded at a density of 100 μL per well in the previously coated 96-well plates. Then, the cells were allowed to attach to the plates for 1.5 h at 37°C.

After the cells were washed gently with PBS twice, 20 μL of 3-(4,5-dimethyl-2-thiazolyl)-2,5-diphenyltetrazolium bromide (MTT) was added to each well for 4 h. Then, the MTT was removed, and 200 μL of dimethylsulfoxide (DMSO) was added to each well. The optical density (OD) at 570 nm of each well was measured with a microplate reader 15 min later. The experiments were performed three times. The control cells were not treated with matrine. The cell adhesion ratio was calculated using the following formula:

$$\text{The cell adhesion ratio} = \frac{\text{OD570}_{\text{treated group}}}{\text{OD570}_{\text{untreated group}}} \times 100\%. \quad (1)$$

2.14. Statistical Analyses. Data are reported as mean ± standard error. Data were analyzed using Student's two-tailed unpaired or paired (fed/fasting experiments) t-tests. Statistical analysis of data having equal variance was performed by one-way or two-way analysis of variance (ANOVA) followed by Tukey's post hoc test when appropriate. Associations between variables were investigated using Spearman correlation coefficient with SPSS 13.0 software. The differences at $P < 0.05$ were considered statistically significant. The data were analyzed using SPSS 13.0.

3. Results

3.1. The Concentration of S1P in Serum and Urine Was Positively Correlated with Chronic Kidney Disease Renal Injury. Mild and moderate clinical IgA nephropathy are characterized by hematuria and proteinuria. Thus, we selected IgA nephropathy as the representative disease of chronic kidney disease. Lee's histological classification (grades I~IV) was employed. Total 40 patients, average age 36.80 ± 13.77 years (range within 19–67), have varying degrees of hematuria and proteinuria, with or without renal dysfunction. We randomly selected 10 healthy volunteers and collected their serum and urine. The clinical characteristics of all participants are presented in Table 1. In this study, of 40 IgA nephropathy patients 18 were male. There was a slight female preponderance. The 24 h urinary protein excretion was 0.56–4.3 g/24 h. The patients' gender, age, serum urea nitrogen, serum creatinine, HDL, complement C3, and systolic and diastolic blood pressure did not show statistically significant differences ($P > 0.05$). However, the serum total protein, albumin, 24 h urinary protein excretion, complement C4, serum IgA, cholesterol, and triglycerides exhibited statistically significant differences ($P < 0.05$). In IgA nephropathy group, serum total protein and albumin levels were lower than those of the control group, but 24 h urine protein, complement C4, serum IgA, cholesterol, and triglycerides in IgA nephropathy group were significantly increased versus the control group (data not shown).

Concentrations of S1P in plasma and urine were measured using ELISA. As shown in Figures 1(a) and 1(b), there was a significant difference between the control and IgA nephropathy groups in plasma (9.22 ± 2.2 versus 13.00 ± 0.60 μmol/L, $P < 0.05$) and urine concentrations of S1P (0.04 ± 0.02 versus 0.16 ± 0.08 μmol/L, $P < 0.05$). The concentration of S1P in plasma and urine in IgA nephropathy patients was significantly higher than healthy volunteers.

Based on the total amount of 24 h urinary protein excretion, IgA nephropathy patients were divided into three groups: low-level proteinuria (0.15~1 g/24 h, 13 cases), moderate proteinuria (1~3.5 g/24 h, 16 cases), and heavy proteinuria (≥3.5 g/24 h, 11 cases). The plasma S1P levels in heavy proteinuria, moderate proteinuria, and low-level proteinuria were 12.15 ± 1.05, 8.98 ± 1.23, and 7.51 ± 2.38 μmol/L, respectively. Plasma S1P levels showed statistically significant differences between these three groups ($P < 0.05$) (Figure 1(c)). In addition, the urine S1P levels in heavy proteinuria, moderate proteinuria, and low-level proteinuria were 0.23 ± 0.09, 0.11 ± 0.02, and 0.04 ± 0.01 μmol/L, respectively, which showed statistically significant differences ($P < 0.05$) (Figure 1(d)). Spearman correlation analysis showed that plasma and urine S1P levels and 24 h urinary protein excretion were positively correlated ($P < 0.05$).

Table 1: Renal function and albumin Ang II-infusion rat and FTY720 intervention rat.

Index	Healthy volunteers	IgA nephropathy patients	t	P
Number	10	40	—	—
Sex (male/female)	6/4	18/22	—	0.60
Age (year)	24.8 ± 1.30	36.80 ± 13.77	17.03	0.07
Serum total protein (g/L)	75.9 ± 3.18	61.99 ± 7.91	1.89	<0.001
Serum albumin (g/L)	47.04 ± 2.23	34.93 ± 4.44	5.53	<0.001
Serum urea nitrogen (mmol/L)	3.80 ± 1.11	5.06 ± 1.20	1.06	0.15
Serum creatinine (μmol/L)	48.80 ± 5.11	89.06 ± 63.20	1.98	0.18
24 h urinary protein excretion (g/24 h)	0.03 ± 0.01	2.43 ± 1.87	10.51	0.01
Cholesterol (mmol/L)	3.31 ± 0.14	4.53 ± 0.91	6.16	<0.001
Triglycerides (mmol/L)	1.28 ± 0.19	1.58 ± 0.64	7.16	<0.001
Hemoglobin (g/L)	126.20 ± 9.06	124.00 ± 20.60	4.37	0.32
Red blood cell ($\times 10^{12}$/L)	4.12 ± 0.89	3.71 ± 1.23	3.54	0.89

Podocyte is a major component of the glomerular filtration barrier. Podocyte foot processes effacement is a characteristic hallmark of podocyte damage and associated with the onset of proteinuria [47]. Electron microscopic was used to analyze ultrastructural alterations of podocytes in Ang II-infusion and FTY720 intervention rats. Partial foot processes of podocytes are retracted and effaced in Ang II-infusion rats, resulting in displacement and disruption of the specialized slit diaphragms that span the filtration slits between foot processes. As shown in Figure 2(h), diffuse foot process fusion in podocytes and the basement membrane and diffuse uneven thickness in Ang II-infusion rats were observed under electron microscopy. Foot process fusion was often associated with detachment from the underlying glomerular basement membrane. Severe podocyte detachment from areas of denuded glomerular basement results in defects of glomerular filtration barrier, leading to development of severe proteinuria [48]. FTY720 intervention ameliorated these changes.

3.2. FTY720 Alleviated Renal Injury in Ang II-Infusion Rat. Our previous studies have found that systemic infusion of Ang II-infusion into normal rats caused renal pathological changes including glomerular mesangial cell proliferation, extracellular matrix deposition, tubular atrophy, dilation, urinary cast formation, inflammatory cell and inflammatory factors infiltration in tubulointerstitial lesion, and interstitial fibrosis [49, 50]. It is well known that Ang II results in the progression of glomerular injury via its hemodynamic or nonhemodynamic effects [51]. Here, a rat model of Ang II-infusion was established to evaluate the role of Ang II in glomerular, podocyte, and tubulointerstitial lesion.

As shown in Figure 2, serum creatinine, blood urea nitrogen, and 24-hour urinary protein excretion in 14 days or 28 days of Ang II-infused rats were higher than those in normal saline-infused control rats and they were significantly resorted by FTY720 pretreatment ($P < 0.05$) (Figures 2(a) and 2(b)). However, after Ang II-infusion for 14 days, the serum albumin concentration in rats showed no significant difference compared to the normal saline infusion control group ($P > 0.05$). However, after Ang II-infusion for 28 days, serum albumin concentration was significantly lower than the control group ($^*P < 0.05$) (Figure 2(c)). Ang II concentrations in both plasma and renal tissues detected by RIA in Ang II-infused rats were significantly increased versus control group ($P < 0.05$) (Figures 2(d) and 2(e)), thus indicating a successful Ang II-infusion rat model. 24-hour urinary protein excretion in Ang II-infused rats after 14 days or 28 days was higher than that in normal saline infusion control rats and was significantly blocked by pretreatment of FTY720, an S1PR agonist ($P < 0.05$) (Figure 2(f)). These results suggested that FTY720 blocked S1P-evoked physiological effects. After 28 days of Ang II-infusion, rat kidney histopathological changes were observed by HE staining. Compared with the normal saline infusion rats, light microscopy displayed significant mesangial and interstitial expansion, proximal tubular epithelial swelling, inflammatory cell infiltration in tubulointerstitial lesion in rats receiving 28 days of Ang II-infusion (Figure 2(g)). Ang II-infusion in rats on day 14 did not cause obvious renal histological lesions. Light microscopy only revealed mild mesangial and tubulointerstitial accumulation of matrix (Figure 2(g)). Thus, we demonstrated that 28 days of Ang II-infusion induced more obvious kidney damage in rats. FTY720 oral administration for 28 days dramatically reduced mesangial and tubulointerstitial accumulation of matrix, proximal tubular epithelial swelling, and inflammatory cell infiltration in tubulointerstitial lesion under light microscopy in Ang II-infusion rats (Figure 2(g)). Thus, we conclude that FTY720 can reduce renal histological lesions induced by Ang II-infusion in rats.

3.3. FTY720 Decreased S1P Synthesis in Ang II-Infusion Rats via Downregulation of Inflammatory Cytokines. After 28 days of Ang II-infusion, the animals were sacrificed. S1P concentrations in plasma and urine were measured using ELISA, but S1P concentrations in urine were not detectable. Plasma S1P levels in Ang II-infusion rats were much higher

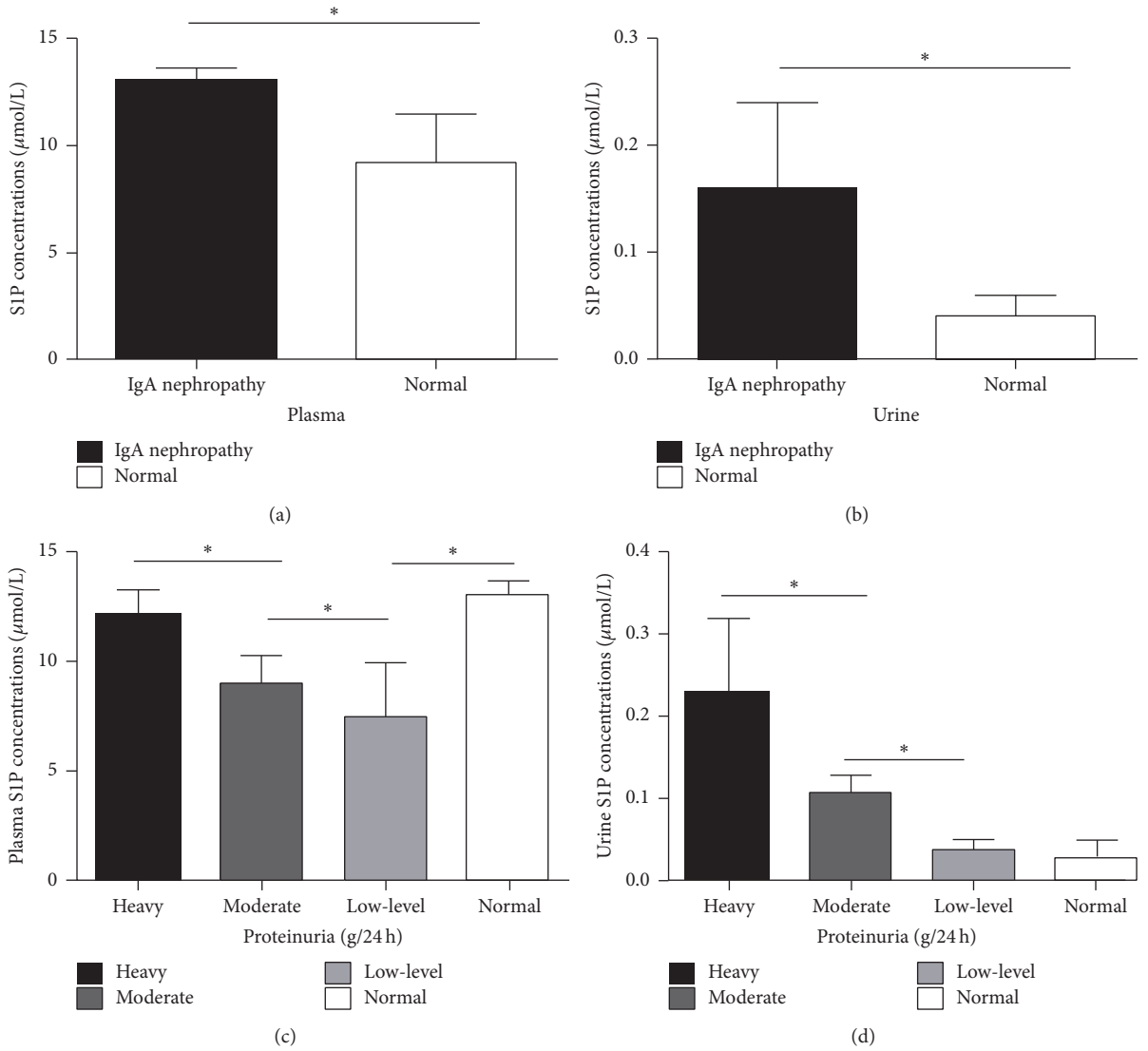

Figure 1: The concentration of S1P in serum and urine was positively correlated with chronic kidney disease renal injury. Forty IgA nephropathy patients and 10 healthy volunteers were selected. The 24 h urine and plasma were collected. Concentrations of S1P in plasma and urine were measured by using ELISA. (a) Concentrations of S1P in plasma in IgA nephropathy patients and healthy volunteers. (b) Concentrations of S1P in 24 h urine in IgA nephropathy patients and healthy volunteers. (c) Concentrations of S1P in plasma in IgA nephropathy patients with different level of proteinuria and healthy volunteers. (d) Concentrations of S1P in 24 h urine from IgA nephropathy patients with different level of proteinuria and healthy volunteers. Data were expressed as means ± standard error of the mean from the independent sample in the same group. $^*P < 0.05$, versus normal group in (a) and (b). $^*P < 0.05$, versus heavy group or low-level group in (c) and (d).

than those in control group. However, FTY720 intervention significantly decreased the concentrations of plasma S1P in Ang II-infusion rats ($P < 0.05$) (Figure 3(a)). Next, TNF-α and IL-6 expression in rat kidney tissues were detected by using an immunohistochemical technique. We demonstrated that TNF-α and IL-6 were mainly expressed in renal tubule after Ang II-infusion, and a very low level of IL-6 and TNF-α was expressed in glomeruli. Compared to the normal saline infusion rats, TNF-α and IL-6 expressions were elevated in Ang II-infusion rats. However, FTY720 administration inhibited TNF-α and IL-6 expression in the renal tissues from Ang II-infusion rats (Figure 3(b)), suggesting that FTY720 intervention can alleviate Ang II-infusion-induced rat renal tissue inflammation. The IL-6 and TNF-α mRNA levels in both renal tissue and rat plasma were also detected by real-time PCR. Ang II-infusion elevated the levels of IL-6 and TNF-α mRNA expression, which were inhibited by FTY720 intervention (Figures 3(c) and 3(d)).

Next, we investigated the mechanism underlying FTY720-induced decrease in S1P concentration. Sphingosine kinases (SPHK), including SPHK1 and SPHK2, are a conserved lipid kinase family that catalyzes S1P formation. SPHK1 is found in the cytosol of eukaryotic cells and migrates to the plasma membrane upon activation, whereas

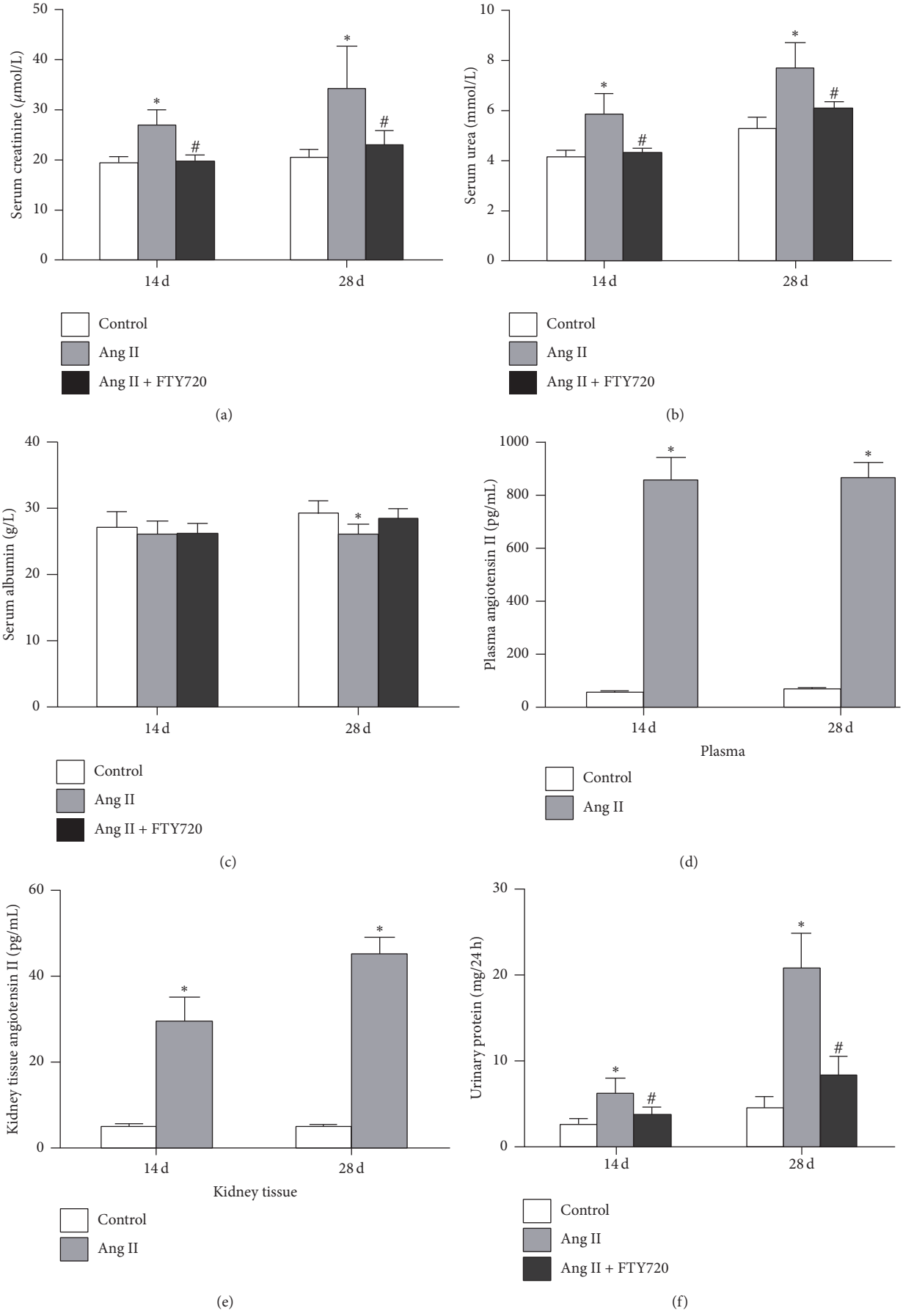

Figure 2: Continued.

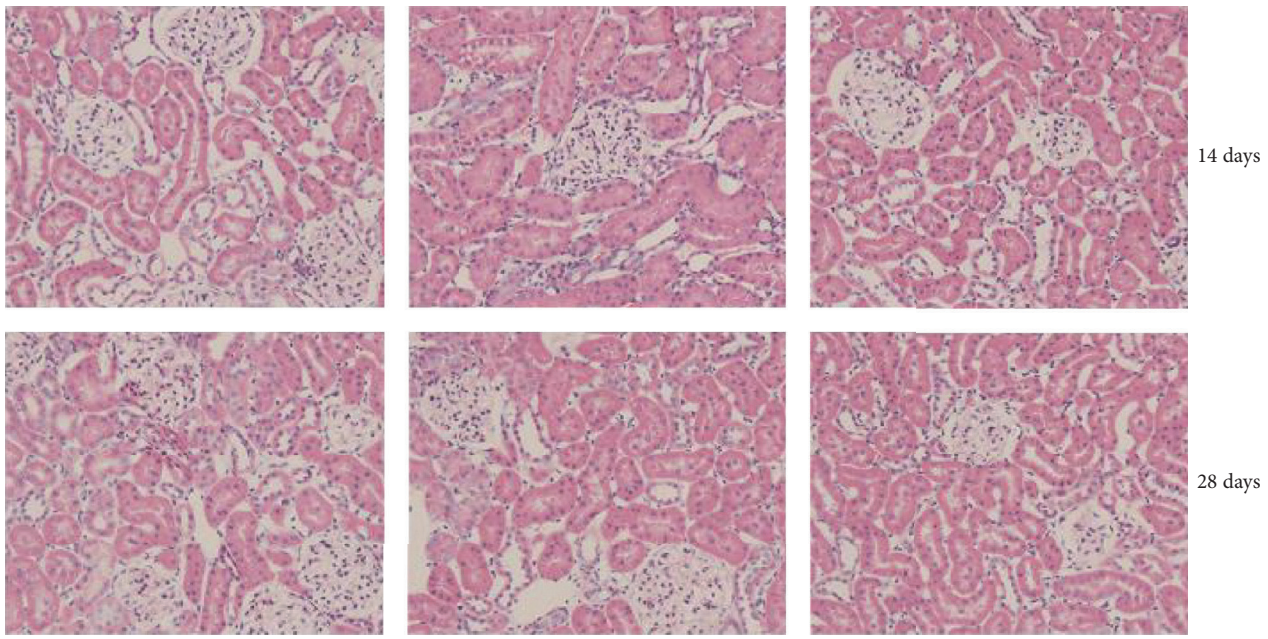

(g)

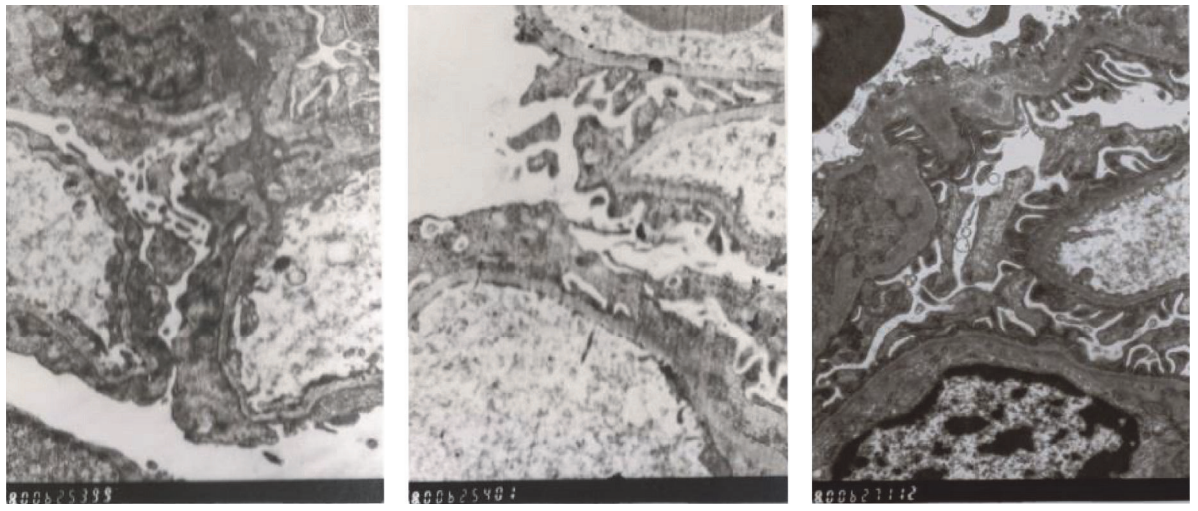

(h)

Figure 2: FTY720 could protect Ang II-induced kidney tissue injury in rats. The rats were subjected to subcutaneously continuous Ang II-infusion (400 ng/kg·min) for 14 or 28 days and were sacrificed. Rats given FTY720 (0.5 g/kg·d gavage) for 14 or 28 days also received Ang II-infusion. After the mice were sacrificed, the kidneys were fixed in paraformaldehyde for HE staining. The other parts of renal cortex were fixed in glutaraldehyde and podocytes were analyzed using transmission electron microscope. Kidney homogenate was used for RIA analysis. The plasma and serum were separated for biochemical analysis. Data represented is means ± SD of six independent experiments performed in triplicate. ($n = 6$) $^{*}P < 0.05$, versus normal saline infusion control rats; $^{\#}P < 0.05$, versus Ang II-infusion rats. (a) Serum creatinine levels in Ang II and FTY720-treated rats. (b) Serum urea nitrogen levels in Ang II and FTY720-treated rats. (c) Serum albumin levels in rats treated with Ang II and FTY720 for 14 and 28 days. (d) Concentration of Ang II in plasma from rats treated with Ang II and FTY720 for 14 and 28 days. (e) Concentration of Ang II in renal tissue homogenate from rats treated with Ang II and FTY720 for 14 and 28 days. (f) Twenty-four-hour urinary protein excretion levels in rats treated with Ang II and FTY720 for 14 and 28 days. (g) Light microscopy evaluation of rat kidney pathological changes with hematoxylin and eosin (H&E) staining (magnification, ×200). (h) Transmission electron microscopy evaluation of micrographs of podocyte ultrastructure in rats (magnification, ×8000).

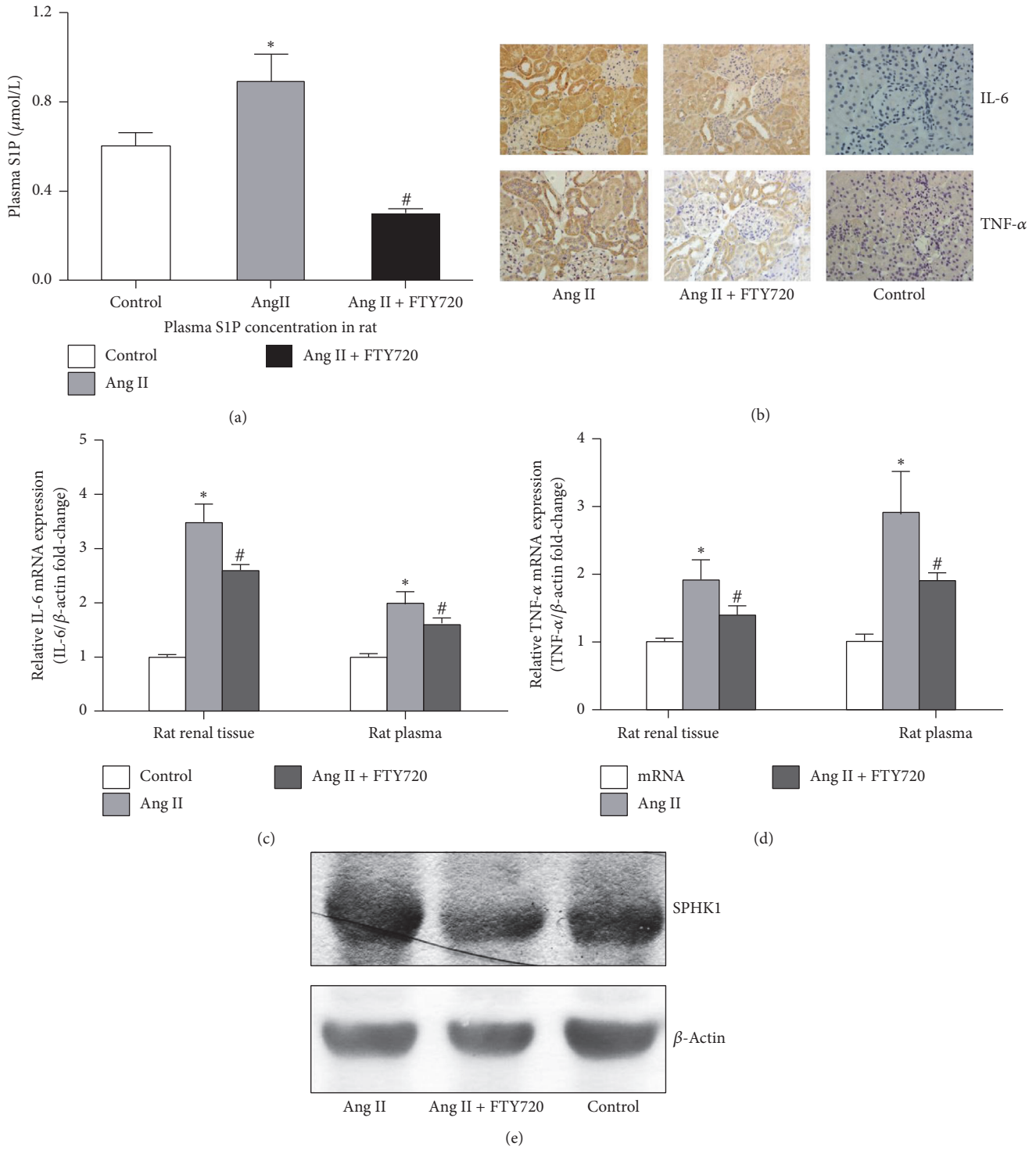

Figure 3: FTY720 decreased S1P synthesis in Ang II-infusion rats via downregulation of inflammatory cytokines. Subcutaneous continuous Ang II-infusion at 400 ng/kg·min concentration in rats for day 28: we sacrificed rats at day 28. FTY720 (0.5 g/kg·d) was orally administered to rats for 28 days and at the same time rats also received Ang II-infusion. When the mice were sacrificed, the kidney was fixed in paraformaldehyde; immunohistochemical analysis of TNF-α and IL-6 protein expression in kidney sections. Rat blood samples were collected and plasma was separated for analyzing S1P concentration by ELISA and SPHK1 protein expression level by western blot. Part of the rat kidney tissue homogenate was used to detect IL-6 and TNF-α mRNA expression level. Data represented is the means ± SD of 6 independent experiments performed in triplicate. ($n = 6$) $^{*}P < 0.05$, versus normal saline infusion control rats; $^{\#}P < 0.05$, versus Ang II-infusion rats. (a) S1P concentration in rat plasma were analyzed by ELISA. (b) TNF-α and IL-6 were detected by immunohistochemical in rat kidney. (c) IL-6 mRNA expression level was detected by RT-PCR in rat kidney tissue homogenate. (d) TNF-α mRNA expression level was detected by RT-PCR in rat kidney tissue homogenate. (e) SPHK1 protein expression level in rat plasma was detected by western blot. β-Actin was used to ensure an equal amount of protein was loaded in each lane. Data represented is the means ± SD of six independent experiments performed in triplicate.

SPHK2 is localized to the nucleus. Here, SPHK1 protein expression was measured by western analysis. As shown in Figure 3(e), FTY720 intervention significantly inhibited Ang II-induced increase in rat plasma SPHK1 protein expression.

3.4. FTY720 Can Alleviate Exogenous S1P-Induced Podocyte Damage. To further substantiate the protective effects of FTY720 against S1P-induced damage, we pretreated cultured immortalized murine podocytes with 5 μM FTY720 for 30 min, followed by S1P treatment (2 μM) for 24 h. Podocyte migration was measured by using wound-healing assay. As shown in Figure 4(a), S1P accelerated podocyte migration, while FTY720 could inhibit S1P-induced podocyte migration. In addition, FTY720 significantly blocked S1P-induced inhibition of podocyte adhesion ($P < 0.05$) (Figure 4(b)). Focal adhesion kinase (FAK) is a nonreceptor tyrosine kinase that plays a critical role in cell motility [52]. Glomerular injury leads to activation of podocyte FAK [53]; thus FAK can be used as a podocyte injury marker. Here, we demonstrated that S1P increased FAK protein expression in a concentration-dependent manner. However, pretreatment with 5 μM FTY720 could inhibit S1P-induced FAK protein expression ($P < 0.05$) (Figure 4(c)).

Next, we observed F-actin in podocyte. The expression of F-actin in the cytoplasm in S1P-treated group was lower than that in the control group. Moreover, in the normal podocyte stress fibers gathered by F-actin were arranged predominantly in one direction. After S1P treatment, some irregular actin filaments were observed with no stress fibers in the cell periphery. Importantly, FTY720 rescued S1P-induced cytoskeleton destruction (Figure 4(d)).

4. Discussion

The present study demonstrates a novel finding that FTY720 has protective effects against chronic kidney disease renal damage in an Ang II-infusion rat model. The concentration of S1P in serum and urine was positively correlated with chronic kidney disease renal injury. Moreover, FTY720 decreased S1P synthesis in Ang II-infusion rats via downregulation of inflammatory cytokines, including TNF-α and IL-6, and controlled glomerular permeability and podocyte function. FTY720 alleviated renal injury in Ang II-infusion rat. In addition, we observed that FTY720 can relieve exogenous S1P-induced podocyte damage. Angiotensin II (Ang II), the main effector peptide of the renin-angiotensin system (RAS), plays a central role in the pathophysiology of renal diseases. Apart from contribution to the progression of glomerular injury through its hemodynamic and/or non-hemodynamic effects, Ang II is considered as a cytokine with an active role in renal pathology. Since progressive kidney disease caused by Ang II arises from aberrations of the glomerulus and the tubulointerstitium, the wide ranging effects of S1PR agonists may be more efficient than current therapies.

Multiple receptor system empowers S1P to have pleiotropic actions and modulate a number of imperative cellular functions [54, 55]. The physiological functions of S1P have been studied extensively in various tissues. Nonetheless, the particular pathophysiology role of S1P in kidney is not clear. Kidney expresses S1PRs [25, 56], which play a significant role in sustaining endothelial cell integrity [57, 58] and in transferring lymphocytes [59]. S1P and SPHK1 are associated with the actions of TNF-α, a cytokine critical for inflammation and autoimmune disorders, for example, inflammatory bowel disease, rheumatoid arthritis, and asthma. TNF-α stimulates ERK1/2-mediated phosphorylation and translocation of SPHK1 to the plasma membrane, catalyzing the formation of S1P [60]. TRAF2, an important signaling intermediate in TNF-α pathway, activates NF-kB by binding directly to SPHK1 [61].

Specifically, S1P regulates vascular barrier integrity in inflammatory conditions and S1P1 fundamentally protects the vasculature from leak with countering effects of S1P2/3. Furthermore, S1P signaling controls the trafficking of several types of immune cells, such as lymphocytes, monocyte, macrophages, and neutrophils [62], influencing functions of these cells, for example, formation of inflammatory mediators. Therefore, therapeutic intervention targeting S1P pathway has advantageous effects. It would be important to develop tissue-/receptor subtype-specific interventions of S1P signaling.

TNF-α is secreted by macrophages and functions as a crucial inflammatory mediator regulating inflammation responses and immune cell activity [63]. TNF-α regulates cell growth by activating NF-kB, a proinflammatory transcription factor [64–66]. TNF-α/NF-kB are promising targets for developing novel chronic kidney disease drugs. It is intriguing to speculate that some drugs with inhibitory effect on TNF-α activation show imperative benefits for kidney damage. In the present study, we demonstrate that TNF-α, IL-6 expression, and S1P levels were elevated in Ang II-infusion rats. However, FTY720 administration inhibited TNF-α, IL-6 expression, and S1P content in the renal tissues from Ang II-infusion rats, suggesting that FTY720 intervention can alleviate Ang II-infusion-induced rat renal tissue inflammation. Our results illuminate that the TNF-α/S1P cascade-mediated kidney inflammatory response induced by Ang II can be repressed by FTY720. The kidney-protective effects of FTY720 might be associated, at least partially, with its ability to inhibit TNF-α and S1P activity.

In conclusion, this study deepens our understanding of the role of S1P in Ang II-induced kidney damage and reveals that administration of S1P1R agonists decreases renal dysfunction. The protective effect of S1P1R agonist on kidney tissue is mediated by a directly beneficial effect on kidney-derived cells, namely, podocytes. We conclude that S1P1R activation might represent a novel therapeutic approach for the early-stage chronic kidney disease.

Competing Interests

The authors declare that there is no conflict of interests regarding the publication of this article.

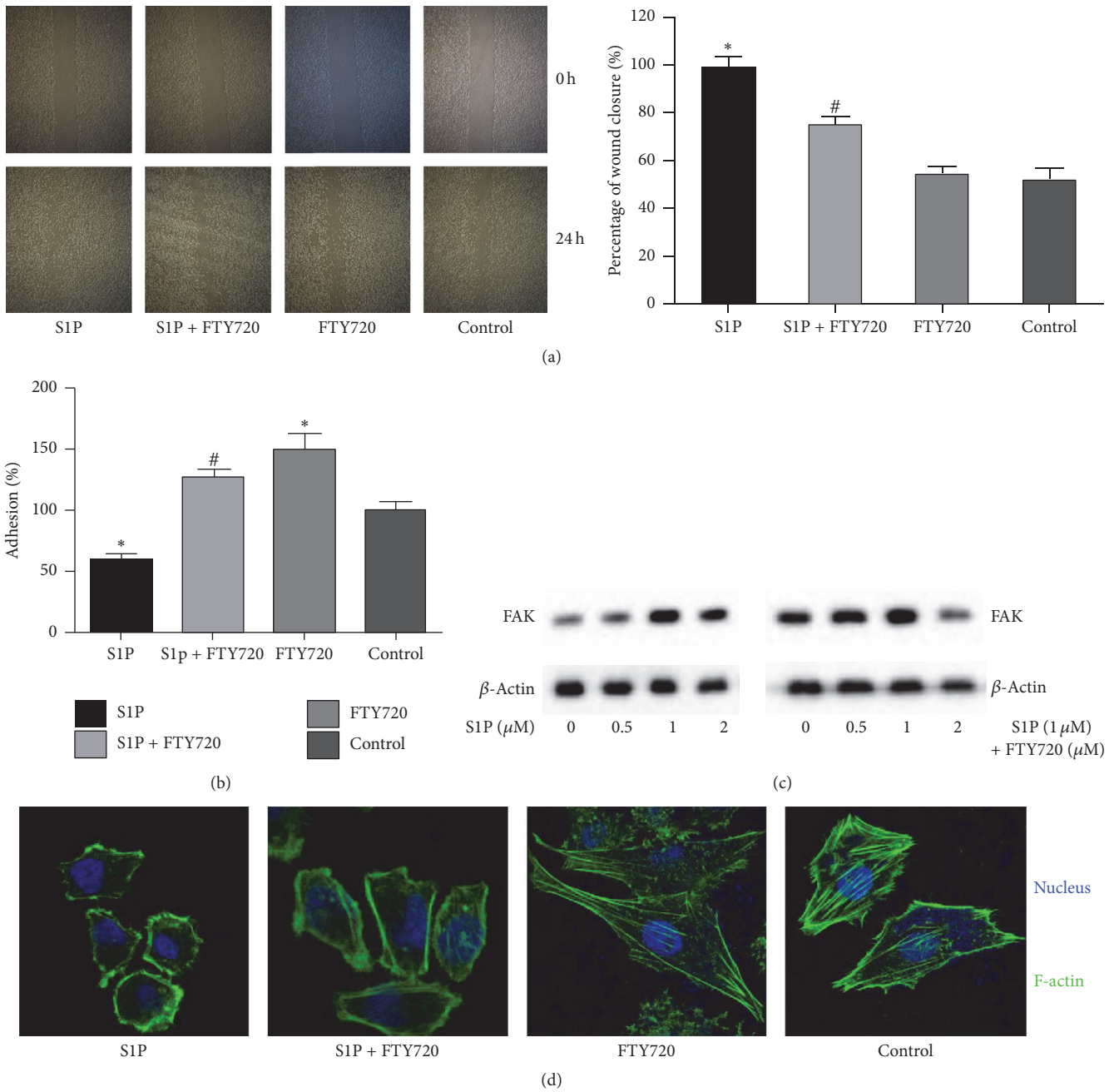

Figure 4: FTY720 could alleviate exogenous S1P-induced podocyte damage. Immortalized murine podocytes were cultured. Using 5 μM FTY720 pretreated for 30 min, followed by S1P treatment (2 μM) for 24 h. Using different doses of S1P within 0~2 μM S1P treated podocyte for 24 h. Or using 5 μM FTY720 treated for 24 h. Podocyte migration was measured by using wound-healing assay. Podocyte migration was measured by using adhesion assay and measured by MTT assay for adhesion cells in plate. FAK protein expression level in rat plasma was detected by western blot. β-Actin was used to ensure an equal amount of protein was loaded in each lane. Data represented is the means ± SD of six independent experiments performed in triplicate. Immunofluorescence was used to observe F-actin change. Three independent experiments were performed. Results are presented as mean cell migration velocity ± SD of the independent experiments, $^{*}P < 0.05$, versus control podocyte; $^{\#}P < 0.05$, versus S1P treated podocyte. (a) The migration ability of podocyte cells was measured using wound-healing assay. The percentage of wound closure was significantly reduced in response to treatment with either S1P or FTY720. Podocyte was treated with S1P which showed a higher cell migration velocity than FTY720-treated or control cells. Podocyte pretreated with FT720 and then treated with S1P showed a slower migration velocity than S1P treated podocyte. (b) The adhesion ability of podocyte cells was measured using adhesion assay. (c) FAK protein expression level in rat plasma was detected by western blot. (d) Representative confocal microscopy images from 3 separate experiments of podocyte cells were treated with S1P or FTY720 for 24 h. F-actin (stained with phalloidin): green; and nuclei: blue. Original magnification ×1,000.

Authors' Contributions

Ke Su and Ping Zeng contributed equally to this work.

Acknowledgments

The authors thank Guohua Ding for advice and stimulating discussion; Ke Wu for critical reading of the manuscript; Hongxia Yang and Heng Zhou for excellent technical assistance for the immunohistochemistry. This work was supported by Chinese Society of Nephrology Clinical Research and Special Funds of Chinese Medical Association (14050470584), National Natural Science Foundation of China (no. 81470912), and Innovative Experiment Project of College Students in Wuhan University School of Medicine (MS2015046).

References

[1] J. M. López-Novoa, A. B. Rodríguez-Peña, A. Ortiz, C. Martínez-Salgado, and F. J. López Hernández, "Etiopathology of chronic tubular, glomerular and renovascular nephropathies: clinical implications," *Journal of Translational Medicine*, vol. 9, article 13, 2011.

[2] X. Tan, X. Wen, and Y. Liu, "Paricalcitol inhibits renal inflammation by promoting vitamin D receptor-mediated sequestration of NF-κB signaling," *Journal of the American Society of Nephrology*, vol. 19, no. 9, pp. 1741–1752, 2008.

[3] S. Segerer, P. J. Nelson, and D. Schlöndorff, "Chemokines, chemokine receptors, and renal disease: from basic science to pathophysiologic and therapeutic studies," *Journal of the American Society of Nephrology*, vol. 11, no. 1, pp. 152–176, 2000.

[4] C. Guijarro and J. Egido, "Transcription factor-κB (NF-κB) and renal disease," *Kidney International*, vol. 59, no. 2, pp. 415–424, 2001.

[5] J. L. Gorriz and A. Martinez-Castelao, "Proteinuria: detection and role in native renal disease progression," *Transplantation Reviews*, vol. 26, no. 1, pp. 3–13, 2012.

[6] M. Maceyka, K. B. Harikumar, S. Milstien, and S. Spiegel, "Sphingosine-1-phosphate signaling and its role in disease," *Trends in Cell Biology*, vol. 22, no. 1, pp. 50–60, 2012.

[7] G. T. Kunkel, M. MacEyka, S. Milstien, and S. Spiegel, "Targeting the sphingosine-1-phosphate axis in cancer, inflammation and beyond," *Nature Reviews Drug Discovery*, vol. 12, no. 9, pp. 688–702, 2013.

[8] J. J. Aarthi, M. A. Darendeliler, and P. N. Pushparaj, "Dissecting the role of the S1P/S1PR axis in health and disease," *Journal of Dental Research*, vol. 90, no. 7, pp. 841–854, 2011.

[9] P. Hänel, P. Andréani, and M. H. Gräler, "Erythrocytes store and release sphingosine 1-phosphate in blood," *FASEB Journal*, vol. 21, no. 4, pp. 1202–1209, 2007.

[10] R. Pappu, S. R. Schwab, I. Cornelissen et al., "Promotion of lymphocyte egress into blood and lymph by distinct sources of sphingosine-1-phosphate," *Science*, vol. 316, no. 5822, pp. 295–298, 2007.

[11] W. L. Santos and K. R. Lynch, "Drugging sphingosine kinases," *ACS Chemical Biology*, vol. 10, no. 1, pp. 225–233, 2015.

[12] T. Hla, M.-J. Lee, N. Ancellin et al., "Sphingosine-1-phosphate: extracellular mediator or intracellular second messenger," *Biochemical Pharmacology*, vol. 58, no. 2, pp. 201–207, 1999.

[13] M. Kono, Y. Mi, Y. Liu et al., "The sphingosine-1-phosphate receptors S1P1, S1P2, and S1P3 function coordinately during embryonic angiogenesis," *The Journal of Biological Chemistry*, vol. 279, no. 28, pp. 29367–29373, 2004.

[14] H. Rosen, R. C. Stevens, M. Hanson, E. Roberts, and M. B. A. Oldstone, "Sphingosine-1-phosphate and its receptors: structure, signaling, and influence," *Annual Review of Biochemistry*, vol. 82, pp. 637–662, 2013.

[15] G. Zhang, J. J. A. Contos, J. A. Weiner, N. Fukushima, and J. Chun, "Comparative analysis of three murine G-protein coupled receptors activated by sphingosine-1-phosphate," *Gene*, vol. 227, no. 1, pp. 89–99, 1999.

[16] I. Ishii, B. Friedman, X. Ye et al., "Selective loss of sphingosine 1-phosphate signaling with no obvious phenotypic abnormality in mice lacking its G protein-coupled receptor, LP B3/EDG-3," *Journal of Biological Chemistry*, vol. 276, no. 36, pp. 33697–33704, 2001.

[17] C. H. Liu and T. Hla, "The mouse gene for the inducible G-protein-coupled receptor edg-1," *Genomics*, vol. 43, no. 1, pp. 15–24, 1997.

[18] Y. Liu, R. Wada, T. Yamashita et al., "Edg-1, the G protein-coupled receptor for sphingosine-1-phosphate, is essential for vascular maturation," *The Journal of Clinical Investigation*, vol. 106, no. 8, pp. 951–961, 2000.

[19] T. Imasawa, H. Kitamura, R. Ohkawa, Y. Satoh, A. Miyashita, and Y. Yatomi, "Unbalanced expression of sphingosine 1-phosphate receptors in diabetic nephropathy," *Experimental and Toxicologic Pathology*, vol. 62, no. 1, pp. 53–60, 2010.

[20] Q. Zhu, M. Xia, Z. Wang, P.-L. Li, and N. Li, "A novel lipid natriuretic factor in the renal medulla: sphingosine-1-phosphate," *American Journal of Physiology—Renal Physiology*, vol. 301, no. 1, pp. F35–F41, 2011.

[21] E. Birgbauer and J. Chun, "New developments in the biological functions of lysophospholipids," *Cellular and Molecular Life Sciences*, vol. 63, no. 23, pp. 2695–2701, 2006.

[22] S. E. Gardell, A. E. Dubin, and J. Chun, "Emerging medicinal roles for lysophospholipid signaling," *Trends in Molecular Medicine*, vol. 12, no. 2, pp. 65–75, 2006.

[23] V. Brinkmann, "Sphingosine 1-phosphate receptors in health and disease: mechanistic insights from gene deletion studies and reverse pharmacology," *Pharmacology and Therapeutics*, vol. 115, no. 1, pp. 84–105, 2007.

[24] H. M. Perry, L. Huang, H. Ye et al., "Endothelial sphingosine 1-phosphate receptor-1 mediates protection and recovery from acute kidney injury," *Journal of the American Society of Nephrology*, vol. 27, no. 11, pp. 3383–3393, 2016.

[25] A. S. Awad, H. Ye, L. Huang et al., "Selective sphingosine 1-phosphate 1 receptor activation reduces ischemia-reperfusion injury in mouse kidney," *American Journal of Physiology—Renal Physiology*, vol. 290, no. 6, pp. F1516–F1524, 2006.

[26] Y.-H. H. Lien, K.-C. Yong, C. Cho, S. Igarashi, and L.-W. Lai, "$S1P_1$-selective agonist, SEW2871, ameliorates ischemic acute renal failure," *Kidney International*, vol. 69, no. 9, pp. 1601–1608, 2006.

[27] V. Brinkmann, M. D. Davis, C. E. Heise et al., "The immune modulator FTY720 targets sphingosine 1-phosphate receptors," *Journal of Biological Chemistry*, vol. 277, no. 24, pp. 21453–21457, 2002.

[28] H. Ni, J. Chen, M. Pan et al., "FTY720 prevents progression of renal fibrosis by inhibiting renal microvasculature endothelial dysfunction in a rat model of chronic kidney disease," *Journal of Molecular Histology*, vol. 44, no. 6, pp. 693–703, 2013.

[29] O. J. David, J. M. Kovarik, and R. L. Schmouder, "Clinical pharmacokinetics of fingolimod," *Clinical Pharmacokinetics*, vol. 51, no. 1, pp. 15–28, 2012.

[30] M. H. Gräler and E. J. Goetzl, "The immunosuppressant FTY720 down-regulates sphingosine 1-phosphate G-protein-coupled receptors," *The FASEB Journal*, vol. 18, no. 3, pp. 551–553, 2004.

[31] H. Müller, S. Hofer, N. Kaneider et al., "The immunomodulator FTY720 interferes with effector functions of human monocyte-derived dendritic cells," *European Journal of Immunology*, vol. 35, no. 2, pp. 533–545, 2005.

[32] K. A. Vora, E. Nichols, G. Porter et al., "Sphingosine 1-phosphate receptor agonist FTY720-phosphate causes marginal zone B cell displacement," *Journal of Leukocyte Biology*, vol. 78, no. 2, pp. 471–480, 2005.

[33] T. Kimura, A. M. Boehmler, G. Seitz et al., "The sphingosine 1-phosphate receptor agonist FTY720 supports CXCR4-dependent migration and bone marrow homing of human CD34+ progenitor cells," *Blood*, vol. 103, no. 12, pp. 4478–4486, 2004.

[34] H. Kitabayashi, M. Isobe, N. Watanabe, J.-I. Suzuki, Y. Yazaki, and M. Sekiguchi, "FTY720 prevents development of experimental autoimmune myocarditis through reduction of circulating lymphocytes," *Journal of Cardiovascular Pharmacology*, vol. 35, no. 3, pp. 410–416, 2000.

[35] M. Fujino, N. Funeshima, Y. Kitazawa et al., "Amelioration of experimental autoimmune encephalomyelitis in Lewis rats by FTY720 treatment," *Journal of Pharmacology and Experimental Therapeutics*, vol. 305, no. 1, pp. 70–77, 2003.

[36] S. Kurose, E. Ikeda, M. Tokiwa, N. Hikita, and M. Mochizuki, "Effects of FTY720, a novel immunosuppressant, on experimental autoimmune uveoretinitis in rats," *Experimental Eye Research*, vol. 70, no. 1, pp. 7–15, 2000.

[37] P. Keul, M. Tölle, S. Lucke et al., "The sphingosine-1-phosphate analogue FTY720 reduces atherosclerosis in apolipoprotein E-deficient mice," *Arteriosclerosis, Thrombosis, and Vascular Biology*, vol. 27, no. 3, pp. 607–613, 2007.

[38] X. Montalban, G. Comi, P. OConnor et al., "Oral fingolimod (FTY720) in relapsing multiple sclerosis: impact on health-related quality of life in a phase II study," *Multiple Sclerosis Journal*, vol. 17, no. 11, pp. 1341–1350, 2011.

[39] A. J. Hoitsma, E. S. Woodle, D. Abramowicz, P. Proot, and Y. Vanrenterghem, "FTY720 combined with tacrolimus in de novo renal transplantation: 1-year, multicenter, open-label randomized study," *Nephrology Dialysis Transplantation*, vol. 26, no. 11, pp. 3802–3805, 2011.

[40] M. Ishii, J. G. Egen, F. Klauschen et al., "Sphingosine-1-phosphate mobilizes osteoclast precursors and regulates bone homeostasis," *Nature*, vol. 458, no. 7237, pp. 524–528, 2009.

[41] J. Kikuta, K. Iwai, Y. Saeki, and M. Ishii, "S1P-targeted therapy for elderly rheumatoid arthritis patients with osteoporosis," *Rheumatology International*, vol. 31, no. 7, pp. 967–969, 2011.

[42] X. Chen, Z. Ren, W. Liang et al., "c-Abl mediates angiotensin II-induced apoptosis in podocytes," *Journal of Molecular Histology*, vol. 44, no. 5, pp. 597–608, 2013.

[43] Z. Ren, W. Liang, C. Chen, H. Yang, P. C. Singhal, and G. Ding, "Angiotensin II induces nephrin dephosphorylation and podocyte injury: role of caveolin-1," *Cellular Signalling*, vol. 24, no. 2, pp. 443–450, 2012.

[44] A. Sheryanna, G. Bhangal, J. McDaid et al., "Inhibition of p38 mitogen-activated protein kinase is effective in the treatment of experimental crescentic glomerulonephritis and suppresses monocyte chemoattractant protein-1 but not IL-1β or IL-6," *Journal of the American Society of Nephrology*, vol. 18, no. 4, pp. 1167–1179, 2007.

[45] Y. Izumiya, S. Kim, Y. Izumi et al., "Apoptosis signal-regulating kinase 1 plays a pivotal role in angiotensin II-induced cardiac hypertrophy and remodeling," *Circulation Research*, vol. 93, no. 9, pp. 874–883, 2003.

[46] J.-W. Zhang, K. Su, W.-T. Shi et al., "Matrine inhibits the adhesion and migration of BCG823 gastric cancer cells by affecting the structure and function of the vasodilator-stimulated phosphoprotein (VASP)," *Acta Pharmacologica Sinica*, vol. 34, no. 8, pp. 1084–1092, 2013.

[47] R. Kalluri, "Proteinuria with and without renal glomerular podocyte effacement," *Journal of the American Society of Nephrology*, vol. 17, no. 9, pp. 2383–2389, 2006.

[48] R. P. Scott and S. E. Quaggin, "Review series: the cell biology of renal filtration," *Journal of Cell Biology*, vol. 209, no. 2, pp. 199–210, 2015.

[49] M. Alique, E. Civantos, E. Sanchez-Lopez et al., "Integrin-linked kinase plays a key role in the regulation of angiotensin II-induced renal inflammation," *Clinical Science*, vol. 127, no. 1, pp. 19–31, 2014.

[50] R. J. Johnson, C. E. Alpers, A. Yoshimura et al., "Renal injury from angiotensin II-mediated hypertension," *Hypertension*, vol. 19, no. 5, pp. 464–474, 1992.

[51] M. E. Rosenberg, L. J. Smith, R. Correa-Rotter, and T. H. Hostetter, "The paradox of the renin-angiotensin system in chronic renal disease," *Kidney International*, vol. 45, no. 2, pp. 403–410, 1994.

[52] M. A. Westhoff, B. Serrels, V. J. Fincham, M. C. Frame, and N. O. Carragher, "Src-mediated phosphorylation of focal adhesion kinase couples actin and adhesion dynamics to survival signaling," *Molecular and Cellular Biology*, vol. 24, no. 18, pp. 8113–8133, 2004.

[53] H. Ma, A. Togawa, K. Soda et al., "Inhibition of podocyte FAK protects against proteinuria and foot process effacement," *Journal of the American Society of Nephrology*, vol. 21, no. 7, pp. 1145–1156, 2010.

[54] T. Hla, M.-J. Lee, N. Ancellin, J. H. Paik, and M. J. Kluk, "Lysophospholipids—receptor revelations," *Science*, vol. 294, no. 5548, pp. 1875–1878, 2001.

[55] H. Rosen and E. J. Goetzl, "Sphingosine 1-phosphate and its receptors: an autocrine and paracrine network," *Nature Reviews Immunology*, vol. 5, no. 7, pp. 560–570, 2005.

[56] M. J. Kluk and T. Hla, "Signaling of sphingosine-1-phosphate via the S1P/EDG-family of G-protein-coupled receptors," *Biochimica et Biophysica Acta*, vol. 1582, no. 1–3, pp. 72–80, 2002.

[57] M.-J. Lee, S. Thangada, K. P. Claffey et al., "Vascular endothelial cell adherens junction assembly and morphogenesis induced by sphingosine-1-phosphate," *Cell*, vol. 99, no. 3, pp. 301–312, 1999.

[58] V. Krump-Konvalinkova, S. Yasuda, T. Rubic et al., "Stable knock-down of the sphingosine 1-phosphate receptor S1P1 influences multiple functions of human endothelial cells," *Arteriosclerosis, Thrombosis, and Vascular Biology*, vol. 25, no. 3, pp. 546–552, 2005.

[59] E. J. Goetzl and H. Rosen, "Regulation of immunity by lysosphingolipids and their G protein-coupled receptors," *Journal of Clinical Investigation*, vol. 114, no. 11, pp. 1531–1537, 2004.

[60] S. M. Pitson, P. A. B. Moretti, J. R. Zebol et al., "Activation of sphingosine kinase 1 by ERK1/2-mediated phosphorylation," *The EMBO Journal*, vol. 22, no. 20, pp. 5491–5500, 2003.

[61] P. Xia, L. Wang, P. A. B. Moretti et al., "Sphingosine kinase interacts with TRAF2 and dissects tumor necrosis factor-α signaling," *The Journal of Biological Chemistry*, vol. 277, no. 10, pp. 7996–8003, 2002.

[62] M. L. Allende, M. Bektas, B. G. Lee et al., "Sphingosine-1-phosphate lyase deficiency produces a pro-inflammatory response while impairing neutrophil trafficking," *The Journal of Biological Chemistry*, vol. 286, no. 9, pp. 7348–7358, 2011.

[63] S.-C. Sensken, C. Bode, and M. H. Gräler, "Accumulation of fingolimod (FTY720) in lymphoid tissues contributes to prolonged efficacy," *Journal of Pharmacology and Experimental Therapeutics*, vol. 328, no. 3, pp. 963–969, 2009.

[64] H.-M. Ni, X. Chen, Y.-H. Shi et al., "Genetic delineation of the pathways mediated by bid and JNK in tumor necrosis factor-α-induced liver injury in adult and embryonic mice," *The Journal of Biological Chemistry*, vol. 284, no. 7, pp. 4373–4382, 2009.

[65] H. Z. Huo, B. Wang, Y. K. Liang, Y. Y. Bao, and Y. Gu, "Hepatoprotective and antioxidant effects of licorice extract against CCl 4-induced oxidative damage in rats," *International Journal of Molecular Sciences*, vol. 12, no. 10, pp. 6529–6543, 2011.

[66] R. Cheung, F. Shen, J. H. Phillips et al., "Activation of MDL-1 (CLEC5A) on immature myeloid cells triggers lethal shock in mice," *Journal of Clinical Investigation*, vol. 121, no. 11, pp. 4446–4461, 2011.

Hindawi
Mediators of Inflammation
Volume 2017, Article ID 3709874, 10 pages
https://doi.org/10.1155/2017/3709874

Research Article

Elucidation of the Anti-Inflammatory Mechanisms of Bupleuri and Scutellariae Radix Using System Pharmacological Analyses

Xia Shen,[1] Zhenyu Zhao,[1] Hao Wang,[1] Zihu Guo,[2] Benxiang Hu,[1] and Gang Zhang[1]

[1]*College of Pharmacy, Shaanxi University of Chinese Medicine, Xi'an, Shaanxi, China*
[2]*Bioinformatics Center, College of Life Science, Northwest A&F University, Yangling, Shaanxi, China*

Correspondence should be addressed to Gang Zhang; jay_gumling2003@aliyun.com

Received 20 October 2016; Revised 13 December 2016; Accepted 22 December 2016; Published 16 January 2017

Academic Editor: Yunzhou Dong

Objective. This study was aimed at elucidating the molecular mechanisms underlying the anti-inflammatory effect of the combined application of Bupleuri Radix and Scutellariae Radix and explored the potential therapeutic efficacy of these two drugs on inflammation-related diseases. *Methods.* After searching the databases, we collected the active ingredients of Bupleuri Radix and Scutellariae Radix and calculated their oral bioavailability (OB) and drug-likeness (DL) based on the absorption-distribution-metabolism-elimination (ADME) model. In addition, we predicted the drug targets of the selected active components based on weighted ensemble similarity (WES) and used them to construct a drug-target network. Gene ontology (GO) analysis and KEGG mapper tools were performed on these predicted target genes. *Results.* We obtained 30 compounds from Bupleuri Radix and Scutellariae Radix of good quality as indicated by ADME assays, which possess potential pharmacological activity. These 30 ingredients have a total of 121 potential target genes, which are involved in 24 biological processes related to inflammation. *Conclusions.* Combined application of Bupleuri Radix and Scutellariae Radix was found not only to directly inhibit the synthesis and release of inflammatory cytokines, but also to have potential therapeutic effects against inflammation-induced pain. In addition, a combination therapy of these two drugs exhibited systemic treatment efficacy and provided a theoretical basis for the development of drugs against inflammatory diseases.

1. Introduction

Multiple chronic diseases are caused by inflammation, and the failure of resolution of inflammation increases the risk of development of such diseases [1]. Furthermore, inflammation is involved in many diseases, such as depression, bipolar disorder, atherosclerosis, and coronary artery disease [2–5].

In China, Traditional Chinese Medicine (TCM) has been used for the effective treatment of such diseases abovementioned for a long history. Amongst various TCM drugs, Bupleuri Radix and Scutellariae Radix are reported to possess anti-inflammation properties and similar patterns of therapeutic action against different diseases [6, 7]. In clinical application, prescription of Bupleuri Radix and Scutellariae Radix in combination is the most common therapy against inflammatory diseases. Saikosaponin constitutes the major anti-inflammatory components of Bupleuri Radix [8]. Baicalin and wogonoside, the main components in Scutellariae Radix, exhibit anti-inflammatory effects by suppressing the expression of IL-6, IL-8, and TNF-α, thus blocking the NF-κB signaling pathway in HBE16 airway epithelial cells [9]. Although the therapeutic requirements against inflammatory diseases are different, a combination of Bupleuri Radix and Scutellariae Radix is frequently used with good therapeutic effects. However, the application of these two drugs against anti-inflammatory diseases is limited owing to the lack of information regarding their mechanisms of action.

Systems pharmacology based research strategy has been widely used in many TCM herbal medicines and formulas researching, such as *Folium Eriobotryae* [10], licorice [11], and Danggui-Shaoyao-San decoction [12], which is helpful for the understanding of the molecular mechanism of TCM treatment from a microcosmic view. It mainly contains ADME screening, interactions network analysis, and

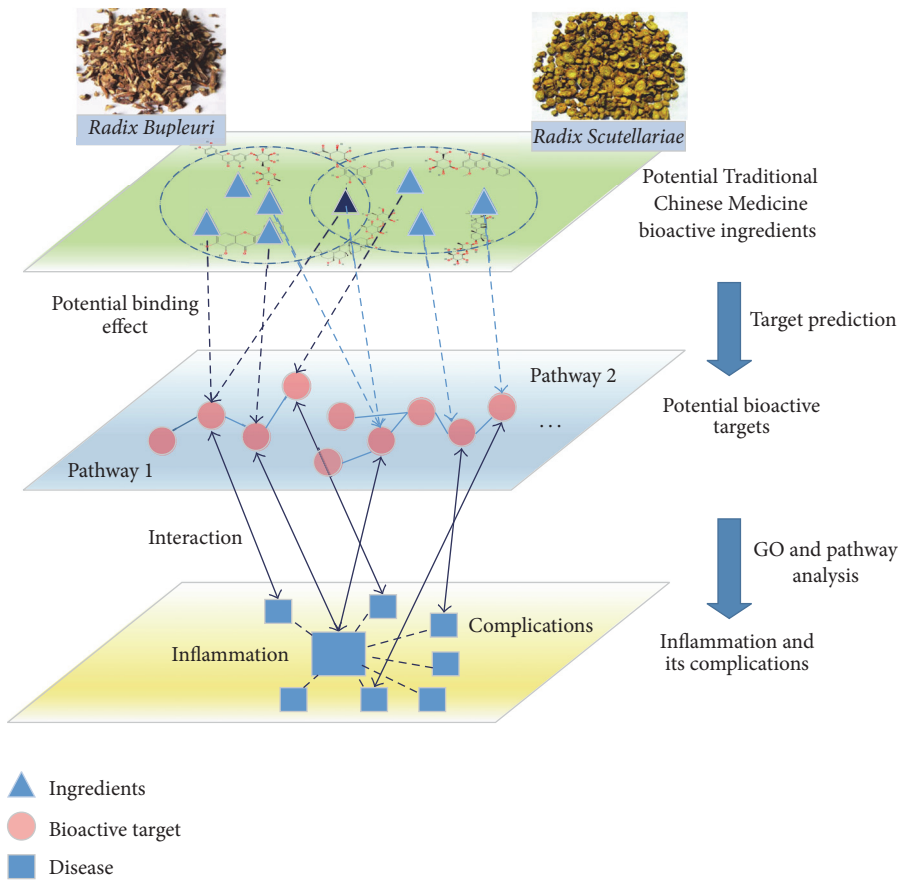

FIGURE 1: The brief workflow of system pharmacological analyses in searching *Bupleuri-Scutellariae Radix* anti-inflammation mechanism.

pathway analysis [13]. Therefore, in order to broaden our knowledge on Bupleuri Radix and Scutellariae Radix, we analyzed the ingredients of these two drugs using systems pharmacology. And we predicted the target genes of the active components and traced the inflammatory pathways related to these targets. Our study explored the cellular mechanisms underlying the anti-inflammatory activities of these two drugs, providing a molecular basis for the treatment of various diseases and their complications using Traditional Chinese Medicine (TCM), as shown in our brief workflow (Figure 1).

2. Materials and Methods

2.1. Materials. The ingredients structures of two herbal medicines were collected from Traditional Chinese Medicines for Systems Pharmacology Database and Analysis Platform (TCMSP http://lsp.nwsuaf.edu.cn/tcmsp.php) and Traditional Chinese Medicines Integrated Database (TCMID http://www.megabionet.org/tcmid/) and supplement the lacking ingredients by the literature from NCBI PubChem database (https://pubchem.ncbi.nlm.nih.gov/) and CNKI database (http://www.cnki.net/).

2.2. Active Ingredients Screening. Previous prediction is very necessary for the drug development process. Accurate identification of the active ingredients from herbal medicines is a basic step to assess the therapeutic mechanism of herbal medicines. And it is helpful for understanding the molecular mechanisms through pharmacokinetic characteristics research. Thus, ADME screening method and a series of pharmacokinetic parameters containing oral bioavailability (OB) and drug-likeness (DL) prediction were employed as our first step. Oral bioavailability is usually used to determine that the orally administered drugs could overcome several barriers and delivery into systemic circulation. A computer model OBioavail which integrates with the metabolism (cytochromes P450 3A4 and 2D6) and transport (P-glycoprotein) information is applying to predict the OB value of herbal ingredients [14]. In our present work, we chose the ingredients with OB $\geq$ 30%. Drug-likeness (DL) prediction allowed us to remove the ingredients deemed to be chemically unsuitable for drug here. It can be deduced that the absorption, distribution, metabolism, and excretion of the herbal medicine ingredients in human body are affected. This model was based on Tanimoto similarity defined as

$$T(A,B) = \frac{A \cdot B}{|A|^2 + |B|^2 - A \cdot B}. \quad (1)$$

In the formula above, "A" represents the ingredients from two herbal medicines, and "B" represents the average drug-likeness index of all molecules in DrugBank database based

on Dragon software descriptors. The DL value represents the possibility that the compound may possess certain biological properties. In our work, we choose the ingredients with suitable DL (DL $\geq$ 0.18), because the average DL index of DrugBank molecules is 0.18.

2.3. Potential Targets Fishing. In order to identify the molecular targets, a novel weighted ensemble similarity (WES) algorithm was employed to predict the potential treatment targets of 60 potential ingredients [15]. This model was built on a large data set involving 98,327 drug-target relations based on BindingDB (http://www.bindingdb.org/bind/index.jsp), DrugBank (http://www.drugbank.ca/), PDB database (http://www.rcsb.org/pdb/), and GoPubMed (http://www.ncbi.nlm.nih.gov/). And the algorithm mainly contains three parts: (1) the first is identifying the key ligand structural and physicochemical features by CDK and Dragon software; (2) in order to improve the accuracy, the overall similarities were converted into the size-bias-free normalized values to eliminate the relevant similarities from random; (3) finally, Bayesian network was used to predict the ensemble similarities (Z score). Then we chose the targets, which score greater than 5, as the potential targets.

Next, we standard the related targets and their related genes by using the BLAST tool in Uniprot database (http://www.uniprot.org/blast/). Then we collected the inflammatory diseases and potential diseases from CTD (http://ctdbase.org/), TTD (http://bidd.nus.edu.sg/group/cjttd/), and PharmGKB database (https://www.pharmgkb.org/).

2.4. Network Construction and Pathway Analysis. TCM prescriptions are considered as multicomponent therapeutics like multiple herbal medicines ingredients interacting with multiple targets. In order to explore the molecular mechanism of Bupleuri Radix and Scutellariae Radix for inflammation and complication diseases, we mapped the ingredients, targets, and potential diseases relevant to inflammation.

And the ClueGO, a plugin from Cytoscape, was utilized to interpret the related gene biology processes. Meanwhile, we used the KEGG Mapper analysis tool (http://www.genome.jp/kegg/tool/map_pathway2.html) to construct the pathways of these genes relevant to inflammatory diseases.

In order to find a disease with a potential comechanism with inflammation, the related disease information based on the potential bioactive was obtained from CTD database (http://ctdbase.org/), PharmGKB (https://www.pharmgkb.org/index.jsp), and TTD database (http://bidd.nus.edu.sg/group/cjttd/). And we classified these related diseases by NIH MeSH (https://meshb.nlm.nih.gov/#/fieldSearch). Finally, a target-disease-MeSH network was built by Cytoscape software.

3. Results and Discussion

3.1. Active Natural Ingredients. Based on the administration-distribution-metabolism-elimination (ADME) model, 30 active constituents out of 99 (Table S1 in Supplementary Material available online at https://doi.org/10.1155/2017/3709874) were selected (OB > 30%, DL > 0.18), as shown in Table 1. These 30 natural products all possess high oral bioavailability and drug-likeness. Among them, 21 components were discovered in Scutellariae Radix and 9 in Bupleuri Radix. Interestingly, this finding, consistent with the crucial nature of the function performed by Scutellariae Radix (clearing away heat and removing toxins), suggests that Scutellariae Radix would be more commonly used against inflammatory diseases than Bupleuri Radix [2].

Not surprisingly, most of the selected active ingredients are directly or indirectly related to inflammation. Several ingredients including saikogenin G, stigmasterol, salvigenin, ganhuangenin, and norwogonin have a direct therapeutic effect against inflammatory diseases. In a previous study, Saikogenin G was demonstrated to exhibit an anti-inflammatory activity against carrageenan produced plantar edema in rats [16]. Stigmasterol has exhibited anti-inflammatory and immunomodulatory effects through the downregulation of proinflammatory cytokines; moreover, it has been shown to inhibit herpes simplex virus replication in nervous cells in vitro [17, 18]. Devi and Periyanayagam found that Salvigenin derived from *Plectranthus amboinicus* exerted anti-inflammatory effects through human red blood cell (HRBC) membrane stabilization [19]. Bo et al. found that ganhuangenin obtained from Scutellariae Radix inhibited the release of histamine and leukotriene B4, thus inducing antioxidation and anti-inflammatory effects [20]. Norwogonin, an active component of Scutellariae Radix, selectively suppresses the activity of COX-1, COX-2, and 5-LOX and exhibits anti-inflammatory activity in arachidonic acid-induced mouse auricular edema. Skullcapflavone II, a potential bradykinin antagonist, was reported to relieve the inflammation in mouse asthma via regulation of the TGF-β1/Smad signaling pathway [21]. More importantly, Scutellariae Radix and Bupleuri Radix modulate immune function. Campesterol is an active ingredient acting as an anti-inflammatory and immunoregulatory compound [22]. Campesterol, a common type of plant sterol, exhibits both anti-inflammatory activity and immunomodulatory effects in Jurkat T cells through IL-2-mediated cAMP modulation and/or a calcium/calcineurin-independent pathway [23].

Inflammation is a common pathological process in many diseases. This means that natural products against inflammation have a wide range of therapeutic mechanisms of action. For instance, chrysin exhibits antitumor, antioxidation, and anti-inflammation activities; Bae et al. found that chrysin suppressed systemic anaphylaxis, histamine release, and IgE-mediated local anaphylaxis in mast cells. Therefore, it can be concluded that chrysin modulates allergic inflammation better than sodium cromoglycate (Intal) [24]. Shin et al. found that chrysin also exhibited anti-inflammatory effects by inhibiting the activation of NF-κB [25]. Meanwhile, chrysin could suppress NF-κB activity through the sensitization of TNF-α by inducing tumor cell apoptosis [26]. Therefore, chrysin may be developed into a drug for the treatment of tumors concomitant with inflammation. Saikosaponin C, a major component in Bupleuri Radix, exhibited good ADME properties in our study. Moreover, it has been reported to suppress caspase-3 activity and caspase-3-mediated FAK degradation to prevent LPS-induced cell injury and apoptosis [27].

Table 1: Potential active constituents in *Bupleuri Radix* and *Scutellariae Radix*.

ID	Ingredient name	OB	DL
CH08	Stigmasterol	43.82985	0.75664
CH22	Areapillin	55.14803	0.41394
CH26	Octalupine	47.82225	0.27864
CH29	Saikogenin G	51.83940	0.63197
CH39	Sainfuran	81.60749	0.23333
CH40	Thymonin	43.16284	0.40714
CH54	Saikosaponin c_qt	30.51828	0.63193
CH57	α-Spinasterol	42.97937	0.75693
CH60	Cubebin	57.12813	0.63980
HQ01	Campesterol	35.02838	0.71579
HQ02	Norwogonin	40.44827	0.20723
HQ03	5,2′-Dihydroxy-6,7,8-trimethoxyflavone	30.07322	0.35463
HQ04	Coptisine	30.40885	0.85647
HQ05	Supraene	33.54594	0.42162
HQ13	Carthamidin	40.28190	0.24188
HQ14	Dihydrobaicalin	41.53938	0.20722
HQ15	Salvigenin	53.87782	0.33279
HQ16	Ganhuangenin	93.43294	0.37375
HQ19	5,7,2′,6′-Tetrahydroxyflavone	35.42827	0.24383
HQ24	5,7,4′-Trihydroxy-8-methoxyflavone	34.76242	0.26666
HQ29	11,13-Eicosadienoic acid	39.27534	0.22891
HQ31	5,7,4′-Trihydroxy-6-methoxyflavanone	37.00241	0.26833
HQ32	5,2′-Dihydroxy-7,8,6′-trimethoxyflavone	38.39282	0.36629
HQ36	Chrysin	48.03082	0.18140
HQ39	Dihydrooroxylin A	46.37778	0.23057
HQ43	Oroxylin A	45.40775	0.23231
HQ44	Rivularin	43.74214	0.36628
HQ46	Skullcapflavone I	51.70113	0.29148
HQ47	Skullcapflavone II	43.90662	0.43793
HQ48	Tenaxin I	32.77480	0.35463

In addition, saikosaponin C inhibits the release of amyloid beta proteins 1-40 and 1-42 as well as abnormally phosphorylated tau, suggesting that saikosaponin C could be applied in the treatment of Alzheimer's disease [28].

3.2. Drug-Target Network Analyses. To elucidate the molecular mechanisms underlying the anti-inflammatory properties of the two drugs, we predicted the drug targets of the 30 selected active components based on weighted ensemble similarity (WES) analysis. The results showed that these 30 ingredients had 121 potential targets (Table S2). Moreover, we established a drug-target network using Cytoscape 3.2.0 software, and the target gene ID, as given in Uniprot, is shown in Figure 2.

The drug targets with a high degree and multiple ingredients were further identified and summarized. Some of these drug targets were directly correlated with cytokine synthesis and release, such as adenylate cyclase type V (ADCY5). In a model of neurogenic inflammation in mouse ear, ADCY5 was found to play a critical role in sensory neuropeptide release and neurogenic inflammation [29]. Katoh et al. discovered the crucial role of sialidase (Neu) in the hyaluronan receptor function of CD44 in T helper type 2-mediated airway inflammation in a murine acute asthmatic model [30]. It is well known that 5-lipoxygenase (ALOX5) is a key enzyme in the biosynthesis of leukotrienes from arachidonic acid in inflammatory and allergic processes. ALOX5 is therefore critical in multiple inflammatory diseases [31]. Fibrosis is a common complication in inflammation. PLA2G2A gene expression is elevated in ulcerative colitis and Crohn's disease, suggesting that this gene is important in inflammation in these two diseases [32]. Toll-like receptor (TLR) pathway is important in inflammation and critical in the migration of pancreatic cancer cells. MAP2K4 is a key protein involved in the migratory process in cancer cells [33]. TNFRSF1A and TLR4 are reported to be implicated in inflammation, and TNFRSF1A is involved in the inflammatory response syndrome [34, 35].

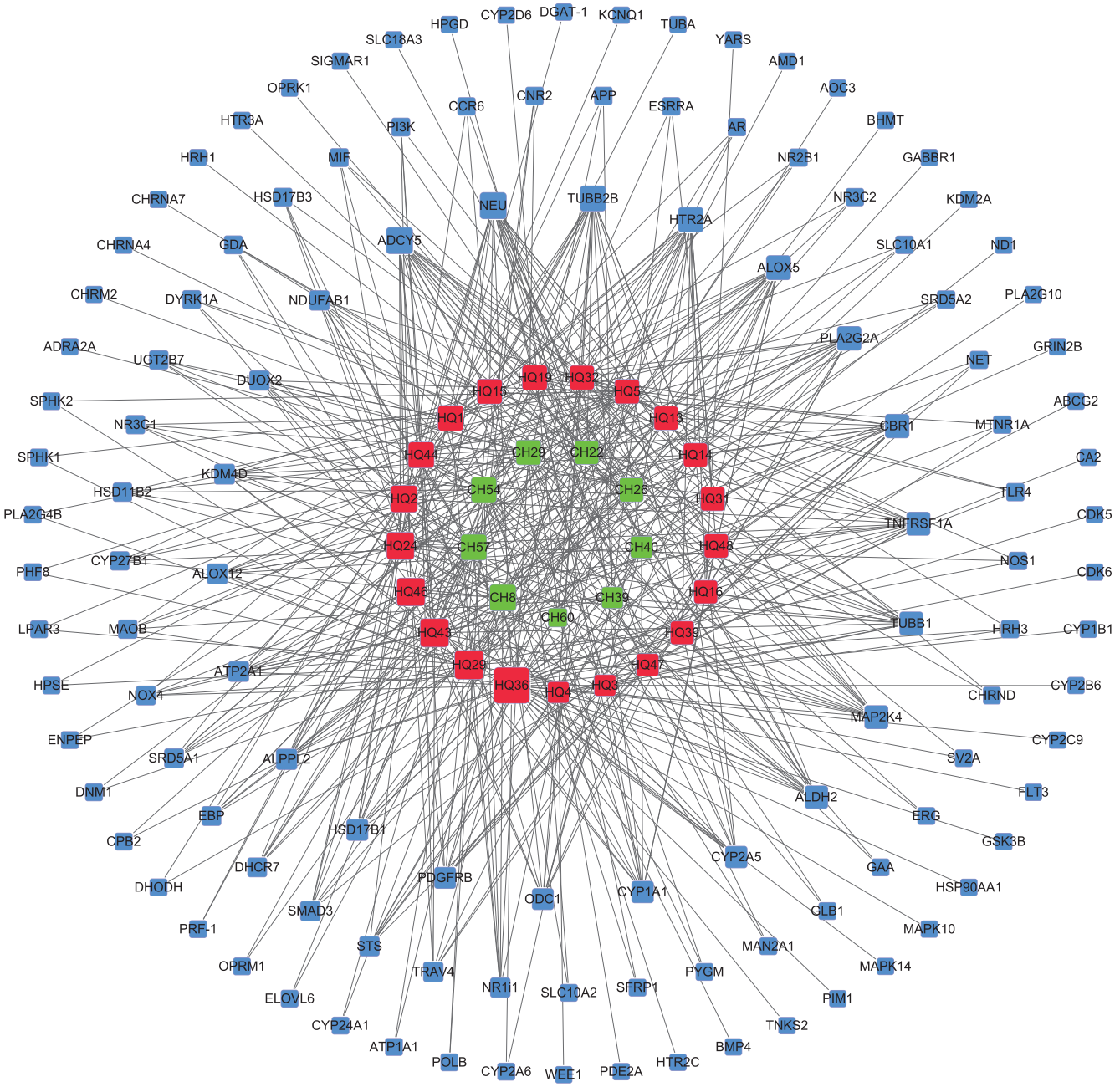

Figure 2: Bupleuri Radix-Scutellariae Radix active ingredients and potential drug targets. Blue: target gene ID; green: active ingredient in Bupleuri Radix; red: active ingredient in Scutellariae Radix. Node size indicates the degree in the network—bigger nodes represent more target genes and smaller nodes indicated fewer targets.

Another kind of drug targets is involved in complications in inflammatory diseases. The neurotransmitter 5-hydroxytryptamine (5-HT) plays an important role in immune responses and inflammatory diseases, such as inflammatory bowel disease, airway inflammation, and rheumatoid arthritis. HTR2A regulates the expression of 5-HT and is closely associated with inflammatory processes [36]. ALDH2 is involved in oxidative stress and inflammation in diabetes [37]. It can thus clearly be seen that the predicted drug targets in our study are associated with inflammation in an either direct or indirect manner.

From the network, we observed interaction between the 30 components and their predicted drug targets. In addition, the degrees of chrysin (HQ36), norwogonin (HQ02), saikosaponin C (CH54), and thymonin (CH40) were 39, 21, 18, and 11, respectively. These active components interacted with their predicted drug targets, such as ADCY5, NEU, ALOX5, HTR2A, MAP2K4, and TLR4; these drug

targets are critical in the inflammatory process, and multiple components exhibited synergistic effects through the concurrent regulation of inflammation-related targets. For instance, chrysin interacted not only with the genes directly related to inflammation, such as ALOX5, TLR4, MAPL10, MAPK14, and MAPK2K4, but also with genes indirectly related to inflammation, such as HTR2A, HSP90AA1, and ADCY5. Norwogonin had 21 targets including ALOX5 and MAP2K4, which are directly involved in inflammation. Thymonin interacted with the inflammation-related targets Alox5, Alox12 TNFRSF1A, and PDGFRB. PDGFRB plays a key role in inflammatory and noninflammatory breast cancer [38]. Saikosaponin C (SSc), a major component of *Bupleuri Radix*, interacted with CNR2. Activation of CNR2 inhibits the release of lymphokine and angiogenic factors, thus influencing the inflammation process and carcinogenesis [39]. Meanwhile, the SSc target SFRP1 is closely related to cancers such as prostate cancer [40], bladder cancer [40], and acute myeloid leukemia [41]. Moreover, these active ingredients exhibited systemic therapeutic efficacy by acting on targets indirectly involved in inflammation and its complications. In this way, the active ingredients of Bupleuri Radix and Scutellariae Radix exhibit anti-inflammatory effects by regulating not only those targets critical for inflammation but also those targets indirectly involved in inflammation and its complications.

3.3. GO and KEGG Pathway Analysis of the Inflammation-Related Drug Targets. To elucidate the molecular mechanisms underlying the anti-inflammatory effects of the two drugs, we performed gene set enrichment analysis using the Cytoscape plugin "ClueGO." As a result, we obtained 24 significant biological processes ($P < 0.05$). To better show the corresponding targets in pathway, we collate the targets associated with each pathway into the table, as shown in Table S3. In this section, we mainly aimed at the inflammation-related pathways and try to dig out underlying disease with the same pathogenesis.

As shown in Figure 3, we found that a number of the targets were involved in the classic inflammatory pathways and in transmitting mediators of inflammation. The other targets were associated with the complications and symptoms of inflammation. Some drug targets are related to MAPK activation, such as MAP2K4, TLR4, MAPK10, MAPK14, NOX4, ADAR2A, CHRNA7, ERBB2, FLT3, HTR2A, and LPAR3. Among these genes, TLR4 regulates LPS-induced inflammation through modulation of the P38 MAPK signaling pathway [42]. Others are involved in the metabolism of arachidonic acid, such as ALOX12, PLA2G10, PLA2G4B, CYP1B1, and CYP2A6. ALOX12 regulates the concentration of arachidonic acid in the peripheral blood via lipoxygenase [43]. Steroids exhibit anti-inflammatory effects through inhibition of the release of arachidonic acid and synthesis of prostaglandin [44]. Therefore, related target genes were also listed, such as ATP1A1, CYP27B1, DHCR7, EBP, GLB1, HSD11B2, HSD17B1, HSD17B3, SRD5A1, and SRD5A2.

In order to clearly explain the two Chinese medicines' corresponding pathway, we built a pathway figure by KEGG Mapper analysis tool (as shown in Figure 4). We have found that Bupleuri Radix and Scutellariae Radix may be beneficial for the treatment of inflammation-induced pain. NO is an inflammatory cytokine released by multiple cells. GO analysis showed that NO was closely related to CYP1B1, HSP90AA1, NOS1, OPRM1, and SMAD3. NOS1 in particular is a key enzyme in NO synthesis [45]. For example, we found target genes involved in the opioid receptor pathway (OPRK1, OPRM1, and SIGMAR1) and in pathways relating to synaptic release of neurotransmitters and hydroxytryptamine (HT) transmission (HTR2A and CHRNA4). Targeting the opioid receptor is a common strategy to achieve pain relief [46]. HTR2A, which is important for 5-HT transmission and nerve conduction, presents elevated expression levels in the punctured rat disc [47].

Combining with the information above, we speculated that the active ingredients in Bupleuri Radix and Scutellariae Radix not only act on the MAPK pathway, NO synthesis pathway, and the arachidonic acid pathway to directly regulate the synthesis and release of inflammatory cytokines, but also affect synaptic release of neurotransmitters in order to achieve pain relief. As a result, these two drugs exhibit systemic anti-inflammatory activity.

Interestingly, according to the targets from above and disease database mining, 344 diseases in 45 classifications were related to 96 targets (Figure 5), which are mostly neoplasms-related diseases (see the details in Table S4). In summary, common targets of these diseases are mostly binding by the ingredients from herbal medicines of Bupleuri Radix and Scutellariae Radix. Thus, these two herbal medicines may relieve complications and secondary disease of inflammatory diseases and treat them in common targets through some common signaling pathways. This may indirectly prove that these natural ingredients can be developed as the core drug of these diseases. Thus, our result provides new information and methodology reference on clinical using for these two herbal medicines and the prodrug discovery of their natural ingredients.

4. Conclusion

Inflammation is a complex pathologic process usually accompanying other diseases, and long-term inflammation increases the risk of cancer [48, 49]. This complexity means that resolution of inflammation is not enough to eradicate diseases. It is critical to systemically treat both inflammation and its complications.

Previously, antipathogen drugs including cephalosporins, aminoglycosides, and penicillin were often used to treat inflammation, leading to severe renal/nerve toxicity and amino glycosides-induced allergic reactions in some patients. Moreover, single-target drugs such as COX-2 inhibitor are limited in clinical application. TCM has multiple components and thus exhibits diverse pharmaceutical activities. Therefore, it is practical to develop novel anti-inflammation drugs from these and other natural products.

In the present study, we first analyzed the components of the selected TCM, Bupleuri Radix and Scutellariae Radix, using a systems pharmacology computer model and database mining technology. Second, the molecular mechanisms

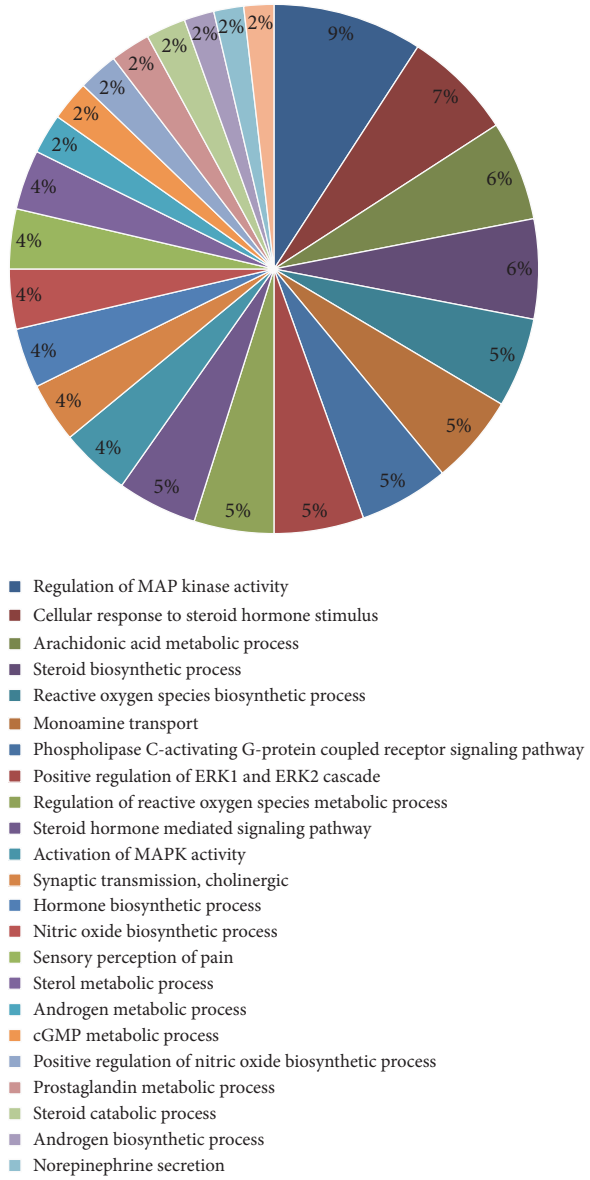

Figure 3: The gene count of inflammation-related gene ontology (GO) term classification.

underlying the anti-inflammation of the active ingredients were elucidated. Our study revealed that TCM has multiple components and multiple targets. The active ingredients of TCM interacted with key targets to inhibit the release of inflammatory cytokines and promote the production of immune cytokines in order to systemically improve the body's immunity. We selected 30 active ingredients with potential anti-inflammatory activity. Among them, several ingredients including saikogenin G, stigmasterol, salvigenin, ganhuangenin, and norwogonin are directly involved in the production and release of inflammatory cytokines. Campesterol, chrysin, and saikosaponin C not only are related to the production and release of inflammatory cytokines, but also exhibit activity against cancer-related inflammation. Thus, these ingredients could possibly be developed into therapeutics for treating inflammation and associated tumors. In addition, the abovementioned ingredients interacted with TLR4, ALOX5, ALOX12, and MAPK10, all of which are critical for the inflammatory process. Disruption of these targets affected the biosynthesis of leukotrienes from arachidonic acid. Interestingly, the selected components potentially interacted with OPRK1 and HTR2A, two target genes involved in pain, suggesting that TCM could relieve both inflammation and its common complication: pain. The multiple components and targets of TCM endow it with diverse pharmacological effects. However, the inflammation-related targets have not been adequately analyzed because of limited specific investigation of these genes. We will further

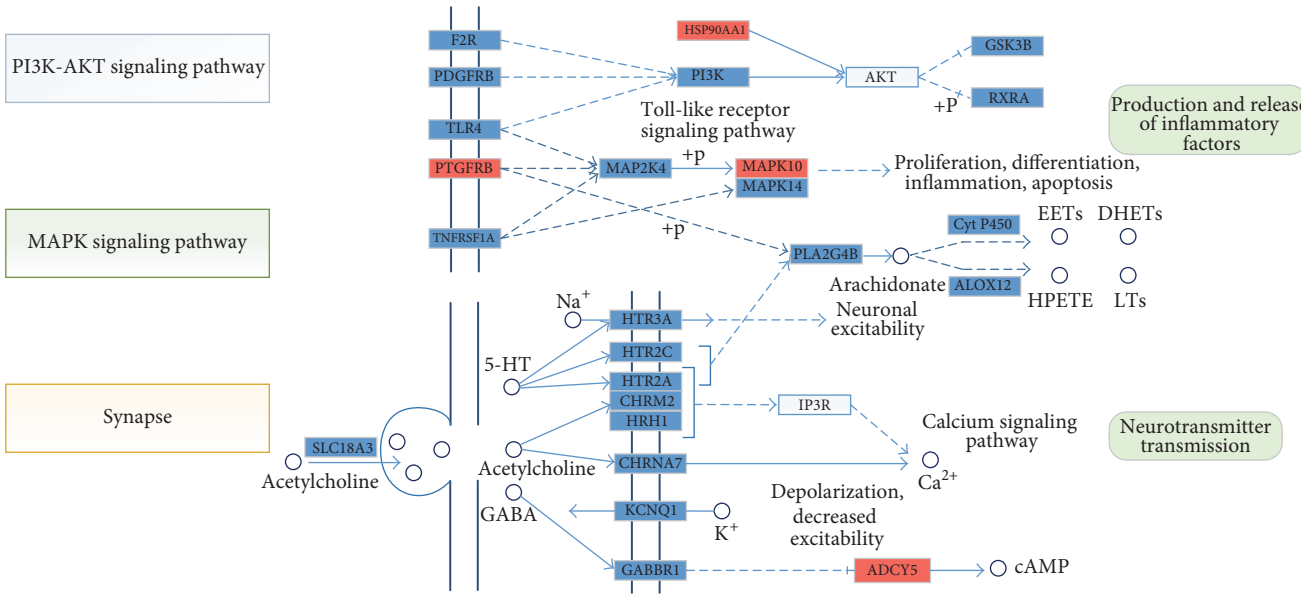

Figure 4: KEGG pathways of inflammation-related bioactive targets. Blue block: the target can be affected by the ingredients from two herbal medicines; red block: cancer-related targets in the KEGG database; white block: key target in the related pathway, but having no binding effect with our herbal ingredients; small circle: chemical metabolites in pathway.

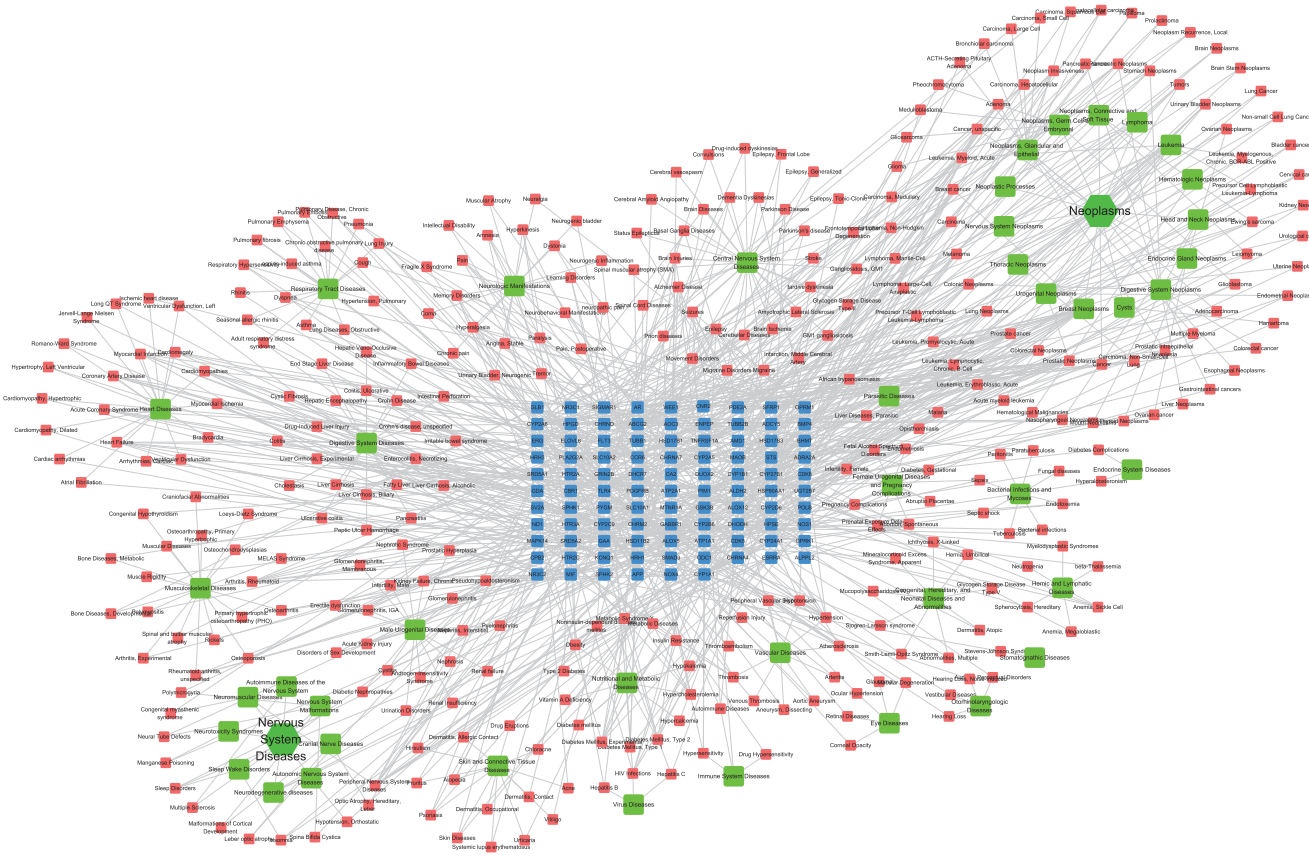

Figure 5: Target-disease-MeSH network. Blue node: the potential bioactive targets. Red node: potentially relevant diseases from CTD, TTD, and PharmGKB databases. Green node: MeSH classifications of potentially relevant disease.

explore the mechanism of action of anti-inflammatory effects of various TCM products and provide a rational basis for drug development in the future.

Disclosure

Xia Shen and Zhenyu Zhao are co-first authors.

Competing Interests

The authors declare that there is no conflict of interests regarding the publication of this paper.

Authors' Contributions

Xia Shen and Zhenyu Zhao contributed equally to this work. Gang Zhang and Xia Shen proposed the main ideas and designed the study. Zhenyu Zhao performed the experiments. Zhenyu Zhao, Hao Wang, and Zihu Guo built the calculation model and analyzed the experimental data. Benxiang Hu provided guidance and advice on TCM theory. Xia Shen, Zhenyu Zhao, and Gang Zhang wrote the manuscript.

Acknowledgments

Thanks are due to the Center of Bioinformatics, College of Life Science, Northwest A&F University, for the technical support. This research is financially supported by the Natural Science Fund of Science and Technology Department of Shaanxi Province (2014JQ4148) and the Key Laboratory Project of Education Department of Shaanxi Province (15JS023).

References

[1] B. Luo, J. Wang, Z. Liu et al., "Phagocyte respiratory burst activates macrophage erythropoietin signalling to promote acute inflammation resolution," *Nature Communications*, vol. 7, Article ID 12177, 2016.

[2] L. Capuron, J. Lasselin, and N. Castanon, "Role of adiposity-driven inflammation in depressive morbidity," *Neuropsychopharmacology*, vol. 42, no. 1, pp. 115–128, 2017.

[3] N. Alie, M. Eldib, Z. A. Fayad et al., "Inflammation, atherosclerosis, and coronary artery disease: PET/CT for the evaluation of atherosclerosis and inflammation," *Clinical Medicine Insights: Cardiology*, vol. 8, supplement 3, pp. 13–21, 2014.

[4] M. Berk, F. Kapczinski, A. C. Andreazza et al., "Pathways underlying neuroprogression in bipolar disorder: focus on inflammation, oxidative stress and neurotrophic factors," *Neuroscience and Biobehavioral Reviews*, vol. 35, no. 3, pp. 804–817, 2011.

[5] P. M. Ridker, C. H. Hennekens, J. E. Buring, and N. Rifai, "C-reactive protein and other markers of inflammation in the prediction of cardiovascular disease in women," *The New England Journal of Medicine*, vol. 342, no. 12, pp. 836–843, 2000.

[6] W.-Y. Jiang, "Therapeutic wisdom in traditional Chinese medicine: a perspective from modern science," *Trends in Pharmacological Sciences*, vol. 26, no. 11, pp. 558–563, 2005.

[7] S.-B. Yoon, Y.-J. Lee, S. K. Park et al., "Anti-inflammatory effects of *Scutellaria baicalensis* water extract on LPS-activated RAW 264.7 macrophages," *Journal of Ethnopharmacology*, vol. 125, no. 2, pp. 286–290, 2009.

[8] Y. Ma, Y. Bao, S. Wang et al., "Anti-inflammation effects and potential mechanism of saikosaponins by regulating nicotinate and nicotinamide metabolism and arachidonic acid metabolism," *Inflammation*, vol. 39, no. 4, pp. 1453–1461, 2016.

[9] S.-J. Dong, Y.-Q. Zhong, W.-T. Lu, G.-H. Li, H.-L. Jiang, and B. Mao, "Baicalin inhibits lipopolysaccharide-induced inflammation through signaling NF-κB pathway in HBE16 airway epithelial cells," *Inflammation*, vol. 38, no. 4, pp. 1493–1501, 2015.

[10] J. Zhang, Y. Li, S.-S. Chen et al., "Systems pharmacology dissection of the anti-inflammatory mechanism for the medicinal herb *Folium Eriobotryae*," *International Journal of Molecular Sciences*, vol. 16, no. 2, pp. 2913–2941, 2015.

[11] H. Liu, J. Wang, W. Zhou, Y. Wang, and L. Yang, "Systems approaches and polypharmacology for drug discovery from herbal medicines: an example using licorice," *Journal of Ethnopharmacology*, vol. 146, no. 3, pp. 773–793, 2013.

[12] Y. Luo, Q. Wang, and Y. Zhang, "A systems pharmacology approach to decipher the mechanism of danggui-shaoyao-san decoction for the treatment of neurodegenerative diseases," *Journal of Ethnopharmacology*, vol. 178, pp. 66–81, 2016.

[13] C. Huang, C. Zheng, Y. Li, Y. Wang, A. Lu, and L. Yang, "Systems pharmacology in drug discovery and therapeutic insight for herbal medicines," *Briefings in Bioinformatics*, vol. 15, no. 5, pp. 710–733, 2013.

[14] X. Xu, W. Zhang, C. Huang et al., "A novel chemometric method for the prediction of human oral bioavailability," *International Journal of Molecular Sciences*, vol. 13, no. 12, pp. 6964–6982, 2012.

[15] C. Zheng, Z. Guo, C. Huang et al., "Large-scale direct targeting for drug repositioning and discovery," *Scientific Reports*, vol. 5, Article ID 11970, 2015.

[16] M. P. Utrilla, A. Zarzuelo, S. Risco, M. A. Ocete, J. Jimenez, and M. J. Gamez, "Isolation of a saikosaponin responsible for the antiinflammatory activity of *Bupleurum gibraltaricum* Lam. root extract," *Phytotherapy Research*, vol. 5, no. 1, pp. 43–45, 1991.

[17] F. Villa-de la Torre, R. Kinscherf, G. Bonaterra et al., "Anti-inflammatory and immunomodulatory effects of *Critonia aromatisans* leaves: downregulation of pro-inflammatory cytokines," *Journal of Ethnopharmacology*, vol. 190, pp. 174–182, 2016.

[18] E. Petrera, A. G. Níttolo, and L. E. Alché, "Antiviral action of synthetic stigmasterol derivatives on herpes simplex virus replication in nervous cells in vitro," *BioMed Research International*, vol. 2014, Article ID 947560, 9 pages, 2014.

[19] K. N. Devi and K. Periyanayagam, "In vitro anti-inflammatory activity of *Plectranthus amboinicus* (Lour) Spreng by HRBC membrane stabilization," *International Journal of Pharmaceutical Sciences and Research*, vol. 1, no. 1, pp. 26–29, 2010.

[20] B. O. Lim, "Effect of ganhuangenin obtained from *Scutellaria radix* on the chemical mediator production of peritoneal exudate cells and immunoglobulin E level of mesenteric lymph node lymphocytes in Sprague-Dawley rats," *Phytotherapy Research*, vol. 16, no. 2, pp. 166–170, 2002.

[21] H.-Y. Jang, K.-S. Ahn, M.-J. Park, O.-K. Kwon, H.-K. Lee, and S.-R. Oh, "Skullcapflavone II inhibits ovalbumin-induced airway inflammation in a mouse model of asthma," *International Immunopharmacology*, vol. 12, no. 4, pp. 666–674, 2012.

[22] A. Navarro, B. De las Heras, and A. Villar, "Anti-inflammatory and immunomodulating properties of a sterol fraction from

Sideritis foetens CLEM," *Biological and Pharmaceutical Bulletin*, vol. 24, no. 5, pp. 470–473, 2001.

[23] S. A. Aherne and N. M. O'Brien, "Modulation of cytokine production by plant sterols in stimulated human Jurkat T cells," *Molecular Nutrition and Food Research*, vol. 52, no. 6, pp. 664–673, 2008.

[24] Y. Bae, S. Lee, and S.-H. Kim, "Chrysin suppresses mast cell-mediated allergic inflammation: involvement of calcium, caspase-1 and nuclear factor-κB," *Toxicology and Applied Pharmacology*, vol. 254, no. 1, pp. 56–64, 2011.

[25] E. K. Shin, H.-S. Kwon, Y. H. Kim, H.-K. Shin, and J.-K. Kim, "Chrysin, a natural flavone, improves murine inflammatory bowel diseases," *Biochemical and Biophysical Research Communications*, vol. 381, no. 4, pp. 502–507, 2009.

[26] X. Li, Q. Huang, C.-N. Ong, X.-F. Yang, and H.-M. Shen, "Chrysin sensitizes tumor necrosis factor-α-induced apoptosis in human tumor cells via suppression of nuclear factor-kappaB," *Cancer Letters*, vol. 293, no. 1, pp. 109–116, 2010.

[27] T. H. Lee, J. Chang, and B. M. Kim, "Saikosaponin C inhibits lipopolysaccharide-induced apoptosis by suppressing caspase-3 activation and subsequent degradation of focal adhesion kinase in human umbilical vein endothelial cells," *Biochemical and Biophysical Research Communications*, vol. 445, no. 3, pp. 615–621, 2014.

[28] T. H. Lee, S. Park, M.-H. You, J.-H. Lim, S.-H. Min, and B. M. Kim, "A potential therapeutic effect of saikosaponin C as a novel dual-target anti-Alzheimer agent," *Journal of Neurochemistry*, vol. 136, no. 6, pp. 1232–1245, 2016.

[29] J. Németh, D. ReglÖdi, G. Pozsgai et al., "Effect of pituitary adenylate cyclase activating polypeptide-38 on sensory neuropeptide release and neurogenic inflammation in rats and mice," *Neuroscience*, vol. 143, no. 1, pp. 223–230, 2006.

[30] S. Katoh, S. Maeda, H. Fukuoka et al., "A crucial role of sialidase Neu1 in hyaluronan receptor function of CD44 in T helper type 2-mediated airway inflammation of murine acute asthmatic model," *Clinical and Experimental Immunology*, vol. 161, no. 2, pp. 233–241, 2010.

[31] D. Steinhilber, "5-lipoxygenase: a target for antiinflammatory drugs revisited," *Current Medicinal Chemistry*, vol. 6, no. 1, pp. 71–85, 1999.

[32] F. Wu and S. Chakravarti, "Differential expression of inflammatory and fibrogenic genes and their regulation by NF-κB inhibition in a mouse model of chronic colitis," *Journal of Immunology*, vol. 179, no. 10, pp. 6988–7000, 2007.

[33] J. Liu, D. Xu, Q. Wang, D. Zheng, X. Jiang, and L. Xu, "LPS induced miR-181a promotes pancreatic cancer cell migration via targeting PTEN and MAP2K4," *Digestive Diseases and Sciences*, vol. 59, no. 7, pp. 1452–1460, 2014.

[34] S. Bank, P. Skytt Andersen, J. Burisch et al., "Polymorphisms in the inflammatory pathway genes TLR2, TLR4, TLR9, LY96, NFKBIA, NFKB1, TNFA, TNFRSF1A, IL6R, IL10, IL23R, PTPN22, and PPARG are associated with susceptibility of inflammatory bowel disease in a Danish cohort," *PLoS ONE*, vol. 9, no. 6, Article ID e98815, 2014.

[35] S. Borghini, D. Ferrera, I. Prigione et al., "Gene expression profile in TNF receptor-associated periodic syndrome reveals constitutively enhanced pathways and new players in the underlying inflammation," *Clinical and Experimental Rheumatology*, vol. 34, supplement 102, no. 6, pp. 121–128, 2016.

[36] M. S. Shajib and W. I. Khan, "The role of serotonin and its receptors in activation of immune responses and inflammation," *Acta Physiologica*, vol. 213, no. 3, pp. 561–574, 2015.

[37] H.-J. Wang, P.-F. Kang, W.-J. Wu et al., "Changes in cardiac mitochondrial aldehyde dehydrogenase 2 activity in relation to oxidative stress and inflammatory injury in diabetic rats," *Molecular Medicine Reports*, vol. 8, no. 2, pp. 686–690, 2013.

[38] F. Chai, Y. Liang, F. Zhang, M. Wang, L. Zhong, and J. Jiang, "Systematically identify key genes in inflammatory and non-inflammatory breast cancer," *Gene*, vol. 575, no. 2, part 3, pp. 600–614, 2016.

[39] R. I. Staiano, S. Loffredo, F. Borriello et al., "Human lung-resident macrophages express CB1 and CB2 receptors whose activation inhibits the release of angiogenic and lymphangiogenic factors," *Journal of Leukocyte Biology*, vol. 99, no. 4, pp. 531–540, 2016.

[40] P. García-Tobilla, S. R. Solórzano, I. Salido-Guadarrama et al., "*SFRP1* repression in prostate cancer is triggered by two different epigenetic mechanisms," *Gene*, vol. 593, no. 2, pp. 292–301, 2016.

[41] C. An, H. Guo, X.-M. Wen et al., "Clinical significance of reduced SFRP1 expression in acute myeloid leukemia," *Leukemia and Lymphoma*, vol. 56, no. 7, pp. 2056–2060, 2015.

[42] Q. Li, F. Bao, D. Zhi et al., "Lipopolysaccharide induces SBD-1 expression via the P38 MAPK signaling pathway in ovine oviduct epithelial cells," *Lipids in Health and Disease*, vol. 15, no. 1, article 127, 2016.

[43] C. C. Berthelot, S. G. Kamita, R. Sacchi et al., "Changes in PTGS1 and ALOX12 gene expression in peripheral blood mononuclear cells are associated with changes in arachidonic acid, oxylipins, and oxylipin/fatty acid ratios in response to omega-3 fatty acid supplementation," *PLoS ONE*, vol. 10, no. 12, Article ID e0144996, 2015.

[44] Y. Floman and U. Zor, "Mechanism of steroid action in inflammation: inhibition of prostaglandin synthesis and release," *Prostaglandins*, vol. 12, no. 3, pp. 403–413, 1976.

[45] J. W. Coleman, "Nitric oxide in immunity and inflammation," *International Immunopharmacology*, vol. 1, no. 8, pp. 1397–1406, 2001.

[46] M. Spetea, M. F. Asim, G. Wolber, and H. Schmidhammer, "The opioid receptor and ligands acting at the μ opioid receptor, as therapeutics and potential therapeutics," *Current Pharmaceutical Design*, vol. 19, no. 42, pp. 7415–7434, 2013.

[47] Y. Fujioka, A. Stahlberg, M. Ochi, and K. Olmarker, "Expression of inflammation/pain-related genes in the dorsal root ganglion following disc puncture in rats," *Journal of Orthopaedic Surgery*, vol. 24, no. 1, pp. 106–112, 2016.

[48] A. K. Roseweir, A. G. M. T. Powell, L. Bennett et al., "Relationship between tumour PTEN/Akt/COX-2 expression, inflammatory response and survival in patients with colorectal cancer," *Oncotarget*, 2016.

[49] I. Benedetti, A. Bettin, and N. Reyes, "Inflammation and focal atrophy in prostate needle biopsy cores and association to prostatic adenocarcinoma," *Annals of Diagnostic Pathology*, vol. 24, pp. 55–61, 2016.

Hindawi Publishing Corporation
Mediators of Inflammation
Volume 2016, Article ID 1320365, 10 pages
http://dx.doi.org/10.1155/2016/1320365

Research Article

Hydrogen-Rich Saline Attenuates Cardiac and Hepatic Injury in Doxorubicin Rat Model by Inhibiting Inflammation and Apoptosis

Yunan Gao,[1] Hongxiao Yang,[2] Yanbin Fan,[2] Lin Li,[2] Jiahui Fang,[2] and Wei Yang[2]

[1]*Department of Cardiology, The Fourth Affiliated Hospital of Harbin Medical University, 37 Yiyuan Street, Harbin, Heilongjiang 150001, China*
[2]*Department of Cardiology, The First Affiliated Hospital of Harbin Medical University, 23 Youzheng Street, Harbin, Heilongjiang 150001, China*

Correspondence should be addressed to Wei Yang; hydyangwei@tom.com

Received 1 October 2016; Revised 12 November 2016; Accepted 17 November 2016

Academic Editor: Yong Wu

Doxorubicin (DOX) remains the most effective anticancer agent which is widely used in several adult and pediatric cancers, but its application is limited for its cardiotoxicity and hepatotoxicity. Hydrogen, as a selective antioxidant, is a promising potential therapeutic option for many diseases. In this study, we found that intraperitoneal injection of hydrogen-rich saline (H_2 saline) ameliorated the mortality, cardiac dysfunction, and histopathological changes caused by DOX in rats. Meanwhile, serum brain natriuretic peptide (BNP), aspartate transaminase (AST), alanine transaminase (ALT), albumin (ALB), tissue reactive oxygen species (ROS), and malondialdehyde (MDA) levels were also attenuated after H_2 saline treatment. What is more, we further demonstrated that H_2 saline treatment could inhibit cardiac and hepatic inflammation and apoptosis relative proteins expressions by western blotting test. In conclusion, our results revealed a protective effect of H_2 saline on DOX-induced cardiotoxicity and hepatotoxicity in rats by inhibiting inflammation and apoptosis.

1. Introduction

Anthracyclines remain the most widely prescribed and effective anticancer agents. Doxorubicin (DOX), an anthracycline anticancer drug of secondary metabolite of *Streptomyces peucetius* var. *caesius*, is widely used in several adult and pediatric cancers such as thyroid cancer, ovarian cancer, leukemia, lymphomas, and breast cancer [1]. But the application is limited for its cytotoxicity in normal organs like heart and liver [2, 3].

Anthracycline cardiotoxicity is exponentially dose-dependent, with an average incidence of 5.1% at 400 mg/m^2 that becomes higher above 500 mg/m^2, albeit with substantial individual variation. Cardiomyopathy may develop at lower doses in the presence of risk factors like age, hypertension, arrhythmias, coronary disease, and so forth [4, 5]. Using clinical criteria, adult survivors of childhood cancer with a median time from diagnosis of 25 years (range: 10–47 years) were assessed for the prevalence of adverse health outcomes. Among them, cardiac dysfunction reaches up to 56.4% [6, 7]. Doxorubicin-induced cardiomyopathy is a lethal disease, because it may not be detected for many years and remains a lifelong threat. When congestive heart failure develops, mortality is approximately 50% [8].

It has been reported that about 40% of patients suffered liver injury after doxorubicin treatment [9]. It is still a challenge to find a favorable treatment for prevention of the toxicity or intervention after toxicity develops [10].

Now it is known that the mechanisms of doxorubicin-mediated cell death include oxidative stress, apoptosis, intracellular calcium dysregulation, topoisomerase II poisoning, DNA adduct formation, and ceramide overproduction [11, 12]. However, it seems that some drugs can protect the organs from the attack of oxidative stress theoretically. Besides, several pharmacologic agents, like antioxidants, hematopoietic cytokines, and iron-chelating agents, are reported to be used

to reduce the toxic effects to some extent [13, 14]. However, the exact mechanism of cardiotoxicity and hepatotoxicity induced by doxorubicin remains poorly understood.

Hydrogen (H_2), the most abundant and smallest element in the universe, has advantageous distribution characteristics for its capability to penetrate biomembranes and diffuse into the organelles and nucleus [15]. In 2007, Ohsawa et al. [16] used an acute rat model in which oxidative stress damage was induced in the brain by focal ischemia and reperfusion; they found that hydrogen acts as a therapeutic antioxidant by selectively reducing cytotoxic oxygen radicals, especially hydroxyl radical ($OH^{\bullet}$), the most cytotoxic reactive oxygen species (ROS). Overproduction of reactive oxygen can result in not only direct organ injury but also exacerbation of the inflammatory reaction simultaneously. The release of proinflammatory cytokines and chemokines, including tumor necrosis factor-α (TNF-α), interleukin-1β (IL-1β), and interleukin-6 (IL-6), the most important cytokines mediating the inflammatory response, normally triggers beneficial host innate immune response to confine tissue damage [17]. Nowadays, the inhibition of inflammation by hydrogen makes sense. Its rapid gaseous diffusion makes it highly effective for reducing cytotoxic radicals, and it has been proven to be protective against injury to various organs including the brain, liver, heart, and lung [18–21].

Studies have confirmed that DOX-derived ROS could act as an intrinsic stress that activates mitogen activated protein kinases (MAPK), p38, JNK, and NF-κB pathways as well as intracellular p53 accumulation, leading to an increase in proinflammatory cytokines (TNF-α and IL-1β) and alteration in the ratio of proapoptotic proteins to antiapoptotic proteins (e.g., Bax to Bcl-2), cytochrome C (Cyto C) release, and caspase-3 (C3) activation [22–24]. The present study aims to investigate the potential anti-inflammation and antiapoptosis effect of hydrogen-rich saline on DOX-induced cardiotoxicity and hepatotoxicity in Wistar albino rats.

2. Materials and Methods

2.1. Animals. Ninety male Wistar albino rats (Changsheng Biotechnology Co. Ltd., Liaoning, China) weighing an average of 200 g were used in this study in accordance with the Guidelines of Laboratory Animals of the First Affiliated Hospital of Harbin Medical University's protocol for care and use. They were housed with free access to food and water in a rodent facility under 12 h light-dark cycle and the temperature of 20–25°C. All rats were acclimated for seven days prior to any experimental procedures.

2.2. Preparation and Estimation of Hydrogen-Rich Saline. Hydrogen, produced from a hydrogen generator (HA300, Dura Safer Technology, Ltd., Beijing, China), was dissolved in normal saline in a thick plastic bag with no dead volume until reaching 4 atm for 1 hour. It was prepared freshly and sterilized by gamma radiation before injection. The concentration of hydrogen-rich saline was measured by oxidimetry method with a reagent containing methylene blue and colloidal platinum (Miz Company, Kanagawa, Japan) [25], and it was maintained at about 0.55 mmol/L to keep the concentrations of hydrogen in the heart and liver above 20 ppb/g [26].

2.3. Experimental Protocol. Ninety rats were divided into three groups at random as the normal-saline group (NS, n = 30), the doxorubicin group (DOX, n = 30), and the doxorubicin plus hydrogen-rich saline group (HS, n = 30). The DOX group and the HS group were treated by intraperitoneal injection with a dose of 2 mg/kg doxorubicin (Adriamycin®, Pfizer, Nerviano (MI), Italy) every 3 days for 30 days while the NS group was given saline of the same dose by the same way. Meanwhile, the HS group was given intraperitoneal injection of hydrogen-rich saline (10 mL/kg) but the other two groups were given the same dose of normal saline every day. On the 30th day, all rats were sacrificed by euthanasia to collect the blood and tissue samples.

2.4. Echocardiography. On the 30th day, the rats were subjected to induction of anesthesia at a concentration of 4% and maintained deeply anesthetized at a concentration of 2% with isoflurane (R510-22, RWD Life Science, Co. Ltd., Shenzhen, China). Transthoracic echocardiography was performed by an experienced ultrasonographic doctor who was blinded to the grouping of the rats. The interventricular septal thickness at diastole (IVSd), left ventricular internal diameter in diastole and systole (LVDd and LVDs), left ventricular posterior wall at diastole (LVPWd), ejection fraction (EF), and shortening fraction (FS) of each rat were assessed using a 12 MHz transducer connected to a commercially available echocardiographic system (SONOS 7500, Philips). All measurements are averages from three consecutive cardiac cycles.

2.5. Serum Parameter. Blood samples of all survived rats from aorta were collected into heparin-containing tubes, centrifuged at 3000g for 15 min at 4°C, and measured within 2 hours. The serum concentrations of BNP were detected using ELISA kits in accordance with the manufacturers' instructions (Nanjing Jiancheng Bioengineering Institute, Nanjing, China). Serum concentrations of AST, ALT, and ALB in different treatment groups were measured by an automatic biochemical analyzer (TMS-1024, Tokyo, Japan).

2.6. ROS and MDA Levels of Tissue. After euthanasia, cardiac and hepatic tissues of all survived rats were, respectively, washed in icy phosphate buffer saline. ROS was quantified by ELISA (Lanpai Biotech. Co. Ltd., Shanghai, China). MDA concentration, a presumptive marker of oxidant-mediated lipid peroxidation, was measured using a commercial kit (KeyGEN Biotech. Co. Ltd., Nanjing, China).

2.7. Histological Study. After blood sample collection, the rats were sacrificed and their hearts and livers were rapidly excised for histopathological and biochemical analyses. Tissues were fixed with 10% buffered formalin, embedded in paraffin, sectioned into 2 μm thick sections, and stained with hematoxylin and eosin (H&E). 10 random fields at 400x magnification in each specimen were observed and photographed with a light microscope (DP73, Olympus Co., Japan) by 3 pathologists of blinded method.

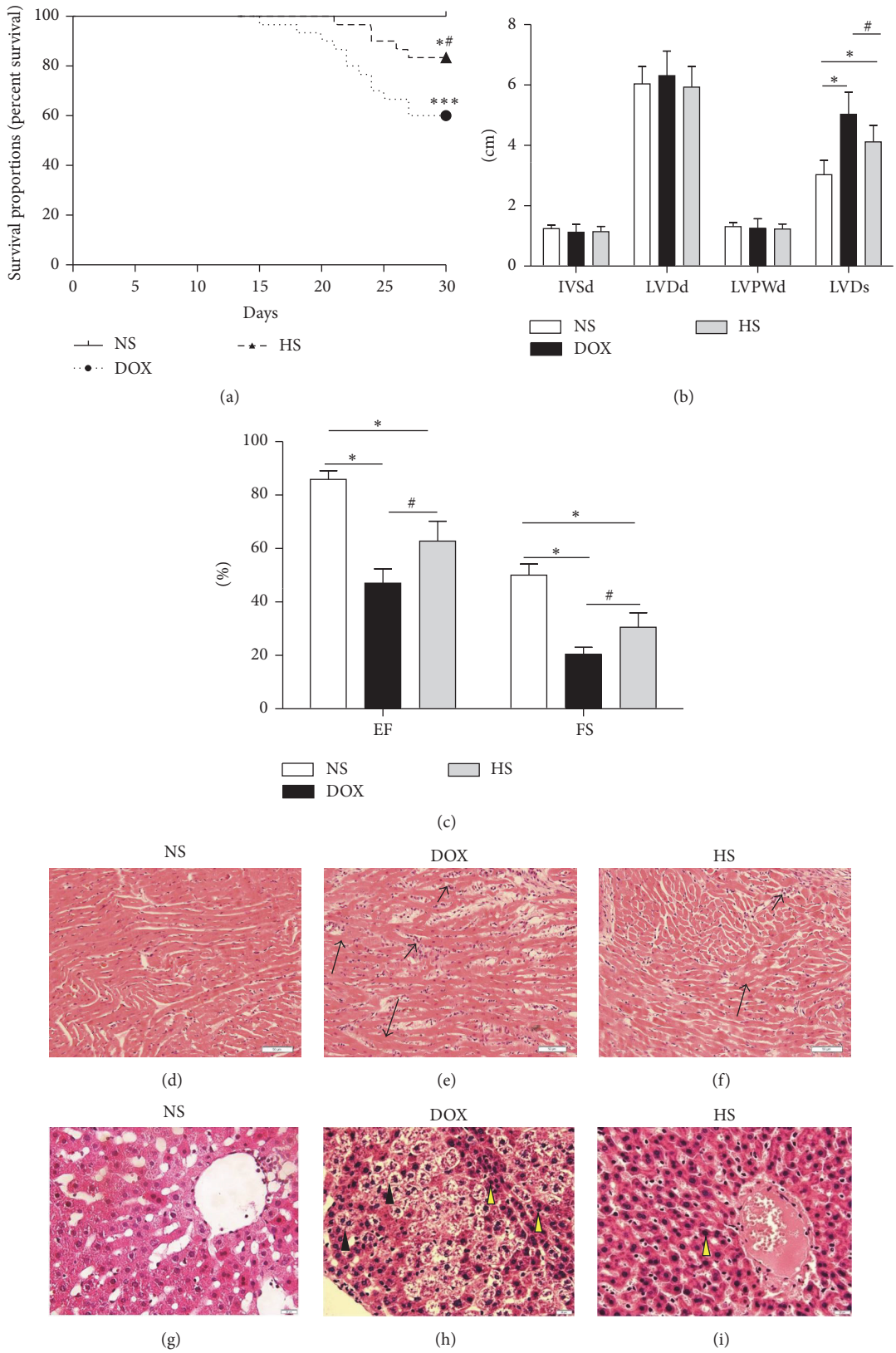

FIGURE 1: Effects of hydrogen-rich saline treatment on mortality, cardiac dysfunction, and pathological changes. Kaplan–Meier analyses of cumulative survival at 30 days after different treatments (a). The IVSd, LVDd, LVPWd, LVDs, EF, and FS of each rat were assessed ((b) and (c)). Morphologic changes of the heart (200x magnification; (d–f)) and liver (400x magnification; (g–i)) were processed for HE staining at 30 days (short arrows for infiltrated inflammatory cells and long arrows for focal myolysis; yellow arrowheads for karyopyknosis and black arrowheads for vacuolar degeneration). $^{*}P < 0.05$ versus NS group; $^{***}P < 0.001$ versus NS group; $^{\#}P < 0.05$ versus DOX group.

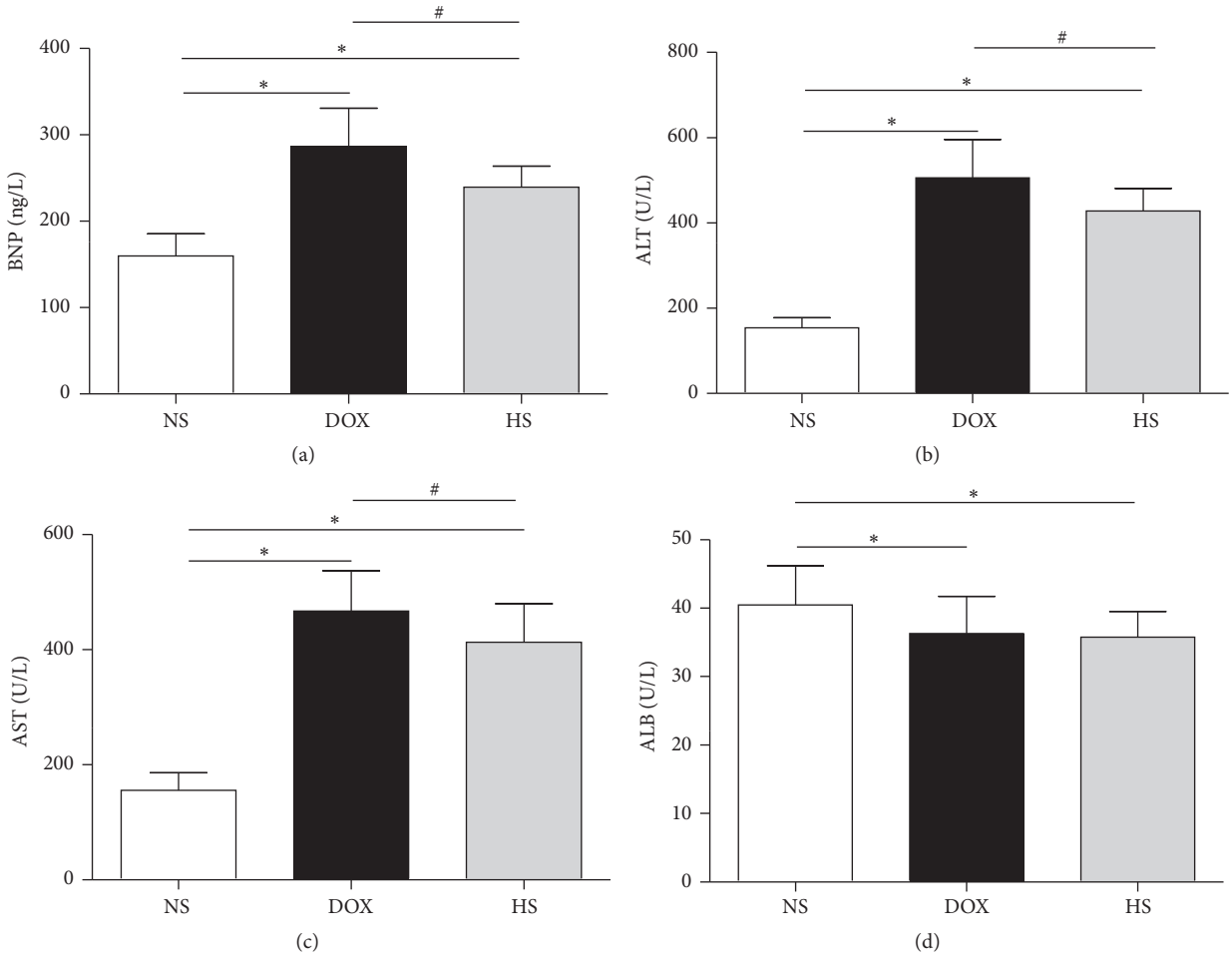

Figure 2: Effect of hydrogen-rich saline on serum parameters. Serum BNP (a), ALT (b), AST (c), and ALB (d) levels in three groups were detected. Data are shown as mean ± SD. $^{*}P < 0.05$ versus NS group; $^{\#}P < 0.05$ versus DOX group.

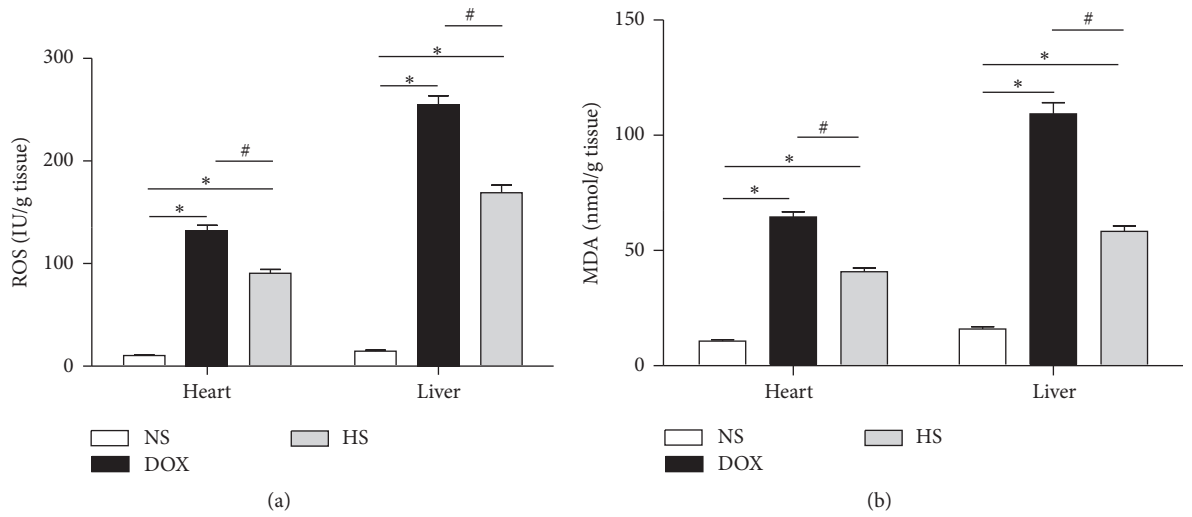

Figure 3: Effects of hydrogen-rich saline on ROS and MDA levels. The ROS (a) and MDA (b) levels of cardiac and hepatic tissues in three groups were detected. Data are shown as mean ± SD. $^{*}P < 0.05$ versus NS group; $^{\#}P < 0.05$ versus DOX group.

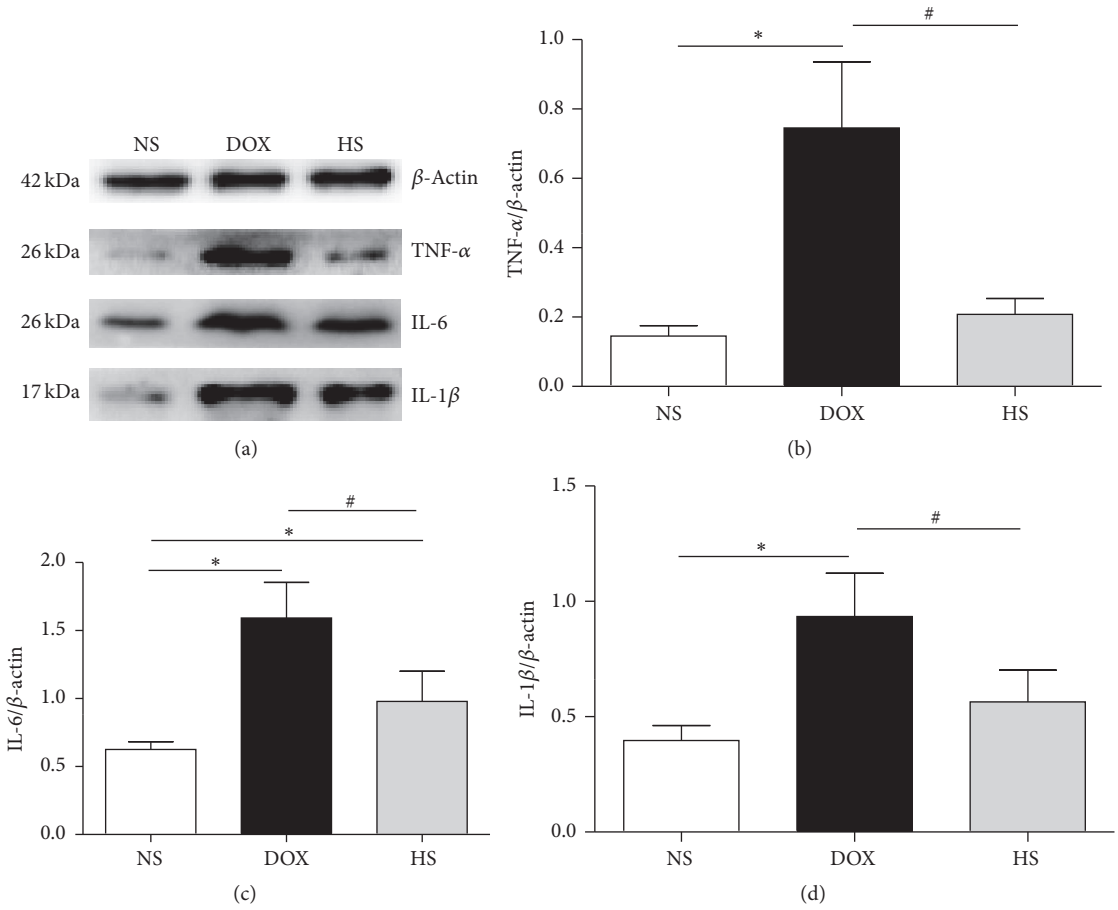

Figure 4: The anti-inflammatory effect of hydrogen-rich saline on cardiac tissue. Representative expression of inflammatory-related proteins in the heart after the treatment was detected (a–d). Data are shown as mean ± SD, $n \geq 3$. $^{*}P < 0.05$ versus NS group; $^{\#}P < 0.05$ versus DOX group.

2.8. Terminal Deoxynucleotidyl Transferase-Mediated dUTP-Biotin End Labeling (TUNEL) Staining Method. The TUNEL assay was performed to label the 3′-end of fragmented DNA in tissue sections according to the manufacturer's instructions (Roche, Switzerland) and stained with DAB kit (ZSGB-BIO, China). Stained cells area was counted on 10 random sections of liver from each rat without knowledge of the group of rats from which the tissue was taken. The TUNEL-positive area was expressed as a percentage of the total area. Finally, slides were examined by a light microscope (DP73, Olympus Co., Japan), and quantitative statistical analysis was performed with the KS400 Image Analysis System (KS400, Zeiss, Germany).

2.9. Assessment of Inflammation and Apoptosis. Western blotting was performed according to the commercial instruction. Total proteins were extracted from the tissues with the lysis buffer for protein immunoblotting. Protein concentrations were measured by BCA protein assay kit with bovine serum albumin (BSA) as standard (Beyotime, China). Protein samples were separated in each well of 12.5% sodium dodecylsulfate-polyacrylamide gel electrophoresis (SDS-PAGE) and blotted to Polyvinylidene fluoride (PVDF) membranes. The blots were blocked with 5% fat-free milk for 1 h at room temperature and then probed with primary antibodies including TNF-α (1 : 500 dilution, number ab6671, Abcam), IL-1β (1 : 1000 dilution, number ab9722, Abcam), IL-6 (1 : 500 dilution, number MAB5011, R&D), Bax (1 : 1000 dilution, number ab182733, Abcam), Bcl-2 (1 : 1000 dilution, number ab59348, Abcam), cleaved caspase-8 (C8) (1 : 1000 dilution, NB100-56116SS, NOVUS), cleaved caspase-3 (C3) (1 : 1000 dilution, number Asp175, CST), and β-actin (1 : 1000 dilution, number TA-09, ZSGB). They were incubated at 4°C overnight. The membranes were washed with TBS-T and then incubated with horseradish peroxidase-conjugated secondary antibody (1 : 2000 dilution; ZB-2301, ZB-2305, and ZSGB) for 1 hour at room temperature. Finally, the bands were collected by Imaging System (Bio-Rad, Hercules, CA, USA). β-Actin was used as the control for equal loading of the protein.

2.10. Data Processing and Statistical Analysis. Recipient survival was plotted using the Kaplan–Meier method and was analyzed using the log-rank test. Quantitative data were expressed as mean ± standard deviation (SD). Analysis of variance (one-way ANOVA) was used for multiple comparisons, with a posttest of Student-Newman-Keuls. Statistical significance was considered at a P value of <0.05. Statistical

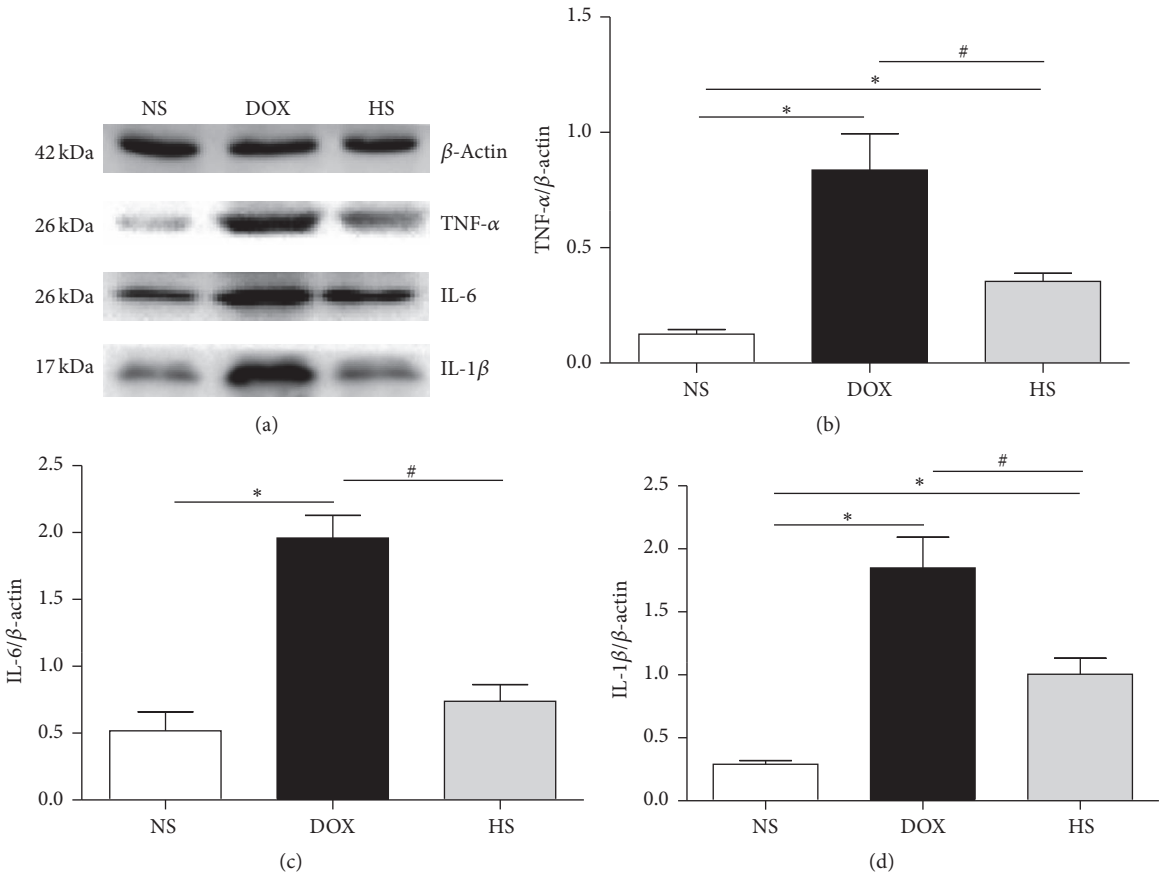

Figure 5: The anti-inflammatory effect of hydrogen-rich saline on hepatic tissue. Representative expression of inflammatory-related proteins in the liver after the treatment was detected (a–d). Data are shown as mean ± SD, $n \geq 3$. $^{*}P < 0.05$ versus NS group; $^{\#}P < 0.05$ versus DOX group.

analyses were performed using SPSS software (SPSS Inc., Chicago, USA).

3. Results

3.1. Effects of Hydrogen-Saline Treatment on Mortality, Cardiac Dysfunction, and Pathological Changes. By the end of the 30th day, all 30 rats in the NS group were alive, while 18 out of 30 (60%) rats in the DOX group ($P < 0.05$ versus NS group; Figure 1(a)) and 25 out of 30 (83.33%) rats survived in the HS group ($P < 0.05$ versus DOX group; Figure 1(a)). The LVD was significantly increased in the DOX group ($P < 0.05$; Figure 1(b)), whereas it was dramatically reduced by the hydrogen-rich saline treatment ($P < 0.05$; Figure 1(b)). However, there were no noted differences between the three groups about the IVSd, LVDd, and LVPWd ($P > 0.05$; Figure 1(b)). In addition, the EF and FS of DOX group were notably decreased compared with the NS group ($P < 0.05$; Figure 1(c)), but they were both remarkably increased in the HS group ($P < 0.05$; Figure 1(c)). Representative histological sections are shown in Figures 1(d)–1(f) (heart) and Figures 1(g)–1(i) (liver). Histopathological results from the H&E light micrographs showed that the NS group showed normal cardiac and hepatic architecture, and pathological injuries were obviously found in the DOX group, including infiltration of inflammatory cells, focal myolysis, karyopyknosis, and vacuolar degeneration, while they were significantly ameliorated in the HS group. According to these results, we further investigated the protective effect of H_2 saline on serum parameters of heart and liver injuries.

3.2. Effect of Hydrogen-Saline on Serum Parameters. Compared with NS group, serum BNP, ALT, and AST levels of DOX group were significantly increased ($P < 0.05$; Figures 2(a)–2(c)), but they were all remarkably reduced in the HS group ($P < 0.05$; Figures 2(a)–2(c)). Although DOX treatment decreased serum ALB levels ($P < 0.05$; Figure 2(d)), H_2 saline treatment was of no significance compared with the DOX group ($P > 0.05$; Figure 2(d)). These data suggest that hydrogen-rich saline effectively protects heart and liver function against doxorubicin-induced cardiotoxicity and hepatotoxicity. In addition, we investigated the ROS and MDA levels of cardiac and hepatic tissues because of the proven antioxidation of hydrogen.

3.3. Effect of Hydrogen-Saline Treatment on ROS and MDA Levels. ROS and MDA levels in cardiac and hepatic tissue were measured, showing that both ROS and MDA levels were

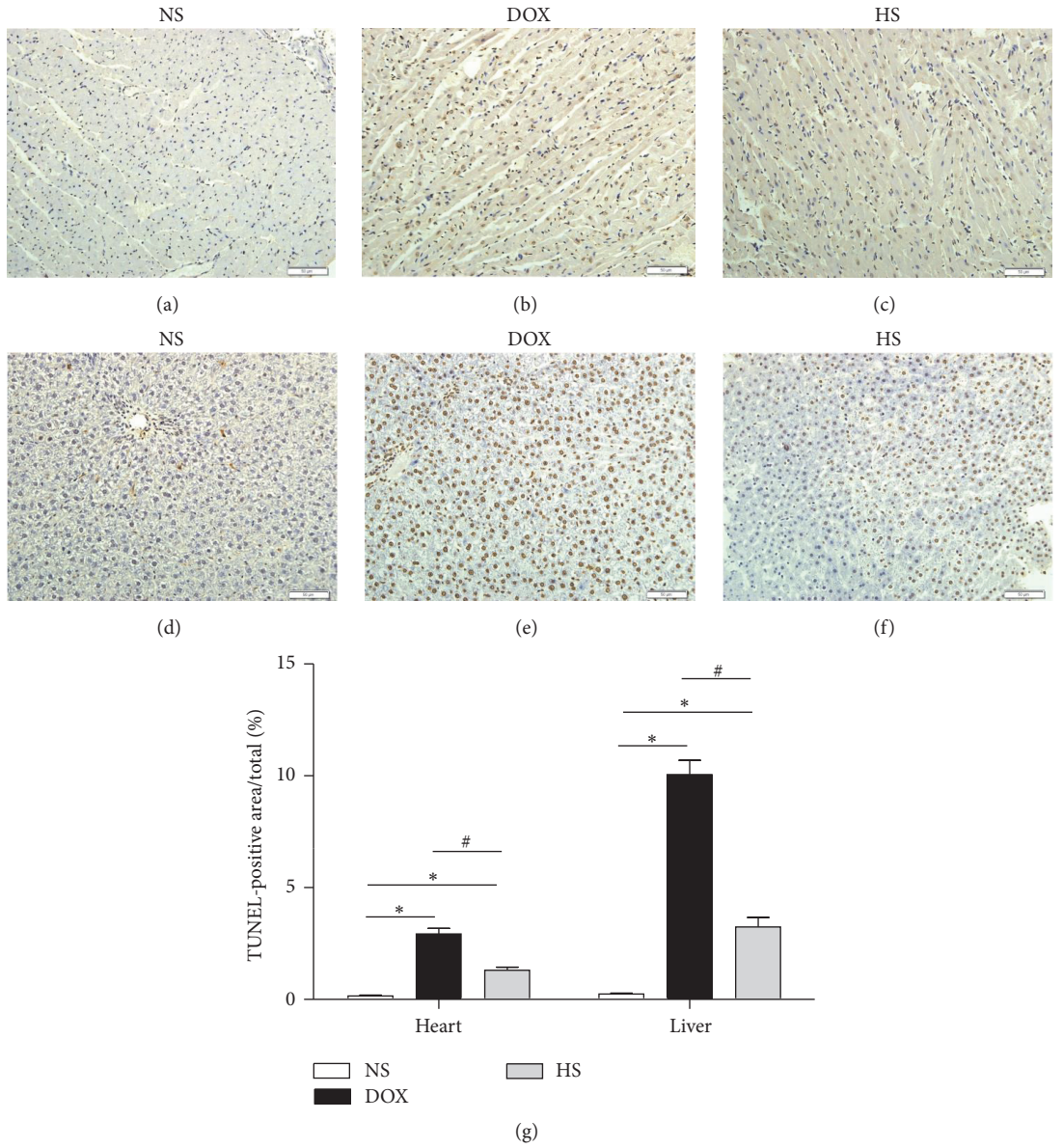

Figure 6: The antiapoptosis of hydrogen-rich saline on cardiac and hepatic tissue in TUNEL staining. Heart (200x magnification; (a–c)) and liver (200x magnification; (d–f)) sections of different treatment groups were stained by TUNEL, and the percentage of TUNEL-positive area (brown staining) of cardiac and hepatic (g) tissues was calculated for each group. Data are shown as mean ± SD. $^{*}P < 0.05$ versus NS group; $^{\#}P < 0.05$ versus DOX group.

significantly higher in the DOX group when compared with the NS group ($P < 0.05$; Figures 3(a) and 3(b)). In addition, they were significantly reduced in the HS group ($P < 0.05$; Figures 3(a) and 3(b)). These findings indicate that hydrogen-rich saline may act as an antioxidant to decrease the cardiac and hepatic ROS and MDA levels. Because oxidative stress injury could induce inflammation and apoptosis, we further investigated the changes of inflammation and apoptosis protein levels by western blotting.

3.4. The Anti-Inflammatory Effect of Hydrogen-Saline Treatment on Cardiac and Hepatic Tissue. The results of expressions of inflammation relative proteins are presented in Figures 4(a)–4(d) (heart) and Figures 5(a)–5(d) (liver). The expressions of TNF-a, IL-1β, and IL-6 in both cardiac and hepatic tissue were markedly increased after doxorubicin injection, and hydrogen-rich saline treatment could reduce the elevation of these inflammatory-related proteins expressions ($P < 0.05$; Figures 4 and 5). These results demonstrate that hydrogen-rich saline protects against heart and liver injury by inhibiting inflammatory responses.

3.5. The Antiapoptosis of Hydrogen-Saline Treatment on Cardiac and Hepatic Tissue in TUNEL Staining. The TUNEL assay findings are shown in Figures 6(a)–6(c) (heart) and Figures 6(d)–6(f) (liver). The percentages of TUNEL-positive

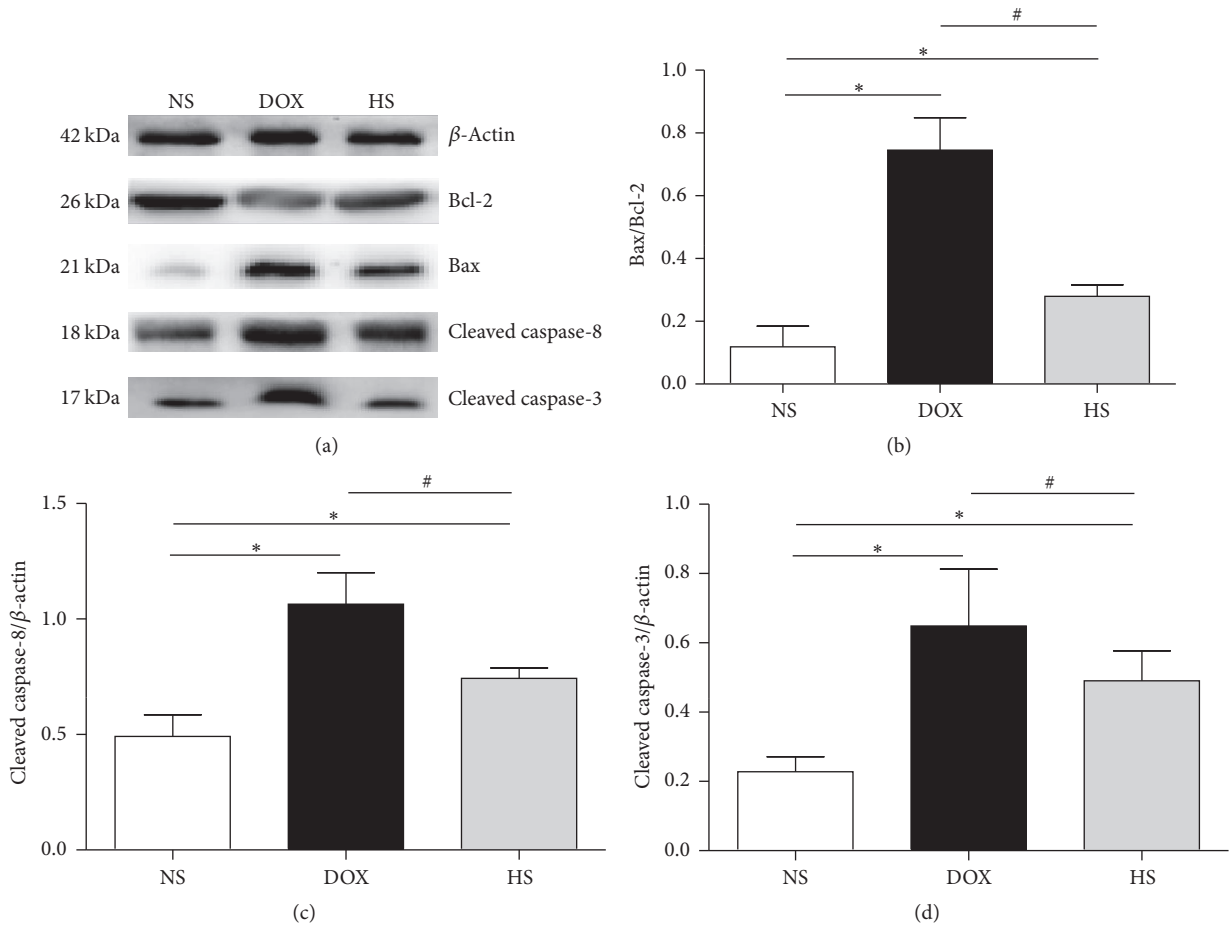

Figure 7: The antiapoptosis effect of hydrogen-rich saline on cardiac tissue. Representative expression of apoptosis-related proteins in the heart of three groups was detected (a–d). Data are shown as mean ± SD, $n \geq 3$. $^{*}P < 0.05$ versus NS group; $^{\#}P < 0.05$ versus DOX group.

area in the cardiac and hepatic (Figure 6(g)) slides were significantly increased in the DOX group ($P < 0.05$), whereas they were obviously reduced in the HS group ($P < 0.05$). These findings demonstrate that hydrogen-rich saline could decrease DOX-induced cell apoptosis.

3.6. The Antiapoptosis of Hydrogen-Saline Treatment on Cardiac and Hepatic Tissue. The results of expressions of apoptosis relative proteins are presented in Figures 7(a)–7(d) (heart) and Figures 8(a)–8(d) (liver). We found that the Bax/Bcl-2, cleaved C8, and cleaved C3 levels were higher in the DOX group compared with the NS group but were significantly reduced in the HS group ($P < 0.05$; Figures 7 and 8). These findings indicate that hydrogen-rich saline protects heart and liver from injury by inhibiting cell apoptosis.

4. Discussion

This study demonstrated a protective effect of hydrogen-rich saline on doxorubicin-induced cytotoxicity and hepatotoxicity, such as reduction in mortality, attenuation of heart and liver dysfunction, structural damage, and infiltration of inflammatory cells.

It is known that the main side effect of doxorubicin is the formation of free radicals in normal cells. Considerable evidence has demonstrated the antineoplastic activity by intercalation into DNA structure and production of ROS [27]. Recent studies have reported that hydrogen-rich saline prevents organ injury by decreasing ROS generation [16, 28], same as we detected. What is more, in this study, MDA, which is the end product of oxidative injury and an indicator of lipid peroxidation, rapidly increased both in the cardiac and in the hepatic tissues in the group with doxorubicin treatment. The ROS and MDA levels were both decreased remarkably after hydrogen-rich saline treatment, which indicated that hydrogen-rich saline could reduce oxidative stress induced by doxorubicin. Because hydrogen-rich saline reduced the product of lipid peroxidation, the instability induced by doxorubicin of cellular structures might be ameliorated.

Lines of evidence have confirmed that inflammation could be induced by the burden of ROS and doxorubicin. Doxorubicin-dependent cell death induces the release of high-mobility group protein B1 (HMGB1) which targets Toll-like receptors 2 and 4 (TLR2 and TLR4). These membrane receptors, in turn, promote immune responses by upregulating the transcription factor NF-κB and then upregulate the expressions of inflammatory factors [29]. Our study

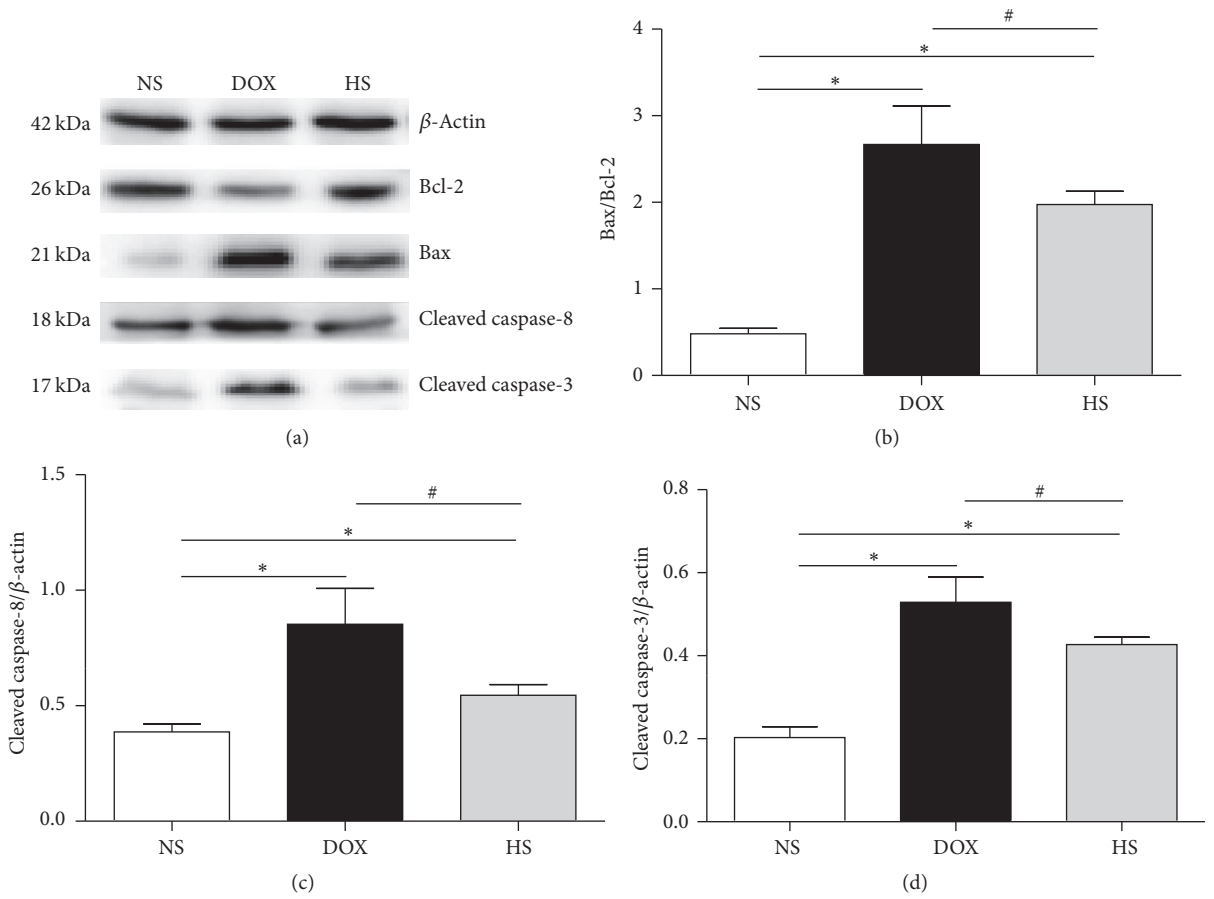

FIGURE 8: The antiapoptosis effect of hydrogen-rich saline on hepatic tissue. Representative expression of apoptosis-related proteins in the liver of three groups was detected (a–d). Data are shown as mean ± SD, $n \geq 3$. $^{*}P < 0.05$ versus NS group; $^{\#}P < 0.05$ versus DOX group.

also showed infiltration of inflammatory cell in cardiac and hepatic tissue after doxorubicin treatment in HE staining, and this could be reduced by hydrogen-rich saline treatment. In addition, we detected TNF-a, IL-1β, and IL-6 levels in cardiac and hepatic tissue; meanwhile, we found that hydrogen-rich saline significantly decreased the expressions of those cytokines, suggesting that hydrogen-rich saline may reduce heart and liver injury by reducing inflammatory responses.

During the past several decades, lots of studies have indicated that DOX-induced cytotoxicity is associated with cell apoptosis from extrinsic and intrinsic signaling pathways. In the extrinsic pathway, the binding of death ligands (FasL, TNFα, and TRAIL) with their receptors induces recruitment and activation of caspase-8, which subsequently activates downstream effector caspases such as caspase-3. The intrinsic pathway is regulated by the members of the Bcl-2 family, enhancing apoptosis via inhibition of antiapoptotic Bcl-2 proteins or activation of proapoptotic Bax and Bak. [30]. We investigated the effects of hydrogen-rich saline on doxorubicin-induced cell apoptosis. The TUNEL finding showed that hydrogen-rich saline treatment significantly ameliorated cell apoptosis in both cardiac and hepatic tissues. In addition, we detected the expressions of the Bax/Bcl-2, cleaved C8, and cleaved C3 in three groups, and the western blotting results showed that they were all decreased with the hydrogen-rich saline treatment. These findings may support the amelioration of heart and liver function and mortality by hydrogen-rich treatment.

In conclusion, our present study investigates the potential mechanism of the protective effect of hydrogen-rich saline on doxorubicin and demonstrates that hydrogen-rich saline treatment could inhibit the inflammatory TNF-α/IL-6 pathway, increase the cleaved C8 expression and Bcl-2/Bax ratio, and attenuate cell apoptosis in both heart and liver tissue. Due to its safety, efficacy, and convenience, intraperitoneal injection of hydrogen-rich saline should be considered as a potential therapy for heart and liver injury caused by doxorubicin.

Competing Interests

The authors have no competing interests to disclose.

Acknowledgments

This work was supported in part by the National Natural Science Foundation of China (Grant no. 81271676). Thanks are due to the Center Lab of the Department of Cardiology of

the First Affiliated Hospital of Harbin Medical University for providing the test site and essential equipment.

References

[1] W. G. Hozayen and H. S. Abou Seif, "Protective effects of rutin and hesperidin against doxorubicin-induced lipodystrophy and cardiotoxicity in albino rats," *Journal of American Science*, vol. 7, pp. 765–775, 2011.

[2] L. Gianni, E. H. Herman, S. E. Lipshultz, G. Minotti, N. Sarvazyan, and D. B. Sawyer, "Anthracycline cardiotoxicity: from bench to bedside," *Journal of Clinical Oncology*, vol. 26, no. 22, pp. 3777–3784, 2008.

[3] M. Yagmurca, O. Bas, H. Mollaoglu et al., "Protective effects of erdosteine on doxorubicin-induced hepatotoxicity in rats," *Archives of Medical Research*, vol. 38, no. 4, pp. 380–385, 2007.

[4] S. M. Swain, F. S. Whaley, and M. S. Ewer, "Congestive heart failure in patients treated with doxorubicin: a retrospective analysis of three trials," *Cancer*, vol. 97, no. 11, pp. 2869–2879, 2003.

[5] D. D. von Hoff, M. W. Layard, P. Basa et al., "Risk factors for doxorubicin-induced congestive heart failure," *Annals of Internal Medicine*, vol. 91, no. 5, pp. 710–717, 1979.

[6] M. M. Hudson, K. K. Ness, J. G. Gurney et al., "Clinical ascertainment of health outcomes among adults treated for childhood cancer," *The Journal of the American Medical Association*, vol. 309, no. 22, pp. 2371–2381, 2013.

[7] D. Strumberg, S. Brügge, M. W. Korn et al., "Evaluation of long-term toxicity in patients after cisplatin-based chemotherapy for non-seminomatous testicular cancer," *Annals of Oncology*, vol. 13, no. 2, pp. 229–236, 2002.

[8] S. A. van Acker, K. Kramer, J. A. Grimbergen, D.-J. Van den Berg, W. J. F. Van der Vijgh, and A. Bast, "Monohydroxyethylrutoside as protector against chronic doxorubicin-induced cardiotoxicity," *British Journal of Pharmacology*, vol. 115, no. 7, pp. 1260–1264, 1995.

[9] X. L. Yang, C. H. Fan, and H. S. Zhu, "Photo-induced cytotoxicity of malonic acid [C_{60}] fullerene derivatives and its mechanism," *Toxicology in Vitro*, vol. 16, no. 1, pp. 41–46, 2002.

[10] L. M. Grant and D. C. Rockey, "Drug-induced liver injury," *Current Opinion in Gastroenterology*, vol. 28, no. 3, pp. 198–202, 2012.

[11] Y. Octavia, C. G. Tocchetti, K. L. Gabrielson, S. Janssens, H. J. Crijns, and A. L. Moens, "Doxorubicin-induced cardiomyopathy: from molecular mechanisms to therapeutic strategies," *Journal of Molecular and Cellular Cardiology*, vol. 52, no. 6, pp. 1213–1225, 2012.

[12] F. Yang, S. S. Teves, C. J. Kemp, and S. Henikoff, "Doxorubicin, DNA torsion, and chromatin dynamics," *Biochimica et Biophysica Acta (BBA)—Reviews on Cancer*, vol. 1845, no. 1, pp. 84–89, 2014.

[13] L. Li, G. Takemura, Y. Li et al., "Preventive effect of erythropoietin on cardiac dysfunction in doxorubicin-induced cardiomyopathy," *Circulation*, vol. 113, no. 4, pp. 535–543, 2006.

[14] X. Zhao, J. Zhang, N. Tong, Y. Chen, and Y. Luo, "Protective effects of berberine on doxorubicin-induced hepatotoxicity in mice," *Biological and Pharmaceutical Bulletin*, vol. 35, no. 5, pp. 796–800, 2012.

[15] A. M. James, H. M. Cochemé, and M. P. Murphy, "Mitochondria-targeted redox probes as tools in the study of oxidative damage and ageing," *Mechanisms of Ageing and Development*, vol. 126, no. 9, pp. 982–986, 2005.

[16] I. Ohsawa, M. Ishikawa, K. Takahashi et al., "Hydrogen acts as a therapeutic antioxidant by selectively reducing cytotoxic oxygen radicals," *Nature Medicine*, vol. 13, no. 6, pp. 688–694, 2007.

[17] J. Zhang, Q. Wu, S. Song et al., "Effect of hydrogen-rich water on acute peritonitis of rat models," *International Immunopharmacology*, vol. 21, no. 1, pp. 94–101, 2014.

[18] K. Hayashida, M. Sano, N. Kamimura et al., "Hydrogen inhalation during normoxic resuscitation improves neurological outcome in a rat model of cardiac arrest independently of targeted temperature management," *Circulation*, vol. 130, no. 24, pp. 2173–2180, 2014.

[19] K.-I. Fukuda, S. Asoh, M. Ishikawa, Y. Yamamoto, I. Ohsawa, and S. Ohta, "Inhalation of hydrogen gas suppresses hepatic injury caused by ischemia/reperfusion through reducing oxidative stress," *Biochemical and Biophysical Research Communications*, vol. 361, no. 3, pp. 670–674, 2007.

[20] Y. F. Zhang, Q. Sun, B. He, J. Xiao, Z. Wang, and X. Sun, "Anti-inflammatory effect of hydrogen-rich saline in a rat model of regional myocardial ischemia and reperfusion," *International Journal of Cardiology*, vol. 148, no. 1, pp. 91–95, 2011.

[21] J. Zheng, K. Liu, Z. Kang et al., "Saturated hydrogen saline protects the lung against oxygen toxicity," *Undersea and Hyperbaric Medicine*, vol. 37, pp. 185–192, 2010.

[22] P. Angsutararux, S. Luanpitpong, and S. Issaragrisil, "Chemotherapy-induced cardiotoxicity: overview of the roles of oxidative stress," *Oxidative Medicine and Cellular Longevity*, vol. 2015, Article ID 795602, 13 pages, 2015.

[23] M. I. Morsi, A. E. Hussein, M. Mostafa, E. El-Abd, and N. A. Abd El-Moneim, "Evaluation of tumour necrosis factor-α, soluble P-selectin, γ-glutamyl transferase, glutathione S-transferase-π and α-fetoprotein in patients with hepatocellular carcinoma before and during chemotherapy," *British Journal of Biomedical Science*, vol. 63, no. 2, pp. 74–78, 2006.

[24] S. Mukherjee, S. K. Banerjee, M. Maulik, A. Kumar Dinda, K. K. Talwar, and S. Kumar Maulik, "Protection against acute adriamycin-induced cardiotoxicity by garlic: role of endogenous antioxidants and inhibition of TNF-α expression," *BMC Pharmacology*, vol. 3, article 16, 2003.

[25] T. Seo, R. Kurokawa, and B. Sato, "A convenient method for determining the concentration of hydrogen in water: use of methylene blue with colloidal platinum," *Medical Gas Research*, vol. 2, no. 1, 2012.

[26] C. Liu, R. Kurokawa, M. Fujino, S. Hirano, B. Sato, and X.-K. Li, "Estimation of the hydrogen concentration in rat tissue using an airtight tube following the administration of hydrogen via various routes," *Scientific Reports*, vol. 4, article 5485, 2014.

[27] H. Malhi and G. J. Gores, "Cellular and molecular mechanisms of liver injury," *Gastroenterology*, vol. 134, no. 6, pp. 1641–1654, 2008.

[28] H. Sun, L. Chen, W. Zhou et al., "The protective role of hydrogen-rich saline in experimental liver injury in mice," *Journal of Hepatology*, vol. 54, no. 3, pp. 471–480, 2011.

[29] A. Ghigo, M. Li, and E. Hirsch, "New signal transduction paradigms in anthracycline-induced cardiotoxicity," *Biochimica et Biophysica Acta*, vol. 1863, pp. 1916–1925, 2016.

[30] J. Shi and L. Wei, "Rho kinase in the regulation of cell death and survival," *Archivum Immunologiae et Therapiae Experimentalis*, vol. 55, no. 2, pp. 61–75, 2007.

Hindawi Publishing Corporation
Mediators of Inflammation
Volume 2016, Article ID 3825037, 8 pages
http://dx.doi.org/10.1155/2016/3825037

Research Article

Association of Insulin Resistance with Glucose and Lipid Metabolism: Ethnic Heterogeneity in Far Western China

Yi-Zhong Yan,[1] Ru-Lin Ma,[1] Jing-Yu Zhang,[1] Jia He,[1] Jiao-Long Ma,[1] Hong-Rui Pang,[1] La-Ti Mu,[1] Yu-Song Ding,[1,2] Heng Guo,[1] Mei Zhang,[1] Jia-Ming Liu,[1] Dong-Sheng Rui,[1] Kui Wang,[1] and Shu-Xia Guo[1,2]

[1]*Department of Preventive Medicine, University of Shihezi, Shihezi 832000, China*
[2]*Department of Pathology and Key Laboratory of Xinjiang Endemic and Ethnic Diseases (Ministry of Education), Shihezi University School of Medicine, Shihezi 832000, China*

Correspondence should be addressed to Shu-Xia Guo; pge888@sina.com

Received 18 August 2016; Revised 11 October 2016; Accepted 3 November 2016

Academic Editor: Yong Wu

Objective. To study the relationships between IR and glucose and lipid metabolism in far western China and these relationships' ethnic heterogeneity. *Methods*. From the baseline survey, 419 Uygur cases, 331 Kazak cases, and 220 Han cases were randomly selected, resulting in a total of 970 cases for study. FINS concentration was measured by radioimmunoassay. *Results*. (1) In the Kazak population, IR was correlated with hyperglycemia; high levels of TC, TG, and LDL-C; and low levels of HDL-C and abdominal obesity (all $P < 0.05$). (2) In the Uygur population, the influence of IR on hyperglycemia and abdominal obesity was the greatest. In the Kazak population, IR was associated with hyperglycemia most closely. In the Han population, IR may have had an impact on the incidence of low HDL-C levels. (3) After adjusting for sex, age, smoking status, and alcohol consumption, IR was still associated with anomalies in the metabolism of the Uygur, Kazak, and Han populations. *Conclusion*. IR was involved in the process of glucose and lipid metabolism, and its degree of involvement differed among the ethnicities studied. We could consider reducing the occurrence of abnormal glucose and lipid metabolism by controlling IR and aiming to reduce the prevalence of metabolic syndrome and related diseases.

1. Introduction

In recent years, the prevalence of diabetes, dyslipidemia, and obesity has still been a growing trend, affecting human health seriously. Studies have found that metabolic diseases often occur simultaneously in an individual and manifest as metabolic syndrome (MS), which can greatly increase a person's risk of cardiovascular disease [1, 2]. However, although the reasons for this clustering are still unclear, a large number of studies have agreed that insulin resistance (IR) is the root cause and has a common pathophysiological origin [3–5]. IR is most closely related to glucose metabolism [6]. As a predictor of diabetes, IR is an important precursor to and warning sign for type 2 diabetes. Obesity, and especially abdominal obesity, is a key factor leading to the development of IR. Current epidemiological evidence has demonstrated a strong correlation between obesity and IR among patients with MS [7]. However, the relationship between abnormal lipid metabolism and IR remains controversial, as the common changes related to IR-related dysfunction are high TG and low HDL-C levels but the link between IR and both TC and LDL-C is weaker [8, 9].

China is a multiethnic country and there are more than 10 ethnic groups in Xinjiang Uyghur Autonomous Region, where Uygur, Kazak, and Han are three large inhabitant ethnic groups. However, there are many differences among these ethnic groups, such as religion, culture, lifestyle, diet, and genetic background. Concerning the diet of Uygur and Kazak population, especially, their primary foods are wheat, beef, mutton, and dairy products containing high fat,but they consume less fruits and vegetables than Han. Due to limited resources in public health and poor transportation, there have

Table 1: General situation.

Ethnic	Group	Male/female	Age (years)	TG (mmol/L)	TC (mmol/L)	HDL-C (mmol/L)	LDL-C (mmol/L)	FPG (mmol/L)	WC (cm)
Uygur	IR	153/162	41.61 ± 12.29	1.48 ± 0.96	4.54 ± 1.10	1.14 ± 0.29	2.51 ± 0.76	4.53 ± 0.79	86.69 ± 11.77
	Non-IR	46/58	41.82 ± 11.81	1.16 ± 0.72	4.40 ± 1.24	1.25 ± 0.27	2.44 ± 0.67	4.03 ± 0.64	83.49 ± 10.19
	P	0.897	0.653	<0.001	0.012	0.005	0.023	<0.001	0.008
Kazak	IR	110/137	45.83 ± 11.40	1.38 ± 1.37	4.52 ± 1.04	1.37 ± 0.39	2.34 ± 0.74	4.94 ± 1.50	89.08 ± 11.69
	Non-IR	36/48	46.33 ± 9.95	1.10 ± 0.61	4.39 ± 1.00	1.41 ± 0.38	2.27 ± 0.73	4.26 ± 0.84	86.64 ± 10.86
	P	0.472	0.800	<0.001	<0.001	<0.001	0.032	0.017	0.028
Han	IR	66/99	49.44 ± 11.23	1.89 ± 1.41	4.81 ± 1.12	1.41 ± 0.37	2.82 ± 0.80	5.40 ± 2.46	88.22 ± 10.00
	Non-IR	32/23	49.62 ± 9.38	1.40 ± 0.68	4.65 ± 0.96	1.52 ± 0.26	2.70 ± 0.63	4.87 ± 0.75	84.80 ± 9.50
	P	0.502	0.823	<0.001	<0.001	0.037	0.029	<0.001	<0.001

Notes: TG = triglyceride, HDL-C = high-density lipoprotein cholesterol, FPG = fasting plasma glucose, LDL-C = low-density lipoprotein cholesterol, TC = total cholesterol, and WC = waist circumference.

not been serious investigations to analyze local public health including MS and related diseases; we need to pay more attention to their health and we need to improve health.

We have found that the prevalence of metabolic diseases such as obesity, hyperglycemia, and lipid metabolism disorders differs among the Uygur, Kazak, and Han populations. Numerous studies have confirmed that IR is the common thread of these metabolic diseases; thus, among the ethnic groups in Xinjiang, we examined the relationships between these diseases and IR. This study aimed to analyze the relationships between IR and glucose and lipid metabolism as well as these relationships' ethnic heterogeneity. Furthermore, we aimed to identify information relevant to preventing MS and related diseases, which may contribute to establishing appropriate preventive public health policies for different ethnic groups.

2. Subjects and Methods

(1) Subjects. Our survey was conducted from 2009 to 2012 in Yili, Kashi, Shihezi, Tacheng, and Changji prefectures. This survey collected information about MS from residents (≥18 years old). On this basis, we randomly selected 419 Uygur cases, 331 Kazak cases, and 220 Han cases, resulting in a total of 970 cases for study.

(2) Diagnostic Criteria and Related Definitions. (1) Dyslipidemia is TC ≥ 6.22 mmol/L as hypercholesterolemia; TG ≥ 2.26 mmol/L as hypertriglyceridemia; LDL-C ≥ 4.14 mmol/L as high low-density lipoprotein cholesterol; HDL-C < 1.04 mmol/L as low high-density lipoprotein cholesterol. Any of these lipids is abnormal that is judged as dyslipidemia [10]. (2) Hyperglycemia is FBG ≥ 6.1 mmol/L and (or) diagnosed with diabetes and treatment [11]. (3) Abdominal obesity is waist circumference for men ≥ 85 cm and women ≥ 80 cm [12]. The homeostasis model assessment of insulin resistance (HOMA-IR) index was defined as follows: [fasting insulin (mU/L) × fasting glucose (in mM)]/22.5. The Chinese Diabetes Society (CDS) states that IR can be estimated using this formula in epidemiological or clinical studies, and the upper quartile of the subjects was the split point [13].

(3) Laboratory Tests. (1) TC, TG, LDL-C, HDL-C, and fasting glucose levels were assessed by a biochemical autoanalyzer (Olympus AU 2700, Olympus Diagnostics, Hamburg, Germany) in a clinical laboratory. (2) FINS was determined by radioimmunoassay with kit purchased from Beijing Atomic-Tech Co. Ltd. (Beijing, China).

(4) Statistical Analysis. All of the analyses were performed using the SPSS statistical package for Windows (version 19.0). Continuously and normally distributed variables were analyzed using variance analysis, and the results are presented as the mean ± standard deviation (M ± SD). Variables with a skewed distribution were analyzed using the Mann–Whitney *U*-test, and the results are expressed as the median (upper quartile, lower quartile) ($M(Q_u, Q_L)$). Factors were analyzed using multivariate logistic regression analysis.

3. Results

3.1. Description of the General Situation. There was a total of 970 cases, including 419 cases of Uygur (43.2%), 331 cases of Kazak (34.1%), and 220 cases of Han (22.7%). The nationalities were divided into two groups (IR and Non-IR) according to the upper quartile of IR (Uygur: 1.17 mmol/L, Kazak: 0.97 mmol/L, and Han: 0.31 mmol/L), and average age and gender were not significantly different ($P > 0.05$ for each comparison); TG, TC, HDL-C, LDL-C, FBG, and WC were different ($P < 0.05$ for each comparison) (Table 1).

3.2. The Relationships of IR and Glucose and Lipid Metabolism

3.2.1. Univariate Logistic Regression Analysis. The results of univariate logistic regression analysis using hyperglycemia, low HDL-C, high TG, high LDL-C, high TC, and abdominal obesity as dependent variables and IR as the independent variable showed that when stratifying by IR quartiles the rates of detection of hyperglycemia showed an increasing trend with an increased IR incidence in the Uygur, Kazak, and Han populations. The Kazak and Han groups showed statistical significance in the fourth quintile, whereas the Uygur group had the highest odds ratio (OR) value in the

Table 2: The detection rates of glucose and lipid metabolism by IR level in Uygur.

Metabolism	Quartile of IR	n	Detection rates	P	OR	95% CI for OR
Hyperglycemia	<1.17*	1/104	0.96%	—	—	—
	1.17~	6/106	5.66%	0.094	6.180	(0.731, 52.255)
	1.74~	10/104	9.62%	0.024	10.957	(1.376, 87.232)
	3.28~	12/105	11.43%	0.014	13.290	(1.695, 104.189)
Low HDL-C	<1.17*	26/104	25.00%	—	—	—
	1.17~	35/106	33.02%	0.172	1.522	(0.833, 2.778)
	1.74~	39/104	37.50%	0.066	1.746	(0.964, 3.163)
	3.28~	41/105	39.05%	0.031	1.922	(1.063, 3.475)
High TG	<1.17*	9/104	8.65%	—	—	—
	1.17~	15/104	14.42%	0.215	1.740	(0.725, 4.174)
	1.74~	17/106	16.04%	0.098	2.063	(0.874, 4.868)
	3.28~	19/105	18.10%	0.034	4.056	(1.258, 8.985)
High LDL-C	<1.17*	2/104	1.92%	—	—	—
	1.17~	3/106	2.83%	0.668	1.485	(0.243, 9.077)
	1.74~	3/104	2.88%	0.653	1.515	(0.248, 9.258)
	3.28~	9/105	8.57%	0.040	4.680	(1.646, 16.154)
High TC	<1.17*	3/104	2.88%	—	—	—
	1.17~	5/104	4.81%	0.782	1.188	(0.351, 4.020)
	1.74~	6/106	5.66%	0.757	1.212	(0.358, 4.103)
	3.28~	6/105	5.71%	0.475	1.455	(0.858, 7.985)
Abdominal obesity	<1.17*	41/104	39.42%	—	—	—
	1.17~	53/104	50.96%	0.095	1.597	(0.921, 2.768)
	1.74~	60/106	56.60%	0.013	2.004	(1.157, 3.473)
	3.28~	65/105	61.90%	0.001	2.497	(1.431, 4.357)

Notes: TG = triglyceride, HDL-C = high-density lipoprotein cholesterol, LDL-C = low-density lipoprotein cholesterol, TC = total cholesterol, IR = insulin resistance, OR = odds ratio, CI = confidence interval, and ∗ = control group.

third quintile. The detection of low HDL-C levels showed an increasing trend with an increased incidence of IR, with the Uygur and Kazak groups showing statistical significance in the fourth quintile, whereas the Han group had the highest OR value in the second quintile. The detection of high TG levels showed an increasing trend with an increased incidence of IR, with the Uygur, Kazak, and Han groups showing statistical significance in the fourth quintile. The detection of high LDL-C levels showed an increasing trend with an increased incidence of IR, with the Uygur and Kazak groups showing statistical significance in the fourth quintile, whereas the Han population showed statistical significance in none of the quintiles. The detection of high TC levels showed an increasing trend with an increased incidence of IR, with the Kazak and Han groups showing statistical significance in the fourth quintile, whereas the Uygur population showed statistical significance in none of the quintiles. The detection of abdominal obesity showed an increasing trend with an increased incidence of IR, with the Kazak and Han groups showing statistical significance in the fourth quintile, whereas the Uygur group had the highest OR value in the third quintile (Tables 2–4).

3.2.2. Multivariate Logistic Regression Analysis. To exclude the influence of confounding factors (age, gender, smoking, and drinking), we had used multivariate Logistic regression with hyperglycemia, low HDL-C, high TG, high LDL-C, high TC, and abdominal obesity as the dependent variable and IR as the independent variable; the results showed that, in Uygur, high TC was not included by the equation, but smoking entered, and OR value of abdominal obesity was highest. IR of Kazak was still associated with all of the indicators, and OR value of hyperglycemia was highest. However, there was no relationship between IR and high LDL-C for Han, but smoking entered the equation, and OR value of low HDL-C was highest (Table 5–7).

4. Discussion

IR can exist before the development of diabetes and cardiovascular disease [14]. A prospective study found significant correlations among hyperinsulinemia, low HDL-C, and diabetes [15]. In addition, IR showed certain differences among different ethnic groups. In the present study, after stratifying the subjects according to the IR quartiles, we found that in the fourth quintile the IR of the Kazak population was highest and that of the Han population was lowest, which indicated that IR may be a more serious risk factor in the Kazak population; this finding was consistent with other reports [16, 17].

Table 3: The detection rates of glucose and lipid metabolism by IR level in Kazak.

Metabolism	Quartile of IR	n	Detection rates	P	OR	95% CI for OR
Hyperglycemia	<0.97*	8/84	9.52%	—	—	—
	0.97~	10/83	12.05%	0.600	1.301	(0.487, 3.480)
	2.24~	14/83	16.87%	0.166	1.928	(0.762, 4.875)
	5.83~	33/81	40.74%	0.000	6.531	(2.784, 15.323)
Low HDL-C	<0.97*	11/83	13.25%	—	—	—
	0.97~	12/83	14.46%	0.822	1.106	(0.458, 2.671)
	2.24~	13/83	15.66%	0.659	1.216	(0.510, 2.895)
	5.83~	21/81	25.93%	0.044	2.291	(1.023, 5.129)
High TG	<0.97*	4/83	4.82%	—	—	—
	0.97~	5/83	6.02%	0.732	1.266	(0.328, 4.891)
	2.24~	7/83	8.43%	0.355	1.819	(0.512, 6.466)
	5.83~	16/81	19.75%	0.007	4.862	(1.549, 15.258)
High LDL-C	<0.97*	1/83	1.21%	—	—	—
	0.97~	3/83	3.61%	0.500	1.350	(0.293, 6.229)
	2.24~	4/83	4.82%	0.256	2.023	(0.566, 9.812)
	5.83~	7/82	8.54%	0.036	4.569	(1.632, 11.238)
High TC	<0.97*	1/83	1.20%	—	—	—
	0.97~	4/83	4.82%	0.517	1.539	(0.418, 5.667)
	2.24~	6/83	7.23%	0.492	1.580	(0.429, 5.821)
	5.83~	6/81	7.41%	0.027	1.862	(1.549, 8.258)
Abdominal obesity	<0.97*	46/81	56.79%	—	—	—
	0.97~	53/81	65.43%	0.260	1.440	(0.763, 2.717)
	2.24~	53/79	67.09%	0.181	1.551	(0.815, 2.950)
	5.83~	62/82	75.61%	0.012	2.359	(1.208, 4.604)

Notes: TG = triglyceride, HDL-C = high-density lipoprotein cholesterol, LDL-C = low-density lipoprotein cholesterol, TC = total cholesterol, IR = insulin resistance, OR = odds ratio, CI = confidence interval, and ∗ = control group.

As early as 1988, studies found that obesity and IR have a causal relationship, as the accumulation of excessive adipose tissue can induce IR [18]. The characteristics of IR caused by obesity are the inhibition of hepatic glucose output and the promotion of glucose uptake by muscle and adipose tissue. Shao et al. found that 11β-HSD1 inhibition can exert a potential benefit in terms of reducing obesity and lowering IR by modulating the insulin signaling pathway and adipocytokine production [19]. However, the prevalence of obesity has increased on an annual basis. According to one survey, the prevalence of adult obesity (male 35.5%, female 35.8%) in the US in 2010 had reached 30.0% in advance [20] of the levels projected for 2015 [21]. In our study, among the Uygur, Kazak, and Han populations, we found that IR was associated with abdominal obesity; this relationship was observed at the third quintile of IR in the Uygur population, while the Kazak and Han groups showed this association in the fourth quintile. These data suggest that lower levels of IR could influence the Uygur population. In addition, the OR was highest in the Han population, which indicated that the correlation between IR and abdominal obesity was strongest in the Han population.

IR is most closely related to glucose metabolism and is a predictor of diabetes. Type 2 diabetes is always accompanied by IR, and hyperglycemia may appear 10 years earlier than other clinical symptoms of diabetes [22, 23]. The UKPDS study found that at the time of diagnosis with type 2 diabetes patients' islet β cell function was only 50% of that in normal humans and that this function gradually declined if the diabetes continued its course [24]. Cusi [25] found that the IR was most obvious in patients with diabetes after comparing between patients with normal glucose tolerance and patients with impaired glucose tolerance. These data were consistent with the clinical findings, which also showed that IR and diabetes were closely related. Our study found that the rate of detection of hyperglycemia increased with an increased incidence of IR, which suggests that IR is associated with hyperglycemia. Interestingly, the Kazak and Han populations showed statistical significance in the fourth quintile, whereas the Uygur group had the highest OR value, at 13.490, in the third quintile, which showed that the impact of IR on hyperglycemia was greatest in the Uygur population.

Related studies have reported that the most common factors associated with IR were high TG levels and low HDL-C levels but that the relationships between IR and both LDL-C and TC were weaker [9] . The present study was consistent, with the conclusion that among the Uygur, Kazak, and Han populations, overall, IR was closely related to high TG levels and low HDL-C levels, whereas there was no relationship between IR and either high LDL-C in the Han population or

Table 4: The detection rates of glucose and lipid metabolism by IR level in Han.

Metabolism	Quartile of IR	n	Detection rates	P	OR	95% CI for OR
Hyperglycemia	<0.31*	7/54	12.96%	—	—	—
	0.31~	8/55	14.55%	0.811	1.075	(0.294, 2.608)
	1.18~	10/57	17.54%	0.754	1.302	(0.392, 3.097)
	2.86~	20/54	37.04%	0.009	3.456	(1.362, 8.769)
Low HDL-C	<0.31*	1/55	1.82%	—	—	—
	0.31~	7/57	12.28%	0.043	7.560	(1.098, 63.636)
	1.18~	9/54	16.67%	0.027	10.800	(1.318, 88.506)
	2.86~	9/54	16.67%	0.027	10.800	(1.318, 88.506)
High TG	<0.31*	9/55	16.36%	—	—	—
	0.31~	14/54	25.93%	0.225	1.789	(0.700, 4.573)
	1.18~	14/57	24.56%	0.286	1.664	(0.653, 4.238)
	2.86~	21/54	38.89%	0.010	3.253	(1.323, 7.998)
High LDL-C	<0.31*	2/55	3.64%	—	—	—
	0.31~	2/54	3.70%	0.985	1.019	(0.138, 7.508)
	1.18~	4/57	7.02%	0.398	2.120	(0.372, 12.088)
	2.86~	5/54	9.26%	0.276	2.548	(0.473, 13.725)
High TC	<0.31*	2/55	3.64%	—	—	—
	0.31~	5/54	9.26%	0.247	2.704	(0.501, 14.585)
	1.18~	7/57	12.28%	0.112	3.710	(0.735, 18.715)
	2.86~	8/54	14.81%	0.041	4.829	(1.323, 20.998)
Abdominal obesity	<0.31*	26/55	47.27%	—	—	—
	0.31~	35/57	61.40%	0.135	1.774	(0.837, 3.762)
	1.18~	35/54	64.81%	0.067	2.055	(0.952, 4.435)
	2.86~	45/54	83.33%	0.000	5.577	(2.290, 13.583)

Notes: TG = triglyceride, HDL-C = high-density lipoprotein cholesterol, LDL-C = low-density lipoprotein cholesterol, TC = total cholesterol, IR = insulin resistance, OR = odds ratio, CI = confidence interval, and * = control group.

Table 5: Multivariate logistic regression analysis of IR with glucose and lipid metabolism in Uygur.

Metabolism	Quartile of IR	β	SE	Wald χ^2	P	OR	95% CI for OR
Hyperglycemia	<1.17*	—	—	—	—	—	—
	1.17~	0.65	0.40	0.53	0.099	1.320	(0.641, 2.599)
	1.74~	1.02	0.52	7.02	0.014	2.432	(1.290, 5.097)
	3.28~	2.12	0.78	12.03	0.001	4.277	(1.702, 9.029)
Low HDL-C	<1.17*	—	—	—	—	—	—
	1.17~	0.36	0.42	1.12	0.343	1.560	(1.098, 5.636)
	1.74~	0.47	0.42	1.24	0.227	1.801	(1.018, 7.506)
	3.28~	1.15	0.44	6.04	0.017	2.832	(1.218, 9.506)
High TG	<1.17*	—	—	—	—	—	—
	1.17~	0.28	0.35	0.52	0.505	1.289	(0.700, 4.573)
	1.74~	0.77	0.36	4.45	0.046	2.664	(1.253, 4.238)
	3.28~	1.29	0.38	11.88	0.009	3.553	(1.323, 8.798)
High LDL-C	<1.17*	—	—	—	—	—	—
	1.17~	0.30	0.38	0.60	0.585	1.019	(0.138, 5.508)
	1.74~	0.35	0.42	3.89	0.068	1.320	(0.772, 6.088)
	3.28~	1.09	0.50	9.79	0.023	2.248	(1.273, 8.725)
Abdominal obesity	<1.17*	—	—	—	—	—	—
	1.17~	0.28	0.39	0.59	0.435	1.274	(0.837, 5.762)
	1.74~	1.02	0.42	7.23	0.009	3.055	(1.952, 8.435)
	3.28~	2.88	0.45	20.35	0.000	5.277	(2.390, 11.583)
Smoking	Nonsmoking	—	—	—	—	—	—
	Smoking	0.76	0.29	6.64	0.010	2.13	(1.202, 3.792)

Notes: TG = triglyceride, HDL-C = high-density lipoprotein cholesterol, LDL-C = low-density lipoprotein cholesterol, IR = insulin resistance, OR = odds ratio, CI = confidence interval, and * = control group.

Table 6: Multivariate logistic regression analysis of IR with glucose and lipid metabolism in Kazak.

Metabolism	Quartile of IR	β	SE	Wald χ^2	P	OR	95% CI for OR
Hyperglycemia	<0.97*	—	—	—	—	—	—
	0.97~	0.38	0.42	1.23	0.311	1.475	(0.694, 3.608)
	2.24~	1.01	0.66	7.59	0.008	4.302	(1.392, 8.097)
	5.83~	2.88	0.86	40.20	0.001	18.456	(8.362, 44.769)
Low HDL-C	<0.97*	—	—	—	—	—	—
	0.97~	0.26	0.32	0.66	0.543	1.260	(0.108, 3.636)
	2.24~	0.32	0.35	1.01	0.427	1.800	(0.318, 5.506)
	5.83~	0.99	0.45	5.64	0.037	2.832	(1.318, 8.526)
High TG	<0.97*	—	—	—	—	—	—
	0.97~	0.32	0.40	1.33	0.225	1.889	(0.802, 4.573)
	2.24~	2.12	0.52	8.60	0.026	3.464	(1.643, 6.238)
	5.83~	2.79	0.60	10.08	0.009	4.653	(1.333, 10.998)
High LDL-C	<0.97*	—	—	—	—	—	—
	0.97~	0.45	0.42	1.13	0.285	1.571	(0.638, 3.508)
	2.24~	0.47	0.42	1.24	0.271	1.592	(0.672, 3.588)
	5.83~	1.12	0.43	6.64	0.010	3.148	(1.473, 7.725)
High TC	<0.97*	—	—	—	—	—	—
	0.97~	0.38	0.40	1.20	0.247	2.704	(0.501, 14.585)
	2.24~	0.42	0.42	1.29	0.112	3.710	(0.735, 18.715)
	5.83~	0.87	0.45	5.59	0.041	4.829	(1.323, 20.998)
Abdominal obesity	<0.97*	—	—	—	—	—	—
	0.97~	0.27	0.39	1.12	0.635	1.274	(0.857, 3.562)
	2.24~	0.37	0.40	1.20	0.467	2.055	(0.952, 4.435)
	5.83~	1.02	0.50	7.02	0.001	5.677	(2.380, 13.653)

Notes: TG = triglyceride, HDL-C = high-density lipoprotein cholesterol, LDL-C = low-density lipoprotein cholesterol, TC = total cholesterol, IR = insulin resistance, OR = odds ratio, CI = confidence interval, and * = control group.

high TC in the Uygur population. Bao et al. [26] reported that in all types of dyslipidemia, both high TG levels and high TG-induced hyperlipidemia were associated with the presence of other IR-related lipid abnormalities as well as with an increasing degree of aggravated dyslipidemia. Certain studies have shown that TG is an independent variable that is involved in serum lipid-induced IR and that is positively correlated with high TG-induced IR lipid marker levels [27]. In the present study, the high TG detection rates in the Uygur, Kazak, and Han ethnic groups were stratified by increasing levels of IR, and this relationship displayed significance in the fourth quintile. One of the hallmarks of IR is a reduced plasma concentration of HDL-C, suggesting that IR and HDL-C are closely related [28]. In this study, lower rates of IR in the Han population showed a correlation with HDL-C, with an OR of 10.800. However, in the other two ethnic groups, this correlation was significant in the fourth quintile, which showed a more obvious correlation between IR and HDL-C than in the Han population.

In short, the degree of correlation between IR and various metabolic disruptions was inconsistent; one explanation for this finding was ethnic heterogeneity. In the Uygur population, IR affected hyperglycemia and abdominal obesity less and was more closely associated with hyperglycemia, without any correlation with TC. In the Kazak population, the relationships of IR with various metabolic dysfunctions occurred in the group in the fourth quintile and were most closely related to hyperglycemia. Finally, in the Han population, the influence of IR on low HDL-C was most obvious, with the highest OR value, whereas high LDL-C levels did not show any correlation with IR.

5. Conclusion

In summary, IR is the common pathophysiological cause of a variety of metabolic abnormalities. In the present study, among the Uygur, Kazak, and Han populations, there were significant differences, but because this was only a cross-sectional study we could not identify the real reason for these differences. However, this study highlights the relevance of the relationship between IR and various metabolic disorders; based on this, we can observe and analyze larger groups and possibly perform experimental studies to eventually identify fundamental differences. These potential studies may provide a scientific foundation for formulating measures and strategies for the prevention and treatment of metabolic diseases that are suitable for different ethnic groups, with the aim of improving the quality of human life.

Table 7: Multivariate logistic regression analysis of IR with glucose and lipid metabolism in Han.

Metabolism	Quartile of IR	β	SE	Wald χ^2	P	OR	95% CI for OR
Hyperglycemia	<0.31*	—	—	—	—	—	—
	0.31~	0.29	0.35	0.55	0.511	1.275	(0.594, 2.608)
	1.18~	0.92	0.37	5.59	0.044	2.302	(1.192, 5.097)
	2.86~	1.33	0.40	12.65	0.001	3.456	(1.362, 8.769)
Low HDL-C	<0.31*	—	—	—	—	—	—
	0.31~	0.78	0.50	2.56	0.083	6.560	(2.098, 59.636)
	1.18~	1.23	0.55	8.52	0.037	11.023	(1.318, 80.506)
	2.86~	2.77	0.60	36.20	0.001	17.156	(2.318, 91.506)
High TG	<0.31*	—	—	—	—	—	—
	0.31~	0.31	0.42	0.66	0.225	1.789	(0.700, 4.573)
	1.18~	0.35	0.44	0.56	0.286	1.664	(0.653, 4.238)
	2.86~	1.03	0.50	3.56	0.020	4.253	(1.323, 8.998)
High TC	<0.31*	—	—	—	—	—	—
	0.31~	0.28	0.31	0.48	0.247	2.704	(0.501, 14.585)
	1.18~	0.32	0.39	0.99	0.112	3.710	(0.735, 18.715)
	2.86~	0.38	0.42	2.89	0.041	4.829	(1.323, 20.998)
Abdominal obesity	<0.31*	—	—	—	—	—	—
	0.31~	0.25	0.35	0.51	0.435	1.274	(0.637, 2.762)
	1.18~	0.92	0.36	6.44	0.012	2.455	(1.252, 4.435)
	2.86~	1.27	0.37	11.75	0.001	3.577	(1.690, 7.583)
Smoking	Nonsmoking	—	—	—	—	—	—
	Smoking	1.22	0.34	13.08	0.001	3.39	(1.752, 6.592)

Notes: TG = triglyceride, HDL-C = high-density lipoprotein cholesterol, TC = total cholesterol, IR = insulin resistance, OR = odds ratio, CI = confidence interval, and * = control group.

Abbreviations

BP: Blood pressure
CI: Confidence interval
FBG: Fasting blood glucose
HDL-C: High-density lipoprotein cholesterol
HOMA-IR: Homeostasis model assessment of insulin resistance
IR: Insulin resistance
LDL-C: Low-density lipoprotein cholesterol
MS: Metabolic syndrome
OR: Odds ratio
TC: Total cholesterol
TG: Triglyceride
WC: Waist circumference
FINS: Fasting serum insulin.

Competing Interests

The authors declare that there are no competing interests regarding the publication of this paper.

Authors' Contributions

Yi-Zhong Yan and Shu-Xia Guo contributed equally to this work.

Acknowledgments

This work was supported by grants from the National Science and Technology Support Projects for the "Eleventh Five-Years Plan" of China (no. 2009BAI82B04) and National Natural Science Foundation of China (no. 81560551).

References

[1] Cooperative Group for the Study of Metabolic Syndrome in Chinese Diabetes Society, "Recommendations of Chinese Medical Association Diabetes Society for metabolic syndrome," *Chinese Journal of Diabetes*, vol. 12, no. 3, pp. 156–161, 2004.

[2] G. Y. Wang, W. J. Tong, Y. S. Li et al., "Relationship of insulin resistance with cardiovascular disease among Mongoalian people," *Chinese Journal of Public Health*, vol. 23, no. 12, pp. 1455–1456, 2007.

[3] G. M. Reaven, "Banting lecture 1988. Role of insulin resistance in human disease. 1988," *Nutrition*, vol. 13, no. 1, pp. 65–66, 1997.

[4] C. F. Semenkovich, "Insulin resistance and a long, strange trip," *The New England Journal of Medicine*, vol. 374, no. 14, pp. 1378–1379, 2016.

[5] A. J. Krentz and G. A. Hitman, "The expanding pathogenic role of insulin resistance in human disease," *Diabetic Medicine*, 2014.

[6] H. Fan, P. R. Zhang, and Y. Xu, "Relationship between non-alcohol fatty liver disease and insulin resistance/cardiovascular diseases in patients with type 2 diabetes mellitus," *Chinese General Practice*, vol. 14, no. 1, pp. 147–150, 2011.

[7] W. J. Wang, K. A. Wang, T. L. Li et al., "A discussion on utility and purposed value of obesity and abdomen obesity when body mass index, waist circamference, waist to hip ratio used as indexes predicting hypertension and hyper-blood glucose," *Chinese Journal of Epidemiology*, vol. 23, no. 1, pp. 16–19, 2002.

[8] S. M. Haffner, R. A. Valdez, H. P. Hazuda, B. D. Mitchell, P. A. Morales, and M. P. Stern, "Prospective analysis of the insulin-resistance syndrome (Syndrome X)," *Diabetes*, vol. 41, no. 6, pp. 715–722, 1992.

[9] X. Hua and Z. X. Hong, "Effects of individualized prescriptive diet and single prescriptive diet on blood lipids and insulin resistance in type 2 diabetes mellitus patients," *Chinese General Practice*, vol. 14, no. 1, pp. 133–135, 2011.

[10] Joint Committee for Developing Chinese Guidelines on Prevention and Treatment of Dyslipidemia in Adults, "Guidelines on prevention and treatment of blood lipid abnormality in Chinese adults," *Chinese Journal of Cardiology*, vol. 35, no. 5, pp. 133–135, 2007.

[11] Y. Cheng and C. Y. Pan, "Definition and diagnosis of diabetes and intermediate hyperglycaemiap," *Chinese Journal of Endocrinology and Metabolism*, vol. 20, no. 5, pp. 6b 1–6b 11, 2004.

[12] Disease Control Department of Ministry of Health in China, *Prevention and Control Guidelines for Overweight and Obesity Adults in China*, People's Medical Publishing House, Beijing, China, 2006 (Chinese).

[13] G. W. Li, C. M. Li, S. X. Sun et al., "Is insulin resistance a common pathway for hereditary and environmental factors-induced hypertension," *Chinese Journal of Internal Medicine*, vol. 42, no. 1, pp. 11–15, 2003.

[14] L. Li and G. Y. Yang, "Lipid dysmetabolism, adipocytokine and insulin resistance," *Chinese Journal of Diabetes*, vol. 15, no. 3, pp. 129–131, 2007.

[15] C. K. Zhou, Y. H. Lu, M. S. An et al., "Association of insulin resistance and cardiovascular disease risk factors," *Sichuan Medical Journal*, vol. 25, no. 12, pp. 1310–1312, 2004.

[16] S. X. Guo, Z. M. Yang, J. Y. Zhang et al., "Relationship of free fatty acid and insulin resistance to hypertension in Kazakh and Han race of Xinjiang," *Chinese Journal of Hypertension*, vol. 18, no. 5, pp. 459–464, 2010.

[17] Y. Li, R. L. Ma, H. Guo et al., "Investigation and analysis of dyslipidemia among the Han population in northern Xinjiang aged 18 and older," *Journal of Shihezi University*, vol. 29, no. 3, pp. 318–321, 2011.

[18] G. R. Freidenberg, D. Reichart, J. M. Olefsky, and R. R. Henry, "Reversibility of defective adipocyte insulin receptor kinase activity in non-insulin-dependent diabetes mellitus. Effect of weight loss," *The Journal of Clinical Investigation*, vol. 82, no. 4, pp. 1398–1406, 1988.

[19] S. Shao, X. Zhang, and M. Zhang, "Inhibition of 11β-hydroxysteroid dehydrogenase type 1 ameliorates obesity-related insulin resistance," *Biochemical and Biophysical Research Communications*, vol. 478, no. 1, pp. 474–480, 2016.

[20] K. M. Flegal, D. Carroll, B. K. Kit, and C. L. Ogden, "Prevalence of obesity and trends in the distribution of body mass index among US adults, 1999–2010," *The Journal of the American Medical Association*, vol. 307, no. 5, pp. 491–497, 2012.

[21] A. von Ruesten, A. Steffen, A. Floegel et al., "Trend in obesity prevalence in European adult cohort populations during follow-up since 1996 and their predictions to 2015," *PLoS ONE*, vol. 6, no. 11, Article ID e27455, 2011.

[22] G. Z. Zhang, T. Qiu, X. J. Li et al., "Clinical analysis of insulin resistance and differentiation of metabolic syndrome of TCM syndrome," *Chinese Journal of Misdiagnosis*, vol. 10, no. 36, pp. 8827–8828, 2010.

[23] S. H. Zheng and X. F. Lv, "Relationship of oxLDL and insulin resistance in new-diagnosed type 2 diabetes mellitus," *Chinese General Practice*, vol. 13, no. 4, pp. 1167–1169, 2010.

[24] R. Harris, K. Donahue, S. S. Rathore, P. Frame, S. H. Woolf, and K. N. Lohr, "Screening adults for type 2 diabetes: a review of the evidence for the U.S. Preventive Services Task Force," *Annals of Internal Medicine*, vol. 138, no. 3, pp. 215–229, 2003.

[25] K. Cusi, "The role of adipose tissue and lipotoxicity in the pathogenesis of type 2 diabetes," *Current Diabetes Reports*, vol. 10, no. 4, pp. 306–315, 2010.

[26] Y. Q. Bao, W. P. Jia, K. S. Xiang, L. Chen, and J. Lu, "Dyslipidaemia and insulin resistance in Chinese in Shanghai," *Chinese Journal of Internal Medicine*, vol. 40, no. 5, pp. 299–302, 2001.

[27] Z. Y. Lu, Y. H. Lin, H. Shao et al., "Association of dyslipidemia profile with insulin resistance," *Chinese Journal of Endocrinology and Metabolism*, vol. 20, no. 5, pp. 447–449, 2004.

[28] A. López-Candales, "Metabolic syndrome X: a comprehensive review of the pathophysiology and recommended therapy," *Journal of Medicine*, vol. 32, no. 5, pp. 283–300, 2001.

Hindawi Publishing Corporation
Mediators of Inflammation
Volume 2016, Article ID 5147571, 10 pages
http://dx.doi.org/10.1155/2016/5147571

Research Article

Dalbergioidin Ameliorates Doxorubicin-Induced Renal Fibrosis by Suppressing the TGF-β Signal Pathway

Xianguo Ren,[1,2] Yun Bo,[3] Junting Fan,[4] Maosheng Chen,[5] Daliang Xu,[6,7] Yang Dong,[6,7] Haowei He,[8] Xianzhi Ren,[7] Rong Qu,[6,7] Yulian Jin,[6,7] Weihong Zhao,[3] and Changliang Xu[1,7]

[1]*National Clinical Research Center of Kidney Diseases, Jinling Hospital, Nanjing University School of Medicine, Nanjing, China*
[2]*Department of Pediatrics, Jinling Hospital, Nanjing University School of Medicine, Nanjing, China*
[3]*Department of Geriatrics, The First Affiliated Hospital of Nanjing Medical University, Nanjing, China*
[4]*School of Pharmacy, Nanjing Medical University, Nanjing, China*
[5]*Department of Nephrology, Zhejiang Provincial People's Hospital, Hangzhou, China*
[6]*Department of Nephrology, Anhui Provincial Children's Hospital, Hefei, China*
[7]*Nanjing University of Traditional Chinese Medicine, Nanjing, China*
[8]*Department of Urology, Jinling Hospital, Nanjing University School of Medicine, Nanjing, China*

Correspondence should be addressed to Weihong Zhao; zhaoweihong1966@163.com
and Changliang Xu; how11are22you33@163.com

Received 5 July 2016; Accepted 21 November 2016

Academic Editor: Lin Deng

We investigated the effect of Dalbergioidin (DAL), a well-known natural product extracted from *Uraria crinita*, on doxorubicin-(DXR-) induced renal fibrosis in mice. The mice were pretreated for 7 days with DAL followed by a single injection of DXR (10 mg/kg) via the tail vein. Renal function was analyzed 5 weeks after DXR treatment. DXR caused nephrotoxicity. The symptoms of nephrotic syndrome were greatly improved after DAL treatment. The indices of renal fibrosis, the phosphorylation of Smad3, and the expression of alpha-smooth muscle actin (α-SMA), fibronectin, collagen III (Col III), E-cadherin, TGF-β, and Smad7 in response to DXR were all similarly modified by DAL. The present findings suggest that DAL improved the markers for kidney damage investigated in this model of DXR-induced experimental nephrotoxicity.

1. Introduction

Doxorubicin (DXR) is an anthracycline glycoside antibiotic that has broad-spectrum antitumor activity against a variety of human solid tumors—such as ovarian, breast, and lung cancers—as well as several other cancers and hematologic malignancies [1–3]. However, DXR does not discriminate between cancer and normal cells and eradicates not only fast-growing cancer cells but also other rapidly growing cells in the body; therefore, its use in chemotherapy has been restricted. DXR has a variety of toxicities, including cardiac, hepatic, renal, and hematologic toxicity [4–8]. Although the mechanism underlying the severe cytotoxicity from DXR is not fully understood, reactive oxygen species (ROS) are assumed to be a key factor. It is very important to understand the events controlling this oxidative injury. DXR treatment leads to the overproduction of hydroxyl radicals, hydrogen peroxide, and superoxide anions, which cause membrane lipid peroxidation [9]. Therefore, increasing data suggest that simultaneous treatment with DXR and an antioxidant may alleviate the toxicity of DXR.

Uraria crinite, which has some great health benefits, is widely distributed throughout India, Thailand, Indonesia, and China. It has long been used as a herbal medicine, having bioactive properties, such as antioxidant activity, antiulcer effects, and osteogenic activity. Its roots, because of their anti-inflammatory activity, have also been used to treat chills, edema, and stomachache [10, 11]. The aim of the present study was to investigate the effect of Dalbergioidin (DAL), a well-known anthocyanin from *Uraria crinita*, on DXR-induced renal fibrosis in mice. The study was performed to determine whether treatment with DAL could counteract

renal fibrosis induced by DRX in vivo. We also investigated DAL's mechanism of action.

2. Methods

2.1. Reagents. DAL was purchased from BioBioPha Co., Ltd. SMAD3, p-SMAD3, SMAD7, α-SMA, fibronectin, Col I, E-cadherin, and TGF-β were purchased from Santa Cruz Biotechnology, Inc. Bovine serum albumin (BSA), DXR, sodium hydroxide, ferric nitrate, trichloroacetic acid (TCA), and perchloric acid (PCA) were obtained from Sigma-Aldrich.

2.2. Animals. The mice were housed and used as previously described [12].

2.3. Experimental Procedure. The mice were randomly divided into 3 groups of 8 mice each. Group I served as the control group for 42 days. Group II served as the model group and received a single IV injection of DXR (10 mg/kg) on day 7. Group III served as the treatment group and was pretreated with DAL (30 mg/kg IP) for 42 days; on day 7, a single IV injection of DXR (10 mg/kg) was administered. On day 42, the mice were sacrificed by cervical dislocation and, after perfusion to evaluate the various biochemical parameters, kidney and blood samples were taken.

2.4. Measurement of Urine and Plasma. Urine and blood samples were collected as previously described [13]. Urine albumin, plasma triglyceride levels, plasma urea levels, and serum creatinine levels were determined using commercial kits, an enzyme-linked immunosorbent assay kit (Exocell), a Urea Nitrogen Direct Kit (Stanbio Laboratory), a LabAssay Triglyceride ELISA Kit (Wako), and a Creatinine Liquicolor Kit (Stanbio Laboratory).

2.5. Masson-Trichrome Staining. Masson-trichrome staining was done as previously described [14].

2.6. Determination of GSH In Vivo. The effect of DAL treatment on Glutathione (GSH) levels was evaluated using a commercial kit (Cayman Chemical Co.) following the manufacturer's protocol.

2.7. Determination of MDA Levels In Vivo. The lipid peroxidation of the kidney tissue was studied by measuring the malondialdehyde (MDA) levels in a colorimetric method involving thiobarbituric acid (TBA) adduct formation. MDA was measured by a commercial TBARS Assay Kit (Cayman Chemical Co.) following the manufacturer's protocol.

2.8. Reverse Transcription Polymerase Chain Reaction (RT–PCR). Total RNA was isolated from the cells using a commercial TRIzol reagent kit (Invitrogene); the RNA concentrations were measured spectrophotometrically. The first cDNA synthesis was performed following the manufacturer's instructions (Takara, JPN). The specific primers for fibronectin, α-SMA, E-cadherin, Col III, SMAD7, TGF-β, and GAPDH (loading control) were as follows:

fibronectin: sense 5′-CGAGGTGACAGAGACCACAA-3′, antisense 5′-CTGGAGTCAAGCCAGACACA-3′; α-SMA: sense 5′-TGTGCTGGACTCTGGAGATG-3′, antisense 5′-ATGTCACGGACAATCTCACG-3′; E-cadherin: sense 5′-AATGGCGGCAATGCAATCCCAAGA-3′, antisense 5′-TGCCACAGACCGATTGTGGAGATA-3′; Col III: sense 5′-AGGCAACAGTGGTTCTCCTG-3′, antisense 5′-GACCTCGTGCTCCAGTTAGC-3′; smad7: sense 5′-AGGTGTTCCCCGGTTTCTCCA-3′; antisense: 5′-TTCACAAAGCTGATCTGCACGGT-3′; TGF-β: sense 5′-GCAACATGTGGAACTCTACCAGAA-3′, antisense 5′-GACGTCAAAAGACAGCCACTCA-3′; GAPDH: sense 5′-AACTTTGGCATTGTGGAAGG-3′, antisense 5′-ACACATTGGGGGTAGGAACA-3′. The protocol was as follows: 50°C for 2 minutes, 95°C for 10 minutes, 40 cycles of 95°C for 15 seconds, and 60°C for 30 seconds.

2.9. Western Blot Analyses. Using the western blotting method as previously described [12], the tissues were homogenized and the supernatant was then decanted. First antibodies were added and incubated with membranes at 4°C overnight. HRP-conjugated secondary antibodies were diluted and incubated with the membranes at 20°C. The blots were then incubated with a chemiluminescent substrate (Millipore) and exposed to Kodak Film.

2.10. ELISA Assay. TGF-β was measured using a TGF-β ELISA Quantitation Kit following the manufacturer's protocol (R & D, Inc.).

2.11. Statistical Analysis. Differences between the groups were analyzed by Student's t-test. All the data points are presented as the treatment group's mean ± standard deviation (SD) of the mean. p values less than 0.05 were considered significant.

3. Results

3.1. Effect of DAL on Renal Dysfunction. As shown in Figure 1(a), the 24-hour urinary protein excretion of the mice progressively increased after the injection of DXR. On day 21, the urinary protein of the DXR-treated mice was significantly higher than that of the control mice. Beginning on day 28, the urinary protein of DXR-treated mice rapidly increased. Treatment with DAL significantly decreased urinary protein at the weeks 5 and 6. The DXR-treated mice developed severe hyperlipidemia (plasma triglyceride 3.63 ± 0.44 mg/mL), which was less severe in the treatment group (plasma triglyceride 1.52 ± 0.31 mg/mL) (Figure 1(b)). The treatment of mice with DXR caused a significant increase in BUN and plasma creatinine levels by 2.3- and 4.1-fold, respectively, compared with the control group (Figures 1(c) and 1(d)). Pretreatment with DAL for 7 days resulted in the restoration of BUN and plasma creatinine to near control levels ($p < 0.01$). Therefore, DAL attenuates nephrotoxicity in a mouse model of DXR.

3.2. Effect of DAL on Renal Fibrosis. Like many other organ systems, the kidney stiffens after injury, a process increasingly recognized as an important driver of renal fibrosis [15]. To correlate the reduction of kidney injury with the effect of the drug treatments, renal fibrosis was assessed by Masson

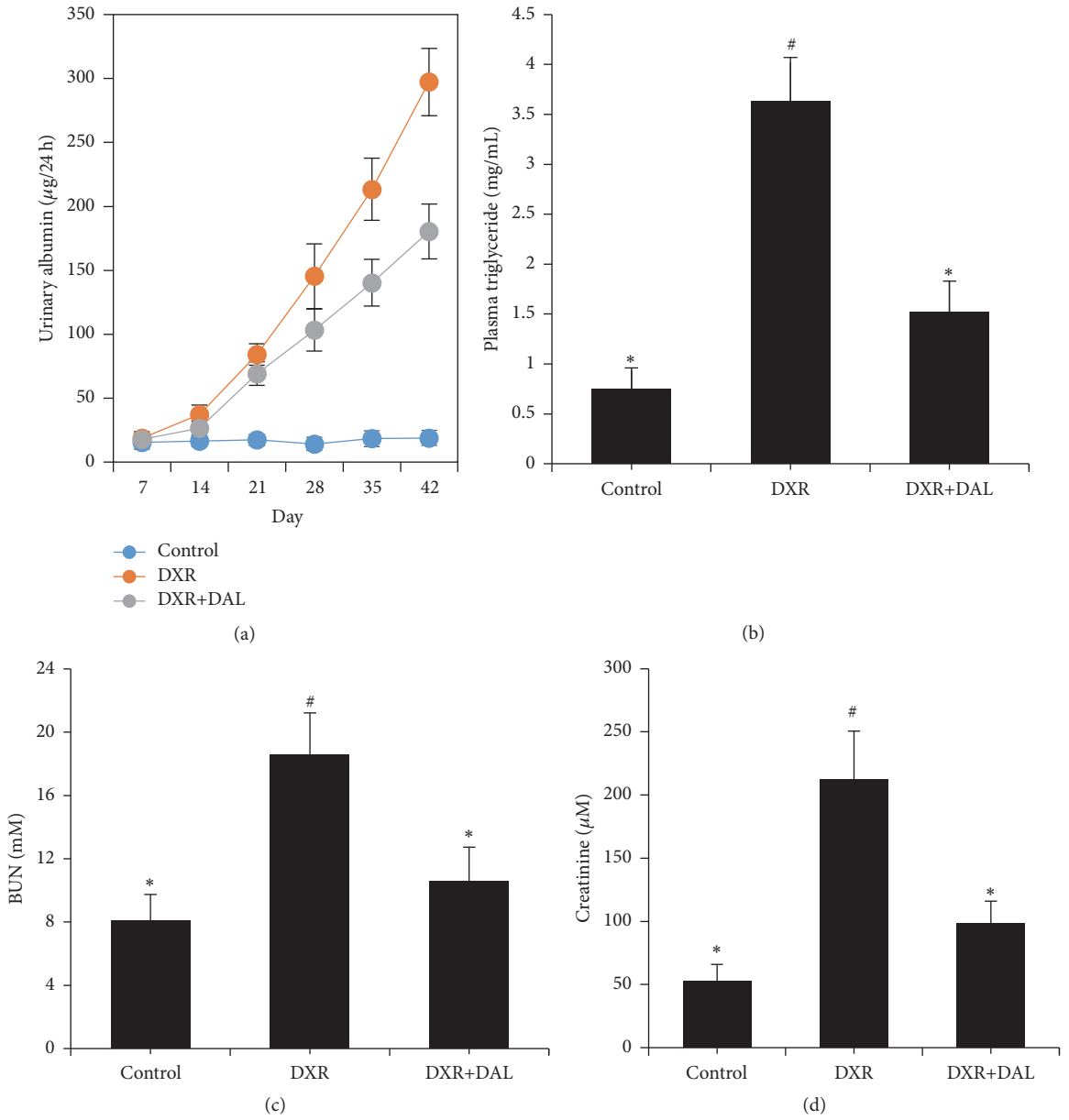

Figure 1: Kidney injury at 5 weeks after DXR injection in different groups of mice as indicated. (a) Effect of DAL on albuminuria against DXR-induced nephrotoxicity; (b) effect of DAL on hyperlipidemia against DXR-induced nephrotoxicity; (c) effect of DAL on blood urea nitrogen (BUN) against DXR-induced nephrotoxicity; (d) effect of DAL on serum creatinine against DXR-induced nephrotoxicity. The control and DAL treatment groups are compared with the DXR group. Values are statistically significant at $^{*}p < 0.05$; the DXR group is compared with the control group. Values are statistically significant at $^{\#}p < 0.05$.

staining (Figure 2(a)). The renal fibrosis marker of alpha-smooth muscle actin (α-SMA), fibronectin, and the epithelial cell marker of E-cadherin were assessed by western blotting [16, 17]. Consistent with the albuminuria data, the results from the DXR mice showed marked renal fibrosis, as evidenced by the increased expression of fibroblasts markers (Figures 2(b)–2(d)). The treatment of mice with DXR caused a significant increase in the renal protein expression of well-known fibroblasts markers and increased the expression of E-cadherin in renal tissue (Figures 2(b)–2(d)). DAL ameliorates renal fibrosis in a mouse model of DXR.

3.3. Effect of DAL on Kidney Redox Potential. The elevated production of reactive oxygen species (ROS) is a primary mechanism of DXR-induced cytotoxicity [18, 19]. MDA and GSH serve to assess the level of ROS. In this study, there was a significant increase of MDA in the kidneys of the DXR group compared with the control group ($p < 0.01$). Compared with the DXR group, the mice with DXR-induced nephrotoxicity that were treated with DAL showed a significant reduction in MDA levels (Figure 3(a)). We also measured the GSH concentration as an indicator of cellular redox status in the kidney tissue to investigate the antioxidant action of DAL.

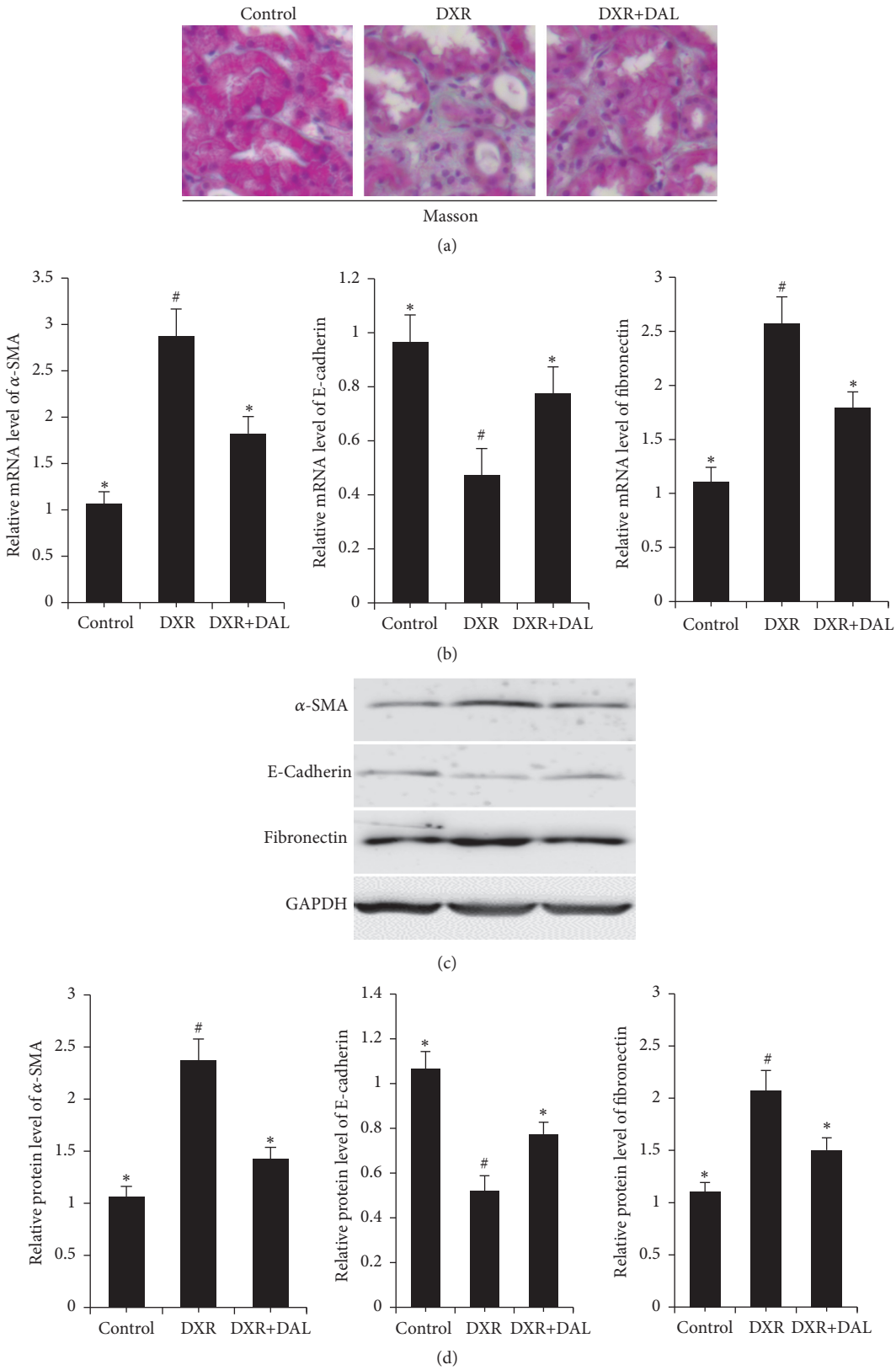

Figure 2: Renal fibrosis at 5 weeks after DXR injection in different groups of mice as indicated. (a) Kidney sections were subjected to Masson-trichrome staining; (b) kidney sections expressed the mRNA of α-SMA, and E-cadherin, fibronectin; (c) kidney sections expressed the protein of α-SMA, E-cadherin, and fibronectin; (d) the relative protein expression of fibronectin, α-SMA, and E-cadherin as seen in the kidney sections. The control and DAL treatment groups are compared with the DXR group. Values are statistically significant at $^{*}p < 0.05$; the DXR group is compared with the control group. Values are statistically significant at $^{\#}p < 0.05$.

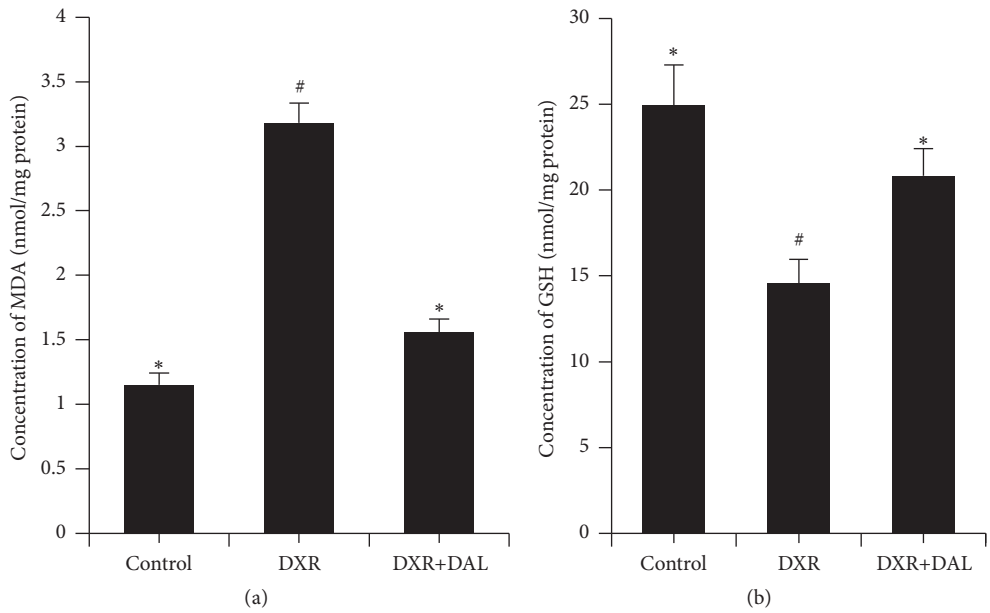

Figure 3: Redox microenvironment in kidney tissue at 5 weeks after DXR injection in different groups of mice as indicated. (a) Effect of DAL on kidney MDA levels; (b) Effect of DAL on kidney GSH levels. The control and DAL treatment groups are compared with the DXR group. Values are statistically significant at $^{*}p < 0.05$; the DXR group is compared with the control group. Values are statistically significant at $^{\#}p < 0.05$.

After the DXR treatment, the levels of GSH were significantly depleted, as shown in Figure 3(b) ($p < 0.01$). Compared with the DXR group, the group that received DAL showed a significantly reversed GSH depletion. This shows that DAL maintains the redox balance of kidney tissue.

3.4. DAL Effects on the TGF-β Signaling Pathway. TGF-β is a key mediator in the pathogenesis of renal fibrosis and induces renal scarring largely by activating its downstream Smad signaling pathway [20]. Although the TGF-β signaling pathway is mediated by Smad2 and Smad3, Smad2 protects against TGF-beta/Smad3-mediated renal fibrosis [21]. Thus, phosphorylated Smad3 is the effector of TGF-β-mediated renal fibrosis. The levels of phosphorylated Smad3 in the kidney were increased by DXR (Figure 4(a)). As shown in Figure 4(a), the DAL-treated groups exhibited a significant decrease in the phosphorylation level of SMAD3 compared with the DXR groups ($p < 0.01$). Because collagen III is a target gene of TGF-beta/SMAD3, the mRNA and protein expression of collagen III in the kidney was evaluated by q-PCR and western blotting. As shown in Figures 4(b) and 4(c), collagen III mRNA and protein levels in the DAL-treated groups showed a significant decrease compared with those in the DXR groups. Smad7 acts as an antagonist of the TGF-β signaling pathway by preventing R-Smads from interacting with their receptors or by competing with Co-Smads for the generation of R-Smad/Co-Smad complexes [22, 23]. Smad7 mRNA and protein levels were reduced after DXR treatment, but this effect was reversed by DAL treatment ($p < 0.01$; Figures 5(a) and 5(b)). DAL suppresses the TGF-β signaling pathway in kidney tissue.

3.5. Effect of DAL on TGF-β Protein Expression. TGF-β is a protein that controls proliferation, cellular differentiation, and other functions in most cells. TGF-β is important for the induction of fibrosis and the EMT often associated with the chronic phases of inflammatory diseases [24]. As shown in Figure 6, the mRNA and protein levels of TGF-β in the DAL-treated groups showed a significant decrease compared with those in the DXR-treated groups.

4. Discussion

In the current study, DAL ameliorated the severe nephritic syndrome induced by DXR in mice. Urine albumin and plasma urea and creatinine are the most sensitive markers of nephrotoxicity implicated in the diagnosis of renal injury [25, 26]. DXR treatment significantly increased serum creatinine, BUN, and hyperlipidemia. In contrast, treatment with DAL resulted in a significant decrease of these parameters in the DXR-treated animals. These results indicate that DAL may offer a considerable nephroprotective effect against DXR toxicity.

Renal fibrosis is a well-known cause of kidney failure in DXR-induced nephropathy [27]. Several cellular pathways, including fibroblast activation and tubular epithelial-mesenchymal transition, have been identified as the major causes of renal fibrosis [28]. In this study, the administration of DAL significantly improved renal fibrosis. One of the major mechanisms in the protection of DAL in this model involves the inhibition of fibroblast activation. After 35 days of DXR injection, fibronectin and α-SMA mRNA and protein levels were markedly upregulated and DAL significantly inhibited

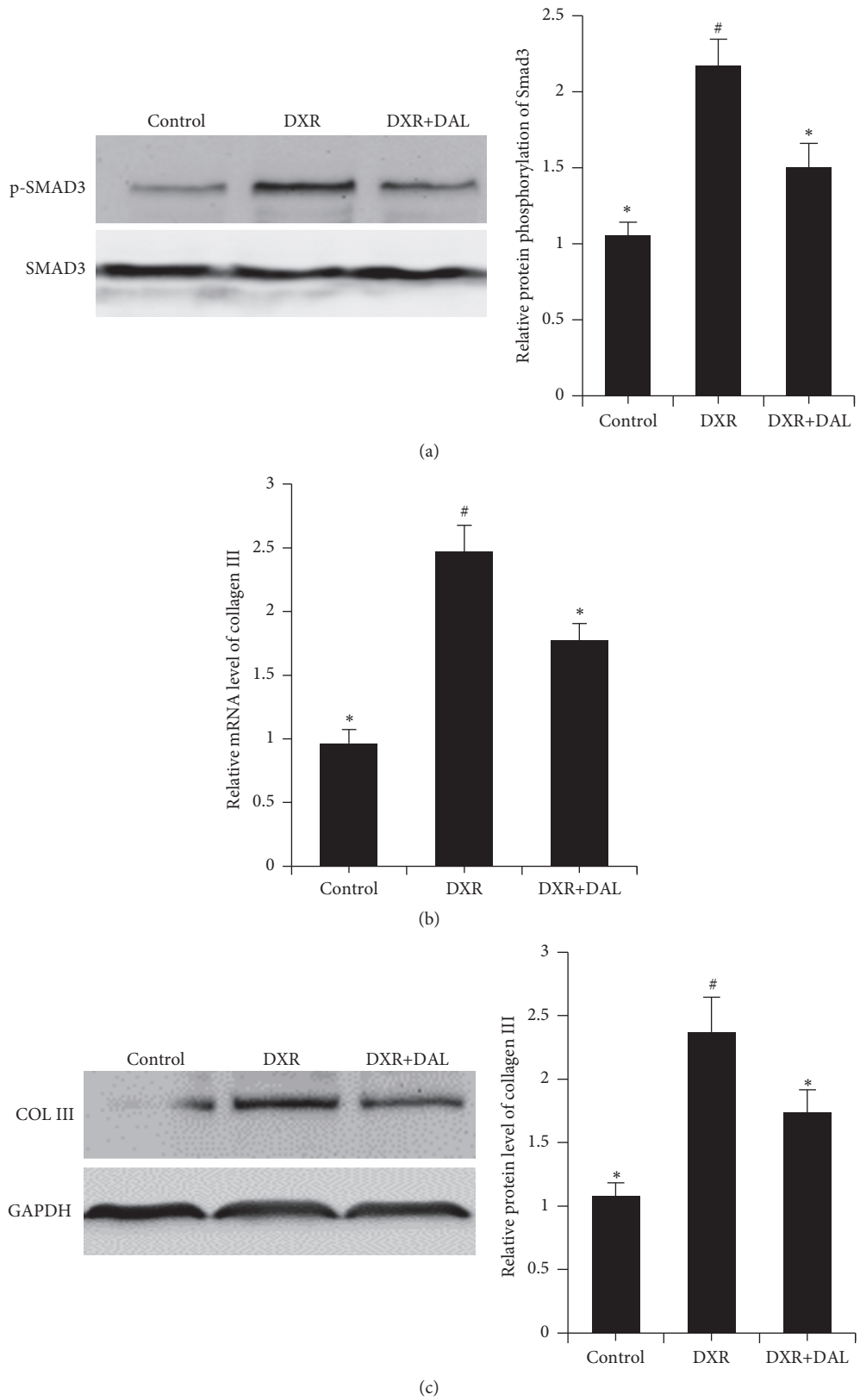

Figure 4: The TGF-β signaling pathway in kidney tissue 5 weeks after DXR injection in different groups of mice as indicated. (a) DAL inhibits the phosphorylation of Smad3; (b) DAL inhibits the gene expression of collagen III, which is the target gene of Smad3; (c) DAL inhibits the protein expression of collagen III, which is the target protein expression of Smad3. The control and DAL treatment groups are compared with the DXR group. Values are statistically significant at $^{*}p < 0.05$; the DXR group is compared with the control group. Values are statistically significant at $^{\#}p < 0.05$.

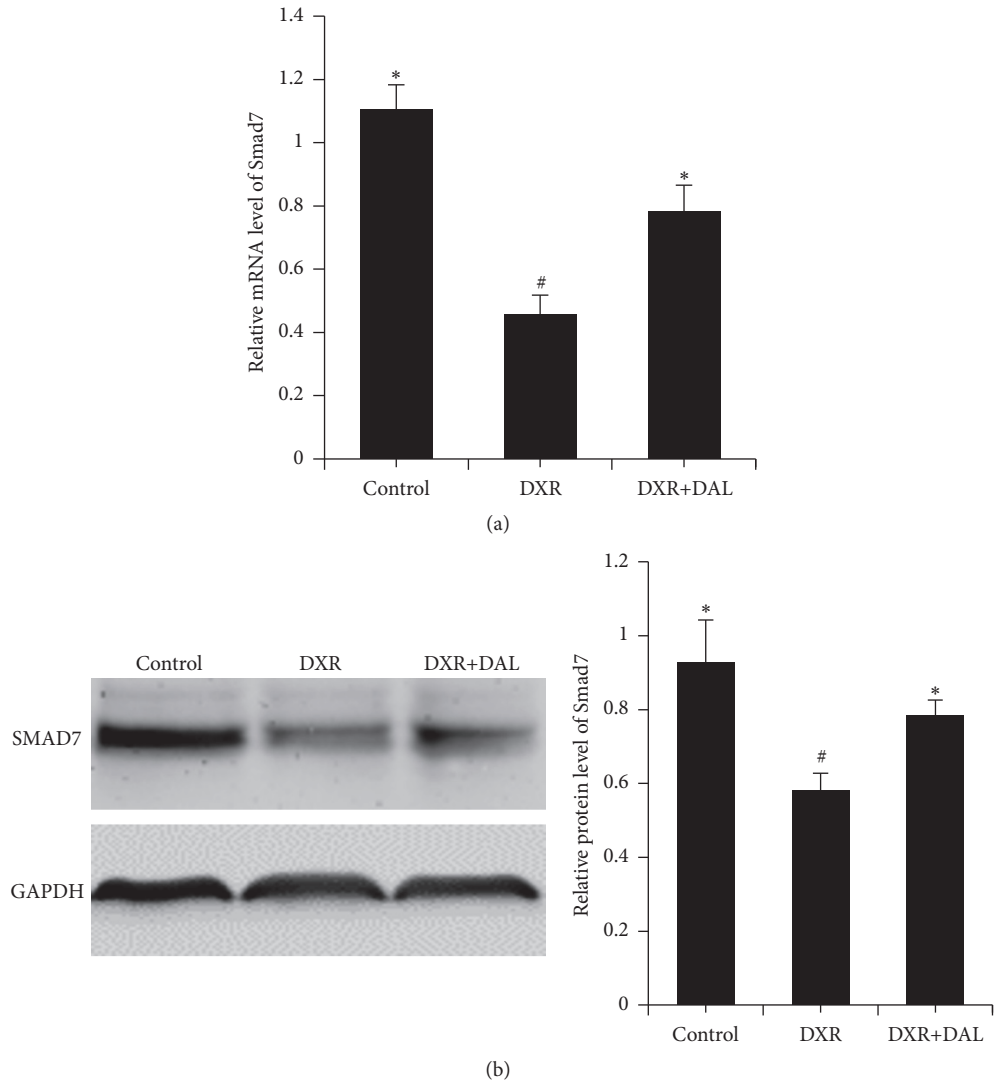

Figure 5: The expression of Smad7, an inhibitor of the TGF-β signaling pathway, in kidney tissue 5 weeks after DXR injection in different groups of mice as indicated. (a) DAL increases the gene expression of Smad7; (b) DAL increases the protein expression of Smad7. The control and DAL treatment groups are compared with the DXR group. Values are statistically significant at $^{*}P < 0.05$; the DXR group is compared with the control group. Values are statistically significant at $^{\#}P < 0.05$.

their levels of expression. We also examined the mRNA and protein levels of the epithelial marker E-cadherin. DAL treatment reversed the reduction of E-cadherin. Consistent with these results histologically, DAL treatment ameliorated DXR-induced renal fibrosis.

TGF-β, which is upregulated in some studies, plays a pivotal role in the progression of the tubular epithelial-mesenchymal transition in renal fibrosis; therapeutic intervention targeting TGF-β has been successful and well tolerated in animal models [9, 21, 23]. It has recently been postulated that ROS mediate fibrosis via a TGF-β-dependent pathway [29, 30]. Moreover, ROS have emerged in the pathogenesis of DXR-induced nephropathy [31, 32]. It has been suggested that a DXR semiquinone plays a major role in DXR nephrotoxicity. Although semiquinones have a short life, they initiate a stream of reactions, producing ROS after interacting with molecular oxygen [5, 33]. It has been shown that DXR increases the production of free radicals such as superoxide, hydroxyl radicals, and hydrogen peroxide, which have a great ability to react rapidly with lipids and cause lipid hydroperoxide (LPO) [9]. LPO is known to be one of the toxic manifestations of DXR ingestion; its presence is determined by measuring MDA levels. Excessive LPO has been reported in the kidneys of DXR-treated mice [34]. In the current study, the DXR-treated mice showed increased levels of MDA compared with the control mice. GSH is the most important thiol-containing antioxidant, and it plays a pivotal role in preventing oxidative damage [35, 36]. GSH has also been used as a biomarker of oxidative stress in biological systems [37]. The depletion of GSH has been observed in DXR mice [34]. In our studies, DAL decreased the concentrations of MDA and increased the level of GSH. The recovering redox balance

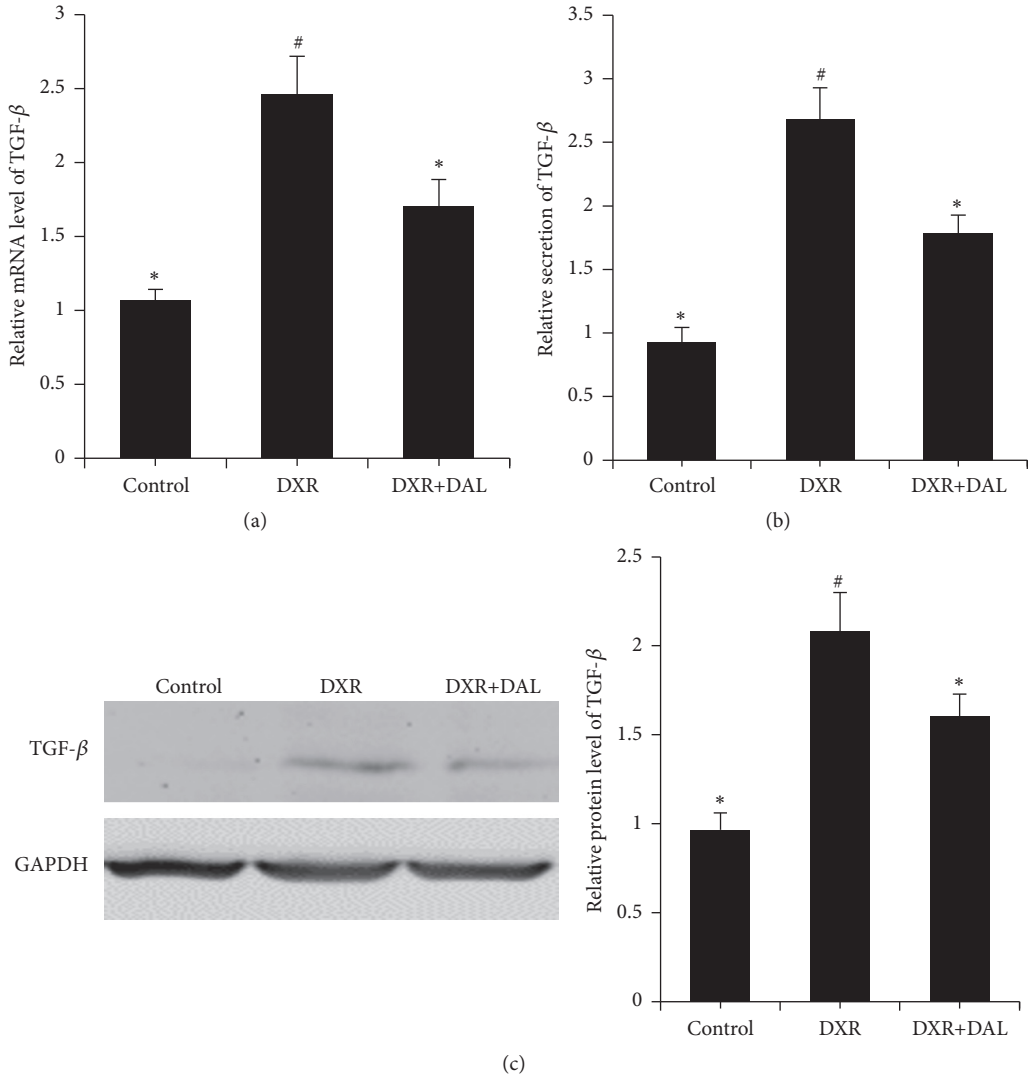

Figure 6: The expression of TGF-β in kidney tissue 5 weeks after DXR injection in different groups of mice as indicated. (a) DAL decreases the gene expression of TGF-β; (b) DAL decreases the protein expression of TGF-β by ELISA; (c) DAL decreases the protein expression of TGF-β as determined by western blotting. The control and DAL treatment groups are compared with the DXR group. Values are statistically significant at $^{*}p < 0.05$; the DXR group is compared with the control group. Values are statistically significant at $^{\#}p < 0.05$.

in the tissue microenvironment is the most likely mechanism by which DAL exerts nephroprotective effect and inhibits a tubular epithelial-mesenchymal transition.

Smad3 is a critical downstream mediator responsible for the biological effects of TGF-β, and their related family members regulate the transcription of several hundred genes. In the context of renal fibrosis, Smad3 are strongly activated in both experimental and human kidney diseases [20]. Phosphorylated Smad3 is increased in the DXR group. This observation indicates that TGF-β/Smad signaling pathways are activated in DXR-induced nephropathy. However, this phenomenon is reversed by DAL. Collagen I, which is a fibrogenic gene, is the downstream target of the TGF-β/Smad3 signaling pathway. DAL reversed the increase of collagen I. Furthermore, Smad7, which is an inhibitor of the TGF-β/Smad signaling pathways, was upregulated by DAL treatment. DAL also increases the mRNA and protein expression of TGF-β in DXR-induced nephropathy.

In conclusion, our results demonstrate that DAL has a potent nephroprotective effect in the DXR mice model. The nephroprotective effect of DAL may be mediated by suppressing the TGF-β-induced renal tubular epithelial-to-mesenchymal transition. This is an early-stage study of the nephroprotective effects of DAL; the detailed mechanisms of action need further clarification.

Competing Interests

The authors declare that there is no conflict of interests regarding the publication of this paper.

Authors' Contributions

Changliang Xu had the initial idea for the project. Xianguo Ren, Yun Bo, Junting Fan, and Maosheng Chen did all the experimental work. Weihong Zhao provided guidance throughout the work. Haowei He, Xianzhi Ren, Rong Qu, and Yulian Jin analyzed the experimental data. Daliang Xu and Yang Dong gave some suggestions about how to arrange the figures. Changliang Xu drafted the manuscript. Changliang Xu and Maosheng Chen provided funding. Xianguo Ren, Yun Bo, Junting Fan, and Maosheng Chen contributed equally to this work and are to be considered first authors.

Acknowledgments

This work was supported by the National Natural Science Foundation of China (no. 81302829) and the Major Program of Traditional Chinese Medicine of Zhejiang Province, China (no. 2015ZZ002).

References

[1] P. W. Burridge, Y. F. Li, E. Matsa et al., "Human induced pluripotent stem cell–derived cardiomyocytes recapitulate the predilection of breast cancer patients to doxorubicin-induced cardiotoxicity," *Nature Medicine*, vol. 22, no. 5, pp. 547–556, 2016.

[2] C.-H. Lai, K.-S. Park, D.-H. Lee et al., "HSP-90 inhibitor ganetespib is synergistic with doxorubicin in small cell lung cancer," *Oncogene*, vol. 33, no. 40, pp. 4867–4876, 2014.

[3] J. Brucker, C. Mayer, G. Gebauer et al., "Non-pegylated liposomal doxorubicin for patients with recurrent ovarian cancer: a multicentric phase II trial," *Oncology Letters*, vol. 12, no. 2, pp. 1211–1215, 2016.

[4] R. Injac, M. Boskovic, M. Perse et al., "Acute doxorubicin nephrotoxicity in rats with malignant neoplams can be successfully treated With fullerenol C60(OH)24 via suppresion of oxidative stress," *Pharmacological Reports*, vol. 60, no. 5, pp. 742–749, 2008.

[5] M. Mohan, S. Kamble, P. Gadhi, and S. Kasture, "Protective effect of *Solanum torvum* on doxorubicin-induced nephrotoxicity in rats," *Food and Chemical Toxicology*, vol. 48, no. 1, pp. 436–440, 2010.

[6] S. Yilmaz, A. Atessahin, E. Sahna, I. Karahan, and S. Ozer, "Protective effect of lycopene on adriamycin-induced cardiotoxicity and nephrotoxicity," *Toxicology*, vol. 218, no. 2-3, pp. 164–171, 2006.

[7] H. C. Lai, Y. C. Yeh, L. C. Wang et al., "Propofol ameliorates doxorubicin-induced oxidative stress and cellular apoptosis in rat cardiomyocytes," *Toxicology and Applied Pharmacology*, vol. 257, no. 3, pp. 437–448, 2011.

[8] V. G. Desai, E. H. Herman, C. L. Moland et al., "Development of doxorubicin-induced chronic cardiotoxicity in the B6C3F1 mouse model," *Toxicology and Applied Pharmacology*, vol. 266, no. 1, pp. 109–121, 2013.

[9] E. Öz and M. N. Ilhan, "Effects of melatonin in reducing the toxic effects of doxorubicin," *Molecular and Cellular Biochemistry*, vol. 286, no. 1-2, pp. 11–15, 2006.

[10] Y.-W. Mao, R.-D. Lin, H.-C. Hung, and M.-H. Lee, "Stimulation of osteogenic activity in human osteoblast cells by edible uraria crinita," *Journal of Agricultural and Food Chemistry*, vol. 62, no. 24, pp. 5581–5588, 2014.

[11] P.-D. Duh, G.-C. Yen, W.-J. Yen, and L.-W. Chang, "Antioxidant effects of water extracts from barley (*Hordeum vulgare* L.) prepared under different roasting temperatures," *Journal of Agricultural and Food Chemistry*, vol. 49, no. 3, pp. 1455–1463, 2001.

[12] D. Xu, M. Chen, X. Ren, X. Ren, and Y. Wu, "Leonurine ameliorates LPS-induced acute kidney injury via suppressing ROS-mediated NF-κB signaling pathway," *Fitoterapia*, vol. 97, pp. 148–155, 2014.

[13] S. Liu, Z. Jia, L. Zhou et al., "Nitro-oleic acid protects against adriamycin-induced nephropathy in mice," *American Journal of Physiology - Renal Physiology*, vol. 305, no. 11, pp. F1533–F1541, 2013.

[14] H. Sugimoto, G. Grahovac, M. Zeisberg, and R. Kalluri, "Renal fibrosis and glomerulosclerosis in a new mouse model of diabetic nephropathy and its regression by bone morphogenic protein-7 and advanced glycation end product inhibitors," *Diabetes*, vol. 56, no. 7, pp. 1825–1833, 2007.

[15] S. G. Szeto, M. Narimatsu, M. Lu et al., "YAP/TAZ are mechanoregulators of TGF-β-Smad signaling and renal fibrogenesis," *Journal of the American Society of Nephrology*, vol. 27, no. 10, pp. 3117–3128, 2016.

[16] M. Zeisberg and E. G. Neilson, "Biomarkers for epithelial-mesenchymal transitions," *The Journal of Clinical Investigation*, vol. 119, no. 6, pp. 1429–1437, 2009.

[17] T. L. Criswell and C. L. Arteaga, "Modulation of NFκB activity and E-cadherin by the type III transforming growth factor β receptor regulates cell growth and motility," *The Journal of Biological Chemistry*, vol. 282, no. 44, pp. 32491–32500, 2007.

[18] Y.-W. Zhang, J. Shi, Y.-J. Li, and L. Wei, "Cardiomyocyte death in doxorubicin-induced cardiotoxicity," *Archivum Immunologiae et Therapiae Experimentalis*, vol. 57, no. 6, pp. 435–445, 2009.

[19] H. Wang, X. Chen, Y. Su et al., "p47(phox) contributes to albuminuria and kidney fibrosis in mice," *Kidney International*, vol. 87, no. 5, pp. 948–962, 2015.

[20] H. Y. Lan, "Diverse roles of TGF-β/Smads in renal fibrosis and inflammation," *International Journal of Biological Sciences*, vol. 7, no. 7, pp. 1056–1067, 2011.

[21] X. M. Meng, X. R. Huang, A. C. K. Chung et al., "Smad2 protects against TGF-β/Smad3-mediated renal fibrosis," *Journal of the American Society of Nephrology*, vol. 21, no. 9, pp. 1477–1487, 2010.

[22] X.-M. Meng, X. R. Huang, J. Xiao et al., "Disruption of Smad4 impairs TGF-β/Smad3 and Smad7 transcriptional regulation during renal inflammation and fibrosis in vivo and in vitro," *Kidney International*, vol. 81, no. 3, pp. 266–279, 2012.

[23] H. Y. Lan, W. Mu, N. Tomita et al., "Inhibition of renal fibrosis by gene transfer of inducible Smad7 using ultrasound-microbubble system in rat UUO model," *Journal of the American Society of Nephrology*, vol. 14, no. 6, pp. 1535–1548, 2003.

[24] D. Pohlers, J. Brenmoehl, I. Löffler et al., "TGF-β and fibrosis in different organs—molecular pathway imprints," *Biochimica et Biophysica Acta—Molecular Basis of Disease*, vol. 1792, no. 8, pp. 746–756, 2009.

[25] R. Sallie, J. M. Tredger, and R. Williams, "Drugs and the liver. Part 1: testing liver function," *Biopharmaceutics and Drug Disposition*, vol. 12, no. 4, pp. 251–259, 1991.

[26] N. Khan and S. Sultana, "Abrogation of potassium bromate-induced renal oxidative stress and subsequent cell proliferation response by soy isoflavones in Wistar rats," *Toxicology*, vol. 201, no. 1–3, pp. 173–184, 2004.

[27] K. Van Beneden, C. Geers, M. Pauwels et al., "Comparison of trichostatin A and valproic acid treatment regimens in a mouse model of kidney fibrosis," *Toxicology and Applied Pharmacology*, vol. 271, no. 2, pp. 276–284, 2013.

[28] Y. Liu, "Renal fibrosis: new insights into the pathogenesis and therapeutics," *Kidney International*, vol. 69, no. 2, pp. 213–217, 2006.

[29] I. Montorfano, A. Becerra, R. Cerro et al., "Oxidative stress mediates the conversion of endothelial cells into myofibroblasts via a TGF-β1 and TGF-β2-dependent pathway," *Laboratory Investigation*, vol. 94, no. 10, pp. 1068–1082, 2014.

[30] R. Samarakoon, J. M. Overstreet, and P. J. Higgins, "TGF-β signaling in tissue fibrosis: redox controls, target genes and therapeutic opportunities," *Cellular Signalling*, vol. 25, no. 1, pp. 264–268, 2013.

[31] H. Wu, Y. M. Wang, Y. Wang et al., "Depletion of $\gamma\delta$ T cells exacerbates murine adriamycin nephropathy," *Journal of the American Society of Nephrology*, vol. 18, no. 4, pp. 1180–1189, 2007.

[32] J. Guo, R. Ananthakrishnan, W. Qu et al., "RAGE mediates podocyte injury in adriamycin-induced glomerulosclerosis," *Journal of the American Society of Nephrology*, vol. 19, no. 5, pp. 961–972, 2008.

[33] N. A. El-Shitany, S. El-Haggar, and K. El-desoky, "Silymarin prevents adriamycin-induced cardiotoxicity and nephrotoxicity in rats," *Food and Chemical Toxicology*, vol. 46, no. 7, pp. 2422–2428, 2008.

[34] S. Rashid, N. Ali, S. Nafees et al., "Alleviation of doxorubicin-induced nephrotoxicity and hepatotoxicity by chrysin in Wistar rats," *Toxicology Mechanisms and Methods*, vol. 23, no. 5, pp. 337–345, 2013.

[35] J. Ø. Moskaug, H. Carlsen, M. C. W. Myhrstad, and R. Blomhoff, "Polyphenols and glutathione synthesis regulation," *The American Journal of Clinical Nutrition*, vol. 81, no. 1, supplement, pp. 277S–283S, 2005.

[36] G. Wu, Y.-Z. Fang, S. Yang, J. R. Lupton, and N. D. Turner, "Glutathione metabolism and its implications for health," *Journal of Nutrition*, vol. 134, no. 3, pp. 489–492, 2004.

[37] D. J. Reed and M. K. Savage, "Influence of metabolic inhibitors on mitochondrial permeability transition and glutathione status," *BBA - Molecular Basis of Disease*, vol. 1271, no. 1, pp. 43–50, 1995.

Hindawi Publishing Corporation
Mediators of Inflammation
Volume 2016, Article ID 6456018, 12 pages
http://dx.doi.org/10.1155/2016/6456018

Review Article

Lactate, a Neglected Factor for Diabetes and Cancer Interaction

Yong Wu,[1,2] Yunzhou Dong,[3] Mohammad Atefi,[1] Yanjun Liu,[1] Yahya Elshimali,[1] and Jaydutt V. Vadgama[1,2]

[1]*Division of Cancer Research and Training, Department of Internal Medicine, Charles R. Drew University of Medicine and Science, Los Angeles, CA 90059, USA*
[2]*David Geffen UCLA School of Medicine and UCLA Jonsson Comprehensive Cancer Center, University of California, Los Angeles, CA 90095, USA*
[3]*Vascular Biology Program, Boston Children's Hospital, Harvard Medical School, Boston, MA 02115, USA*

Correspondence should be addressed to Yong Wu; yongwu@cdrewu.edu

Received 18 August 2016; Revised 17 November 2016; Accepted 23 November 2016

Academic Editor: Mirella Giovarelli

Increasing body of evidence suggests that there exists a connection between diabetes and cancer. Nevertheless, to date, the potential reasons for this association are still poorly understood and currently there is no clinical evidence available to direct the proper management of patients presenting with these two diseases concomitantly. Both cancer and diabetes have been associated with abnormal lactate metabolism and high level of lactate production is the key biological property of these diseases. Conversely, high lactate contribute to a higher insulin resistant status and a more malignant phenotype of cancer cells, promoting diabetes and cancer development and progression. In view of associations between diabetes and cancers, the role of high lactate production in diabetes and cancer interaction should not be neglected. Here, we review the available evidence of lactate's role in different biological characteristics of diabetes and cancer and interactive relationship between them. Understanding the molecular mechanisms behind metabolic remodeling of diabetes- and cancer-related signaling would endow novel preventive and therapeutic approaches for diabetes and cancer treatment.

1. Introduction

Globally, diabetes mellitus (DM) and cancer are two of the most predominant diseases, with cancer the 2nd and diabetes the 12th primary cause of death [1, 2]. The connection between these two diseases was first hypothesized over 75 years ago. More and more evidence proposes that DM is related to an augmented risk of cancer [3] and the higher mortality in cancer patients [4, 5]. Actually, recent studies have suggested that type 2 diabetes (T2DM) is an independent risk factor for the progress of various types of cancer [6]. Although these two diseases share a number of common risk factors, the biological link between them is still not well known [6, 7], which poses a challenge for clinical management. While a thorough picture is yet to emerge, several mechanisms have been suggested to explain this relationship, for example, hyperglycemia itself [3], oxidative stress [8–11], treatment for diabetes, hormonal disorders, insulin resistance with secondary hyperinsulinemia [3], metabolic alterations underlying the diseases [12], insulin-increased bioactivity of IGF-I [13, 14], insulin's positive effect on estrogen bioavailability, the status of chronic inflammation, and obesity [7]. On the other hand, DM might also develop after tumor establishment in certain cancers that progress very rapidly, for example, pancreatic and liver cancers [15].

Lactate (2-hydroxypropanoic acid), formerly deemed a waste product of glycolysis, has drawn more and more attention as a crucial regulator of insulin resistance, DM, cancer development, maintenance, and metastasis. Over the last half century, substantial experiments revealed that lactate is both a powerful fuel and signaling molecule, and it is continuously being produced and circulated through the body [16]. Its presence in diabetes and cancer has been recognized, and recent studies suggest that suppressing it can be therapeutic, after 50 years of disavowal. Recently, cancer and DM have been associated with abnormal lactate metabolism. Lactate

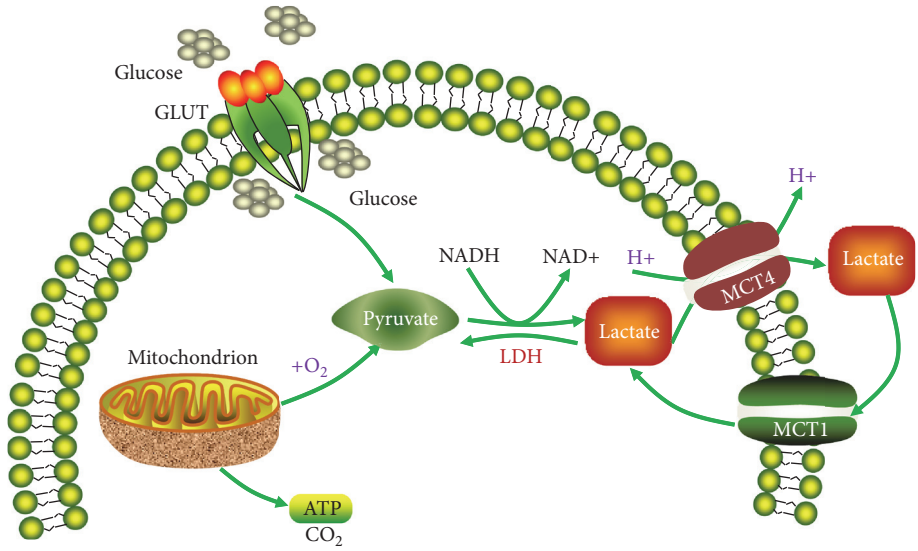

Figure 1: Lactate production and shuttling pathways. GLUT, glucose transporter; LDH, lactate dehydrogenase; MCT, monocarboxylate transporter.

facilitates cancer cell intrinsic effects on metabolism and has extra noncancer cell autonomous effects which can induce tumorigenesis. In addition, lactate plays an important role in stimulating tumor inflammation and in promoting tumor angiogenesis by functioning as a signaling molecule [17]. Given that hyperlactacidemia is the most imperative biological feature of diabetes and cancer, it is reasonable to imagine that hyperlactacidemia might play an important role during diabetes and cancer interaction. Here, we review the available evidence of lactate's role in different biological characteristics of diabetes and cancer and interactive relationship between them. It appears that hyperlactacidemia may function as an interaction hub between diabetes and cancer and contribute to a higher insulin resistant status and a more malignant phenotype of cancer cells.

2. Lactate Production and Metabolism

Lactate, a 3-carbon hydroxycarboxylic acid, is produced in the cytoplasm by the glycolysis pathway under anaerobic conditions, via the reduction of an intermediate metabolite pyruvate, with the simultaneous oxidation of NADH to NAD+. This reaction is catalyzed by lactate dehydrogenase (LDH) [18]. LDH is composed of four subunits of two distinct types (H and M), with each subunit type under distinct genetic control leading to five diverse isozymes including LDH-1 (H4), LDH-2 (H3M1), LDH-3 (H2M2), LDH-4 (H1M3), and LDH-5 (M4) [19]. Under aerobic conditions and in the presence of the enzyme pyruvate dehydrogenase (PDH), pyruvate is converted into acetyl CoA, subsequently entering the tricarboxylic acid (TCA) cycle or Kreb's cycle.

The normal plasma concentration of lactate is 0.3–1.3 mM. In plasma, lactate is buffered by $NaHCO_3$. Lactate may have two stereoisomers, namely, d-lactate and l-lactate. In humans, lactate exists predominantly in the levorotatory isoform. Most tissues in the human body produce lactate, but the majority of production is found in muscles [18]. Lactate is transported across the plasma membrane with the aid of the monocarboxylate transporters (MCTs), which facilitates the proton-linked transport of monocarboxylates, for example, L-lactate, pyruvate, and the ketone bodies [20, 21]. So far four isoforms, MCT1–4, have been functionally substantiated to implement this function in mammals, each with different substrate and inhibitor affinities [20, 21] (Figure 1).

Plasma concentrations of lactate represent an equilibrium between its production and metabolism. Lactate can be metabolized by various cells and tissues, for example, liver, germ cells, and neurons, converting to pyruvate via LDH and subsequently to glycogen or carbon dioxide [22]. Under normally physiological conditions, lactate is cleared by the livers and kidneys [23, 24]. At present, lactate is also considered as a regulator of energy homeostasis [16, 25, 26]. At a generalized level, lactate can be carried to the liver and reconverted into glucose through the Cori cycle, serving as an energy source [27].

3. Lactate Production Increases in Diabetes

Fasting plasma lactate level is increased in patients with DM including T1DM and T2DM versus nondiabetic persons [28–36]. Diabetic patients with obesity exhibit higher fasting plasma lactate levels than nondiabetic individuals with obesity [37, 38]. Barnett et al. proposed that diabetes-associated hyperlactatemia might be an early change in the time course of the disease [39]. Recently, Berhane et al. [40] demonstrated that lactate production progressively rises during hyperinsulinemic euglycemic clamp study, a condition of hyperinsulinemia similar to the early stages in the development of T2DM. Intriguingly, similar previous studies also report elevated lactate concentrations during the early

stages of diabetes, prediabetes, and the hyperinsulinemia condition. In addition, Brouwers et al. [41] reported increased lactate levels in patients with poorly controlled T1DM and glycogenic hepatopathy, implying that enhanced plasma lactate concentrations are part of the clinical spectrum of these diseases. Furthermore, lactate has also been revealed to predict diabetes occurrence in the future [42, 43].

The mechanisms underlying diabetes-associated hyperlactatemia include serious changes in the intracellular glucose metabolism in insulin-sensitive tissues, for example, diminished glycogen synthesis, compromised glucose oxidative metabolism, and increased whole-body rate of nonoxidative glycolysis [28, 31, 44]. Importantly, when compared with controls, nonoxidative glycolysis rate retains higher in T2DM patients during hyperglycemic [31, 44, 45] and hyperinsulinemic [31, 44] status. In addition, the postprandially nonoxidative glycolysis is elevated in these patients relative to healthy controls and blood lactate level rises under this condition [36]. Insulin resistance plays a vital role in the pathogenesis of T2DM [46] and can be used as an early marker for the disease [40]. Under the insulin resistant condition, high levels of insulin promote glycolysis through activating two rate limiting enzymes, namely, phosphofructokinase and pyruvate dehydrogenase [47]. Thus, patients with insulin resistance/diabetes exhibit augmented activity of glycolysis [31, 48]. The elevated glycolysis results in enhanced formation of NADH and pyruvate and reduced NAD+ levels. Pyruvate is converted into lactate by LDH accompanied by NAD+ generation from NADH in a redox reaction. This reaction may be accentuated in insulin resistance since hyperinsulinemia induces enhanced glycolysis.

4. Contribution of Lactate to Insulin Resistance/Diabetes

As an imperative cellular metabolite in the glycolytic pathway, lactate might reflect the cellular metabolism status. Some studies suggest that augmented lactate levels in obesity, which might play a significant role in glucose transport and metabolism, profoundly influence insulin sensitivity [49]. Its high plasma level might be an early indication of the beginning of insulin resistance and can be utilized to identify a state of insulin resistance [40]. In addition, in HIV-infected patients treated with nucleoside reverse transcriptase inhibitors, both resting and postexercise levels of lactate are associated with insulin resistance in skeletal muscle [50]. Lactate alone or combined with other insulin secretagogues, for example, ketone bodies, stimulates insulin release in INS-1 cells and isolated pancreatic islets [51], indicating that increased plasma lactate promotes insulin secretion and pancreatic response to insulin secretagogues. Thus, these results suggest that lactate not only enhances insulin secretion from β-cells but also improves the responsiveness of these cells to insulin [51]. These data may explain that the transiently elevated lactate obtained during physical exercises and aerobic/anaerobic training improves DM symptoms. Instead, lactate concentrations are chronically increased in diabetic patients with obesity [52]. The chronical hyperlactatemia maintained by the enhanced lactate formation from adipocytes in obese individuals [53] is found preceding diabetes onset [52] and might participate in this pathologic process. Together, these data indicate that chronical hyperlactatemia might indicate the early stages of insulin resistance and contributes to the onset of diabetes. Actually, some epidemiologic studies suggest that high lactate levels might predict the occurrence of diabetes [42, 43]. Crawford et al. [43] in their cross-sectional study among white elderly people with severe carotid atheromatosis reveal a relationship between plasma lactate levels and prevailing T2DM; nonetheless no association is detected among African Americans.

While the molecular mechanisms underlying lactate-induced insulin resistance/diabetes are yet uncertain, it has been proposed that inhibition of the ability to oxidize glucose, the repression of glucose transport, and insulin-stimulated glycolysis, as well as reduced insulin-induced glucose uptake is implicated in this phenomenon. Furthermore, it has been suggested that lactate-induced insulin resistance is related to compromised insulin signaling and reduced insulin-triggered glucose transport in skeletal muscle [54].

5. Lactate Production Increases in Cancer

A common feature of primary and metastatic cancers is increase in glycolysis rate, leading to augmented glucose uptake and lactate formation, even under normal oxygen conditions. This is also known as aerobic glycolysis or the "Warburg effect" [55], a metabolic hallmark of cancer. It was first described in the 1920s by Warburg and he hypothesized that cancer is caused by compromised mitochondrial metabolism. While this hypothesis has been proven wrong, the experimental observations of elevated glycolysis in cancers even under normoxic conditions have been repetitively substantiated [56]. Unlike anaerobic glycolysis that stimulates energy generation under hypoxia, the Warburg effect provides a proliferative advantage via converting carbohydrate fluxes from energy generation to biosynthetic processes. To meet cancer cell proliferation requirements, the glycolytic switch is related to increased glucose consumption and lactate accumulation [57]. It is shocking that the lactate levels determined in human cancers, for example, cervix cancer, can range from 4 mM to 40 mM [58], while the physiological levels of lactate in normal tissues are 1.8–2 mM [59].

The molecular mechanisms underlying upregulation of glycolysis in cancer are not well delineated. It is generally assumed that this phenomenon results from defective cellular respiration, oncogenic changes, and overexpression of metabolite transporters and glycolytic enzymes, for example, glucose transporters and hexokinases, which are the crucial regulatory molecules for glycolytic flux [60]. The oncogenes and tumor suppressor genes implicated in the metabolic alteration from oxidative phosphorylation to an increased glycolysis of cancer cells include hypoxia-inducible factor-1α (HIF-1α) [60, 61], epidermal growth factor (EGF), phosphoinositol 3-kinase (PI3-K), myc, nuclear Factor Kappa

Beta, protein kinase B (PKB), insulin-like growth factor I, mTOR, Kirsten rat sarcoma viral oncogene homolog (KRAS), and 5′ adenosine monophosphate-activated protein kinase (AMPK). The majority of these oncogenes stimulate genes encoding proteins that regulate glycolysis and glutaminolysis [55].

Among the aforementioned oncogenes, the transcription factor HIF-1α is the most important controller of the glycolytic response and cellular adaptation [62]. Expression of HIF-1α-regulated genes results in an increased glycolytic flux in cancer cells in an oxygen-independent manner. The targets of HIF-1 include hexokinase II [63], angiogenic growth factors (e.g., VEGF), haematopoietic factors (e.g., erythropoietin and transferrin) [64], and membrane transporters including glucose transporter-1 (GLUT-1) and monocarboxylate transporter-4 (MCT-4). These membrane transporters contribute to both sufficient glucose transport into the cell and release of amassed lactate out of the cell. HIF-1α activates pyruvate dehydrogenase kinase 1 (PDK-1) and subsequently inactivates the pyruvate dehydrogenase complex (PDC), leading to reduced flux into oxidative phosphorylation [55]. In addition, the activated HIF-1α is related to constitutively high rate of glucose consumption. Furthermore, hypoxia-reoxygenation injury in cancers may stabilize HIF-1α [65], indicating that its constitutive upregulation may be caused by the cyclic oxic-hypoxic cycles which happen in premalignant cancers.

In addition to glycolysis, glutaminolysis is another primary pathway for energy generation and cause increased lactate formation in cancer cells. Moreover, glutaminolysis facilitates macromolecule synthesis in proliferating tumor cells [61]. The tumor-specific isoform of pyruvate kinase (PK) M2 (PKM2) offers an additional source of lactate by converting phosphoenolpyruvate (PEP) into pyruvate. Nevertheless, PEP may promote the production of pyruvate independent of PKM2 activity through serving as a phosphodonor for phosphoglycerate mutase 1 (PGAM1) [66].

6. Lactate Facilitates Cancer Development

High concentrations of lactate have been linked to unfavoured clinical outcome in some human cancers [57]. Augmented intratumoral lactate levels are related to elevated incidence of metastasis in cervical, breast, head, and neck cancers [58, 67, 68]. Due to lactate concentrations conversely correlated with overall and disease-free patient survival, tumor lactate generation, serum lactate, and LDH levels have long been recognized as prognostic biomarkers of patients with various types of epithelial cancers [55, 69–79]. Increased lactate alters microenvironment, fuels cancer cells, and results in acidosis, inflammation, angiogenesis, immunosuppression, and radio-resistance [80–83]. In the next paragraphs, we review these biological actions of increased lactate in cancer development and progress by describing the main evidences.

Substantial studies have demonstrated that cancer cells can uptake lactate and use it for energetic production and amino acid formation. Accumulative evidence demonstrates that lactate is a fuel for the oxidative metabolism in oxygenated cancer cells [68, 84–87] and a signaling mediator in cancer and endothelial cells (ECs) [88–90]. Recently, Bonuccelli et al. [68] reveal that ketones and lactate fuel tumor growth and metastasis, which might illuminate why diabetic patients have an augmented cancer incidence and poor prognosis, because of elevated ketone/lactate production. In vitro studies suggest that cervical cancer SiHa cells and breast cancer MDA-MB-231 cells uptake lactate in a pH-dependent manner [84, 91]. Due to lack of sufficient oxygenation or an effective vascular network in the microenvironment, cancer uptake and exploitation of lactate is dependent on oxygen concentrations, lactate levels, amount of healthy mitochondria, and suitable MCT expression [92, 93]. Owing to the significant metastasis-promoting characteristics of lactate, one can reason that it is unwise to use lactate-containing intravenous injection solutions, for example, lactated Ringer's or Hartmann's solution in cancer patients [68].

The tumor microenvironment (TME) refers to a sophisticated network of extracellular matrix molecules, soluble factors, adipocytes, and stromal cells including tumor endothelial cells (TECs), tumor-associated fibroblasts (TAFs), and macrophages. Among the soluble factors in TME, large amounts of lactate are important due to its effects on tumor and stromal cells [18]. In addition, it decreases extracellular pH to 6.0–6.5 [94–96]. Actually, lactic acidosis frequently contributes to death in patients with some types of metastatic cancer, for example, metastatic breast cancer [97–113]. The acidic TME causes pain in cancer patients [114] and results in metastasis of some tumors [115]. Moreover, acidosis per se may be mutagenic [116], probably via suppression of DNA repair [95] and may result in spontaneous transformation of diploid fibroblasts [117]. Under some circumstances, low pH induces in vitro invasion [118] and in vivo metastasis [119], possibly via the metalloproteinases/cathepsins, which stimulate the degradation of the extracellular matrix and basement membranes [120, 121]. Lactic acidosis results in overexpression of matrix metalloproteinase-9 (MMP-9) [122], VEGF-A [123, 124], transforming growth factor-β2 (TGF-β2) [125] and IL-8 [126–128] in various cancer cells, rendering the TME even more complicated. Pavlides et al. [129] suggest that cancer cells stimulate aerobic glycolysis in CAFs. CAFs render tumor survival and a higher proliferative capacity by a number of factors including secreting lactate and pyruvate and alterations in cell metabolism. Accordingly, cancer cells may become accustomed to rapid alterations in the TME via reprograming stromal cells and via the metabolic interchange between oxidative and glycolytic cells [129, 130].

Within the tumor, TAFs exhibit a different lactate metabolic pathway than the cancer cells. TAFs mainly contain low levels of glucose importer GLUT1, lactate dehydrogenase-B and pyruvate dehydrogenase, while cancer cells contain high GLUT1, lactate dehydrogenase-A, pyruvate dehydrogenase kinase and hypoxia inducible factor-1α. Within cancer cells, the imported glucose is metabolized to pyruvate, while pyruvate dehydrogenase is inactive due to its phosphorylation by pyruvate dehydrogenase kinase phosphorylates. Therefore, LDH-5 (made of LDHA subunits) in an anaerobic manner converts pyruvate to lactate which is exported out of

the cell. On the other hand, TAFs import the lactate and by their LDH-1 (containing LDHB subunits) activity convert it back to pyruvate which is funneled to aerobic pathways of mitochondria via the activity of pyruvate dehydrogenase. It seems that these two lactate metabolic pathways in cancer cells and TAFs work in a complementary manner as cancer cells generate high levels of lactate and acidify the microenvironment while TAF consume the lactate in an aerobic manner and decrease the acidity of the microenvironment [131, 132].

The angiogenesis process supports the new blood vessel development and plays an important role in restoring perfusion, oxygenation, and nutrient supply. Lactate is an imperative contributor to wound healing and angiogenesis [133–135]. Lactate itself induces cell migration [134], vascular morphogenesis [136], circulating vascular progenitor cell recruitment [137], and tube formation and promotes angiogenesis by activating the VEGF/VEGFR2 pathway [136, 138] and stimulating endothelial cells via MCT1, which induces the phosphorylation and degradation of IκBα, triggering the NF-kB/IL-8 (CXCL8) signaling pathway [90]. Lactate-stimulated angiogenesis depends on lactate oxidation by LDH-1, exploiting the enzymatic reaction products, for example, pyruvate and NADH, and lactate transporters [136, 137]. The enhancing production of pyruvate from lactate oxidation activates NF-κB and HIF-1, leading to overexpression of some growth factors required for angiogenesis, including VEGF, basic fibroblast growth factor (bFGF), and stromal cell-derived factor-1 (SDF-1) [139, 140]. In addition, Vegran et al. [90] demonstrate that lactate-stimulated NF-κB activation in ECs is associated with IL-8-mediated autocrine angiogenesis and that this pathway promotes EC migration and tube formation in vitro, as well as lactate-triggered tumor angiogenesis in vivo.

Endothelial cells of tumor vasculature import high levels of glucose (high GLUT1 levels). However, since they contain high LDH1 and low HIF-1α and lowLDH5, similar to TAFs, they show an aerobic metabolism. Meanwhile due to low expression of lactate transporters, endothelial cells perhaps do not import much of the lactate in the tumor. Hence, it seems the main role of endothelial cells is to respond to the tumor microenvironment by generating new vessels to support the cancer cells and other tumor associated cells. However, they may not participate in uptake and consumption of lactate within the tumor [132, 141].

One main reason for cancer development is that the immune system loses its ability to effectively eradicate aberrant cells. High levels of lactate have a harmful effect on the tumor infiltrating immune cells. Clinical evidence indicates that lactate restricts immune cell infiltration in renal cell carcinoma (RCC) and damages the metabolism and cytolytic functions of T cells in the TME [80, 142]. Lactate hinders proliferation and cytokine release of human cytotoxic T lymphocytes (CTLs) by 95% and their cytotoxic activity by 50%. Lactate released from melanoma cells impedes TAA-induced IFN-γ generation by specific CTLs in melanoma spheroid cocultures [143]. In addition, other studies substantiated that high levels of lactate suppresses TCR-stimulated cytokine release (IFN-γ, TNF-α, and IL-2) and prompts partial damage of lytic granules exocytosis in CTLs by selectively downregulating the MAPKs p38 and JNK/c-Jun signaling pathways [81]. Moreover, tumor-derived lactate enhances arginase-1 (ARG1) expression in tumor-associated macrophages (TAMs), hindering T-cell activity and proliferation [144], inhibiting antitumor immune responses and promoting tumor growth [145, 146]. Lately, Colegio et al. [145] demonstrated that, under normoxic conditions, lactate stabilizes HIF-1α, resulting in ARG1 and VEGF gene expression in macrophages. Furthermore, tumor-derived lactate changes monocytes' function hinders their differentiation to DCs and inhibits the cytokine production from differentiated DCs and suppresses the activity of NK cells, thus contributing to immune suppression within tumors [82, 147, 148].

Some studies on experimental tumors, including about 1,000 xenografts of individual human head and neck squamous cell carcinoma, indicate that lactate levels are positively correlated with radio-resistance [149]. The mechanisms behind this correlation reside in, at least partially, the antioxidant characteristics of lactate [150]. Anticancer treatments, for example, ionizing radiation and a number of chemotherapeutic drugs, work through inducing overproduction of reactive oxygen species (ROS) in targeted cancer cells, which causes DNA/RNA damage, genomic instability, and lipid peroxidation. Hence, an accretion of lactate may promote resistance to radiation and lead to chemoresistance [151]. Wagner et al. reveal that lactate can modulate cellular DNA damage repair processes in the uterine cervix, leading to the resistance of cervical cancer cells to anticancer therapy [152]. Since animals receiving chemotherapy or radiotherapy exhibit a reduction in lactate [153], checking this metabolite in human cancers might be used to predict therapeutic responses. Accordingly, a recent study [154] proposes that lactate can be used as a quantitative biomarker of acute radiation response.

Finally, lactate is a mediator of inflammation [155, 156] and might be used as a biomarker of inflammatory processes [157]. Lactate and inflammation stimulate each other in a malicious cycle [83]. It promotes IL-4/IL-13 production [158] and stimulates the IL-23/IL17 pathway [18]. Lactate promotes IL-23p19 expression in tumor infiltrating immune cells by stimulating toll-like receptor. In addition, it stimulates splenocytes to secrete IL-17 in an IL-23-dependent manner. These effects stimulate local inflammatory responses, favoring the incidence and development of tumors [159]. In addition, lactate benefits the growth of inflammation-associated colorectal tumor by promoting PGE2 synthesis and gluconeogenesis in monocytes [160]. Together, these studies suggest that lactate plays a significant proinflammatory role in tumor development.

It is believed that in diabetic patients, the adipose tissue plays a major role in induction of metabolic syndrome. In these patients there is an underlying chronic inflammation in adipose tissue and a general increase in levels of cytokines such as TNF-α, IL-1, and IL-6 [161]. While these released factors play important roles in cancer biology, there is evidence that points to their possible reciprocal roles in the lactate level. For instance, TNFα can induce LDHA and lactate production in a short period of time [162], while lactate induces release of TNF-α and IL-6 in some cells

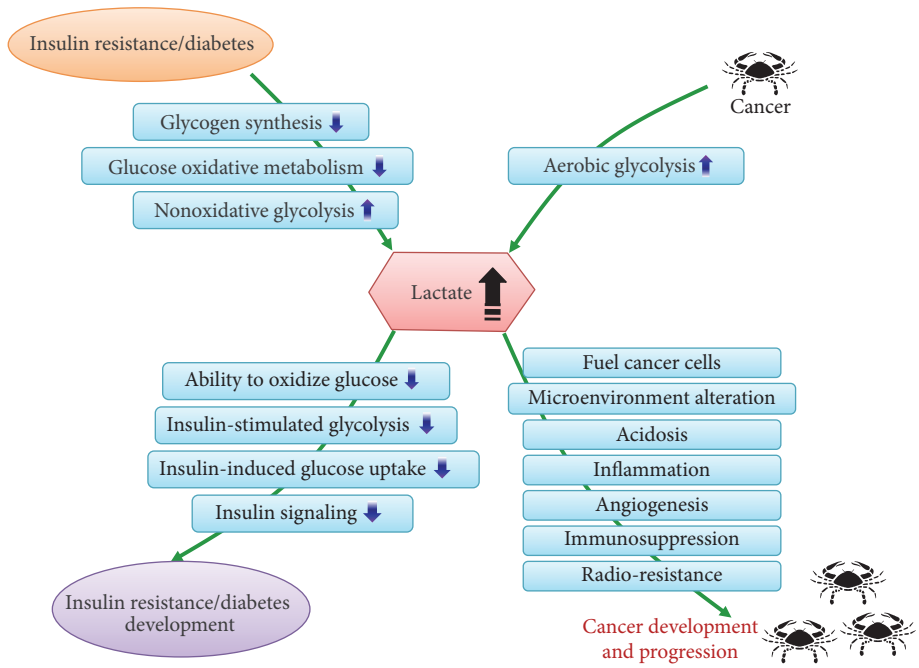

Figure 2: Illustration of lactate as an interaction hub between diabetes and cancer.

[163]. In a study on rats, chronic infusion of IL-1α induced hyperlactacidemia [164] and in another study on rat ovaria cells, IL-1β enhanced glucose uptake and induced aerobic glycolysis [165]. Moreover, it has been shown that high levels of IL-6 correlated with high levels of lactate and can result in poor prognosis of patients with metastatic melanoma [166]. These findings indicate that the release cytokines may play roles in both cancer and metabolic syndrome and may be the connecting points between developments of both diseases.

7. Concluding Remarks and Future Perspectives

Accumulative evidence indicates a high incidence and mortality for a variety of malignancies in patients with diabetes. Diabetes and its risk factors are associated with cancer and they have an intricate and reciprocally reinforcing relationship. Nevertheless, the underlying mechanisms are poorly understood and currently there is no clinical evidence available to direct the proper management of patients presenting with these two diseases concomitantly. Diabetes and cancer interact with each other in a vicious cycle, where lactate plays a pivotal role in this mutual interaction. Insulin resistance/diabetes and cancer conditions produce high levels of lactate and conversely high lactate promotes diabetes and cancer development and progression (Figure 2).

In diabetes, hyperlactacidemia is perhaps due to the high levels of insulin which induces the activity of two glycolytic enzymes phosphofructokinase and pyruvate dehydrogenase [47]. However, glycolytic switch in cancer is due to the increased activity of glycolytic enzymes, for example, glucose transporters and hexokinases [60], which have been attributed to signaling pathways such as HIF-1α [60, 61], EGF, phosphoinositol 3-kinase (PI3-K), myc, NF-kB, PKB, IGF-I, mTOR, KRAS, and AMPK. Among these, HIF-1 signaling seems to be very important as it induces hexokinase II [63], GLUT-1 and MCT4, and pyruvate dehydrogenase kinase 1 (PDK-1), and therefore inactivates the pyruvate dehydrogenase, leading to reduced flux into oxidative phosphorylation [55]. In both diabetes and cancer lactate can induce inflammation through IL-4/IL-13 production [158] and IL-23/IL17 pathway [18]. However, in cancer the effect of lactate is more profound and can alter microenvironment, fuels cancer cells, and results in acidosis, inflammation, angiogenesis, and immunosuppression [80–83].

In this review, we deliberated the mechanisms underlying high lactate induced by diabetes and cancer, as well as the effects of high level of lactate production, and the key property of diabetes and cancer, on diabetes development and different cancer biological behaviors. Besides supplying abundant nutrition for tumor growth, increased lactate level might also activate various signaling pathways, which play imperative roles in cancer development and progression. Existing evidence demonstrates that some diabetes treatments might have significant therapeutic implications in cancer patients and that MCT/lactate transport inhibitors are employed therapeutically to repress cancer metastasis. Understanding the molecular mechanisms behind metabolic remodeling of diabetes- and cancer-related signaling would endow novel preventive and therapeutic approaches for diabetes and cancer treatment. Importantly, combined management of diabetes and cancer probably leads to better improvement in mortality versus treating them individually. Accordingly, more interdisciplinary approaches are required to reveal the mechanisms underlying the links between

these two diseases and, eventually, ameliorate clinical outcomes.

Competing Interests

The authors declare no competing financial interests.

Acknowledgments

This work was supported in part by NIH-NIMHD U54MD007598, NIH/NCI 1U54CA14393; U56 CA101599-01; Department-of-Defense Breast Cancer Research Program Grant BC043180, NIH/NCATS CTSI UL1TR000124 (to Jaydutt V. Vadgama) and Accelerating Excellence in Translational Science Pilot Grant G0812D05, NIH/NCI SC1CA200517 (to Yong Wu).

References

[1] A. D. Lopez, C. D. Mathers, M. Ezzati, D. T. Jamison, and C. J. Murray, "Global and regional burden of disease and risk factors, 2001: systematic analysis of population health data," *The Lancet*, vol. 367, no. 9524, pp. 1747–1757, 2006.

[2] S. Joshi, M. Liu, and N. Turner, "Diabetes and its link with cancer: providing the fuel and spark to launch an aggressive growth regime," *BioMed Research International*, vol. 2015, Article ID 390863, 11 pages, 2015.

[3] H. Noto, A. Goto, T. Tsujimoto, K. Osame, and M. Noda, "Latest insights into the risk of cancer in diabetes," *Journal of Diabetes Investigation*, vol. 4, no. 3, pp. 225–232, 2013.

[4] B. B. Barone, H.-C. Yeh, C. F. Snyder et al., "Long-term all-cause mortality in cancer patients with preexisting diabetes mellitus: a systematic review and meta-analysis," *JAMA*, vol. 300, no. 23, pp. 2754–2764, 2008.

[5] B. B. Barone, H.-C. Yeh, C. F. Snyder et al., "Postoperative mortality in cancer patients with preexisting diabetes: systematic review and meta-analysis," *Diabetes Care*, vol. 33, no. 4, pp. 931–939, 2010.

[6] M. Jalving, J. A. Gietema, J. D. Lefrandt et al., "Metformin: taking away the candy for cancer?" *European Journal of Cancer*, vol. 46, no. 13, pp. 2369–2380, 2010.

[7] E. Giovannucci, D. M. Harlan, M. C. Archer et al., "Diabetes and cancer: a consensus report," *Diabetes Care*, vol. 33, no. 7, pp. 1674–1685, 2010.

[8] A. W. Barclay, P. Petocz, J. McMillan-Price et al., "Glycemic index, glycemic load, and chronic disease risk—a metaanalysis of observational studies," *American Journal of Clinical Nutrition*, vol. 87, no. 3, pp. 627–637, 2008.

[9] H. J. Sun, H. Ohrr, J. W. Sull, J. E. Yun, M. Ji, and J. M. Samet, "Fasting serum glucose level and cancer risk in Korean men and women," *Journal of the American Medical Association*, vol. 293, no. 2, pp. 194–202, 2005.

[10] T. Stocks, K. Rapp, T. Bjørge et al., "Blood glucose and risk of incident and fatal cancer in the metabolic syndrome and cancer project (Me-Can): analysis of six prospective cohorts," *PLOS Medicine*, vol. 6, no. 12, Article ID e1000201, 2009.

[11] R. Abe and S.-I. Yamagishi, "AGE-RAGE system and carcinogenesis," *Current Pharmaceutical Design*, vol. 14, no. 10, pp. 940–945, 2008.

[12] C. García-Jiménez, J. M. García-Martínez, A. Chocarro-Calvo, and A. De la Vieja, "A new link between diabetes and cancer: enhanced WNT/β-catenin signaling by high glucose," *Journal of Molecular Endocrinology*, vol. 52, no. 1, pp. R51–R66, 2013.

[13] R. Kaaks and A. Lukanova, "Energy balance and cancer: the role of insulin and insulin-like growth factor-I," *Proceedings of the Nutrition Society*, vol. 60, no. 1, pp. 91–106, 2001.

[14] M. Pollak, "Insulin and insulin-like growth factor signalling in neoplasia," *Nature Reviews Cancer*, vol. 8, no. 12, pp. 915–928, 2008.

[15] J. Li, G. Cao, Q. Ma, H. Liu, W. Li, and L. Han, "The bidirectional interation between pancreatic cancer and diabetes," *World Journal of Surgical Oncology*, vol. 10, article 171, 2012.

[16] L. B. Gladden, "Lactate metabolism: a new paradigm for the third millennium," *Journal of Physiology*, vol. 558, no. 1, pp. 5–30, 2004.

[17] J. R. Doherty and J. L. Cleveland, "Targeting lactate metabolism for cancer therapeutics," *Journal of Clinical Investigation*, vol. 123, no. 9, pp. 3685–3692, 2013.

[18] S. Romero-Garcia, M. M. Moreno-Altamirano, H. Prado-Garcia, and F. J. Sánchez-García, "Lactate contribution to the tumor microenvironment: mechanisms, effects on immune cells and therapeutic relevance," *Frontiers in Immunology*, vol. 7, article no. 52, 2016.

[19] M. Drent, N. A. M. Cobben, R. F. Henderson, E. F. M. Wouters, and M. Van Dieijen-Visser, "Usefulness of lactate dehydrogenase and its isoenzymes as indicators of lung damage or inflammation," *European Respiratory Journal*, vol. 9, no. 8, pp. 1736–1742, 1996.

[20] A. P. Halestrap and D. Meredith, "The SLC16 gene family—from monocarboxylate transporters (MCTs) to aromatic amino acid transporters and beyond," *Pflügers Archiv*, vol. 447, no. 5, pp. 619–628, 2004.

[21] A. P. Halestrap, "The monocarboxylate transporter family—Structure and functional characterization," *IUBMB Life*, vol. 64, no. 1, pp. 1–9, 2012.

[22] M. Sola-Penna, "Metabolic regulation by lactate," *IUBMB Life*, vol. 60, no. 9, pp. 605–608, 2008.

[23] A. Consoli, N. Nurjhan, J. J. Reilly Jr., D. M. Bier, and J. E. Gerich, "Contribution of liver and skeletal muscle to alanine and lactate metabolism in humans," *American Journal of Physiology—Endocrinology and Metabolism*, vol. 259, no. 5, pp. E677–E684, 1990.

[24] G. Van Hall, "Lactate kinetics in human tissues at rest and during exercise," *Acta Physiologica*, vol. 199, no. 4, pp. 499–508, 2010.

[25] F. Boussouar and M. Benahmed, "Lactate and energy metabolism in male germ cells," *Trends in Endocrinology and Metabolism*, vol. 15, no. 7, pp. 345–350, 2004.

[26] K. Caesar, P. Hashemi, A. Douhou et al., "Glutamate receptor-dependent increments in lactate, glucose and oxygen metabolism evoked in rat cerebellum *in vivo*," *The Journal of Physiology*, vol. 586, no. 5, pp. 1337–1349, 2008.

[27] C. Waterhouse and J. Keilson, "Cori cycle activity in man," *Journal of Clinical Investigation*, vol. 48, no. 12, pp. 2359–2366, 1969.

[28] A. Avogaro, G. Toffolo, M. Miola et al., "Intracellular lactate- and pyruvate-interconversion rates are increased in muscle tissue of non-insulin-dependent diabetic individuals," *Journal of Clinical Investigation*, vol. 98, no. 1, pp. 108–115, 1996.

[29] Y. D. I. Chen, B. B. Varasteh, and G. M. Reaven, "Plasma lactate concentration in obesity and type 2 diabetes," *Diabete et Metabolisme*, vol. 19, no. 4, pp. 348–354, 1993.

[30] A. Consoli, N. Nurjhan, F. Capani, and J. Gerich, "Predominant role of gluconeogenesis in increased hepatic glucose production in NIDDM," *Diabetes*, vol. 38, no. 5, pp. 550–557, 1989.

[31] S. Del Prato, R. C. Bonadonna, E. Bonora et al., "Characterization of cellular defects of insulin action in type 2 (non-insulin-dependent) diabetes mellitus," *Journal of Clinical Investigation*, vol. 91, no. 2, pp. 484–494, 1993.

[32] D. E. Kelley and L. J. Mandarine, "Hyperglycemia normalizes insulin-stimulated skeletal muscle glucose oxidation and storage in noninsulin-dependent diabetes mellitus," *Journal of Clinical Investigation*, vol. 86, no. 6, pp. 1999–2007, 1990.

[33] I. R. Lanza, S. Zhang, L. E. Ward, H. Karakelides, D. Raftery, and K. Sreekumaran Nair, "Quantitative metabolomics by 1H-NMR and LC-MS/MS confirms altered metabolic pathways in diabetes," *PLOS ONE*, vol. 5, no. 5, Article ID e10538, 2010.

[34] C. Meyer, M. Stumvoll, V. Nadkarni, J. Dostou, A. Mitrakou, and J. Gerich, "Abnormal renal and hepatic glucose metabolism in type 2 diabetes mellitus," *Journal of Clinical Investigation*, vol. 102, no. 3, pp. 619–624, 1998.

[35] M.-T. Van Der Merwe, G. P. Schlaphoff, N. J. Crowther et al., "Lactate and glycerol release from adipose tissue in lean, obese, and diabetic women from South Africa," *Journal of Clinical Endocrinology and Metabolism*, vol. 86, no. 7, pp. 3296–3303, 2001.

[36] H. J. Woerle, E. Szoke, C. Meyer et al., "Mechanisms for abnormal postprandial glucose metabolism in type 2 diabetes," *American Journal of Physiology—Endocrinology and Metabolism*, vol. 290, no. 1, pp. E67–E77, 2006.

[37] L. Metz, P. Sirvent, G. Py et al., "Relationship between blood lactate concentration and substrate utilization during exercise in type 2 diabetic postmenopausal women," *Metabolism: Clinical and Experimental*, vol. 54, no. 8, pp. 1102–1107, 2005.

[38] J. K. Zawadzki, R. R. Wolfe, D. M. Mott, S. Lillioja, B. V. Howard, and C. Bogardus, "Increased rate of Cori cycle in obese subjects with NIDDM and effect of weight reduction," *Diabetes*, vol. 37, no. 2, pp. 154–159, 1988.

[39] A. H. Barnett, A. J. Spiliopoulos, D. A. Pyke, W. A. Stubbs, J. Burrin, and K. G. Alberti, "Metabolic studies in unaffected co-twins of non-insulin-dependent diabetics," *British Medical Journal*, vol. 282, no. 6277, pp. 1656–1658, 1981.

[40] F. Berhane, A. Fite, N. Daboul et al., "Plasma lactate levels increase during hyperinsulinemic euglycemic clamp and oral glucose tolerance test," *Journal of Diabetes Research*, vol. 2015, Article ID 102054, 7 pages, 2015.

[41] M. C. G. J. Brouwers, J. C. Ham, E. Wisse et al., "Elevated lactate levels in patients with poorly regulated type 1 diabetes and glycogenic hepatopathy: a new feature of mauriac syndrome," *Diabetes Care*, vol. 38, no. 2, pp. e11–e12, 2015.

[42] L.-O. Ohlson, B. Larsson, P. Björntorp et al., "Risk factors for Type 2 (non-insulin-dependent) diabetes mellitus. Thirteen and one-half years of follow-up of the participants in a study of Swedish men born in 1913," *Diabetologia*, vol. 31, no. 11, pp. 798–805, 1988.

[43] S. O. Crawford, R. C. Hoogeveen, F. L. Brancati et al., "Association of blood lactate with type 2 diabetes: the atherosclerosis risk in communities carotid MRI study," *International Journal of Epidemiology*, vol. 39, no. 6, pp. 1647–1655, 2010.

[44] A. W. Thorburn, B. Gumbiner, F. Bulacan, P. Wallace, and R. R. Henry, "Intracellular glucose oxidation and glycogen synthase activity are reduced in non-insulin-dependent (type II) diabetes independent of impaired glucose uptake," *Journal of Clinical Investigation*, vol. 85, no. 2, pp. 522–529, 1990.

[45] S. Bokhari, P. Emerson, Z. Israelian, A. Gupta, and C. Meyer, "Metabolic fate of plasma glucose during hyperglycemia in impaired glucose tolerance: Evidence for further early defects in the pathogenesis of type 2 diabetes," *American Journal of Physiology—Endocrinology and Metabolism*, vol. 296, no. 3, pp. E440–E444, 2009.

[46] J. H. Warram, B. C. Martin, A. S. Krolewski, J. S. Soeldner, and C. R. Kahn, "Slow glucose removal rate and hyperinsulinemia precede the development of type II diabetes in the offspring of diabetic parents," *Annals of Internal Medicine*, vol. 113, no. 12, pp. 909–915, 1990.

[47] R. A. DeFronzo, "Insulin resistance, lipotoxicity, type 2 diabetes and atherosclerosis: the missing links. The Claude Bernard Lecture 2009," *Diabetologia*, vol. 53, no. 7, pp. 1270–1287, 2010.

[48] J.-A. Simoneau, S. R. Colberg, F. L. Thaete, and D. E. Kelley, "Skeletal muscle glycolytic and oxidative enzyme capacities are determinants of insulin sensitivity and muscle composition in obese women," *FASEB Journal*, vol. 9, no. 2, pp. 273–278, 1995.

[49] E. A. Richter, L. P. Garetto, M. N. Goodman, and N. B. Ruderman, "Muscle glucose metabolism following exercise in the rat. Increased sensitivity to insulin," *Journal of Clinical Investigation*, vol. 69, no. 4, pp. 785–793, 1982.

[50] A. Maagaard, M. Holberg-Petersen, P. A. Torjesen, J. N. Bruun, and D. Kvale, "Insulin resistance is affected by increased levels of plasma lactate but not mitochondrial alterations in skeletal muscle in NRTI-exposed HIV-infected patients," *HIV Clinical Trials*, vol. 8, no. 5, pp. 345–353, 2007.

[51] M. J. MacDonald, M. J. Longacre, S. W. Stoker, L. J. Brown, N. M. Hasan, and M. A. Kendrick, "Acetoacetate and β-hydroxybutyrate in combination with other metabolites release insulin from INS-1 cells and provide clues about pathways in insulin secretion," *American Journal of Physiology—Cell Physiology*, vol. 294, no. 2, pp. C442–C450, 2008.

[52] J. Lovejoy, B. Mellen, and M. Digirolamo, "Lactate generation following glucose ingestion: relation to obesity, carbohydrate tolerance and insulin sensitivity," *International Journal of Obesity*, vol. 14, no. 10, pp. 843–855, 1990.

[53] V. Qvisth, E. Hagström-Toft, E. Moberg, S. Sjöberg, and J. Bolinder, "Lactate release from adipose tissue and skeletal muscle in vivo: Defective insulin regulation in insulin-resistant obese women," *American Journal of Physiology—Endocrinology and Metabolism*, vol. 292, no. 3, pp. E709–E714, 2007.

[54] M. Hamamdzic, B. Hrabac, A. Alic, E. Pasic-Juhas, and A. Hodzic, "Effect of lactate on insulin action in rats," *Bosnian Journal of Basic Medical Sciences*, vol. 8, no. 2, pp. 131–134, 2008.

[55] F. Hirschhaeuser, U. G. A. Sattler, and W. Mueller-Klieser, "Lactate: a metabolic key player in cancer," *Cancer Research*, vol. 71, no. 22, pp. 6921–6925, 2011.

[56] G. L. Semenza, D. Artemov, A. Bedi et al., "'The metabolism of tumours': 70 years later," *Novartis Foundation Symposium*, vol. 240, pp. 251–264, 2001.

[57] S. Dhup, R. K. Dadhich, P. E. Porporato, and P. Sonveaux, "Multiple biological activities of lactic acid in cancer: influences on tumor growth, angiogenesis and metastasis," *Current Pharmaceutical Design*, vol. 18, no. 10, pp. 1319–1330, 2012.

[58] D. M. Brizel, T. Schroeder, R. L. Scher et al., "Elevated tumor lactate concentrations predict for an increased risk of metastases in head-and-neck cancer," *International Journal of Radiation Oncology, Biology, Physics*, vol. 51, no. 2, pp. 349–353, 2001.

[59] S. Walenta, A. Salameh, H. Lyng et al., "Correlation of high lactate levels in head and neck tumors with incidence of metastasis," *American Journal of Pathology*, vol. 150, no. 2, pp. 409–415, 1997.

[60] R. J. DeBerardinis, "Is cancer a disease of abnormal cellular metabolism? New angles on an old idea," *Genetics in Medicine*, vol. 10, no. 11, pp. 767–777, 2008.

[61] A. J. Levine and A. M. Puzio-Kuter, "The control of the metabolic switch in cancers by oncogenes and tumor suppressor genes," *Science*, vol. 330, no. 6009, pp. 1340–1344, 2010.

[62] G. L. Semenza, "Hypoxia-inducible factor 1: master regulator of O_2 homeostasis," *Current Opinion in Genetics and Development*, vol. 8, no. 5, pp. 588–594, 1998.

[63] S. Yasuda, S. Arii, A. Mori et al., "Hexokinase II and VEGF expression in liver tumors: correlation with hypoxia-inducible factor-1α and its significance," *Journal of Hepatology*, vol. 40, no. 1, pp. 117–123, 2004.

[64] P. Carmeliet, Y. Dor, J. M. Herbert et al., "Role of HIF-1α in hypoxia-mediated apoptosis, cell proliferation and tumour angiogenesis," *Nature*, vol. 394, no. 6692, pp. 485–490, 1998.

[65] B. J. Moeller, Y. Cao, C. Y. Li, and M. W. Dewhirst, "Radiation activates HIF-1 to regulate vascular radiosensitivity in tumors: role of reoxygenation, free radicals, and stress granules," *Cancer Cell*, vol. 5, no. 5, pp. 429–441, 2004.

[66] M. G. Vander Heiden, J. W. Locasale, K. D. Swanson et al., "Evidence for an alternative glycolytic pathway in rapidly proliferating cells," *Science*, vol. 329, no. 5998, pp. 1492–1499, 2010.

[67] S. Walenta, M. Wetterling, M. Lehrke et al., "High lactate levels predict likelihood of metastases, tumor recurrence, and restricted patient survival in human cervical cancers," *Cancer Research*, vol. 60, no. 4, pp. 916–921, 2000.

[68] G. Bonuccelli, A. Tsirigos, D. Whitaker-Menezes et al., "Ketones and lactate "fuel" tumor growth and metastasis: evidence that epithelial cancer cells use oxidative mitochondrial metabolism," *Cell Cycle*, vol. 9, no. 17, pp. 3506–3514, 2010.

[69] S. Blatt, N. Voelxen, K. Sagheb et al., "Lactate as a predictive marker for tumor recurrence in patients with head and neck squamous cell carcinoma (HNSCC) post radiation: a prospective study over 15 years," *Clinical Oral Investigations*, vol. 20, no. 8, pp. 2097–2104, 2016.

[70] M. I. Koukourakis, E. Kontomanolis, A. Giatromanolaki, E. Sivridis, and V. Liberis, "Serum and tissue ldh levels in patients with breast/gynaecological cancer and benign diseases," *Gynecologic and Obstetric Investigation*, vol. 67, no. 3, pp. 162–168, 2009.

[71] M. Ryberg, D. Nielsen, K. Osterlind, P. K. Andersen, T. Skovsgaard, and P. Dombernowsky, "Predictors of central nervous system metastasis in patients with metastatic breast cancer. A competing risk analysis of 579 patients treated with epirubicin-based chemotherapy," *Breast Cancer Research and Treatment*, vol. 91, no. 3, pp. 217–225, 2005.

[72] B. Nisman, V. Barak, A. Hubert et al., "Prognostic factors for survival in metastatic breast cancer during first-line paclitaxel chemotherapy," *Anticancer Research*, vol. 23, no. 2, pp. 1939–1942, 2003.

[73] M. Ryberg, D. Nielsen, K. Øterlind, T. Skovsgaard, and P. Dombernowsky, "Prognostic factors and long-term survival in 585 patients with metastatic breast cancer treated with epirubicin-based chemotherapy," *Annals of Oncology*, vol. 12, no. 1, pp. 81–87, 2001.

[74] A. Viganó, E. Bruera, G. S. Jhangri, S. C. Newman, A. L. Fields, and M. E. Suarez-Almazor, "Clinical survival predictors in patients with advanced cancer," *Archives of Internal Medicine*, vol. 160, no. 6, pp. 861–868, 2000.

[75] A. Kher, G. Moghe, and A. Deshpande, "Significance of serum ferritin and lactate dehydrogenase in benign and malignant disease of breast," *Indian Journal of Pathology and Microbiology*, vol. 40, no. 3, pp. 321–326, 1997.

[76] N. Khan, S. P. Tyagi, and A. Salahuddin, "Diagnostic and prognostic significance of serum cholinesterase and lactate dehydrogenase in breast cancer," *Indian Journal of Pathology and Microbiology*, vol. 34, no. 2, pp. 126–130, 1991.

[77] Yeshowardhana, M. M. Gupta, G. Bansal et al., "Serum glycolytic enzymes in breast carcinoma," *Tumori*, vol. 72, no. 1, pp. 35–41, 1986.

[78] P. Malhotra, L. S. Sidhu, and S. P. Singh, "Serum lactate dehydrogenase level in various malignancies," *Neoplasma*, vol. 33, no. 5, pp. 641–647, 1986.

[79] M. I. Koukourakis, A. Giatromanolaki, E. Sivridis et al., "Lactate dehydrogenase-5 (LDH-5) overexpression in non-small-cell lung cancer tissues is linked to tumour hypoxia, angiogenic factor production and poor prognosis," *British Journal of Cancer*, vol. 89, no. 5, pp. 877–885, 2003.

[80] K. Fischer, P. Hoffmann, S. Voelkl et al., "Inhibitory effect of tumor cell-derived lactic acid on human T cells," *Blood*, vol. 109, no. 9, pp. 3812–3819, 2007.

[81] A. N. Mendler, B. Hu, P. U. Prinz, M. Kreutz, E. Gottfried, and E. Noessner, "Tumor lactic acidosis suppresses CTL function by inhibition of p38 and JNK/c-Jun activation," *International Journal of Cancer*, vol. 131, no. 3, pp. 633–640, 2012.

[82] Z. Husain, P. Seth, and V. P. Sukhatme, "Tumor-derived lactate and myeloid-derived suppressor cells: linking metabolism to cancer immunology," *OncoImmunology*, vol. 2, no. 11, Article ID e26383, 2013.

[83] K. Kawauchi, K. Araki, K. Tobiume, and N. Tanaka, "p53 regulates glucose metabolism through an IKK-NF-κB pathway and inhibits cell transformation," *Nature Cell Biology*, vol. 10, no. 5, pp. 611–618, 2008.

[84] P. Sonveaux, F. Végran, T. Schroeder et al., "Targeting lactate-fueled respiration selectively kills hypoxic tumor cells in mice," *The Journal of Clinical Investigation*, vol. 118, no. 12, pp. 3930–3942, 2008.

[85] O. Feron, "Pyruvate into lactate and back: from the Warburg effect to symbiotic energy fuel exchange in cancer cells," *Radiotherapy and Oncology*, vol. 92, no. 3, pp. 329–333, 2009.

[86] U. E. Martinez-Outschoorn, S. Pavlides, A. Howell et al., "Stromal-epithelial metabolic coupling in cancer: integrating autophagy and metabolism in the tumor microenvironment," *International Journal of Biochemistry and Cell Biology*, vol. 43, no. 7, pp. 1045–1051, 2011.

[87] D. Whitaker-Menezes, U. E. Martinez-Outschoorn, Z. Lin et al., "Evidence for a stromal-epithelial "lactate shuttle" in human tumors: MCT4 is a marker of oxidative stress in cancer-associated fibroblasts," *Cell Cycle*, vol. 10, no. 11, pp. 1772–1783, 2011.

[88] H. Lu, R. A. Forbes, and A. Verma, "Hypoxia-inducible factor 1 activation by aerobic glycolysis implicates the Warburg effect in carcinogenesis," *The Journal of Biological Chemistry*, vol. 277, no. 26, pp. 23111–23115, 2002.

[89] H. Lu, C. L. Dalgard, A. Mohyeldin, T. McFate, A. S. Tait, and A. Verma, "Reversible inactivation of HIF-1 prolyl hydroxylases

allows cell metabolism to control basal HIF-1," *Journal of Biological Chemistry*, vol. 280, no. 51, pp. 41928–41939, 2005.

[90] F. Vegran, R. Boidot, C. Michiels, P. Sonveaux, and O. Feron, "Lactate influx through the endothelial cell monocarboxylate transporter MCT1 supports an NF-kappaB/IL-8 pathway that drives tumor angiogenesis," *Cancer Research*, vol. 71, no. 7, pp. 2550–2560, 2011.

[91] Q. Wang and M. E. Morris, "The role of monocarboxylate transporter 2 and 4 in the transport of γ-hydroxybutyric acid in mammalian cells," *Drug Metabolism and Disposition*, vol. 35, no. 8, pp. 1393–1399, 2007.

[92] L. B. Gladden, "A 'lactatic' perspective on metabolism," *Medicine and Science in Sports and Exercise*, vol. 40, no. 3, pp. 477–485, 2008.

[93] G. A. Brooks, "Intra- and extra-cellular lactate shuttles," *Medicine & Science in Sports & Exercise*, vol. 32, no. 4, pp. 790–799, 2000.

[94] H. Xie, J.-I. Hanai, J.-G. Ren et al., "Targeting lactate dehydrogenase-a inhibits tumorigenesis and tumor progression in mouse models of lung cancer and impacts tumor-initiating cells," *Cell Metabolism*, vol. 19, no. 5, pp. 795–809, 2014.

[95] N. Raghunand, R. A. Gatenby, and R. J. Gillies, "Microenvironmental and cellular consequences of altered blood flow in tumours," *British Journal of Radiology*, vol. 76, no. 1, pp. S11–S22, 2003.

[96] R. J. Gillies, N. Raghunand, G. S. Karczmar, and Z. M. Bhujwalla, "MRI of the tumor microenvironment," *Journal of Magnetic Resonance Imaging*, vol. 16, no. 4, pp. 430–450, 2002.

[97] G. M. Colombo, L. R. Del Vecchio, T. Sacco, and M. Cicchinelli, "Fatal lactic acidosis due to widespread diffusion of melanoma," *Minerva Medica*, vol. 97, no. 3, article 295, 2006.

[98] D. Deeren, E. Verbeken, S. Vanderschueren, A. Wilmer, H. Bobbaers, and W. Meersseman, "Cancer presenting as fatal pulmonary tumour embolism," *Acta Clinica Belgica*, vol. 61, no. 1, pp. 30–34, 2006.

[99] J. C. Cheng, S. D. Esparza, V. M. Knez, K. M. Sakamoto, and T. B. Moore, "Severe lactic acidosis in a 14-year-old female with metastatic undifferentiated carcinoma of unknown primary," *Journal of Pediatric Hematology/Oncology*, vol. 26, no. 11, pp. 780–782, 2004.

[100] W. K. Chau, C. F. Yang, Y. H. Chou, and C. H. Ho, "Aggressive undifferentiated carcinoma of unknown primary site complicated by lactic acidosis after bleeding: a case report," *Japanese Journal of Clinical Oncology*, vol. 32, no. 6, pp. 210–214, 2002.

[101] B. M. Wall, N. Mansour, and C. R. Cooke, "Acute fulminant lactic acidosis complicating metastatic cholangiocarcinoma," *American Journal of the Medical Sciences*, vol. 319, no. 2, pp. 126–129, 2000.

[102] T. R. J. Evans, R. C. Stein, H. T. Ford, J. C. Gazet, G. V. Chamberlain, and R. C. Coombes, "Lactic acidosis: a presentation of metastatic breast cancer arising in pregnancy," *Cancer*, vol. 69, no. 2, pp. 453–456, 1992.

[103] E. Warner, "Type B lactic acidosis and metastatic breast cancer," *Breast Cancer Research and Treatment*, vol. 24, no. 1, pp. 75–79, 1992.

[104] M. Odeh and H. Bassan, "The role of malignancy in lactic acidosis and shock," *Postgraduate Medical Journal*, vol. 65, no. 768, pp. 801–803, 1989.

[105] C. R. Thomas Jr. and N. Dodhia, "Common emergencies in cancer medicine: metabolic syndromes," *Journal of the National Medical Association*, vol. 83, no. 9, pp. 809–818, 1991.

[106] J. P. Sculier, C. Nicaise, and J. Klastersky, "Lactic acidosis: a metabolic complication of extensive metastatic cancer," *European Journal of Cancer and Clinical Oncology*, vol. 19, no. 5, pp. 597–601, 1983.

[107] D. S. Sheriff, "Lactic acidosis and small cell carcinoma of the lung," *Postgraduate Medical Journal*, vol. 62, no. 726, pp. 297–298, 1986.

[108] R. N. Raju and C. G. Kardinal, "Lactic acidosis in lung cancer," *Southern Medical Journal*, vol. 76, no. 3, pp. 397–398, 1983.

[109] P. W. Stacpoole, M. J. Lichtenstein, J. Robert Polk, and F. Anthony Greco, "Lactic acidosis associated with metastatic osteogenic sarcoma," *Southern Medical Journal*, vol. 74, no. 7, pp. 868–870, 1981.

[110] U. R. Varanasi, B. Carr, and D. P. Simpson, "Lactic acidosis associated with metastatic breast carcinoma," *Cancer Treatment Reports*, vol. 64, no. 12, pp. 1283–1285, 1980.

[111] G. Wesbey, "Lactic acidosis in oat cell carcinoma with extensive hepatic metastases," *Archives of Internal Medicine*, vol. 141, no. 6, pp. 816–817, 1981.

[112] T. El Imad, L. El Khoury, and A. S. A. Geara, "Warburg's effect on solid tumors," *Saudi journal of kidney diseases and transplantation*, vol. 25, no. 6, pp. 1270–1277, 2014.

[113] R. A. Gatenby and E. T. Gawlinski, "The glycolytic phenotype in carcinogenesis and tumor invasion: insights through mathematical models," *Cancer Research*, vol. 63, no. 14, pp. 3847–3854, 2003.

[114] M. Nagae, T. Hiraga, and T. Yoneda, "Acidic microenvironment created by osteoclasts causes bone pain associated with tumor colonization," *Journal of Bone and Mineral Metabolism*, vol. 25, no. 2, pp. 99–104, 2007.

[115] Y. Kato, S. Ozawa, M. Tsukuda et al., "Acidic extracellular pH increases calcium influx-triggered phospholipase D activity along with acidic sphingomyelinase activation to induce matrix metalloproteinase-9 expression in mouse metastatic melanoma," *FEBS Journal*, vol. 274, no. 12, pp. 3171–3183, 2007.

[116] T. Morita, T. Nagaki, I. Fukuda, and K. Okumura, "Clastogenicity of low pH to various cultured mammalian cells," *Mutation Research*, vol. 268, no. 2, pp. 297–305, 1992.

[117] R. J. Ruch, J. E. Klaunig, G. A. Kerckaert, and R. A. LeBoeuf, "Modification of gap junctional intercellular communication by changes in extracellular pH in Syrian hamster embryo cells," *Carcinogenesis*, vol. 11, no. 6, pp. 909–913, 1990.

[118] R. Martínez-Zaguilán, E. A. Seftor, R. E. B. Seftor, Y.-W. Chu, R. J. Gillies, and M. J. C. Hendrix, "Acidic pH enhances the invasive behavior of human melanoma cells," *Clinical and Experimental Metastasis*, vol. 14, no. 2, pp. 176–186, 1996.

[119] O. K. Schlappack, A. Zimmermann, and R. P. Hill, "Glucose starvation and acidosis: effect on experimental metastatic potential, DNA content and MTX resistance of murine tumour cells," *British Journal of Cancer*, vol. 64, no. 4, pp. 663–670, 1991.

[120] J. Rozhin, M. Sameni, G. Ziegler, and B. F. Sloane, "Pericellular pH affects distribution and secretion of cathepsin B in malignant cells," *Cancer Research*, vol. 54, no. 24, pp. 6517–6525, 1994.

[121] P. Montcourrier, I. Silver, R. Farnoud, I. Bird, and H. Rochefort, "Breast cancer cells have a high capacity to acidify extracellular milieu by a dual mechanism," *Clinical and Experimental Metastasis*, vol. 15, no. 4, pp. 382–392, 1997.

[122] Y. Kato, Y. Nakayama, M. Umeda, and K. Miyazaki, "Induction of 103-kDa gelatinase/type IV collagenase by acidic culture conditions in mouse metastatic melanoma cell lines," *Journal of Biological Chemistry*, vol. 267, no. 16, pp. 11424–11430, 1992.

[123] D. Fukumura, L. Xu, Y. Chen, T. Gohongi, B. Seed, and R. K. Jain, "Hypoxia and acidosis independently up-regulate vascular endothelial growth factor transcription in brain tumors in vivo," *Cancer Research*, vol. 61, no. 16, pp. 6020–6024, 2001.

[124] L. Xu, D. Fukumura, and R. K. Jain, "Acidic extracellular pH induces vascular endothelial growth factor (VEGF) in human glioblastoma cells via ERK1/2 MAPK signaling pathway. Mechanism of low pH-induced VEGF," *Journal of Biological Chemistry*, vol. 277, no. 13, pp. 11368–11374, 2002.

[125] F. Baumann, P. Leukel, A. Doerfelt et al., "Lactate promotes glioma migration by TGF-β2-dependent regulation of matrix metalloproteinase-2," *Neuro-Oncology*, vol. 11, no. 4, pp. 368–380, 2009.

[126] Q. Shi, J. L. Abbruzzese, S. Huang, I. J. Fidler, Q. Xiong, and K. Xie, "Constitutive and inducible interleukin 8 expression by hypoxia and acidosis renders human pancreatic cancer cells more tumorigenic and metastatic," *Clinical Cancer Research*, vol. 5, no. 11, pp. 3711–3721, 1999.

[127] Q. Shi, X. Le, B. Wang, Q. Xiong, J. L. Abbruzzese, and K. Xie, "Regulation of interleukin-8 expression by cellular pH in human pancreatic adenocarcinoma cells," *Journal of Interferon and Cytokine Research*, vol. 20, no. 11, pp. 1023–1028, 2000.

[128] L. Xu and I. J. Fidler, "Acidic pH-induced elevation in interleukin 8 expression by human ovarian carcinoma cells," *Cancer Research*, vol. 60, no. 16, pp. 4610–4616, 2000.

[129] S. Pavlides, D. Whitaker-Menezes, R. Castello-Cros et al., "The reverse Warburg effect: aerobic glycolysis in cancer associated fibroblasts and the tumor stroma," *Cell Cycle*, vol. 8, no. 23, pp. 3984–4001, 2009.

[130] S. Pavlides, I. Vera, R. Gandara et al., "Warburg meets autophagy: cancer-associated fibroblasts accelerate tumor growth and metastasis via oxidative stress, mitophagy, and aerobic glycolysis," *Antioxidants and Redox Signaling*, vol. 16, no. 11, pp. 1264–1284, 2012.

[131] A. Giatromanolaki, M. I. Koukourakis, A. Koutsopoulos, S. Mendrinos, and E. Sivridis, "The metabolic interactions between tumor cells and tumor-associated stroma (TAS) in prostatic cancer," *Cancer Biology and Therapy*, vol. 13, no. 13, pp. 1284–1289, 2012.

[132] M. I. Koukourakis, A. Giatromanolaki, A. L. Harris, and E. Sivridis, "Comparison of metabolic pathways between cancer cells and stromal cells in colorectal carcinomas: a metabolic survival role for tumor-associated stroma," *Cancer Research*, vol. 66, no. 2, pp. 632–637, 2006.

[133] O. Trabold, S. Wagner, C. Wicke et al., "Lactate and oxygen constitute a fundamental regulatory mechanism in wound healing," *Wound Repair and Regeneration*, vol. 11, no. 6, pp. 504–509, 2003.

[134] S. Beckert, F. Farrahi, R. S. Aslam et al., "Lactate stimulates endothelial cell migration," *Wound Repair and Regeneration*, vol. 14, no. 3, pp. 321–324, 2006.

[135] T. K. Hunt, R. Aslam, Z. Hussain, and S. Beckert, "Lactate, with oxygen, incites angiogenesis," *Advances in Experimental Medicine and Biology*, vol. 614, pp. 73–80, 2008.

[136] T. K. Hunt, R. S. Aslam, S. Beckert et al., "Aerobically derived lactate stimulates revascularization and tissue repair via redox mechanisms," *Antioxidants and Redox Signaling*, vol. 9, no. 8, pp. 1115–1124, 2007.

[137] T. N. Milovanova, V. M. Bhopale, E. M. Sorokina et al., "Lactate stimulates vasculogenic stem cells via the thioredoxin system and engages an autocrine activation loop involving hypoxia-inducible factor 1," *Molecular and Cellular Biology*, vol. 28, no. 20, pp. 6248–6261, 2008.

[138] P. E. Porporato, V. L. Payen, C. J. De Saedeleer et al., "Lactate stimulates angiogenesis and accelerates the healing of superficial and ischemic wounds in mice," *Angiogenesis*, vol. 15, no. 4, pp. 581–592, 2012.

[139] B. D. Kelly, S. F. Hackett, K. Hirota et al., "Cell type-specific regulation of angiogenic growth factor gene expression and induction of angiogenesis in nonischemic tissue by a constitutively active form of hypoxia-inducible factor 1," *Circulation Research*, vol. 93, no. 11, pp. 1074–1081, 2003.

[140] D. J. Ceradini, A. R. Kulkarni, M. J. Callaghan et al., "Progenitor cell trafficking is regulated by hypoxic gradients through HIF-1 induction of SDF-1," *Nature Medicine*, vol. 10, no. 8, pp. 858–864, 2004.

[141] I. Marchiq and J. Pouysségur, "Hypoxia, cancer metabolism and the therapeutic benefit of targeting lactate/H^+ symporters," *Journal of Molecular Medicine*, vol. 94, no. 2, pp. 155–171, 2016.

[142] K. Singer, M. Kastenberger, E. Gottfried et al., "Warburg phenotype in renal cell carcinoma: high expression of glucose-transporter 1 (GLUT-1) correlates with low CD8+ T-cell infiltration in the tumor," *International Journal of Cancer*, vol. 128, no. 9, pp. 2085–2095, 2011.

[143] C. Feder-Mengus, S. Ghosh, W. P. Weber et al., "Multiple mechanisms underlie defective recognition of melanoma cells cultured in three-dimensional architectures by antigen-specific cytotoxic T lymphocytes," *British Journal of Cancer*, vol. 96, no. 7, pp. 1072–1082, 2007.

[144] T. Ohashi, T. Akazawa, M. Aoki et al., "Dichloroacetate improves immune dysfunction caused by tumor-secreted lactic acid and increases antitumor immunoreactivity," *International Journal of Cancer*, vol. 133, no. 5, pp. 1107–1118, 2013.

[145] O. R. Colegio, N.-Q. Chu, A. L. Szabo et al., "Functional polarization of tumour-associated macrophages by tumour-derived lactic acid," *Nature*, vol. 513, no. 7519, pp. 559–563, 2014.

[146] V. Bronte, "Tumor cells hijack macrophages via lactic acid," *Immunology and Cell Biology*, vol. 92, no. 8, pp. 647–649, 2014.

[147] E. Gottfried, L. A. Kunz-Schughart, S. Ebner et al., "Tumor-derived lactic acid modulates dendritic cell activation and antigen expression," *Blood*, vol. 107, no. 5, pp. 2013–2021, 2006.

[148] Z. Husain, Y. Huang, P. Seth, and V. P. Sukhatme, "Tumor-derived lactate modifies antitumor immune response: effect on myeloid-derived suppressor cells and NK cells," *The Journal of Immunology*, vol. 191, no. 3, pp. 1486–1495, 2013.

[149] U. G. A. Sattler, S. S. Meyer, V. Quennet et al., "Glycolytic metabolism and tumour response to fractionated irradiation," *Radiotherapy and Oncology*, vol. 94, no. 1, pp. 102–109, 2010.

[150] C. Groussard, I. Morel, M. Chevanne, M. Monnier, J. Cillard, and A. Delamarche, "Free radical scavenging and antioxidant effects of lactate ion: An In Vitro Study," *Journal of Applied Physiology*, vol. 89, no. 1, pp. 169–175, 2000.

[151] U. G. A. Sattler and W. Mueller-Klieser, "The anti-oxidant capacity of tumour glycolysis," *International Journal of Radiation Biology*, vol. 85, no. 11, pp. 963–971, 2009.

[152] W. Wagner, W. M. Ciszewski, and K. D. Kania, "L- and D-lactate enhance DNA repair and modulate the resistance of cervical carcinoma cells to anticancer drugs via histone deacetylase inhibition and hydroxycarboxylic acid receptor 1 activation," *Cell Communication and Signaling*, vol. 13, no. 1, article no. 36, 2015.

[153] C. Plathow and W. A. Weber, "Tumor cell metabolism imaging," *Journal of Nuclear Medicine*, vol. 49, supplement 2, pp. 43S–63S, 2008.

[154] V. C. Sandulache, Y. Chen, H. D. Skinner et al., "Acute tumor lactate perturbations as a biomarker of genotoxic stress: development of a biochemical model," *Molecular Cancer Therapeutics*, vol. 14, no. 12, pp. 2901–2908, 2015.

[155] M. M. Lerch, D. L. Conwell, and J. Mayerle, "The anti-inflammasome effect of lactate and the lactate gpr81-receptor in pancreatic and liver inflammation," *Gastroenterology*, vol. 146, no. 7, pp. 1602–1605, 2014.

[156] R. Hoque, A. Farooq, A. Ghani, F. Gorelick, and W. Z. Mehal, "Lactate reduces liver and pancreatic injury in toll-like receptor- and inflammasome-mediated inflammation via GPR81-mediated suppression of innate immunity," *Gastroenterology*, vol. 146, no. 7, pp. 1763–1774, 2014.

[157] A. Finn and S. C. Oerther, "Can L(+)-lactate be used as a marker of experimentally induced inflammation in rats?" *Inflammation Research*, vol. 59, no. 4, pp. 315–321, 2010.

[158] W. Wagner, W. Ciszewski, K. Kania, and J. Dastych, "Lactate stimulates IL-4 and IL-13 production in activated HuT-78 T lymphocytes through a process that involves monocarboxylate transporters and protein hyperacetylation," *Journal of Interferon & Cytokine Research*, vol. 36, no. 5, pp. 317–327, 2016.

[159] H. Shime, M. Yabu, T. Akazawa et al., "Tumor-secreted lactic acid promotes IL-23/IL-17 proinflammatory pathway," *Journal of Immunology*, vol. 180, no. 11, pp. 7175–7183, 2008.

[160] L. Wei, Y. Zhou, J. Yao et al., "Lactate promotes PGE2 synthesis and gluconeogenesis in monocytes to benefit the growth of inflammation-associated colorectal tumor," *Oncotarget*, vol. 6, no. 18, pp. 16198–16214, 2015.

[161] B. Arcidiacono, S. Iiritano, A. Nocera et al., "Insulin resistance and cancer risk: an overview of the pathogenetic mechanisms," *Experimental Diabetes Research*, vol. 2012, Article ID 789174, 12 pages, 2012.

[162] D. Nehar, C. Mauduit, F. Boussouar, and M. Benahmed, "Tumor necrosis factor-α-stimulated lactate production is linked to lactate dehydrogenase A expression and activity increase in porcine cultured Sertoli cells," *Endocrinology*, vol. 138, no. 5, pp. 1964–1971, 1997.

[163] A. K. Andersson, L. Rönnbäck, and E. Hansson, "Lactate induces tumour necrosis factor-α, interleukin-6 and interleukin-1β release in microglial- and astroglial-enriched primary cultures," *Journal of Neurochemistry*, vol. 93, no. 5, pp. 1327–1333, 2005.

[164] T. C. Vary, P. O'Neill, R. N. Cooney, G. Maish III, and M. Shumate, "Chronic infusion of interleukin 1 induces hyperlactatemia and altered regulation of lactate metabolism in skeletal muscle," *Journal of Parenteral and Enteral Nutrition*, vol. 23, no. 4, pp. 213–217, 1999.

[165] I. Ben-Shlomo, S. Kol, L. M. Roeder et al., "Interleukin (IL)-1β increases glucose uptake and induces glycolysis in aerobically cultured rat ovarian cells: evidence that IL-1β may mediate the gonadotropin-induced midcycle metabolic shift," *Endocrinology*, vol. 138, no. 7, pp. 2680–2688, 1997.

[166] L. Hoejberg, L. Bastholt, J. S. Johansen, I. J. Christensen, J. Gehl, and H. Schmidt, "Serum interleukin-6 as a prognostic biomarker in patients with metastatic melanoma," *Melanoma Research*, vol. 22, no. 4, pp. 287–293, 2012.